

University of Nottingham
UK | CHINA | MALAYSIA

Combustion Characteristics of Methane-Diesel Dual-Fuel Engines at Light Load Conditions with Different Injection Strategies

Abdelrahman H.I. Hegab
B.Sc. (Hons), M.Sc.

Thesis submitted to the University of Nottingham
for the degree of Doctor of Philosophy

October 2017

"Praise be to Allah, Who has guided us to this; never could we have found guidance, had it not been for the guidance of Allah"

The Holy Qur'an [7:43]

ABSTRACT

An experimental investigation has been carried out to examine the combustion process in methane-diesel dual-fuel engines under light load conditions, with different ratios of the two fuels and different injection strategies of the diesel pilot. The study has used a 2.2L turbocharged common rail compression ignition (CI) engine, converted for dual-fuel (DF) operation while retaining the ability to run on diesel fuel only. The main area of interest has been the change of heat release characteristics with methane substitution for diesel fuel, and what gives rise to these changes. The focus has been put on the light load operating conditions, where the engine suffers poor fuel economy and increased instability owing to the very weak mixture strength of the gaseous fuel and air. An effort has been made to identify the minimum size of the diesel pilot required for the ignition of the very lean methane-air mixture at near-idle low-load operating conditions.

The experiments have been carried out at fully-warm steady-state conditions, at a wide range of engine speeds from 1400 to 2000 rpm at 25% engine load, with a wide range of methane substitution for diesel fuel up to 80% (energy basis). The influence of pilot injection strategy has been assessed via comparing the results of dual-fuel operation using a single pilot injection, to those obtained using pilot split-injection strategy. The maximum possible substitution ratio of methane for diesel fuel has been investigated at 5% engine load for a speed range from 1300 to 1600 rpm, and the different limitations on this ratio have been assessed.

The results have demonstrated that the dominant combustion mechanism in the region away from the pilot effect is determined by the relative magnitudes of diesel pilot and gaseous fuel. Gaseous fuel equivalence ratio (ϕ_{CH4}) has to be greater than 0.35 to sustain a flame-propagation event. For ϕ_{CH4} below 0.3, pilot combustion dominates. Small pilot masses (~1.6 mg/stroke) evaporate and locally intermix with the very lean gaseous fuel-air mixture, where the ensuing combustion is governed by the chemical kinetics. The minimum diesel injection mass was 0.8 mg/stroke in the test engine used. This presents a system-limitation on the maximum achievable substitution ratio of methane for diesel

fuel. The maximum substitution ratio achieved was as high as 95% at 1600 rpm, but it decreased at lower engine speeds. Methane substitution beyond these limits is restricted by the operation-limitation on engine stability, as the value of coefficient of variance of the gross indicated mean effective pressure ($COV_{IMEPgross}$) at this point exceeds 8%. Using larger pilot masses allows for the utilization of larger quantities of the gaseous fuel without exceeding the engine stability criterion ($COV_{IMEPgross}$ ~ 5%).

The use of pilot-split injection in DF engines has the capacity to change the combustion mode from the conventional diesel dual fuel (DDF) combustion into a novel two-stage partially premixed dual fuel (PPDF) combustion if the timing and quantity of the pilot pre-injection are optimized. Researches on this field are still in the early stages and in need for further development. The present work has developed an optimum pilot-split injection strategy to approach PPDF combustion mode. The results demonstrated a 17% reduction in the maximum rate of pressure rise (ROPR) and a 5% increase in the brake thermal efficiency (BTE) relative to conventional DDF, while maintaining the engine stability at appropriate levels ($COV_{IMEPgross}$ ~2-3%). The effect of pilot pre-injection mass on PPDF combustion was studied for the first time in this work. It has been found that the pre-injection mass has to be kept above a certain limit (3.2 mg/stroke) to bring about the desirable change of the combustion mode.

LIST OF PUBLICATIONS

Published:

- Hegab A, La Rocca A, Shayler P. Towards keeping diesel fuel supply and demand in balance: Dual-fuelling of diesel engines with natural gas. Renewable Sustainable Energy Revs 2017;70:666–697. (From Chapters 1, 2, and 3).

- Hegab A, Shayler P. The use of biodiesel and its emulsions as pilot fuels for compression ignition engines dual-fuelled with NG. In: Energy Mater. Res. Conf. Lisbon, Portugal: April 2017. (From Chapter 3).

- Hegab A, Shayler P. Effect of Pilot Pre-Injection on Methane-Diesel Dual Fuel Engine Combustion. In Proc. MHMT'17 2nd Int. Conf. Combust. Sci. Processes. Barcelona, Spain: April 2017. (From Chapter 6).

- Hegab A, Shayler P. Influence of Pilot Pre-Injection Mass on Partially Premixed Dual Fuel (PPDF) Engine Combustion. In Proc. MHMT'17 2nd Int. Conf. Combust. Sci. Processes. Barcelona, Spain: April 2017. (From Chapter 6).

Pending:

- Influence of energy substitution ratio on some combustion characteristics of a methane-diesel dual-fuel engine. Under preparation; 2017. (From Chapter 5).

- Investigating combustion modes and maximum substitution ratio of methane for diesel fuel in a dual-fuel engine at light load conditions. Under preparation; 2017. (From Chapter 5).

- Combustion characteristics of a methane-diesel dual fuel engine using pilot split-injection strategy. Under preparation; 2017. (From Chapter 6).

- An experimental study of partially premixed dual fuel (PPDF) engine combustion with fixed pre-injection quantity. Under preparation; 2017. (From Chapter 6).

To My Family

for their support, encouragement, patience, and love

ACKNOWLEDGEMENT

I would like to thank Professor Paul Shayler for giving me the opportunity to be part of the Engine Research Group at the University of Nottingham, where I have developed professionally as well as personally.

I am also grateful to my former and current colleagues in the group, post-grad and post-doc, for their helpful input and useful tips. Particular thanks go to Dr. Richard Gardiner. I would like also to express my appreciation for the valued assistance from the technical staff of the group, especially Mr. Nigel Sykes.

I must acknowledge the sponsorship I received from the Ministry of Higher Education in Egypt for my PhD studies.

To my family, I cannot thank you enough. I will always be indebted to you.

TABLE OF CONTENTS

ABBREVIATIONS **viii**

NOMENCLATURE **xi**

1 INTRODUCTION **1**

1.1 Overview 2
1.2 Background 3
1.2.1 Global energy outlook and transport sector demand 3
1.2.2 NG as an alternative fuel for IC engines 7
1.2.3 NG usage in transport sector 10
1.3 Present Contribution 13
1.3.1 Aim and objectives 13
1.3.2 Experimental approach 14
1.4 Thesis Layout 15
1.5 Contribution to Knowledge 16

2 LITERATURE REVIEW **18**

2.1 Introduction 19
2.2 Overview 19
2.3 Combustion and Exhaust Emissions Characteristics of PINGDEs 20
2.4 Influence of Injection Parameters and Fuel Composition on Combustion and Exhaust Emissions PINGDEs 34
2.4.1 Quantity of diesel fuel pilot 34
2.4.2 Injection timing of the two fuels 40
2.4.3 Injection pressure of the two fuels 49
2.4.4 Composition of natural gas 50
2.5 Conclusions 55

3 FUTURE DIRECTIONS OF NG-DIESEL DUAL-FUEL ENGINES **57**

3.1 Introduction 58
3.2 Splitting the Diesel Pilot into Pre-Injection and Main-Injection 59
3.3 Direct Injection of NG inside the Engine Cylinder 61
3.4 Increasing the Injection Pressure of the Two Fuels 65
3.5 Utilization of Alternative High-Cetane Pilot Fuels 68
3.5.1 Biodiesel fuels 68
3.5.2 Emulsified fuels 73
3.6 Utilization of Various Additives 77
3.6.1 Addition of H_2 77
3.6.2 Addition of EGR 79
3.6.3 Simultaneous addition of EGR and H_2 80
3.6.4 Addition of O_2 81
3.7 Conclusions 83

4 EXPERIMENTAL FACILITIES AND DATA PROCESSING 85

4.1 Introduction 86
4.2 Experimental Facilities and Setup 86
4.2.1 Engines and test bed 86
4.2.2 Data acquisition and instrumentation 94
4.3 Data Collection and Processing 98
4.3.1 Determination of the top dead center (TDC) 98
4.3.2 Synchronization of in-cylinder pressure and crank angle data 100
4.3.3 In-cylinder pressure data post-processing 103
4.3.4 Heat release rate (HRR) analysis 108
4.3.5 Indicated work and engine stability indicator 121

5 COMBUSTION PROCESS IN METHANE-DIESEL DUAL-FUEL ENGINES AT LIGHT LOAD CONDITIONS 124

5.1 Introduction 125
5.2 Overview and Method 125
5.3 Influence of Methane Substitution Ratio on DF Engine Combustion 127
5.4 Investigating Maximum Possible Methane Substitution for Diesel Fuel 134
5.5 Conclusions 151

6 EFFECT OF PILOT PRE-INJECTION ON DUAL-FUEL ENGINES COMBUSTION 153

6.1 Introduction 154
6.2 Overview and Method 154
6.3 PPDF Combustion vs. Conventional DDF Combustion 160
6.4 Influence of Pre-Injection Mass on PPDF Combustion 165
6.5 Conclusions 172

7 DISCUSSION AND CONCLUSIONS 173

7.1 Introduction 174
7.2 Discussion 174
7.3 Further Work to Complement This Thesis 180
7.3.1 Exhaust emissions analysis 180
7.3.2 Test rig development 181
7.4 Suggestions for Future Research 183
7.4.1 Improving light load operation 183
7.4.2 Limitations on methane substitution at high loads 186
7.5 Conclusions 188
7.5.1 Dual-fuel operation at light load 188
7.5.2 Pilot injection strategy 189

REFERENCES 190

APPENDICES 212

ABBREVIATIONS

ADC	Analogue-to-Digital Converter
AFR	Air-to-Fuel Ratio
AFR^{act}	Actual Air-to-Fuel Ratio
AFR^{stoic}	Stoichiometric Air-to-Fuel Ratio
ATDC	After Top Dead Center
APP	Accelerator Pedal Position
BC	Black Carbon
BDC	Bottom Dead Center
BBDC	Before Bottom Dead Center
BMEP	Brake Mean Effective Pressure (bar)
BTDC	Before Top Dead Center
BTE	Brake Thermal Efficiency (%)
BSFC	Brake Specific Fuel Consumption (kg fuel/kWhr)
CA	Crank Angle
CAD	Crank Angle Degree (°)
CDA	Cylinder Deactivation
CDO	Conventional diesel operation
C/H	Carbon-to-Hydrogen Ratio
CI	Compression Ignition
CIE	Compression Ignition Engines
CN	Cetane Number
CNG	Compressed Natural Gas
COHR	Center of Heat Release
COV_{IMEP}	Coefficient of Variation (of the IMEP)
CR	Common Rail
DAQ	Data Acquisition
DC	Direct Current
DDF	Diesel Dual-Fuel
DEE	Diethyl Ether
DF	Dual-Fuel
DFO	Dual-Fuel operation
DI	Direct Injection
DME	Dimethyl-Ether
DOC	Duration of Combustion

DP	Distributor Pump
DSF	Dynamic Skip Fire
DTI	Dial Test Indicator
ECU	Engine Control Unit
EDAQ	External Data Acquisition
EGR	Exhaust Gas Recirculation
EOC	End of Combustion
FAME	Fatty Acid Methyl Esters
FAR^{act}	Actual Fuel-to-Air Ratio
FAR^{stoic}	Stoichiometric Fuel-to-Air Ratio
FDD	Flame Development Duration
FFT	Fast Fourier Transform
FIE	Fuel Injection Equipment
FM	Fixed Mass
FR	Fixed Ratio
GHGs	Greenhouse Gases
GID	Gaseous-Fuel Ignition
HCCI	Homogenous Charge Compression Ignition
HP	High Pressure
HPCR	High-Pressure Common Rail
HPDI	High-Pressure Direct Injection
HR	Heat Release (J)
HRR	Heat Release Rate (J/°)
HTHR	High Temperature Heat Release
HTR	High Temperature Reaction
ICEs	Internal Combustion Engines
ID	Ignition Delay
IDI	Indirect Injection
IHR	Integrated Heat Release
IMEP	Indicated Mean Effective Pressure (bar)
ISFC	Indicated Specific Fuel Consumption (kg fuel/kWhr)
LNG	Liquefied Natural Gas
LTC	Low-Temperature Combustion
LHV	Low Heating Value (kJ/kg)
LP	Low Pressure
LTHR	Low Temperature Heat Release
LTR	Low Temperature Reaction
MAP	Manifold Absolute Pressure

MCC	Mixing-Controlled Combustion
MEUI	Mechanically-actuated Electronically-controlled Unit Injection system
MN	Methane Number
NEDC	New European Driving Cycle
MEP	Mean Effective Pressure (bar)
NG	Natural Gas
NGVs	Natural Gas Vehicles
NTC	Negative Temperature Coefficient
NVH	Noise, Vibration, and Harshness
NVO	Negative Valve Overlap
OEC	Oxygen Enriched Combustion
OECD	Organization for Economic Cooperation and Development
OEM	Original Equipment Manufacturer
PCCI	Premixed Charge Compression Ignition
PES	Percentage of Energy Substitution
PINGDE	Pilot Ignited Natural Gas Diesel Engine
PM	Particulate Matters
PMC	Pre-mixed Combustion
PPCI	Partially Premixed Compression Ignition
PPDF	Partially Premixed Dual Fuel
PPME	Pongamia Pinnata Methyl Ester
PSD	Power Spectral Density
RCCI	Reactivity Controlled Compression Ignition
RME	Rapeseed Methyl Ester
ROPR	Rate of Pressure Rise (bar/°)
R/P	Reserve-to-Production Ratio
SFC	Specific Fuel Consumption (kg fuel/kWhr)
SI	Spark Ignition
SIEs	Spark Ignition Engines
SOC	Start of Combustion
SOI	Start of Injection
TDC	Top Dead Center
TDCi	Turbocharged Diesel Common rail injection
THC	Total Hydrocarbon
VGT	Variable Geometry Turbine
VVT	Variable Valve Timing
W/O	Water-in-Oil

NOMENCLATURE

Latin

A	Area (m^2)
A_p	Top area of the piston (m^2)
A_w	Combustion chamber wall area (m^2)
B	Cylinder bore diameter (m)
c	Speed of sound of the gas (m/s)
C_v	Specific heat at constant volume (J/kg.k)
C_p	Specific heat at constant pressure (J/kg.k)
F_n	Fundamental resonant frequency (Hz)
h_c	Convection hear transfer coefficient ($J/s.m^2.k$)
k	Constant, number of suction strokes per engine revolution
L	Connecting rod length (m); Length of access passage (m)
m	Mass (kg)
$\dot{m_a}$	Mass flow rate of air (kg/s or mg/st)
$\dot{m_{CH4}}$	Mass flow rate of methane (kg/s)
$\dot{m_D}$	Mass flow rate of diesel fuel (kg/s or mg/st)
$\dot{m_{NG}}$	Mass flow rate of natural gas (kg/s)
$\dot{m_{pre}}$	Mass flow rate of pilot pre-injection (kg/s or mg/st)
M	Apparent molar mass of the gas (kg/kmol)
N	Engine speed (rpm or rps)
P	Pressure (Pa)
Q	Heat (J)
Q_{ch}	Fuel chemical energy (J)
Q_{gross}	Gross hear release (J)
Q_{ht}	Heat transfer to cylinder walls (J)
Q_{net}	net heat release (J)
R	Gas constant (J/kg.k); Radius to crank pin (m)
r	Compression ratio; Hydrogen-to-Carbon ratio
$\bar{R}$	Universal gas constant (J/kg.k)
S	Piston displacement from the TDC (m)
T	Temperature (k)
T_{ad}	Adiabatic flame temperature (k)
T_w	Effective wall temperature (k)

U	Internal energy (J)
V	Volume (m^3)
V_c	Clearance volume (m^3)
V_{disp}	Displacement volume (m^3)
$\dot{V}$	Volume flow rate (m^3/hr)
W	Work (J)
W_{cycle}	Work per cycle (J)
W_{brake}	Brake work (J)
$W_{friction}$	Friction work (J)
$W_{ind,\ gross}$	Gross indicated work (J)
$W_{ind,\ net}$	Net indicated work (J)
z	NG substitution ratio

Greek

γ	Specific heat ratio
δ	Infinitesimal change
η_{th}	Thermal efficiency
η_v	Volumetric efficiency
θ	Crank angle position (°)
θ_E	Crank angle at which a certain combustion stage ends (°)
θ_{rad}	Argument of trigonometric function (radians)
θ_{phase}	Phase shift angle (°)
ρ_a	Density of air (kg/m^3)
σ	Standard deviation
ϕ	Equivalence ratio

CHAPTER ONE

INTRODUCTION

1 Introduction

1.1 Overview

The investigation reported in this thesis is focused on providing a better understanding of combustion initiation and development in modern light-duty CI engines dual fuelled with diesel fuel and methane. The operation of these engines at part load conditions that prevail in the city traffic is of particular interest and pose questions as relative to engine combustion, fuel economy, and limitations on methane substitution for diesel fuel. The experimental studies described in the present contribution were directed towards these operating conditions, with a focus on several combustion and heat release characteristic comprising ignition delay, combustion phasing, ROPR, and engine stability.

The work started with investigating the influence of diesel fuel injection strategy on CI engine combustion. The tests were carried out using two versions of modern automotive CI engines with different fuel injection equipment (FIE) configurations. The first has a mechanical injection with distributor pump (DP), while the second has a common rail (CR) system. The comparative study between the two test engines was performed using diesel mono-fuel operation. Only the CR engine was modified to operate in the dual-fuel mode, where the influences of pilot injection strategy and the ratio of diesel fuel to methane on combustion and heat release were assessed and evaluated.

The experimental study reported here was preceded by an assessment and development of the test facility to accommodate the necessary hardware and test measures following the rig overhauling, as the two engines were tested on the same rig; one after the other.

The work carried out in this thesis entailed, in the lead, steering a detailed review of the prevalent literature with regard to NG-diesel dual-fuel engines, to provide an overview of the progress that has been made in recent years and identify the requirement for and the potential of further research. This presented an integrated part of the thesis, to guide the current work and also to lead the path ahead of future contributions in the field.

The overall background of the subject, the significance of the present contribution, and the structure of the thesis are given in the following sections.

1.2 Background

1.2.1 Global energy outlook and transport sector demand

Energy demand worldwide continues to rise as a consequence of the population growth along with the improvement in the standard of living. The last 10-year average rate of growth in world primary energy consumption is 1.8%, although the year 2016 exhibited a below-average growth of just 1.0%; slightly higher than the 0.9% growth recorded in 2015 [1]. This recent slowdown is attributable, in some measure, due to the rebalancing of the Chinese economy away from the energy intensive sectors [1]. While consumption and production reached record levels for every fuel type (except nuclear power), energy consumption will see more increase in the foreseeable future as the world population is expected to grow by more than 2 billion people in the next 30 years to surpass 9.8 billion by 2050 [2]. Figure 1.1 illustrates the total world energy consumption by fuel type from 1990 to 2040 (history/projections). At present, fossil fuels continue to supply more than 75% of total energy consumption [3]. The increased energy demand dictates increased fuel production; draining current fossil fuel reserve levels at a faster rate.

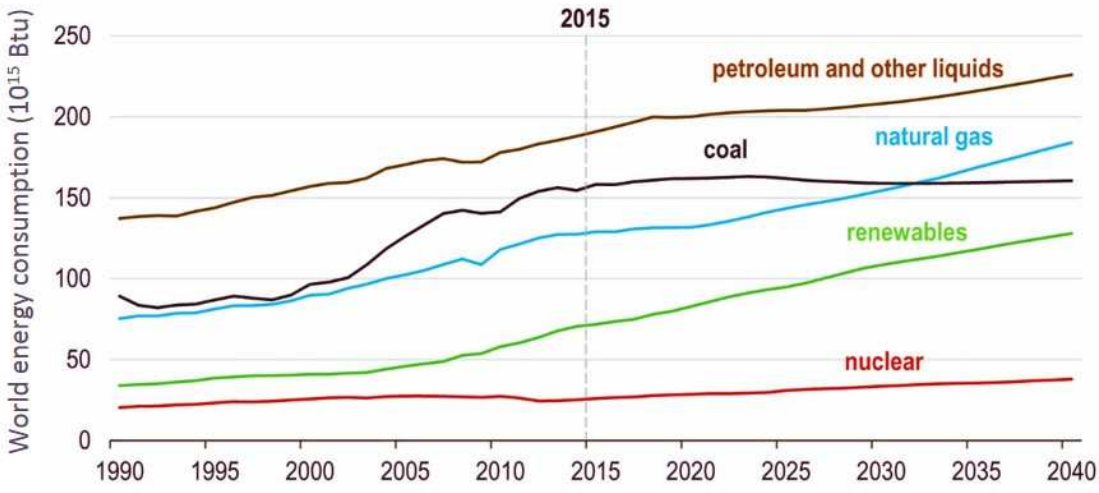


Figure 1.1 World energy consumption by fuel type, 1990-2040 (quadrillion Btu). Adapted from [3].

While oil remains the world's leading fuel at 33% of global energy consumption, more than 60% of the world's current oil reserves are in regions that suffer frequent political turmoil; as demonstrated by Fig. 1.2, which considerably affects the stability of supply distributions [1]. As internal combustion engines (ICEs), fuelled mostly by petroleum-derived liquid fuels, have been the main source of transport power over the past century and expected to continue service into the present century, the road transport sector, in particular, needs more secure and sustainable fuel sources.

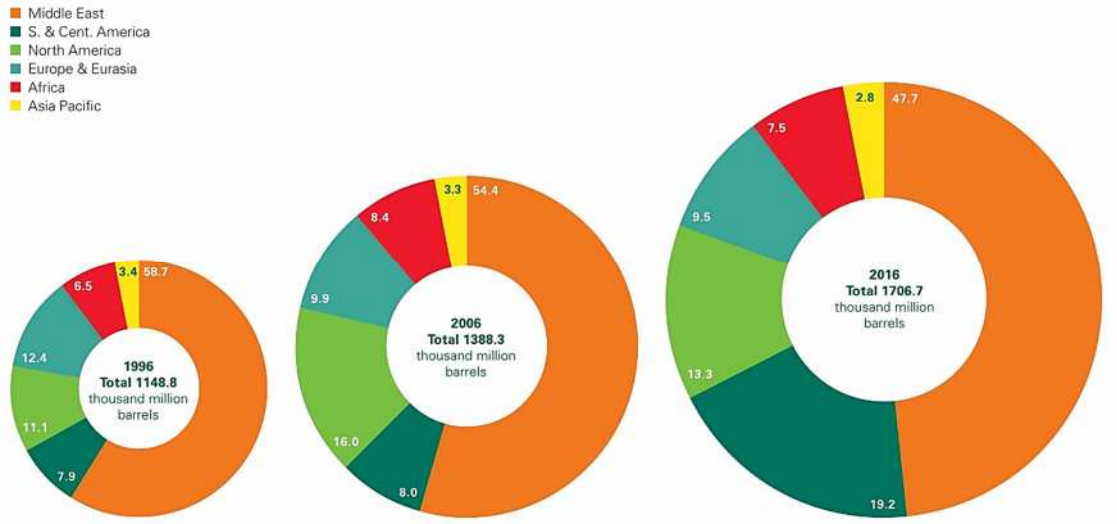


Figure 1.2 Distribution of proven reserves of oil in 1996, 2006 and 2016 – (%). Ref. [1].

World demand for transport fuels accounts for almost 60% of the total oil consumption [4], and it is expected to grow rapidly as the number of vehicles increases. As for overall energy demand, the growth of transport fuels demand is almost entirely from countries outside the Organization for Economic Cooperation and Development (OECD) [3, 4]. Regardless of the fact that the number of personal vehicles is expected to rise to about 1.7 billion in 2040 compared with approximately 825 million at 2010, the fuel demand from this sector is expected to rise only slightly [5]. This is attributed to the prospective reduction in the average vehicle size and the miles driven (compared to today's average vehicle), on top of the improvement in efficiencies and hybridization [5, 6]. Conversely, energy demand for the commercial transport sector, which includes heavy-duty trucks and marine, is expected to increase by about 75% over the same period in spite of some gains in efficiency. Hence, the demand for diesel fuel, the most popular fuel for heavy-

duty vehicles, will rise by 85%, while gasoline demand will fall by about 10% over this period between 2010 and 2040 [6]. That is, the increasing demand for transport energy is strongly skewed towards the heavier fuels (predominantly; middle distillates such as diesel and jet fuels) [7]. Recently, there has been a slight improvement in oil refinery processes with regard to the amounts of heavy fuels yield compared with gasoline yield. For instance, the U.S. refinery yield of “Distillate Fuel Oil” (general classification for one of the petroleum fractions includes diesel fuels and fuel oils [8]) has increased from 23.9% at 2004 to 29.8% at 2014, while the yield of Finished Motor Gasoline during the same period fell from 46.8% to 44.9% [9]. Despite the increased yield in distillate fuel oil, this is probably insufficient to meet the growing demand for diesel fuel. The likely shortfall will stimulate more investments in the current refinery courses to yield more diesel and jet fuels at a cost to gasoline [6].

The legislated reduction of exhaust gas emissions is another critical challenge facing the IC engines that use fossil fuels. For instance, Euro 5 emission standards that came into force in 2009 demanded gasoline and diesel engines to reduce their NOx emissions by 25% and 28%, respectively, relative to the previous emissions standards. Further reduction of diesel engines NOx emissions by 55.5% was called for by Euro 6 standards in 2014 [10]. Yet, carbon emissions from fossil fuel use in transport sector account for almost 25% of global energy-related CO_2 emissions [11]. While there are continuous efforts to develop more energy-efficient and environmentally friendly ICEs [12, 13], significant achievements are considered far from being sustainable in terms of its well-to-wheel efficiency or CO_2 emissions [14]. In the short term, however, the use of light-duty vehicles with improved energy efficiency presents the most cost-effective and thus sustainable mean of reducing oil consumption [14].

Despite their high NOx and PM emissions, which are difficult to control by the after-treatment of the oxygen-rich exhaust through the use of catalysts, the market share of diesel vehicles has been rising, especially in Europe. In countries such as Spain, France, and Belgium, the market share of diesel fuelled passenger cars is close to 60%; as shown in Fig. 1.3 [16]. The recent decline in the number of light-duty diesel vehicles is driven by the increasing concern over their contribution to inner city poor air quality. However,

the use of diesel engines in heavy-duty vehicles and commercial transport continues to grow. The increasing demand for diesel engines (including off-highway equipment) is illustrated by Table 1.1 [15].

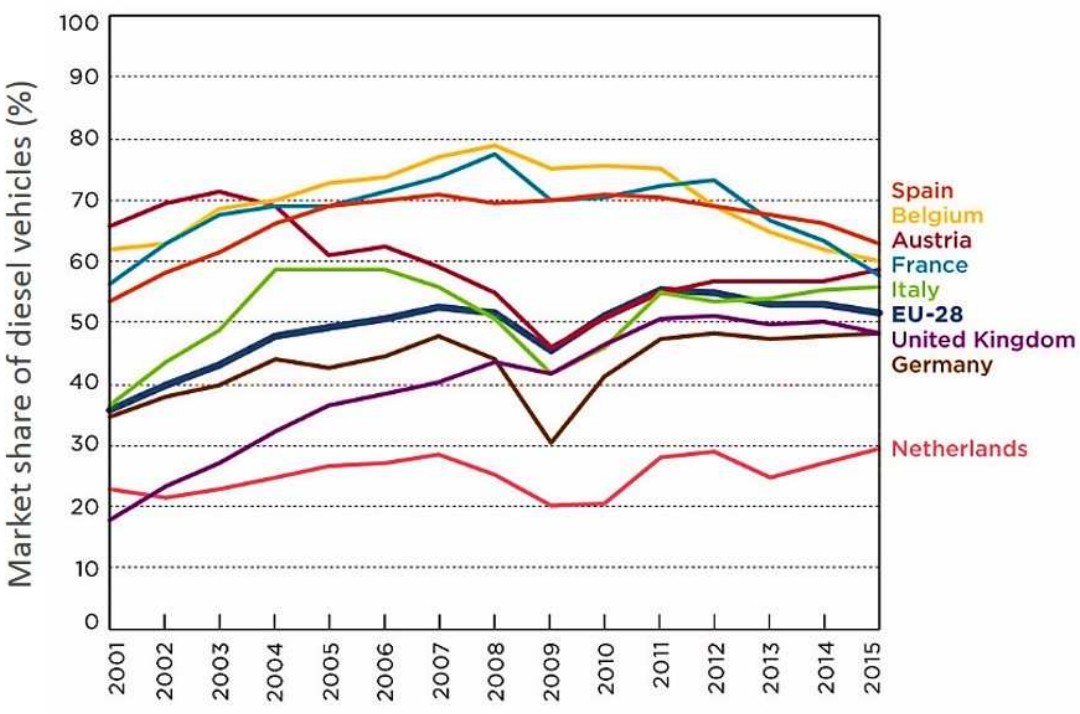


Figure 1.3 Passenger cars market share of diesel vehicles (%) in Europe. Adapted from Ref. [16].

Table 1.1 Global diesel engines demand (billion dollars). Adapted from Ref [15].

Region	2012	2017
North America	23.2	32.3
Western Europe	43.3	57.2
Asia Pacific	74.3	113.5
South America	9.4	14.2
Eastern Europe	13.2	18.7
Africa & Middle East	8.2	12.7
TOTAL	171.6	248.6

The transition into the use of low-carbon fuels, along with hybridization, is regarded a medium-term strategy to approach a more sustainable transport and reduces the reliance on conventional ICEs fuels (diesel and gasoline) [14]. The production costs of a range of alternative fuels and energy carriers, at varying oil price assumptions and technology maturation levels, have been investigated [17]. The potential benefits of using some of these fuels in transport sector have also been studied [18]. The emerging picture is very complex and influenced by socio-economic, political, and environmental factors on top of many direct technical challenges. At present, natural gas (NG) appears to be a very promising candidate fuel that will play a bigger role in transport sector in the near future [5]. The concept of dual-fuelling diesel engines with NG stands as an attractive option to reduce the dependence on diesel fuel and lessen the harmful emissions. With the high market share of diesel-fuelled vehicles in several areas worldwide, dual-fuelling of diesel engines with NG will likely deliver a breakthrough in the existing vehicle market if some technical as well as operational issues are addressed. These include fuel storage, safety measures, and engine modification (intake system for port injection or cylinder head for direct in-cylinder injection).

1.2.2 NG as an alternative fuel for IC engines

NG is the volatile portion of the crude petroleum, which normally occupies, under high pressures, the porous rocks of oil reservoirs above the liquid fuel zone. In addition, it can be found in dry form or non-associated with oil gas fields [19]. The composition of raw NG varies considerably depending on its source, but its main constituent is methane (with an average concentration of 90%). The remainder is composed of various heavier hydrocarbons (ethane, propane, and butane), along with some diluent gases such as N_2, CO_2, on top of traces of other components. The properties of NG and the concentrations of its main constituents are presented in Table 1.2 [20]. However, the detailed nature of different constituents of NG has vital implications on its use as an alternative fuel for ICEs. For instance, the percentages of higher hydrocarbon are significantly influential on engine combustion and emissions [19]. Table 1.3 lists some of the major properties of higher hydrocarbon fuel gases in comparison with methane [19].

Table 1.2 Properties of natural gas. Adapted from Ref. [20].

Property	Value
Relative molar mass	17-20
Carbon content, weight %	73.3
Hydrogen content, weight %	23.9
Oxygen content, weight %	0.4
Relative density, 15°C	0.72-0.81
Boiling point, °C	-162
Autoignition temperature, °C	540-560
Octane number	120-130
Methane number	69-99
Stoichiometric air/fuel ratio, weight	17.2
Vapor flammability limits, volume %	5-15
Lower heating/calorific value, MJ/kg	38-50
Methane concentration, volume %	80-99
Ethane concentration, volume %	2.7-4.6
Nitrogen concentration, volume %	0.1-15
Carbon dioxide concentration, volume %	1-5
Sulfur content, weight % ppm	<5

Table 1.3 Properties of main hydrocarbon fuel gases. Adapted from Ref. [19].

Property	Methane	Ethane	Propane	Propene	Butane	Butene
Energy content LHV (MJ/kg)	50.01	47.48	46.35	45.78	45.74	45.32
Liquid density (kg/L)	0.466	0.572	0.501	0.519	0.601	0.607
Liquid energy density (MJ/L)	23.30	27.16	23.22	23.76	27.49	27.51
Boiling point (ºC)	-164	-89	-42	-47	-0.5	-6.3
Gas energy density (MJ/m^3)	32.6	58.4	84.4	79.4	111.4	113.0

NG is found in several areas worldwide, either together with other fossil fuels or on its own, and it has larger proven reserves than crude oil; the current known reserves-to-production (R/P) ratio for NG approaches 53% [1]. Also, the proven reserve distribution of NG is better than that of oil, with respect to the political stability of the regions where the reserves are found; as shown in Fig. 1.4 [1]. Besides, methane, the main constituent of NG, can be produced in a renewable way from landfill and biomass decomposition. The produced gas from that process is usually referred to as landfill gas or biogas, and it is usually composed of at least 50% methane and up to 50% CO_2, with trace amounts of hydrogen, nitrogen, and hydrogen sulfide [21-23].

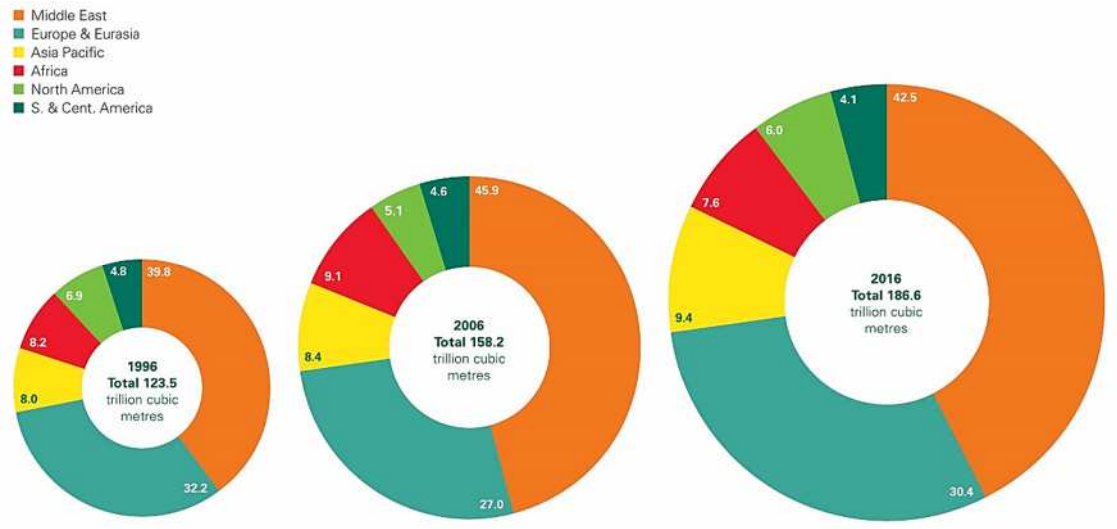


Figure 1.4 Distribution of proven reserves of NG in 1996, 2006 and 2016 – (%). Ref. [1].

As a fuel, NG has a clean nature of combustion, compared with conventional fuels. It can reduce the engine exhaust emissions by about 50% in non-methane hydrocarbons (HC), 50–87% in NOx, 20–30% in CO_2, 70–95% in CO, while it produces almost zero smoke and PM [24]. NG has a higher combustion enthalpy per unit mass (lower heating value) than gasoline or diesel fuel and a very high octane rating that exceeds 120 [25, 26]. As a result, the engine can work at high compression ratios without experiencing the "knock" phenomenon, and thus NG is suitable for CIEs if a high-energy ignition source is available. It also can be utilized in SIEs under higher compression ratios than those with conventional gasoline; producing higher thermal efficiency [27, 28].

From the economic perspective, NG as a fuel is cheaper than conventional motor fuels such as gasoline and diesel (on energy equivalent basis), and thus it offers lower running cost [29]. In addition, the use of NG provides several benefits to the engine components, and effectively reduces the maintenance requirements. NG does not mix with or dilute the lubricating oil, and will not cause deposits in the combustion chambers and on spark plugs like petrol does; thereby extends the piston ring and spark plug life. In diesel dual-fuel operation, evidence of reduced engine wear is reported, leading to longer engine life [15, 24]. As far as the safety is considered, NG seems to be safer than conventional fuels. The low density of NG, coupled with its high auto-ignition temperature and high flammability limits gives it a high dispersal rate and makes the likelihood of ignition in the event of a gas leakage much less than gasoline or diesel [20, 24]. With regard to the

applicability, NG can be easily employed in SIEs and CIEs. The technology of engine conversion is well-known and can be directly applied through several options, where suitable conversion equipment is readily available [30].

1.2.3 NG usage in transport sector

Although NG has a higher energy density per unit mass than gasoline and diesel fuel, the volumetric energy density of NG is much lower; as illustrated by Fig. 1.5 [31]. For that reason, it is unfeasible to use NG as a transportation fuel at ambient temperature and pressure; it must be either compressed or liquefied to increase its volumetric energy density [32]. Despite the fact that liquefied natural gas (LNG) is superior to compressed natural gas (CNG) in terms of energy density, it has worse environmental impact as the gas has to be liquefied and transported. LNG usage in transportation sector is therefore still marginal, although it has begun in recent years to penetrate the fuel market for both marine and long-distance road transportation [33]. In LNG vehicles, NG is stored in the liquid phase at a very low temperature of the order of –162ºC and a volume of 1/600 of its original volume. In advance of being introduced to the engine, LNG must be heated and vaporized; and therefore a distinctive technology is required. Yet, LNG can also be used to refuel CNG vehicles. In this case, an L-CNG filling station is required, in which NG is stored as LNG but sold as CNG, by flowing first through a low-temperature high-pressure pump, then through a gasification device, and finally through the CNG sales machine [34]. In CNG vehicles, NG is compressed to less than 1% of the volume under atmospheric pressure; such a volume is attained at 200 bar. In view of that, conventional liquid fueling systems are no longer usable; where this concerns both the onboard fuel storage and fuel delivery systems. A high-pressure CNG cylinder is required to replace the conventional liquid fuel tank, while a modified fuel delivery system is prerequisite. Regardless of these modifications, the driving range of natural gas vehicles (NGVs) is generally less than that of comparable vehicles running on conventional fuels, owing to the lower energy density of natural gas. Typical CNG cylinder used in onboard carries less fuel energy (in MJ) than a gasoline or diesel fuel tank of the same volume [19, 21].

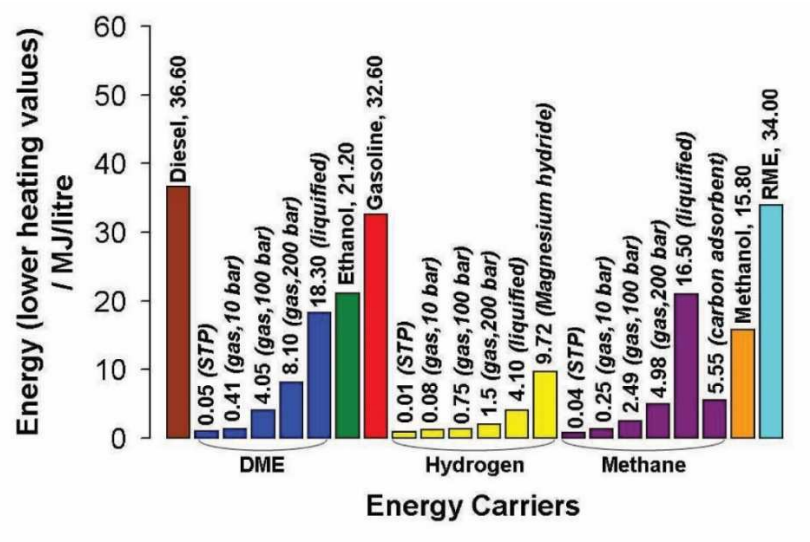


Figure 1.5 **Volumetric energy density (lower heating values) for different energy carriers; gasoline, diesel fuel, and methane; MJ/ Liters. Ref. [31].**

The number of NG-fuelled vehicles has significantly raised in recent years. At present, the total number of NGVs over the world exceeds 22 million, which represents around 2% of the total vehicles population. Asian and Latin America countries take the lead in NGVs population with expectations of further growth, despite the fact that there is still less attention to this alternative in most European countries. Table 1.4 lists the top 10 countries in NGVs population and their share to the total NGVs worldwide [35], and Fig. 1.6 shows the top 10 countries in NGVs share to the local vehicle market [36].

Table 1.4 **Top 10 countries in NGVs population. Adapted from Ref. [35].**

Country	Total NGVs population	% of total NGVs worldwide
Iran	4,000,000	17.91
China	3,994,350	17.88
Pakistan	3,700,000	16.57
Argentina	2,487,349	11.14
India	1,800,000	8.06
Brazil	1,781,102	7.97
Italy	885,300	3.96
Colombia	500,000	2.24
Thailand	462,454	2.07
Uzbekistan	450,000	2.01

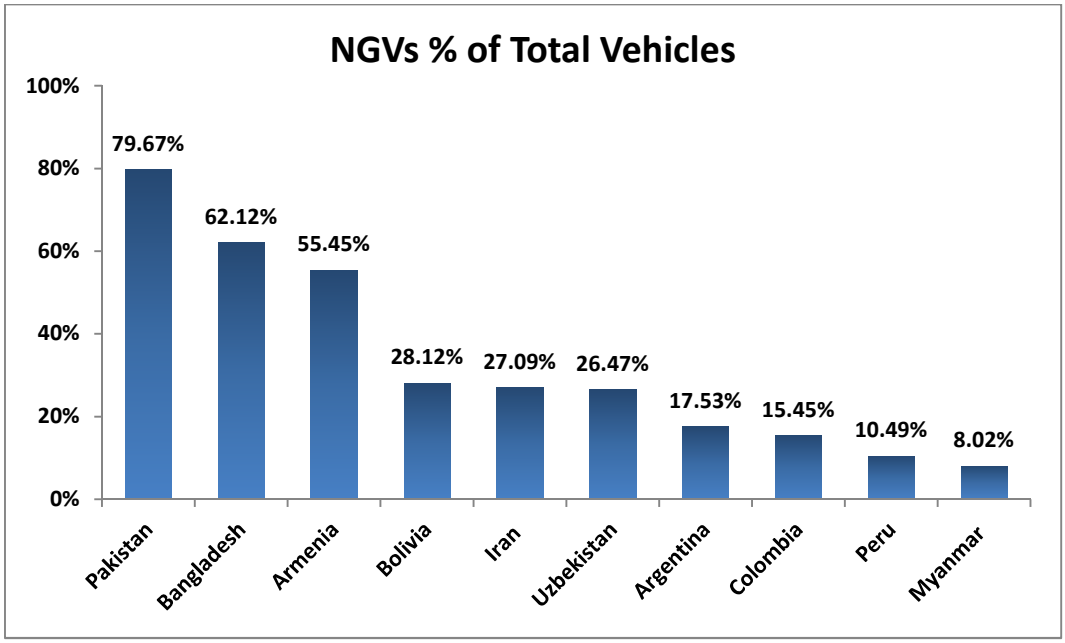


Figure 1.6 Top 10 countries in NGVs share to the local vehicle market. Adapted from Ref. [36].

In recent years, gas-fueled SI engines have fallen increasingly out of favor to dual-fuel engines as the latter display several positive features [19]. The high compression ratios and torque of the diesel engines can be retained in the dual-fuel operation; leading to improvements in power output and efficiency. DDF engines have less cyclic variability even at light load conditions, owing to the reliable source of the energetic pilot ignition. A wider spectrum of gaseous fuels can be used in DDF engines with a less tendency to knock, while the robust construction of the retrofitted diesel engine used can withstand the high in-cylinder pressure values and any incident shocks. Power output in DDF engines is controlled by changing the fuel concentration rather than through throttling, and hence the engine can operate over a wider overall range of mixture equivalence ratios and turbocharging intensity.

Although the concept of dual-fuelling is not new and has been deliberated lengthily in the past two decades, several uncertainties still exist with regard to engine combustion, emissions, and the rates and mechanisms of heat release. There is a need to promote the understanding of how the fuel oxidation processes take place in DF engines, what the stages of combustion are, and how to identify the boundaries between these. The effects of pilot injection strategy and gaseous fuel substitution levels also need to be examined.

Light load operation of DDF engines is the most challenging owing to the small amount of gaseous fuel used, where the resulting weak mixture of the gaseous fuel and air bring many negative outcomes to engine combustion, emissions, stability, and fuel economy [19, 21]. To make the use of these engines more practical at urban driving conditions, light load operation has to be improved. The optimization of the pilot injection strategy could yield novel combustion modes in DF engines that have the capacity to improve light load operation [37]. The use of pilot split-injection strategy is one potent solution to achieve that, but researches on this strategy are still in the early stages and in need for further development. The influence of pilot pre-injection mass is yet to be studied. The present work addresses the above mentioned topics.

1.3 Present Contribution

1.3.1 Aim and objectives

The aim of the investigations described in this thesis has been to establish how the heat release characteristics of a methane-diesel dual-fuel engine depend on the pilot injection strategy and the substitution ratio of methane for diesel fuel, under light load operating conditions.

To attain this aim, the following objectives were identified:

- Investigate how the trending change of the fuel injection equipment (FIE) in modern CI engines from the mechanical injection to the common rail system alters engine combustion and heat release characteristics.
- Examine the practicability of converting modern automotive CI engines to work on dual-fuel (DF) mode using methane as the main fuel and diesel fuel as a pilot.
- Explore the combustion initiation and development in a methane-diesel DF engine, how it compares to classical diesel combustion, and how it would be influenced by the change of fuel injection equipment (FIE) and pilot injection strategy.
- Consider the influence of methane substitution ratio for diesel fuel on the rates and mechanisms of energy release, and assess the different limitations on the maximum possible substitution ratio at light load operating conditions.
- Investigate the effect of using pilot pre-injection in methane-diesel DF engines, how it could change the combustion mode and what the potential benefits are.

1.3.2 Experimental approach

At the time the present work commenced, the Engine Research Group at the University of Nottingham was lacking a test rig for a CI engine dual-fuelled with gaseous fuel. In view of that, it was decided to modify and rebuild an existing test rig. The author of the present contribution was responsible for the design and commissioning of the new test facility. A modern turbocharged diesel common rail (CR) injection (TDCi) engine, by Ford motor company, was allocated for the project. This engine, referred to as the CR-Engine, belongs to the category used in Ford Transit vans, and hence the results of the project could be applied to many large fleets worldwide. The test bed allocated to the project was occupied by a CI engine from the same manufacturer and series of engines (Ford Puma) but with a distributor pump (DP) mechanical injection system. This engine will be referred to in this work as the DP-Engine.

The work started with evaluating the test bed components, auxiliary systems, controls, and data acquisition equipment. The purpose was to investigate the possibility of using any of the rig components when rebuilding it to accommodate the CR-Engine. This job was practically achieved by conducting a baseline testing for the DP-Engine, firstly to evaluate the system, and at the same time to solidify the base of comparison between different FIEs, following the commissioning of the CR-Engine. The comparative study covered the effects of engine speed, load, and injection timing on the heat release rate (HRR) and combustion characteristics under conventional diesel operation (CDO). The detailed results and analysis of the study are presented in Appendix A.

After the test rig was assessed and the data required for the comparison was collected, the process of rig overhauling took place. Special attention was paid to the gaseous fuel system design, selection of components, and safety measures. The target was to execute a practical system that is compact yet efficient as well as safe, so it can be easily applied to vehicular applications with least modifications. Dual-fuel experiments were done on the CR-Engine only, using methane as the main fuel and diesel fuel as a pilot. The study began with investigating combustion initiation and development in dual-fuel engines, then examined the different limitations on methane substitution for diesel fuel. Finally, the effect of pilot pre-injection on methane-diesel dual-fuel combustion was studied.

1.4 Thesis Layout

The research undertaken in this thesis is presented in seven chapters. The objective of each is described briefly in what follows:

Chapter 1 is the introduction. It gives an overview of the present work and a descriptive background of the topic, including the outlook for global energy and transport section demand, as well as the potentials of NG as a fuel and its current use in ICEs. The present contribution respecting the aim, objectives, and approach is then highlighted, followed by outlining the thesis layout.

A critical review of the relevant literature regarding the progress and recent trends in NG-diesel DF engines is given in chapter 2. The concept and challenges are highlighted, and the effects of injection parameters and fuel composition on engine combustion and emissions are investigated. These comprise pilot fuel size, injection timing and pressure of the two fuels, and NG composition.

Chapter 3 builds of the review presented in chapter 2, to categorize the future directions of research in the field, and highlights some topics that need further investigation. These include pilot split-injection strategy, direct injection of NG inside the engine cylinder, using alternative high-cetane pilot fuels (e.g. biodiesel fuels and emulsified fuels), and employing different charge additives (H_2, EGR, and O_2).

A detailed description of the experimental facilities used in this work is presented in Chapter 4. This includes the two test engines used, the test bed, and the data acquisition system and instrumentation. Data collection and post-processing procedures are also explained in this chapter.

In Chapter 5, combustion process in methane-diesel DF engine at light load conditions is discussed through a detailed analysis of the heat release characteristics. The influence of methane substitution ratio for diesel fuel and the limitations on its maximum value are also investigated.

The use of pilot pre-injection in DF engines, how it affects the combustion mode, and the reflections of combustion mode change on the engine combustion and heat release characteristics are examined in Chapter 6. The influence of pilot pre-injection mass is also studied and quantified.

Chapter 7 presents the overall discussion of the work undertaken, together with the final conclusions. Further efforts to complement the present work and suggestions for future research are also highlighted.

1.5 Contribution to Knowledge

The thesis provides a roadmap for future research directions on dual-fuelling of diesel engines with NG. The map outlines a categorization of the new technologies of research in the field, where the diversity of topics discussed and evaluated is unprecedented in a single work. The outcome has been published in “Renewable and Sustainable Energy Reviews” in 2016, while some additional efforts have been presented in the “Energy and Materials Research Conference EMR2017”, Lisbon, Portugal; 2017.

Insight to the combustion process in diesel dual fuel (DFF) engines has been established through experimental studies and analysis of the results without using complex imaging techniques. Most of the research efforts on traditional all-metal engines serve to discuss the general trends of DDF operation yet the detailed analysis of the heat release data is the area that requires further research effort. This has been addressed in this work where the DDF combustion stages, the boundaries between these stages, and the dominant combustion mechanism in each stage have been identified. A wide range of substitution ratios of methane for diesel fuel has been covered, while the limitations on maximum possible substitution ratio have been examined. The study has revealed some important qualitative information and quantitative results that will be submitted for the publication in the “Energy Conversion and Management”.

The present work also bridges some gaps in the knowledge with regard to the influence of pilot injection strategy on DF engine combustion mode. The accurate control of fuel injection parameters could help attaining novel combustion modes that bring several

benefits to engine combustion, emissions, stability and fuel economy. The present work has developed an optimum pilot-split injection strategy to attain partially premixed dual fuel (PPDF) combustion mode. The test results under the novel PPDF mode have been compared to those from conventional DDF operation and presented in the “International Conference on Combustion Science and Processes CSP’17”, Barcelona, Spain; 2017. The influence of pilot pre-injection mass on PPDF combustion is studied for the first time in the present contribution. The results have been conveyed in another contribution presented in the same conference.

CHAPTER TWO

LITERATURE REVIEW

2 Literature Review

2.1 Introduction

This chapter provides a review of previous studies of NG-diesel dual-fuel engines, on the topics that have been well-developed. Following a general overview of the concept of dual-fuelling and its different configurations, the chapter is separated into two parts. The first part covers the research efforts on combustion and emissions characteristics of NG-diesel DF engines, with an effort to fill any voids and explain any discrepancies in the results. In the second part, the effects of injection parameters and gaseous fuel composition on combustion and emissions are considered. The outcomes of this review will help to identify the future directions of research on the topic that require further development, but these will be discussed in Chapter 3 as they present the foundation of the excremental study presented in later chapters of this thesis.

2.2 Overview

The most common natural gas-diesel dual-fuel engine operating mode is referred to as “Pilot Ignited Natural Gas Diesel Engine – PINGDE” [38]; where most of the engine power output is provided by the gaseous fuel while a pilot amount of the diesel fuel is injected near the end of the compression stroke to act as an ignition source of the NG-air mixture. The engine power output is controlled by changing the amount of the main gaseous fuel, while the pilot diesel fuel quantity is kept constant [38].

In most applications to date, NG is inducted or injected into the intake manifold to mix uniformly with the air, and the homogenous NG-air mixture is then introduced into the cylinder to be compressed; like in the conventional diesel mode. In some applications in recent years, NG is directly injected into the cylinder shortly before the end of the compression stroke. This technique provides better fuel economy and more efficient combustion and maintains the power output and the brake thermal efficiency of an equivalently-sized conventional diesel engine. It also enables the use of less pilot mass as it is electronically controlled, in contrast to the relatively large pilot fuel mass with mechanical control systems [19]. Yet, direct injection of NG requires the development of special high pressure gaseous injectors; adding cost and complexity to the process.

Regardless of the way of introducing NG into the engine cylinder, the pilot diesel fuel is introduced into the cylinder through the conventional diesel injection system [21].
Combustion processes of fuels currently used in ICEs depend on the octane number (a measure of knocking resistance, used with SI engines fuels) and the cetane number (a measure of ignition delay characteristics, used with CI engines fuels) [39, 40]. For any given fuel, there is an inverse but not a proportional relationship between octane and cetane numbers. Methane, the main constituent of NG, has a higher octane number than gasoline and a lower cetane number than diesel fuel. Thus, regardless of the way of introducing NG into the combustion chamber in CI engines, NG does not spontaneously ignite under CI compression ratios (and the corresponding temperatures) like diesel. Instead, it does need a source of controlled ignition, and from here the necessity of the utilization of pilot diesel fuel emerges. The injection of the pilot fuel into such a hot environment results in the auto-ignition of the diesel fuel droplets; affecting the part of the gaseous charge entrained into the pilot jet and in its vicinity. Then, flame propagates throughout the combustible gas-air mixture [41, 42].
The following sections review the recent research efforts on PINGDEs combustion and emissions, and the influences of different engine parameters on these characteristics.

2.3 Combustion and Exhaust Emissions Characteristics of PINGDEs

Papagiannakis and Hountalas [43] studied the combustion and emissions characteristics of a DI diesel engine dual-fuelled with NG. They compared the conventional diesel operation (CDO) and dual-fuel operation (DFO), where the pilot fuel amount with CDO was kept constant, while the power output of the engine is adjusted by controlling the amount of gaseous fuel. The percentage of NG substitution *(z)* was expressed on mass basis used; as:

$$z = \frac{\dot{m_{NG}}}{\dot{m_{NG}} + \dot{m_D}} \times 100(\%) \tag{2.1}$$

where ($\dot{m}_{NG}$) and ($\dot{m}_D$) are the mass flow rates for NG and diesel fuel; respectively.
The results indicated that DFO results in lower peak cylinder pressure compared to the one under CDO. The authors pointed out that reduced in-cylinder pressure during the compression stroke under DFO is lower due to the higher specific heat capacity of the natural gas-air mixture [44]. At low load, the combustion duration under DFO is longer

compared to CDO, because of the slow combustion rate due to lower temperature and fuel-air ratio. At high load, it is shorter due to the improved mixture strength. The heat release rate (HRR) is lower under DFO than CDF during the first phase of combustion, while the case is reversed during the second phase of combustion; revealing a late combustion of the gaseous fuel.

The total brake specific fuel consumption (BSFC) for CDO and DFO reported by [43] is shown in Fig. 2.1. It can be seen that BSFC is higher under DFO compared to the one under CDO at the same engine operating conditions; where this is attributed to the poor utilization of the gaseous fuel due mainly to the lower temperature and fuel-air ratio inside the combustion chamber. At high load, however, the values of total BSFC under DFO tend to converge to the ones under CDO, mainly because of the improvement of gaseous fuel utilization, but it remains higher.

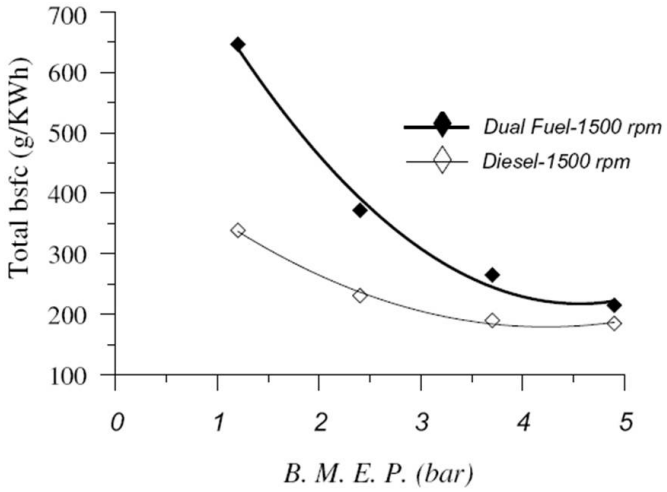


Figure 2.1 BSFC for both conventional diesel and dual fuel modes reported by [43].

BSFC results reported were estimated from the brake power output and the measured mass flow rates of both fuels, without accounting for the difference in the lower heating value (LHV) between NG and Diesel fuel. This data therefore does not actually provide a clear-cut comparison for the brake thermal efficiency. Certainly, the total BSFC under DFO would be even higher if it was corrected to the heating value of Diesel fuel, and hence the brake thermal efficiency will consequently suffer a further reduction. This is demonstrated by Fig. 2.2 that shows a plot of the data retrieved (using a set of digitizing

programs) from the original work for BSFC for CDO and DFO, as well as the corrected values for DFO based on the actual consumptions and LHVs of both fuels reported.

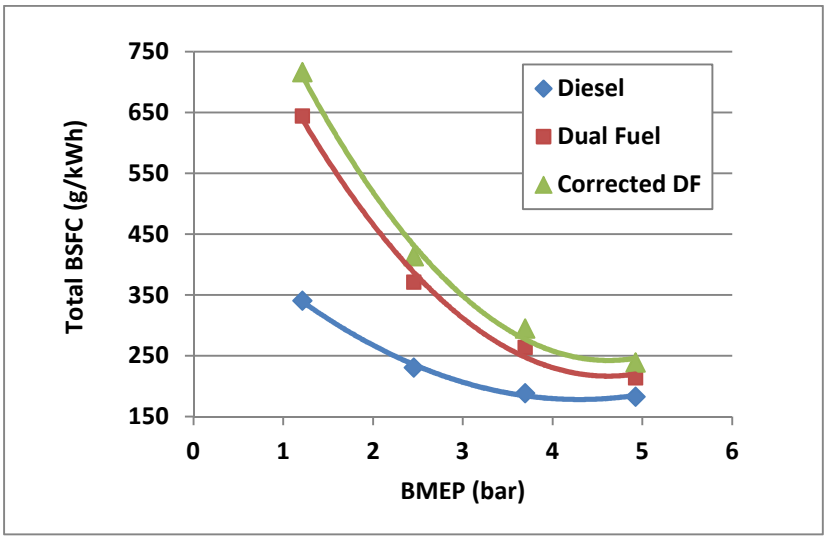


Figure 2.2 **BSFC for CDO and DFO – retrieved from the values reported by [43] and re-plotted – and for corrected values for DFO based on the actual consumptions and LHVs of both fuels reported in the original work. Data is for engine speed of 1500 rpm.**

The use of NG was proven successful in reducing NOx emissions. That the reduction was slight at low loads but considerable at high loads due to the less intense combustion, the lower temperature, and the lower concentration of oxygen due to the utilization of a large amount of gaseous fuel which replaces an equal amount of air. There was also a drastic reduction in soot emissions under DFO regardless of the operating conditions since NG has a very small tendency to produce soot. Conversely, CO and HC emissions were considerably higher relative to the CDO, especially at low loads due to the low cylinder temperature and the slower burning where a considerable part of the gaseous fuel escapes the combustion process. At high load, the improvement in fuel utilization and the increase of burned gas temperature improves the oxidation process, especially at low engine speeds where there is more time to complete combustion, but CO and HC emissions remain much higher than the case with CDO. Reported CO and HC emission traces reflected the quality of the combustion process [39] and demonstrated a good consistency. This could be observed in Fig. 2.3, where the data presented by the authors are retrieved, and then combined and plotted on a single graph.

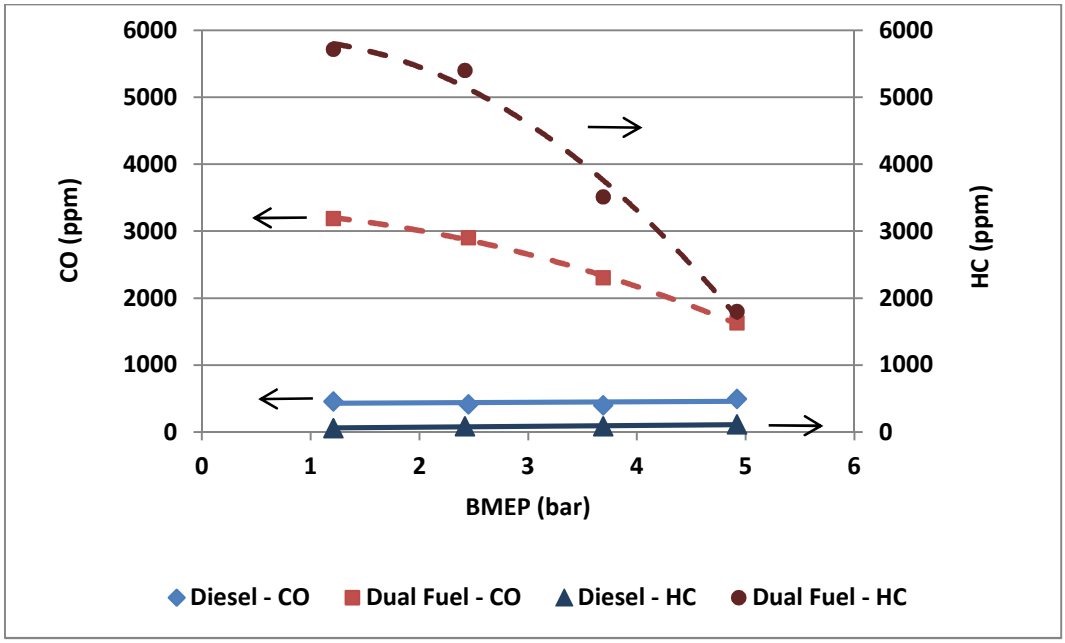


Figure 2.3 **CO and HC emissions for CDO and DFO – retrieved from the values reported by [43] and re-plotted. Plot shows good consistency of emission traces. Data is for engine speed of 1500 rpm.**

Lounici *et al* [45] investigated the influence of DFO on combustion characteristics, performance, and exhaust emissions of a DI diesel engine. The diesel pilot quantity was kept constant at 10% of its rated value (i.e. the value corresponds to the engine rated power), while the engine power was increased by augmenting the NG flow rate. They found that the in-cylinder pressure at low load conditions was slightly lower with DFO than with CDO, owing to the larger specific heat capacity of the NG-air mixtures, the later ignition, and the slower combustion rate. At high loads, in contrast with the results reported by Papagiannakis *et al* [43], the peak cylinder pressure was higher with DFO. The conflict between the two results could be due to the use of a smaller pilot fuel quantity (10%) in [45], and hence the very fast burning rate of the larger amount of the gaseous fuel brings about higher pressure levels. This observation is more evident at high engine speed, where the in-cylinder mixture is well prepared and the cylinder wall is warmer. This result is supported by Selim [46], who also reported that the maximum pressure is higher for DFO than CDO.

DFO demonstrated higher total BSFC than CDO at low load, but the case was reversed at high loads. The higher BSFC at low load reveals a poor utilization of the gaseous fuel due to the combination of low temperature and very poor NG-air mixture inside

the combustion chamber. This result is in keeping with that reported in [43]. At high loads, on the other hand, the improvement of the gaseous fuel utilization due to higher temperatures and richer mixtures, led to a relevant improvement of the total BSFC, and it became lower with DFO. This result contradicts what was reported by Papagiannakis *et al* [43] although they as well reported an improvement of combustion conditions and gaseous fuel utilization at high loads. Like the case with cylinder pressure, the reason of that dissimilarity could be attributed to the utilization of smaller pilot diesel amount in [45], so the burning rate of the mixture became faster and hence a larger amount of the useful heat was released at earlier stages of the expansion stroke closer to the TDC; generating more useful power and reducing the BSFC.

DFO was proven very effective at minimizing soot emissions, particularly at high load conditions, due to the very low tendency of NG to produce soot [47]. DFO also reduced NOx emissions at low and intermediate load, while the case was reversed at high load. At low load, although they reported almost equal temperature inside the cylinder for both CDO and DFO, they attributed the reduced NOx concentrations with the latter to the reduced oxygen concentration. In contrast with Papagiannakis *et al* [43], Lounici *et al* [45] reported higher NOx emissions with DFO compared with CDO. They attributed that to the elevated cylinder temperature with DFO at high loads as a result of the improvement in gaseous fuel combustion. In addition, they suggested that the increase in NOx emissions was due to the increased oxygen concentration in the engine cylinder with DFO at high load compared with CDO. This contradicts what was reported in other studies, including [43], but the authors [45] supported their argument by highlighting that the larger amount of NG (a low carbon fuel) used at high load in the place of diesel requires less quantity of oxygen to completely oxidize the carbon into CO_2, and hence the amount oxygen remaining will be larger. However, a better interpretation of results could be attained if NOx trends were analyzed in conjunction with those of soot. Figure 2.4 presents the data retrieved from [45] with regard NOx and soot for both CDO and DFO. At high loads with CFO, the presence of substantial amount of soot caused the cooling effect of soot radiation (the heat dissipation to soot by radiation) to be sizeable [48]. That is, the fraction of the chemical energy release lost to soot radiation became significant and hence the flame temperature was depressed; reducing the amount of thermal NOx produced [49].

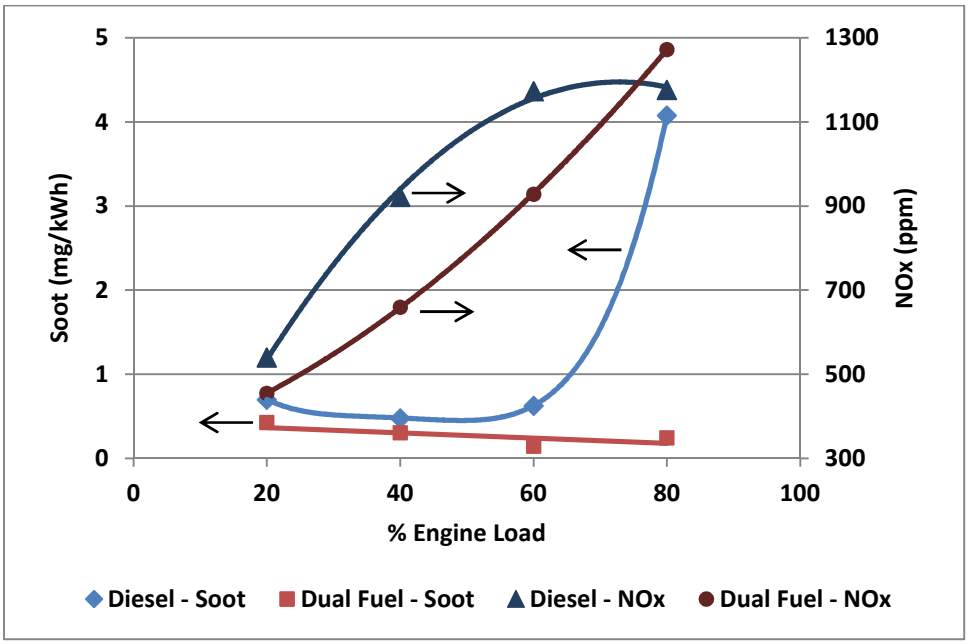


Figure 2.4 **NOx and Soot trends for CDO and DFO – retrieved from the values reported by [45] and re-plotted. Data is for engine speed of 1500 rpm.**

Figure 2.5 shows a plot of CO and THC data retrieved from [45] for CDO and DFO. It can be seen that CO emissions for DFO are higher at low and intermediate loads, but lower at high loads where CDO reaches very high levels. The authors attributed the elevated CO emission at low loads to the very poor mixture. The declining trend of CO under DFO as the load increases is attributed to the improvement in the gaseous fuel utilization. The authors attributed the enormous increase of CO emissions under CDO at high loads to the locally very rich mixture. Whereas this was not highlighted by the authors, the ultimate CO emission with CDO at high loads suggests that the engine at that point was in the smoke zone operation with an equivalence ratio higher than 0.8; the smoke limit for diesel engines as identified by [39]. This analysis is supported by the corresponding value of soot emissions reported in the same work, which clearly demonstrated excessive soot levels as shown in Fig 2.4.

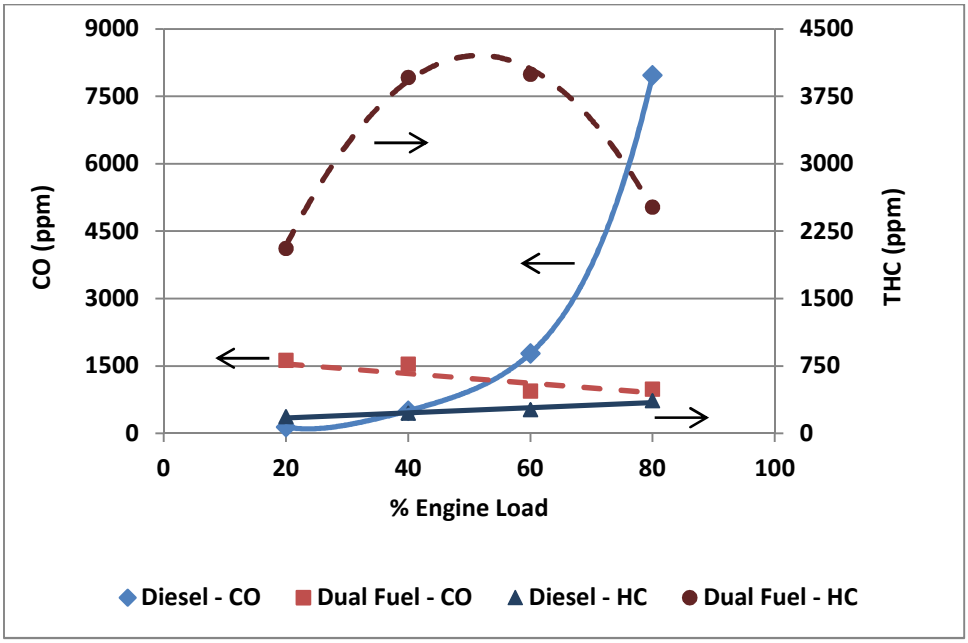


Figure 2.5 **CO and THC trends for CDO and DFO – retrieved from the values reported by [45] and re-plotted. Data is for engine speed of 1500 rpm.**

Figure 2.5 also shows higher THC emission with DFO at all load conditions, and this is consistent with the results reported by other researchers. For high loads, there is an agreement among researchers that higher charge temperature and richer gaseous fuel bring about further improvement in the combustion process, and as a consequence, a decrease in unburned hydrocarbon emissions occurs. However, it can be seen from Fig. 2.5 that the results reported by Lounici *et al* [45] exhibit different pattern from those of other researchers including Papaginakis *et al* [43] who conveyed a sequential decrease in THC as the gaseous fuel increases as shown in Fig. 2.3. In an attempt to interpret this dome-shaped trend, Lounici *et al* [45] said that at low load, the unfavorable combustion conditions for the gaseous fuel (low temperature, very lean mixture) are responsible for the THC emissions, but since the gaseous fuel participation is small THC emissions are relatively lower. As the load increases, at first stage THC emissions will increase since the gaseous fuel participation increases but the combustion quality is not sufficient to reduce THC emissions. This result is not consistent with the reported CO emission results that reflected an improved combustion as the load increases through the increase of NG. The authors reported lower CO_2 emissions at all load conditions, as expected because of the lower carbon-to-hydrogen ratio (C/H) of NG.

Shenghua *et al* [50] studied combustion and exhaust emissions characteristics of a NG-diesel dual-fuel turbocharged CI engine. The engine power was controlled by regulating the natural gas flow rate, while the pilot diesel fuel quantity was kept constant at 20% of the rated value under CDO. They found that DFO causes lower maximum cylinder pressure and rate of pressure rise (ROPR); both at a more retarded CA position. This is because the quantity of diesel premixed combustion is higher in CDO, which makes the cylinder pressure higher and at higher rates than DFO. The authors attributed retarded occurrence of peak pressure and ROPR to the prolonged ignition delay of the diesel pilot with DFO relative to the CDO. This effect has been deliberated by Liu *et al* [51] who explained that the introduction of the gaseous fuel to the cylinder changes both the physical and the chemical processes of the ignition delay. The extension to the physical process is related to changes in the charge temperature, pressure, pre-ignition energy release, heat transfer, on top of the effects of the residual gases, while the extension to the chemical process results from the chemical interaction between the diesel fuel and gaseous fuel [51].

A comparison between heat release characteristics of CDO and DFO in [50] is shown in Fig. 2.6. Diesel combustion process encompasses four phases; ignition delay (θ_1), premixed combustion (θ_2), mixing controlled combustion (θ_3) and late combustion (θ_4); where the typical HRR curve of CI diesel combustion is classically characterized by the presence of two peaks [39]. Combustion process in DF engines could also be divided into four phases; ignition delay of diesel pilot (α_1), premixed diesel combustion and ignition of gaseous fuel (α_2), fast burning of gaseous fuel (α_3) and late combustion (α_4). It is clearly identified that DFO exhibits a longer ignition delay. At the beginning of DF combustion, HRR trend is steeper (compared with the subsequent stages). This can be regarded as the premixed combustion of the diesel pilot; representing the second stage of combustion (α_2). Combustion of the gaseous fuel then takes place at very fast rates since a large amount of gaseous fuel is used at the high load, and hence the HHR curve is characterized by the presence of a single peak (unlike CI diesel combustion). Due to the very fast burning rate of the gaseous fuel at these conditions, more than 90% of the fuel is consumed before 40° CA ATDC, and this is one of the reasons why the dual fuel engine has a higher thermal efficiency at high loads.

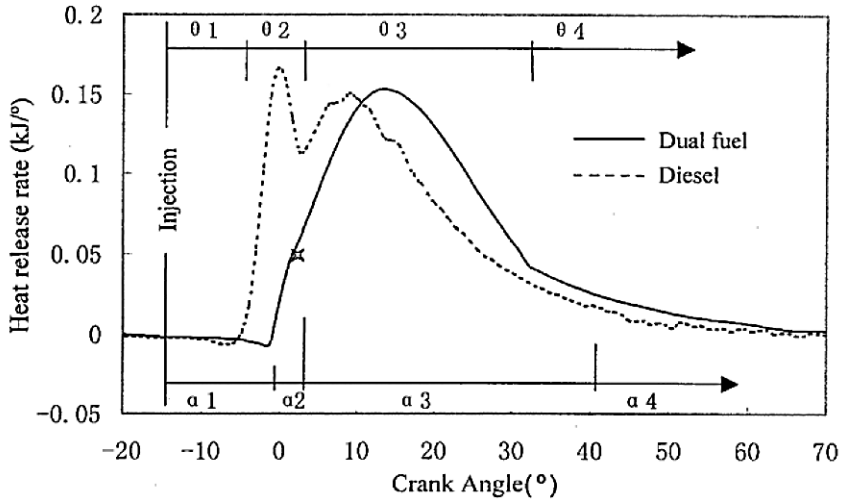


Figure 2.6 **Heat release rate (HRR) curve showing combustion phases for both CDO and DFO; reported by [50]. Data is for engine speed of 1600 rpm and load of 0.9 MPa BMEP. Zero CA stands for the TDC.**

Mittal *et al* [52] studied combustion and exhaust emissions characteristics of a multi-cylinder 18.1 liter (18,100 cc) diesel engine converted to NG fuelling with diesel pilot. The engine used Mechanically-actuated Electronically-controlled Unit Injection system (MEUI) for direct injection of diesel fuel at a pressure of 200MPa. NG substitution levels were restricted at low load by factors like cyclic variability, cylinder-to-cylinder variations, limited combustion efficiency, and elevated HC and CO emissions [53]. At high loads, the exhaust gas temperature limits the percentage of gaseous fuel with DFO; a similar effect is studied by Karnik *et al* [54]. In view of that, higher substitution ratios were achievable only at mid-load conditions.

Fuel injection timing was relatively advanced under DFO relative to CDO at the same load. This action was done automatically by the engine control module as a response to the reduction of diesel fuel flow when the gaseous fuel is introduced into the cylinder. The authors implied that largest amount of advance was 16 crank-angle-degree (CAD) with largest NG substitution; i.e. largest reduction in diesel fuel, which was achieved at 50% load. This might mask the actual effect of NG induction on both the ignition delay and cylinder pressure, as the inevitable result of largely advanced injection is an earlier start of combustion (SOC); irrespective of the possibility of having a prolonged ignition delay due to the introduction of the gaseous fuel. This is demonstrated by Fig. 2.7 that clearly shows an earlier start of combustion (SOC) with DFO compared with CDO as

evident by the sudden rise of pressure and HRR traces. However, a careful look at the figure discloses that CDO combustion commenced after that of DFO by few crank angle degrees (about 5 CAD), as revealed by the sudden rise of the HRR traces; despite 16 CAD injection advance was experienced. That is, the net effect of NG admission is a prolonged ignition delay (by ≈11 CAD), which is consistent with other results [43, 50]. Nevertheless, the influence of gaseous fuel induction on the cylinder pressure is still ambiguous, as the reported results cannot be fully interrupted with the effect of injection advance strongly influential. The retarded injection with CDO results in a late SOC considerably after the TDC as shown by the HRR traces, and hence the pressure rise in this case is moderated since the piston is moving down the expansion stroke away from the TDC, and CDO exhibited a lower peak in-cylinder pressure. It can be seen also from Fig. 2.7 that the HRR pattern for DFO is still dual-peak characterized; unlike the results reported by Shenghua *et al* [50]. The reason for that pattern could be the considerable contribution of diesel fuel to the total energy supplied owing to the use of large pilot, so the resulting HRR pattern still resembles that of the CDO.

DFO observed high CO and HC emissions, mainly due to the larger piston land volume that harbors a relatively large amount of unburned mixture, which is an inherent nature of diesel engines converted to DFO [55]. Also, as the cylinder pressure decreases with NG induction, the resultant lower environmental pressure supplies less resistance to the fuel spray and thus increased spray tip penetration [56, 57]. The excessive penetration led to more impingement hence generates more soot from the diesel pilot.

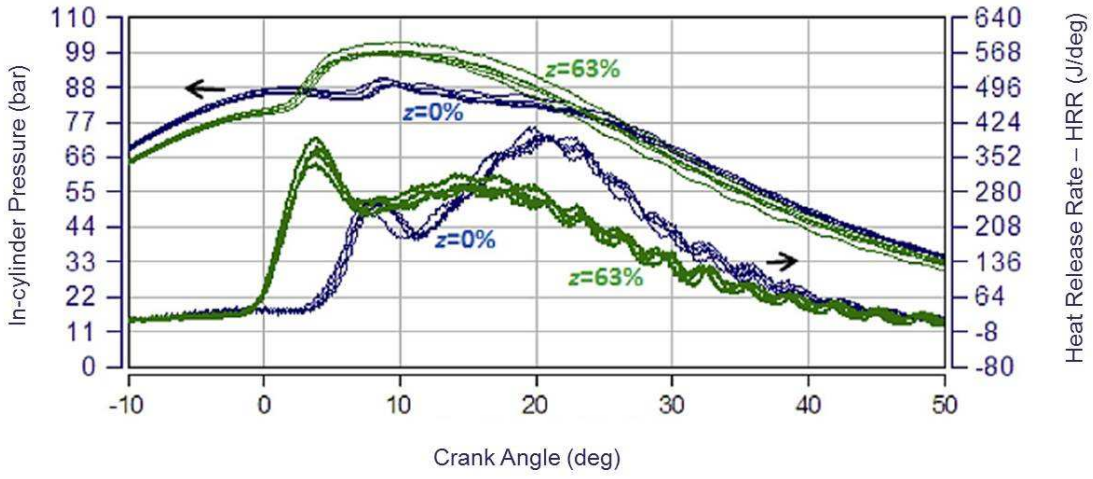


Figure 2.7 **In-cylinder pressure and heat release rate (HRR) curve for both CDO (z=0%) and DFO (z=63%) - adapted from [52]. Data is for 50% of engine full load. Zero CA stands for the TDC.**

Mbarawa and Milton [58] investigated the maximum possible NG fuel substitution for diesel fuel in a DI diesel engine when converted to DFO with gaseous fuel induction. The relative contribution of NG to the total fuel consumption was calculated on energy basis considering the difference in calorific values between diesel fuel and NG; as:

$$\%\, NG = \frac{\dot{m_{NG}} \times LHV_{NG}}{\dot{m_{NG}} \times LHV_{NG} + \dot{m}_D \times LHV_D} \times 100(\%) \qquad (2.2)$$

where (LHV_{NG}) and (LHV_D) are the lower heating values for NG and diesel fuel. The authors identified the criteria of the maximum NG substitution as the occurrence of a severe diesel knock or end gas auto-ignition being evident, or as suffering combustion loss; noticeable as misfire and inability to sustain a steady torque output. They found that a stable engine operation could be maintained with as much as 86% NG substitution for diesel fuel. Figure 2.8 presents the engine map they produced for maximum NG substitution at different engine operating conditions (speeds and loads).

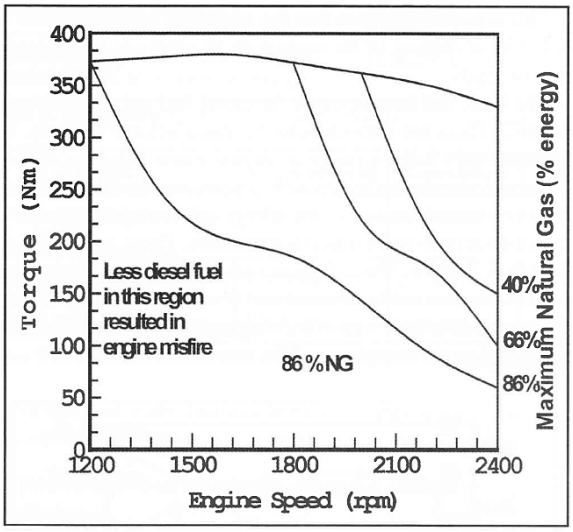


Figure 2.8 Maximum NG substitution levels map (energy basis) at different engine operation conditions (speeds and loads). Ref. [58].

At low engine speed (1200 rpm), a maximum substitution level of 86% was achievable throughout the entire engine load range, and the engine at such speed was capable of providing torque levels equivalent to those obtained under the CDO. Below the 86% contour (i.e. larger NG substitution levels), nevertheless, the engine experienced misfire and unstable combustion. Beyond this contour, the ultimate NG substitution could be

maintained at higher engine speeds only at lower torques. At 2400 rpm, for instance, the 86% NG substitution level could only be employed below about 20% of the rated engine load, as severe engine knock occurred above that level. That is, NG substitution must be reduced if it is required to achieve high torque at high speeds. This is attributed to the effect of engine speed on the degree of turbulence inside the engine cylinder. While increasing engine speed increases the degree of turbulence and accelerates the combustion, this is advantageous only at low loads where mixture strength is weak. At high loads, the fast burning rates of NG as the mixture strength increases put the engine on the verge of knocking conditions, and therefore high turbulence must be avoided. Accordingly, higher speeds and loads are achievable with less NG substitution only.
From the data representing maximum NG substitution levels, the authors constructed the engine maps for DFO at these conditions and compared that to the corresponding CDO results obtained from the baseline testing; with regard to brake thermal efficiency and equivalence ratio. Figure 2.9 shows the brake thermal efficiency map for CDO and DFO at maximum NG substitution; at different operating conditions.

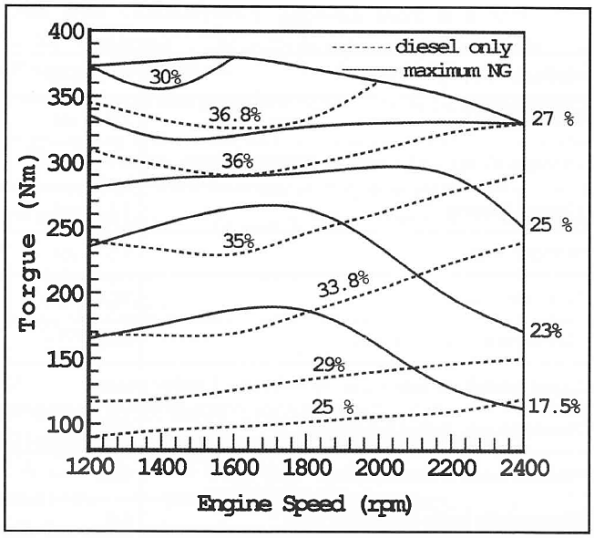


Figure 2.9 Brake thermal efficiency (%) map for CDO and DFO at maximum NG substitution; at different operating conditions. Ref. [58].

It can be seen that CDO always exhibits higher brake thermal efficiency than DFO. This is because introducing NG reduces the partial pressure of oxygen in the intake charge, and reduces the temperature and pressure levels at the end of the compression

stroke (due to the higher specific heat capacity of the mixture). As a result, the ignition delay increases and hence a major part of the combustion process takes place during the expansion stroke; reducing the useful power output and the brake thermal efficient consequently. Also, the poor gaseous fuel utilization and the associated slow burning rate of the lean mixture at low load make the efficiency more deteriorated at these conditions. As the engine torque increases, more NG is introduced into the cylinder and hence more effective rich mixture is produced, which improves the performance even at low speeds where the degree of turbulence is modest. At high-speed regions, the high degree of turbulence limits the substitution of NG, and thus these regions involve the utilization of larger diesel quantity.

Figure 2.10 shows the total equivalence ratio map for CDO and DFO at maximum NG substitution; at different operating conditions. The equivalence ratio *(ϕ)*, defined as the actual fuel/air ratio to stoichiometric fuel/air ratio (or alternatively; the stoichiometric air/fuel ratio to the actual air/fuel ratio), is calculated for DFO that involves the use of two fuels as:

$$\phi_{tot} = \frac{AFR_{NG}^{stoic} \cdot \dot{m}_{NG} + AFR_{D}^{stoic} \cdot \dot{m}_{D}}{\dot{m}_{air}} \tag{2.3}$$

where (AFR_{NG}^{stoic}) and (AFR_{D}^{stoic}) are the stoichiometric air-fuel ratios (mass basis) for NG and diesel fuel; respectively.

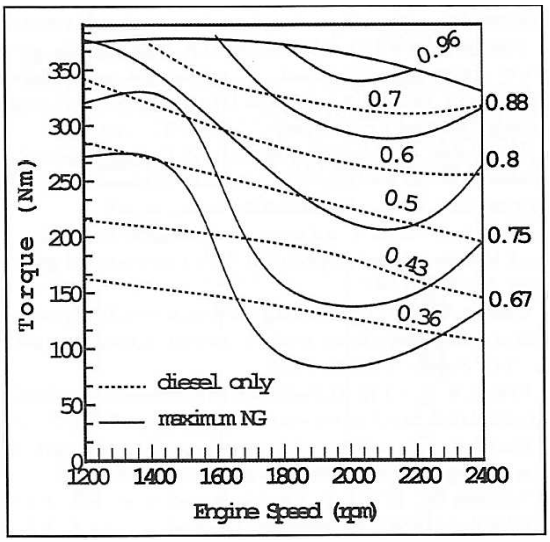


Figure 2.10 Total equivalence ratio (ϕ) map for CDO and DFO at maximum NG substitution; at different operating conditions. Ref. [58].

From the figure, it is evident that for a given torque and speed (i.e. power) level, the total equivalence ratio of DFO is always at a considerably higher level than CDO. For a given engine running on a particular fuel, equivalence ratio is inversely proportional to the product of thermal efficiency and airflow to the engine. That is;

$$\dot{W} = \eta_{th}.\phi.FAR^{stoic}.\dot{m}_{air}.LHV_f \quad (2.4)$$

where ($\dot{W}$) is the engine brake power, (η_{th}) is the brake thermal efficiency, (FAR^{stoic}) is the stoichiometric fuel/air ratio, and (LHV_f) is the lower heating value of the fuel. The equation is derived from the basics in Appendix B.

Substitution of NG displaces some of the intake air; reducing the volumetric efficiency and the air mass flow rate. Hence, engine power is reduced as a direct consequence of the reduced air mass flow if the equivalence ratio remains the same. In other words, the equivalence ratio must be increased to maintain the same level of power if the air mass flow is reduced; as shown in the figure.

Figure 2.10 also demonstrates that for a fixed equivalence ratio value, relatively higher engine power is attained at high load-low speed conditions. The reason behind this is the increased mixture strength and the improved combustion of NG at such conditions, and hence the resulting high thermal efficiency maintains good power levels even with high NG substitution. For high-load-high-speed conditions, in turn, the maximum NG substitution is limited because of the increased degree of turbulence inside the engine cylinder as already discussed. This implies the use of larger amount of diesel (and larger air mass flow), and hence the total equivalence ratios of DFO converge towards their counterparts of CDO. Fixed equivalence ratio contour at low load-mid speed conditions exhibits modest power levels. This is due to the deteriorated thermal efficiency at these conditions on top of the reduced air mass flow, and hence power levels drop for a fixed equivalence ratio, as per equation (2.4).

2.4 Influence of Injection Parameters and Fuel Composition on Combustion and Exhaust Emissions of PINGDEs

2.4.1 Quantity of diesel fuel pilot

The quantity of pilot injection has a strong effect on performance and exhaust emissions of dual-fuel engines, especially at light loads. Whereas it is desirable to replace a larger amount of the liquid diesel fuel by the clean and economic gaseous fuel, the quantity of the pilot fuel should be kept above a certain value to maintain a stable combustion of the gaseous fuel. Inconveniently, most of the diesel fuel mechanical injection systems experience poor atomization, and hence deteriorated combustion, when the amount of fuel injected per cycle is reduced below 5-10% of the ultimate design level. Besides, it should be ensured that the injector does not get overheated when small pilot fuel quantities are injected while a significant energy is released through the combustion of gaseous fuel [59]. Pilot fuel size, however, should be determined such that it keeps the dual-fuel operating mode feasible. Also, large pilot masses might cause knock at high loads. A compromise, therefore, must be made between the benefits and the drawbacks of increasing pilot fuel size.

Abd-Allah *et al* [59] investigated the effect of pilot fuel quantity on performance and emissions of an IDI diesel engine dual-fuelled with methane (or propane). They found that at very light loads with small pilot quantities, CO and HC emissions were relatively high. This was attributed to the very lean mixture where the resulting flame originating from the pilot ignition could not propagate throughout the whole combustion chamber, and consequently, only partial oxidation occurred. With increasing the pilot quantity, the volume of the charge that is affected by the combustion of the pilot fuel envelope became larger, and hence the burned fraction of the gaseous fuel increased; reducing the CO and HC emissions as shown in Fig. 2.11. While the authors presented consistent results as shown in the figure, they did not provide an explanation for the reason behind those dome-shaped curves for CO and HC emissions (where this shape indicates that CO and HC emissions initially increased although mixture strength was increased). One reason behind this trend is that although the mixture strength was increased as a result of increasing the gaseous fuel, it was still weak and suffered deteriorated combustion

because of the flame propagation problem associated with the small pilot fuel quantity. Thus, as the gaseous fuel amount became larger, CO and HC emissions tended to rise until the mixture strength became nearly half stoichiometric, then both decreases due to the improved combustion at higher mixture strength.

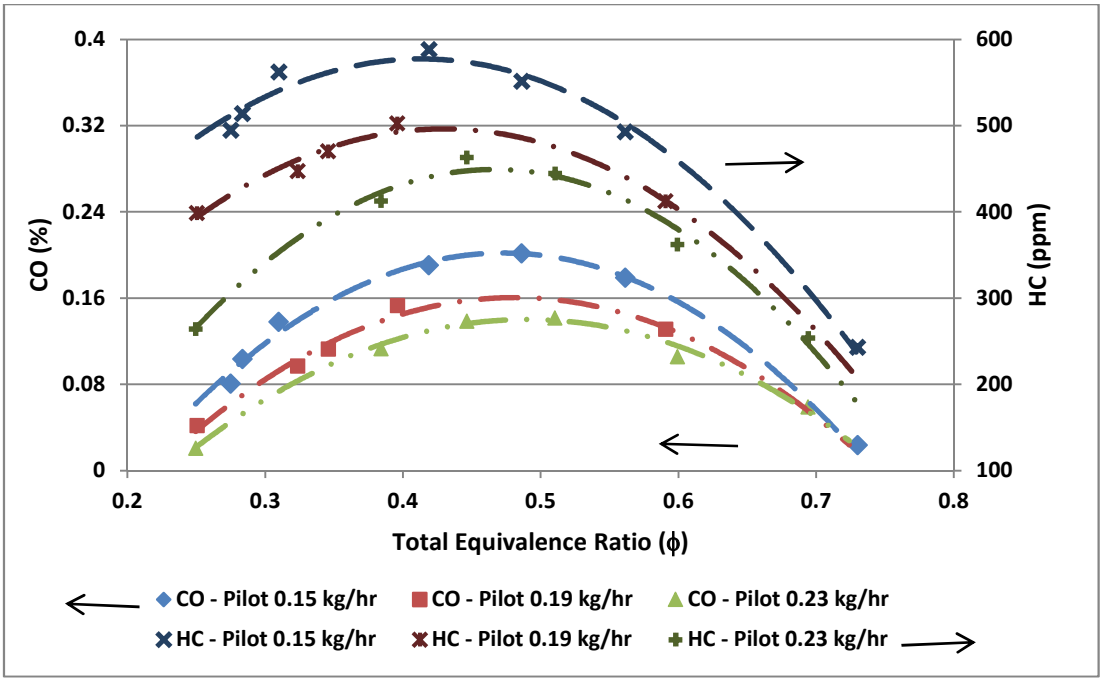


Figure 2.11 **CO and HC emissions for different quantities of pilot fuel – retrieved from the values reported by [59] and re-plotted. Data is for engine speed of 1000 rpm and fixed pilot injection timing of 25° BTDC.**

As shown in Fig. 2.12, the authors also found that for the same total equivalence ratio (ϕ), increasing the pilot fuel quantity increased the charge temperature which tends to increase the production of NOx. For relatively high loads, however, the combustion of gaseous fuel became more efficient and less affected by the pilot fuel quantity, and thus the effect pilot fuel quantity became milder. This explains why the line converges at higher equivalence ratios. The utilization of large pilot fuel quantity was also found to produce higher power output. The increase of pilot fuel quantity leads to an improved flame propagation and, consequently, results in increasing the output power. While the authors did not highlight that, but for the same equivalence ratio the use of larger pilot quantity shortens the ignition delay relative to the one with smaller pilot, and hence the peak cylinder pressure is attained closer to the TDC at earlier stages of the expansion

stroke; generating more useful power and increasing the efficiency. Figure 2.13 shows the brake power and thermal efficiency; where the original data presented by the authors are retrieved, and then combined and re-plotted on a single graph. Nevertheless, the use of large pilot fuel quantities at high loads increases the tendency to knock [59].

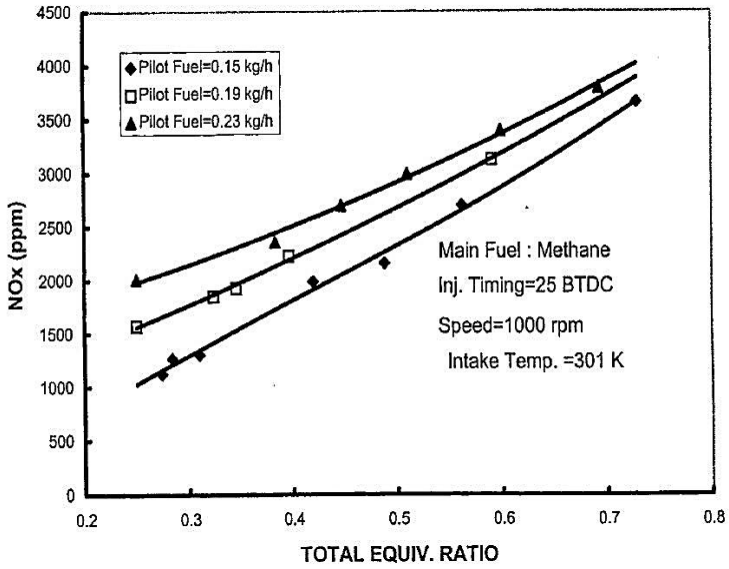


Figure 2.12 NOx emissions for different quantities of pilot fuel; reported by [59].

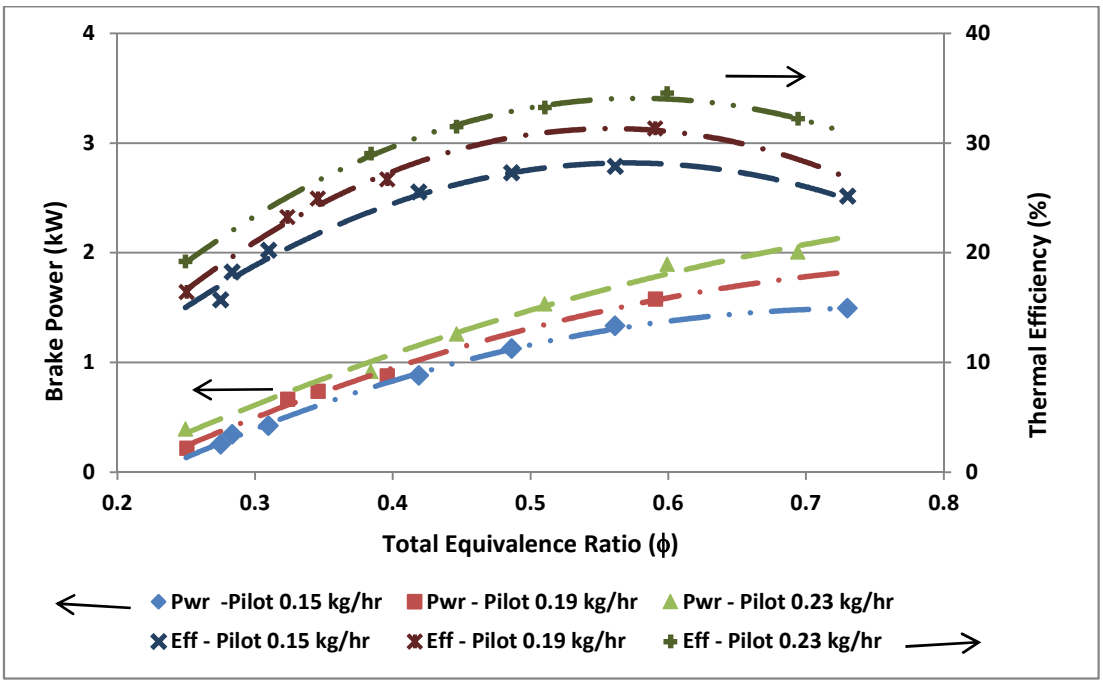


Figure 2.13 Brake power and brake thermal efficiency for different pilot fuel quantities – retrieved from the values reported by [59] and re-plotted. Data is for engine speed of 1000 rpm.

Imran *et al* [60] investigated the effects of pilot fuel quantity on some combustion and emissions characteristics of a DI diesel engine; dual-fuelled with NG (or hydrogen) as the main fuel and diesel fuel (or rapeseed methyl ester –RME) as a pilot. They found that the ignition delay was reduced as the quantity of pilot fuel was increased; where this could be attributed to more ignition centers resulting from the injection of a greater amount of pilot fuel and hence shortening the time between the fuel injection and the start of the ignition process. Also, the specific heat capacity ratio (γ) for the NG-air mixture is considerably higher than the pure air. This higher specific heat capacity ratio results in lower in-cylinder temperatures and hence an increased ignition delay. Figure 2.14 illustrates the in-cylinder pressure as well as the heat release rate (HRR) for CDO as well as DFO for three different pilot settings; at the specified operating condition. It can be seen that the inflection in both the in-cylinder pressure and the HRR, presenting a sudden rise which indicates the start of combustion (SOC), was advanced with the increase of the pilot fuel quantity; indicating a shorter ignition delay. The figure also demonstrates that the peak in-cylinder pressure was increased with the increase of pilot fuel quantity; where this was a reflection of the ignition delay trends. While the authors did not mention this, but the prolonged ignition delay with the larger amount of NG, i.e. small amount of pilot fuel, causes the combustion to commence well-after the TDC, and hence the combustion pressure is moderated as the piston is moving away down the expansion stroke.

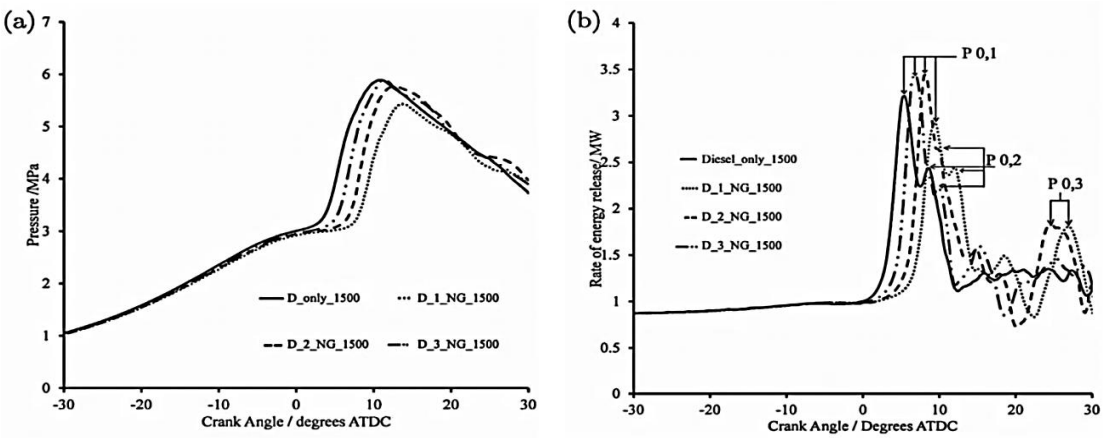


Figure 2.14 (a) In-cylinder pressure and (b) rate of heat release for CDO as well as DFO with three pilot fuel quantity settings; at engine speed of 1500 rpm and BMEP of 0.503 MPa. Adapted from [60].

The peaks (P 0,1), (P 0,2), and (P 0,3) on the figure point towards the first, second, and third (if any) peaks of the HRR patterns for different fuelling settings. For most diesel engines with mechanical injection systems, combustion is characterized by the presence of two peaks for premixed combustion and mixing-controlled combustion phases [39]. For dual-fuelling with larger pilot quantity, the curve still resembles the characteristics of diesel combustion; only two peaks on HRR pattern are present, but both of them are shifted down the expansion stroke as a direct consequence of the increased ignition delay as already discussed. With a smaller amount of pilot fuel, i.e. a larger amount of NG, a third peak occurs revealing late combustion of some of the gaseous fuel that could not get oxidized in the earlier phase of combustion.
Specific NOx emissions (g/MJ) increases as the pilot fuel quantity was increased, where this is attributed to the increase of multi-centered ignition points within the gaseous fuel-air mixture. The relatively higher in-cylinder temperature with larger pilot quantity can ensure timely evaporation of the pilot fuel and hence better distribution of the ignition centers across the charge. Specific HC emission was decreased, in general, as the quantity of the pilot fuel was increased. This is a direct consequence of improved combustion conditions.

Carlucci *et al* [61] examined the influence of pilot fuel quantity on combustion and exhaust emissions of a DI dual-fuel NG-diesel engine. Similar to other results reported here [59, 60], the authors found that introducing larger pilot quantity into the cylinder will enhance the combustion process, as indicated by the observed higher cylinder pressure and HRR. Also, CO and HC levels are decreased and NOx level is increased. The influence is more visible at low speeds and loads where the quantity of NG is barely enough to sustain a stable combustion only in the proximity of combustion locations of diesel pilot. On the contrary, the quantity of NG at high speeds and loads is rich enough to produce stable flame and thus the effect of pilot quantity is relatively insignificant.

Mousavi *et al* [62] numerically investigated the combustion process in a medium duty turbocharged DI diesel engine, converted to work under DF mode using NG and diesel pilot. The focus of the study was the part load operating conditions, due to poor engine performance, retarded thermal efficiency and elevated CO and HC emissions. The work

was done using KIVA-3V code at the closed part of the cycle, with a set of sub-models of the code modified to simulate the fuel spray atomization, combustion and pollutant emissions formation processes. The model has been validated using experimental data previously obtained on the same engine and demonstrated good agreement for the entire load range. In conformity with previous results as [43, 58], the authors found that the methane-air mixture at part load is very lean and suffers slow burning rate. Combustion process is drawn towards the low-temperature profile in the expansion stroke, and less fuel will burn [62]. In these conditions, a remarkable amount of the unburned methane remains in the most remote areas from diesel fuel spray, such as the bottom of the piston bowl. Moreover, it has been demonstrated that the flame structure is noticeably affected by engine operating conditions. As shown in Fig. 2.15, at part load conditions only the areas that are influenced by diesel diffusion flames could be ignited. The premixed methane-air flame could only propagate in the direction of diesel spray and its diffusion flame. At full load, on the contrary, the premixed methane-air flame could propagate throughout the entire combustion chamber. Accordingly, it was concluded that the development of diesel diffusion flame is required to burn lean NG-air mixture at part load conditions. The authors examined the effect of increasing the pilot fuel quantity on improving methane combustion. As illustrated by Fig. 2.16, the increase of the pilot fuel quantity from 12% to 20% (energy basis), while total input energy, fluid flow, and thermodynamic initial conditions were kept constant, resulted in an increased diffusion flame penetration of diesel pilot. Hence, the lean methane-air mixture could be ignited properly and propagated rapidly; owing to the enlarged size of diesel combustion region [62].

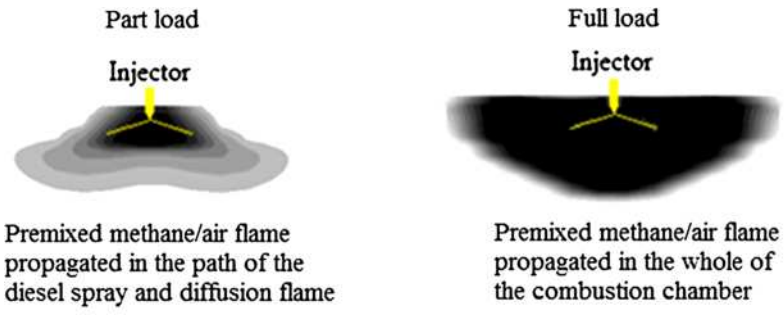


Figure 2.15 Flame structures at part and full load conditions. Ref. [62].

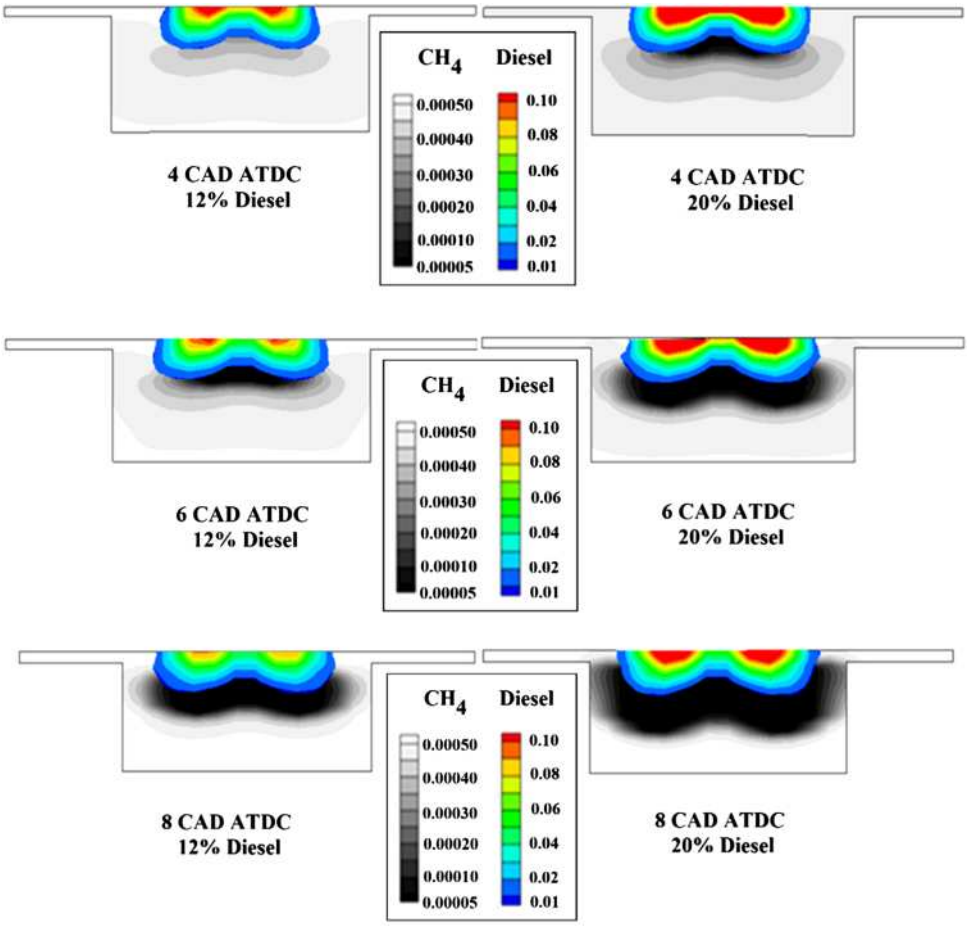


Figure 2.16 **Methane and diesel concentration (g) contours for 12% and 20% diesel pilot quantities (energy basis); at part load conditions. Ref. [62].**

2.4.2 Injection timing of the two fuels

Injection timing of the pilot fuel is a key factor that affects combustion characteristics of DF engines. For a fixed total equivalence ratio, advancing the injection timing means that the combustion occurs earlier in the cycle, and this can increase the peak cylinder pressure because more fuel is burned before the TDC. Charge temperature is expected to increase with the advanced injection timing of the pilot fuel and the associated higher energy release rates of the mixture. Also, the rate of pressure rise during the combustion of the gaseous fuel increases with advancing the injection timing of the pilot fuel [59]. On the other hand, retarding the injection timing delays the combustion of the pilot, and hence the cylinder temperature becomes insufficient to propagate the flame throughout the entire charge. As a result, incomplete combustion of the gaseous fuel-air mixture

takes place. Also, retarding the injection timing decreases the peak cylinder pressure as more of the fuel burns after TDC. It should be noted that, however, too much advanced injection results in a highly erratic engine operation, unacceptable rates of pressure rise, and an increased tendency to knock. To conclude, injection timing must be determined adequately to avoid adverse effects upon combustion process and engine structure.

Abd-Allah *et al* [63] investigated the effect of pilot fuel injection timing on performance and emissions of IDI diesel engine dual-fuelled with methane or propane. They found that for a fixed total equivalence ratio, advancing the injection timing provides better overall combustion. This could be attributed to the longer ignition delay associated with injection advance, where this prolonged delay allows for better spray penetration and development; creating a larger pilot fuel-air-gaseous fuel mixture (an effective flame propagation region) prior to ignition. Higher combustion rates of the larger premixed regions yielded higher combustion temperature. Also, the earlier start of combustion (SOC) with advancing injection timing means that the cylinder charge will spend longer period at higher temperature where better oxidation reactions take place. The resulting improvement in combustion event with advancing injection timing caused a subsequent reduction in both HC and CO emissions for a fixed total equivalence ratio; as shown in Fig. 2.17. Similar to their earlier work [59], the authors in this work [63] did not provide an explanation for the reason behind those dome-shaped curves for HC and somehow for CO emissions. As deliberated above, this could be attributed to the initial increases in gaseous fuel admission while the mixture strength was still weak and suffering flame propagation problem tended to increase both HC and CO emissions until the mixture strength became nearly half stoichiometric.

As expected, the elevated maximum temperature in the cycle due to injection advance increases NOx emissions for any fixed total equivalence ratio. While the authors did not highlight this, the effect was more notable at higher equivalence ratios, where the advanced combustion of the larger gaseous fuel amount use at these conditions highly increased the maximum cycle temperature and pressure. This explains the diversion of NOx trends at higher equivalence ratios; as shown in Fig. 2.18.

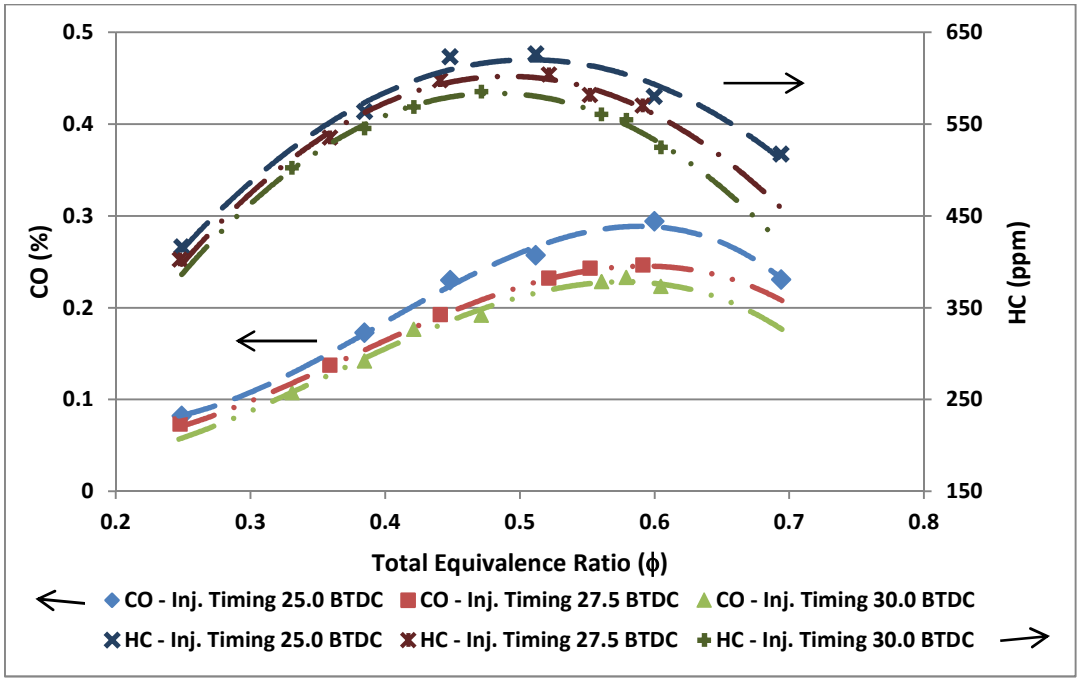


Figure 2.17 **CO and HC emissions for different injection timings of pilot fuel – retrieved from the values reported by [63] and re-plotted. Data is for engine speed of 1000 rpm and fixed pilot fuel quantity of 0.12 kg/hr.**

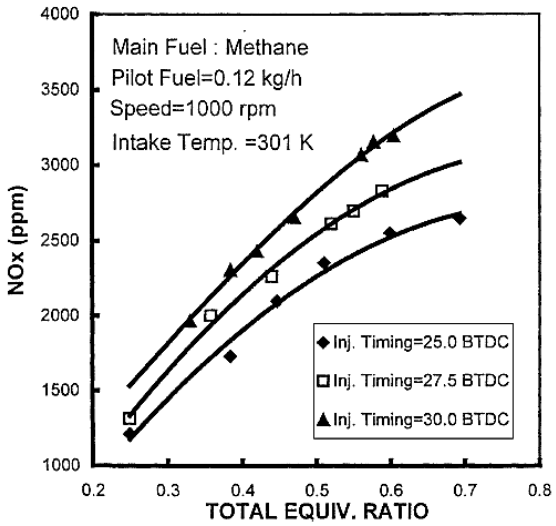


Figure 2.18 **NOx emissions for different injection timings of pilot fuel; reported by [63].**

Higher combustion temperature due to advancing the pilot injection timing leads to increased power output levels and thermal efficiency. Once again, this is credited to the attainment of peak cylinder pressure closer to the TDC at earlier stages of the expansion stroke, generating more useful power and increasing the brake thermal efficiency. The

authors also conveyed that advancing the injection timing at medium and high loads, nevertheless, led to early knocking. It is therefore concluded that advancing the pilot fuel injection timing is not favorable in DFO at medium and high loads.

Wang *et al* [64] investigated the effect of injection timing on pilot diesel ignition mode, and the subsequent impact on combustion and emissions of NG-diesel DF engine with multi-point NG injection into the intake port. The work focused on light load operating conditions; in an attempt to resolve the issues of lower brake thermal efficiency and higher unburned hydrocarbon emissions of dual-fuel engines at these conditions. They found that the significant advancing of injection timing brings about pilot diesel ignition mode different from traditional diesel engine compression ignition mode in the sense that it does not occur at a specific place in the spray, but simultaneously across the combustion chamber [64]. It is to the point to highlight that one of the early attempts to achieve homogenous charge compression ignition (HCCI) combustion in diesel engines was done through largely advancing the injection timing to form homogenous mixture, where the rise of the pressure and temperature during the compression stroke brings about spontaneous ignition [65]. Reactions in HCCI engines generally involve a two-stage process, comprising the so-called low temperature and high temperature reactions [66]. Although the two-stage process for NG-diesel DF engine is different, the authors [64] referred to the ignition mode with advanced injection as “two-stage auto-ignition”; to distinguish it from the classical auto-ignition of diesel. The study covered a wide range of diesel injection timing, varying from -5 to -55 °CA BTDC, at constant flow rates of pilot diesel and NG throughout. Figure 2.19 shows the variations of heat release rate (HRR) profile with pilot diesel injection timing (T_{inj}) at 1335 rpm. It could be seen that up to T_{inj} of 27.5 °CA BTDC, the HRR profile exhibits the general shape of the conventional diesel ignition mode, with a peak value of about 150 J/°CA and the crank angles of the first and also the peak heat release advances with the advance of injection timing. Following a transitional span from 27.5 to 32.5° BTDC, it could be seen that HRR profile exhibits significantly different pattern when T_{inj} changes from 32.5 to 55 °CA BTDC; where a two-stage auto-ignition mode can be seen clearly. That is, the ignition mode in these conditions resembles that of HCCI engines to some extent; Fig. 2.20 shows typical HRR curve for HCCI combustion in diesel-like fuels [67]. HRR

profile exhibits a low-temperature heat release (LTHR) or cool-flame (associated with low-temperature reaction (LTR) kinetics), followed by a high-temperature heat release (HTHR) or hot flame (associated with high-temperature reaction (HTR) kinetics, and considered as the main ignition). In between these two stages, there is a phase of low reactivity (also known as negative temperature coefficient (NTC) regime), where the overall reactivity of the system decreases with rising temperature [68].

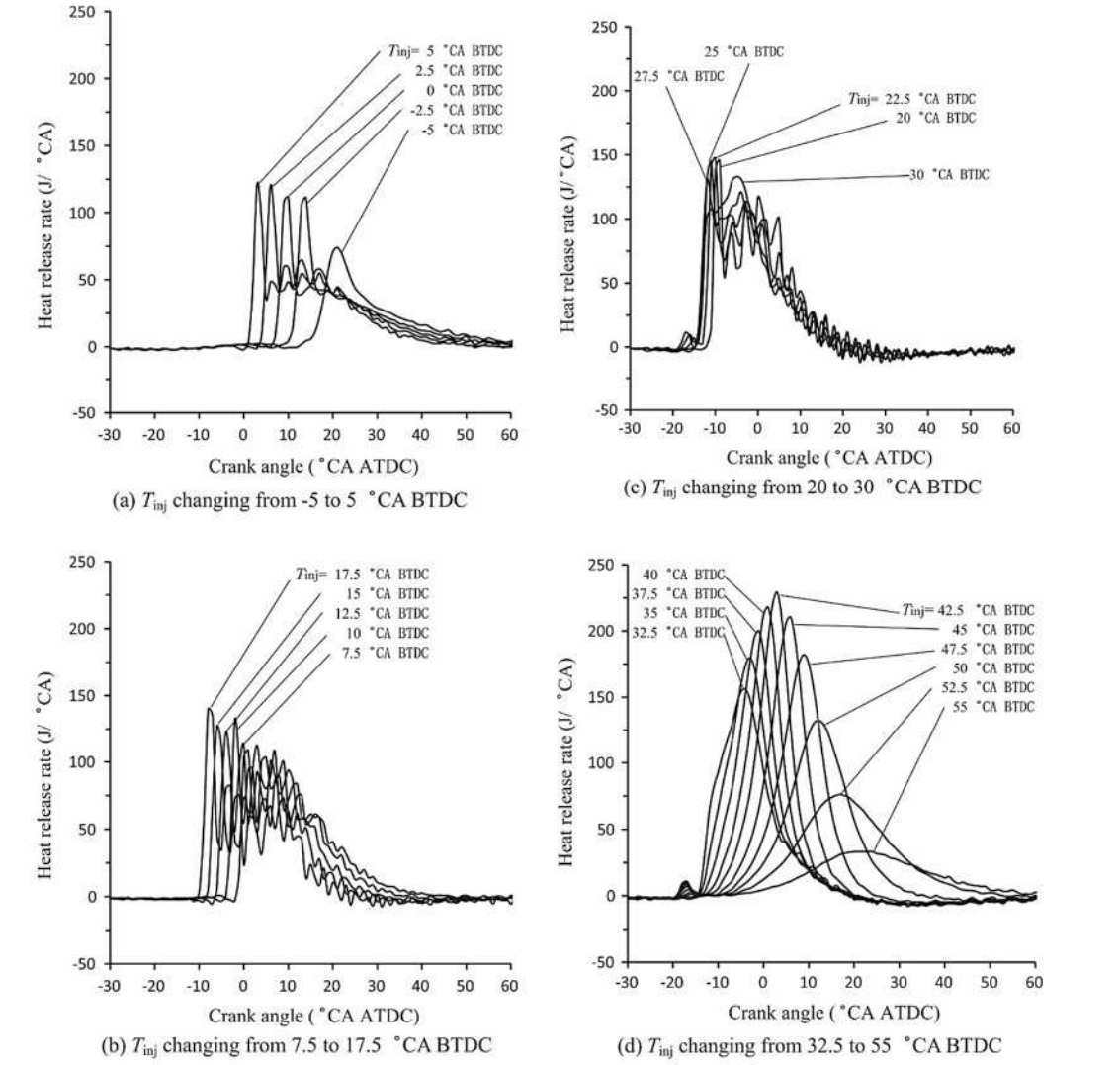


Figure 2.19 Heat release rate (HRR) profiles at different pilot injection timings (T_{inj}). Data is for engine speed of 1335 rpm and light load conditions. Ref. [64].

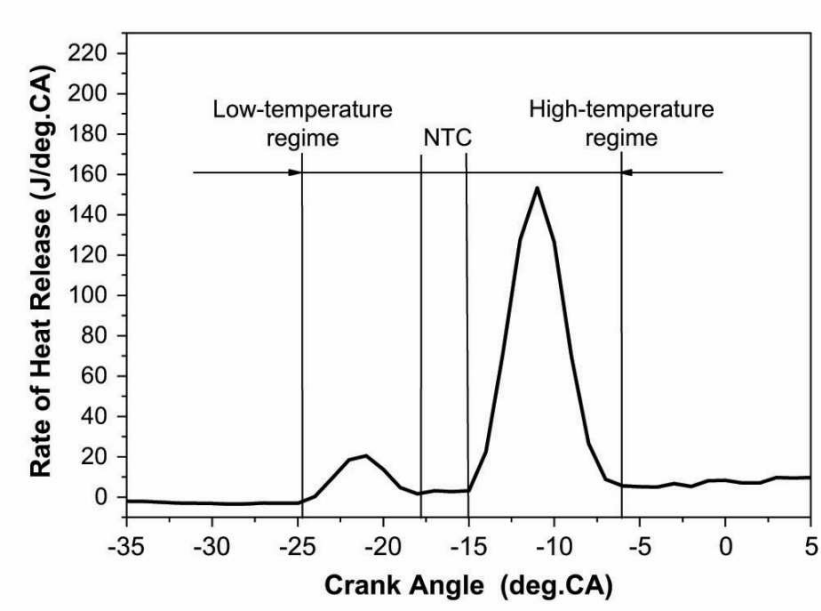


Figure 2.20 Typical HRR curve from HCCI combustion of n-heptane fuel. Ref. [67].

Although the advanced injection in DF engines does not form a homogeneous mixture as it is induced by a spray-type flow, the two-stage auto-ignition pattern is maintained as observed in Fig. 2.19 (d). It could also be noticed that the main heat release rate part becomes symmetrical about the crank angle of the maximum HRR. The maximum HRR value elevates to as much as 225 J/°CA; the reason is not explicitly stated in the work [64], but it could be attributed to the entrainment of the NG-air mixture burning in the second stage of pilot combustion. As shown in Fig. 2.21, the results in [64] exhibited a threshold almost at T_{inj} equals 30 °CA BTDC affecting the start of combustion – SOC (defined as the crank angle of 2% accumulated heat release) and the crank angle of 50% heat release (CA50). Below this value, the SOC as well as the CA50 advance with the advance of T_{inj}, but an opposite trend is observed when T_{inj} exceeds that threshold. This reveals the effect of ignition mode on combustion behavior. For conventional ignition mode associated with normal (and retarded) injection, it is the T_{inj} itself that is the main factor in the determination of the SOC (and CA50). Alternatively, mixture pressure and temperature are more important than T_{inj} for SOC as well as CA50 under the two-stage auto-ignition mode. In general, the authors found that engine performance, combustion and emissions characteristics in two-stage auto-ignition mode are better than those in conventional diesel ignition mode. Nevertheless, too early injection will lead to diesel

spray impingement and poor atomization quality due to lower in-cylinder temperature and pressure. Optimized results in two-stage auto-ignition mode could be achieved with pilot diesel injection timing set to °CA BTDC to yield higher brake thermal efficiency (35%) as well as lower NOx (60 ppm) and THC (0.4%) emissions.

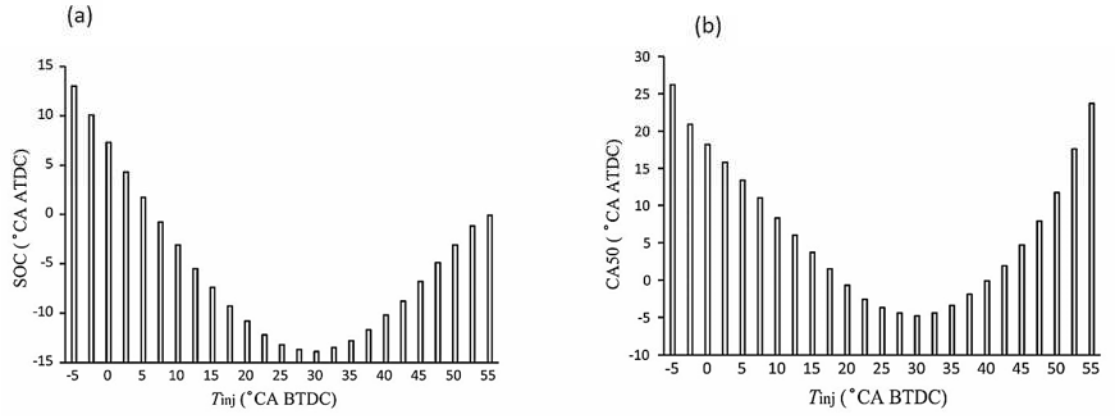


Figure 2.21 Effect of pilot injection timings (T_{inj}) on (a) the start of combustion (SOC), and (b) the crank angle of 50% heat release (CA50). Data is for engine speed of 1335 rpm and light load conditions. Adapted from [64].

Similar to the case of the pilot liquid fuel, the effect of injection timing of the gaseous fuel with port injection configuration is also influential on combustion characteristics of DF engines. Combustion process in these engines strongly depends on the way by which the air-gaseous fuel-diesel mixture is prepared and distributed inside the cylinder at the instant of combustion commencement and during its development [69]. It has been revealed that the degree of charge stratification and the intensity of turbulence generated by the fuel jet have a remarkable effect on combustion phases and heat release pattern [70]. Also, a proper stratification of the in-cylinder charge can be obtained with NG port injection in dual-fuel engines via varying NG injection timing [71]. As this phenomenon has a positive effect on accelerating the combustion process of dual-fuel engines, especially at low and part loads, determination of the optimum injection timing for NG port injection engine configuration becomes crucial.

Yang *et al* [72] investigated the effect of NG injection timing on combustion and emissions of NG-manifold injection DI CR diesel engine. Both injection events of NG and diesel fuel were controlled by a specially developed ECU; as described in details

in another work [73]. They found that changing NG injection timing notably affected the cylinder pressure and HHR trends at all load conditions; as shown in Fig. 2.22. The compression pressure is influenced by NG injection timing in a complex manner mainly due to the interactions of volumetric efficiency, combustion phasing, and specific heat ratio. At part load, retarded NG injection timing results in an increased cylinder pressure and a notably higher second peak of HRR that represents the rapid combustion phase; on the account of late combustion. That is, most of the NG is burned fast in the second phase of combustion. This was mainly due to the time for NG and air mixing is reduced by retarding NG injection, and hence there was not enough time to form homogenous charge. That is, more stratification of the NG-air mixture is formed, which obviously have a positive effect on enhancing the NG burning rate.

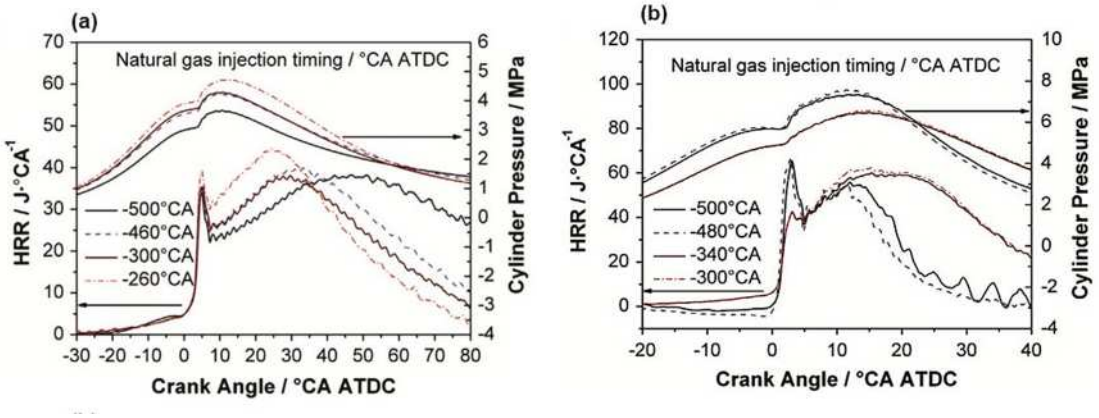


Figure 2.22 Cylinder pressure and HRR traces for different NG injection timing at (a) low load; 0.240 MPa BMEP, and (b) high load; 0.767 MPa BMEP. Adapted from [72].

In comparison, with the very advanced injection timing of –500º CA ATDC that was employed to simulate the conventional dual engines with gas mixer [71], it can be seen from Fig. 2.22 (a) that the major part of the NG at part load was burned in the late stages of combustion; indicating a slower burning rate. At high loads, however, the pressure traces with retarded NG injection timing transformed from the typical two-peak pattern to an almost single-peak one, and the first peak of HRR (representing the first phase of combustion) exceptionally decreased while the second and third phases of combustion increased; as shown in Fig. 2.22 (b). This can be attributed to the reduced mixing timing of NG and air with retarded injection timing, which resulted in a stratified-like gaseous fuel-air mixture in the cylinder. Nevertheless, this stratified-like mixture is probably

over-rich for ignition kernel formation and flame propagation of the pilot fuel, and consequently, less pilot fuel burned in the first stage and more heat of pilot fuel released during the expansion stroke.

With regard to flame development duration – FDD (defined as the interval crank angles between start of ignition and the crank angle at which 10% mass (pilot diesel and NG) fraction burned), and center of heat release – COHR (defined as the crank angle where 50% total heat released; referred to as CA50), data reported in the original work [72] was retrieved and re-plotted on a single graph to illustrate the concurrent effects of NG injection timing on these two combustion characteristics at different loads; as shown in Fig. 2.23.

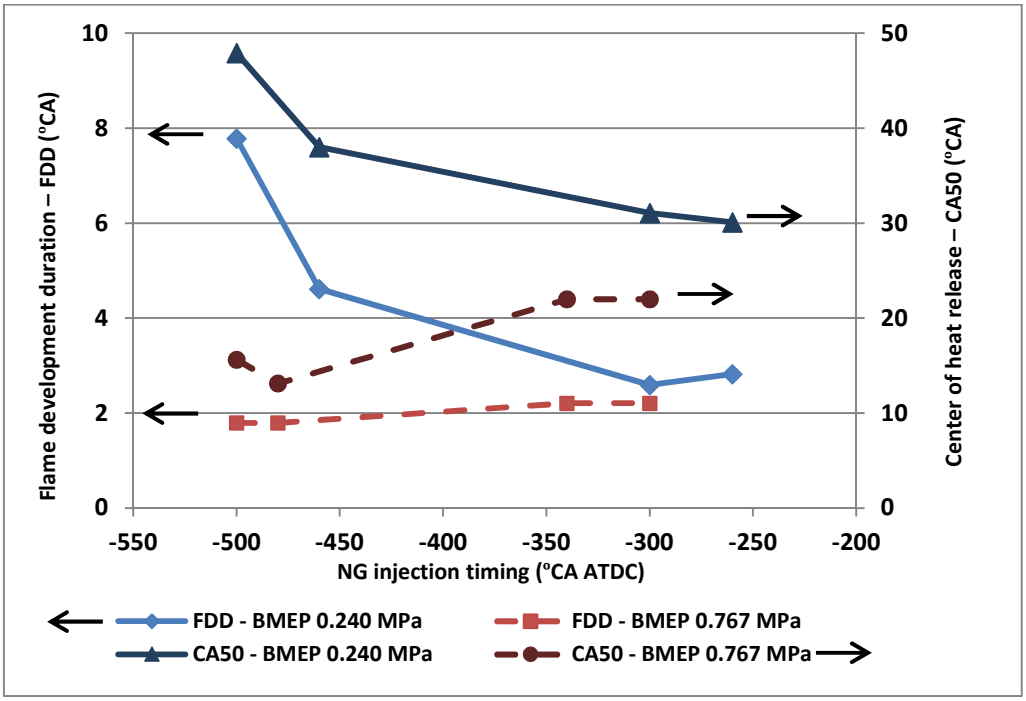


Figure 2.23 **Flame development duration (FDD) and center of heat release (CA50) for different NG injection timing at low (0.240 MPa BMEP) and high (0.767 MPa BMEP) loads. Retrieved from the values reported by [72] and re-plotted.**

The figure shows that at low loads where the NG-air mixture is lean and experiences difficulties to be ignited by the pilot, retarding the injection timing provides a stratified-like mixture with local rich areas, and consequently, combustion is enhanced and flame speed is accelerated. Therefore, the FDD was shortened and the CA50 was attained closer to the TDC. This also improved the brake thermal efficiency. At high loads,

however, it can be seen that FDD slightly increased while the CA50 was getting more distant away from the TDC as the injection timing was retarded. This could be attributed to an undesirable effect of mixture stratification at high load as it may result in the formation of over-rich regions; which may, comparatively, slow down the formation of the flame kernel and thus prolong the initial combustion duration [74]. A corresponding slight decrease in the BTE was therefore observed with retarding NG injection timing at high loads.

The trends of exhaust emissions were consistent with the effect of charge stratification associated with retarding the injection timing. That is, at low load, the general trend of CO and HC emissions showed a decrease as injection timing was retarded, while NOx exhibited a slight increase. This can be attributed to the enhanced combustion owing to the beneficial effect of charge scarification at these load conditions. Yet, the effect of retarded injection timing and the associated charge stratifications on exhaust emissions remained marginal. The reason behind this might be the improved combustion of the NG at high load due to the increased mixture strength; regardless of the presence of any charge stratification.

2.4.3 Injection pressure of the two fuels

Carlucci *et al* [61] studied the effects of pilot fuel injection pressure and main gaseous fuel injection pressure, on combustion and exhaust emissions of a DF NG-diesel engine with DI of diesel fuel and manifold injection of NG. They found that increasing pilot fuel injection pressure provides a better fuel jet penetration throughout the cylinder, and hence results in an improved combustion as the flame spreads well in the combustion chamber. It also leads to a better atomization of the pilot fuel droplets, and hence more ignition nuclei become ready to burn. This globally raises the first peak of rate of heat release (ROHR) that represents the premixed combustion phase, and the maximum in-cylinder pressure; as shown in Fig. 2.24. The effect is larger at engine high speeds and loads where the rich mixture sustains the flame propagation throughout the combustion chamber; in contrast to low speeds and loads conditions where gaseous fuel combustion can only take place in the proximity of the combustion locations of the pilot fuel.

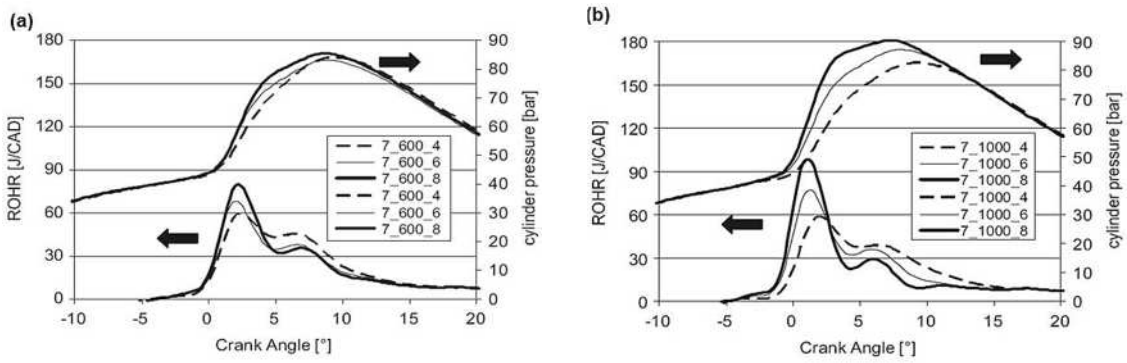


Figure 2.24 **In-cylinder pressure and ROHR traces for different pilot fuel injection pressures of (a) 600 bar, and (b) 1000 bar; at engine speed of 2000 rpm, fixed injection pressure of the gaseous fuel (7 bar) and variable pilot fuel quantities (4,6,8 mm^3). Adapted from [61].**

NG port injection pressure had only a little effect on engine performance and emissions; under different operating conditions. While reasons were not mentioned in the original work [61], it could be attributed to gaseous fuel introduction strategy employed. As the gaseous fuel was injected early in the manifold, the resulting gaseous fuel-air mixture is expected to be homogenous regardless of the injection pressure used. In the absence of any charge stratification, the combustion of the homogenous gaseous fuel-air mixture will simulate that of conventional DF engines with a gas mixer, and hence the effect of gaseous fuel injection pressure becomes insignificant.

2.4.4 Composition of natural gas

While NG is formed predominantly of methane (CH_4), it contains heavier hydrocarbons and inert diluents. The levels of these species vary substantially with the geographical source, time of year, on top of treatments applied during production or transportation. Typical composition of commercial-grade NG varies from 70% to 95% CH_4, with the balance composed of heavier hydrocarbons (mainly ethane; C_2H_6, and propane; C_3H_8) as well as diluents such as molecular nitrogen and carbon dioxide. There are also trace levels of sulfur compounds and other hydrocarbon species.

The variation of NG composition is influential on DF engines combustion and exhaust emissions. For premixed NG combustion, the presence of heavy hydrocarbon (ethane and propane) enhances the ignitability of the mixture due to the increased concentration of the reactive radicals. At high temperatures, enhanced NG ignition is attributed to the

increases in the concentrations of H, OH, HO_2 and H_2O_2 radicals [75]. At temperatures lower than ~1200 K, it is the methyl peroxy (CH_3O_2H) radical that plays the key role [76]. Also, the presence of ethane and propane extends the lean combustion limit and increase the flame propagation. Table 2.1 lists some of the thermodynamic and flame properties of methane compared to ethane and propane [77].

The small levels of N_2 diluent are unlikely to strongly affect NG combustion. However, their principal influence is the reduction of the heating value of the fuel. Higher dilution levels, however, may pose a greater impact on combustion and emissions. For premixed NG combustion, NOx emissions were reduced with N_2 dilution as high as 30% [78]. For heavy-duty DI NG engines, it was demonstrated that diluting the NG with N_2 (while increasing the injection mass to retain the same total fuel energy) resulted in a slower initial combustion but faster and more stable late-stage combustion. This was attributed to the higher kinetic energy of the gas jet and the consequential improvement in mixing process [79].

Table 2.1 Some thermodynamic properties of methane, ethane, and propane. Adapted from [77].

Property	Methane	Ethane	Propane
Chemical formula	CH_4	C_2H_6	C_3H_8
Lean flammability limit in air (% vol.)	5.0	2.9	2.0
Stoichiometric mixture in air (% vol.)	9.47	5.64	4.02
Laminar flame speed in air (cm/s)	34	39	39
Flashpoint temperature (K)	85	138	169
Auto-ignition temperature (K)	810	745	743
Adiabatic flame temperature (K)	2250	2265	2270

McTaggart-Cowan *et al* [80] studied the effects of NG composition on a pilot ignited DI NG diesel engine with DI of NG using a special DF high-pressure direct injection (HPDI) injector at 21 MPa with a fixed pilot quantity of 5% of total fuel (energy basis). The injection timing of NG was always fixed at 1.0 ms after the end of diesel injection, while the latter was adjusted to maintain the mid-point of combustion (or the center of heat release); i.e. 50% IHR (integrated heat resale) at a certain value of 0, 5, 10, or 15°

ATDC (four cases were examined). Ethane, propane, hydrogen, and nitrogen have been added, separately, to the gaseous fuel at two different percentages of each constituent. They found that the gaseous-fuel ignition delay (GID) was reduced by all additives; as shown in Fig. 2.25. For H_2 addition, this was attributed to the increased ignitability of the gaseous fuel, which causes a corresponding reduction in ignition delay as verified by other work of the author [81]. A similar effect was observed with ethane and propane additions, due to the increases of reactive radicals. The absence of these species in the pure methane case results in an increase in the GID. With N_2 addition, the increased jet momentum improves the mixing conditions and reduces the ignition delay [79].

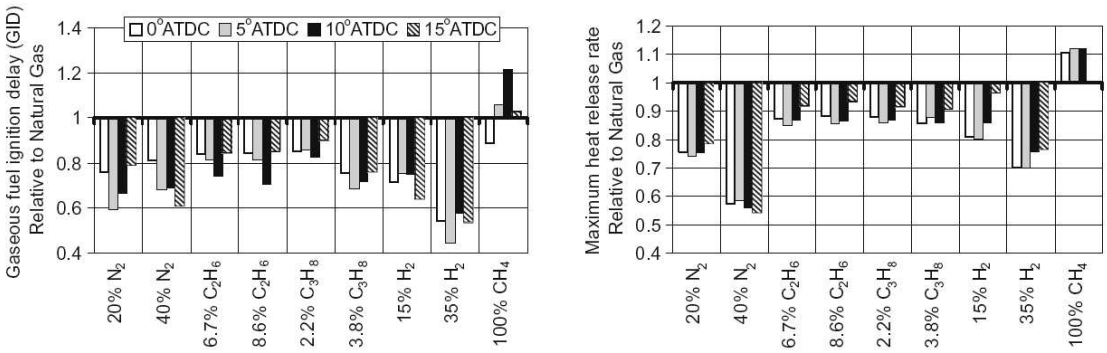


Figure 2.25 Fuel additives effect (relative to NG) on GID and maximum HRR for different combustion timings corresponding to occurrence of 50%IHR at 0, 5, 10, and 15° ATDC. Adapted from [80].

In view of that, the authors developed a correlation between methane number (MN) of different compositions (as a measure of knocking tendency [82]) and the GID, where a 1% change in MN leads to about 1% corresponding change in GID (both relative to NG fuelling for a given timing) for all the fuels excluding N_2; as shown in Fig. 2.26.
Figure 2.25 illustrates also that the maximum HRR follows a trend similar to that of the GID. Reduced GID with fuel additives brings about a corresponding reduction in the amount of premixed fuel, and hence premixed combustion phase and the corresponding maximum HRR are reduced. The authors also developed a linear relationship between these two parameters, where a change of 1% in GID results in an equivalent 1% change in the maximum HRR (both relative to NG fuelling for a given timing) for all the fuels excluding N_2; as shown in Fig. 2.27.

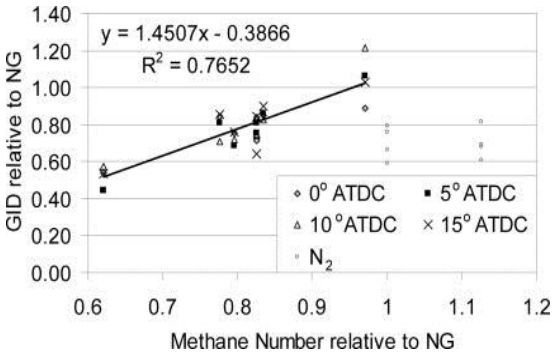


Figure 2.26 **Relationship between methane number (MN) and GID (both relative to NG). Adapted from the online version of [80].**

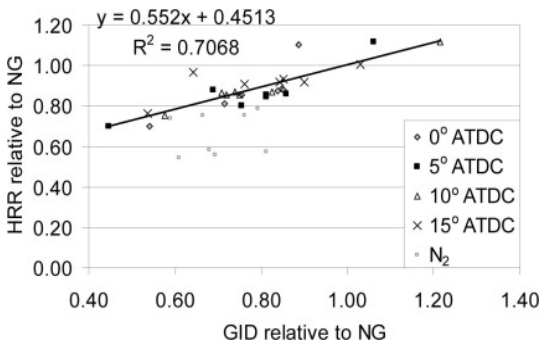


Figure 2.27 **Relationship between GID and maximum HRR (both relative to NG). Adapted from the online version of [80].**

While gaseous fuel additives considerably affect the combustion process, the influence of fuel conversion efficiency ended to be insignificant since the followed experimental methodology involved the adjustment of combustion timing to attain the 50%IHR at certain values. The exception was with N_2 addition, as the significant increase in the injected mass (to maintain the same energy level with elevated N_2 quantity) increased the work done during the expansion stroke. The improved late-cycle combustion with N_2 additions also contributed to the improved efficiency.

It was found that NOx emissions were increased with all additives excluding N_2; as shown in Fig. 2.28. This was attributed to the increased adiabatic flame temperate (T_{ad}) with ethane, propane, and H_2 additions; and hence the strongly temperature-dependent thermal NOx was largely increased [25]. The authors developed a linear relationship between the change in T_{ad} and the corresponding change in NOx emissions; with 1% change in T_{ad} there was a corresponding change of 5% in the generated NOx. Yet, the changes in NOx emissions depends as well on combustion timing in addition to reaction zone stoichiometry and post-combustion mixing; which are also influenced by the fuel composition. Nevertheless, the authors did not highlight the irregular change of NOx with N_2 addition (an increase with low % N_2 and a decrease with high % N_2). That trend could be attributed to the countering effects of improved combustion due to improved mixing from one side, and the reduced T_{ad} as a result of N_2 addition from the other side. Fundamentally, with low % N_2, although T_{ad} is reduced, the effect of improved mixing

on enhancing the combustion conditions dominates, and hence NOx emissions slightly increase (relative to NG). With high % N_2, conversely, the large reduction in T_{ad} is the governing factor and hence NOx emissions decrease (relative to NG).

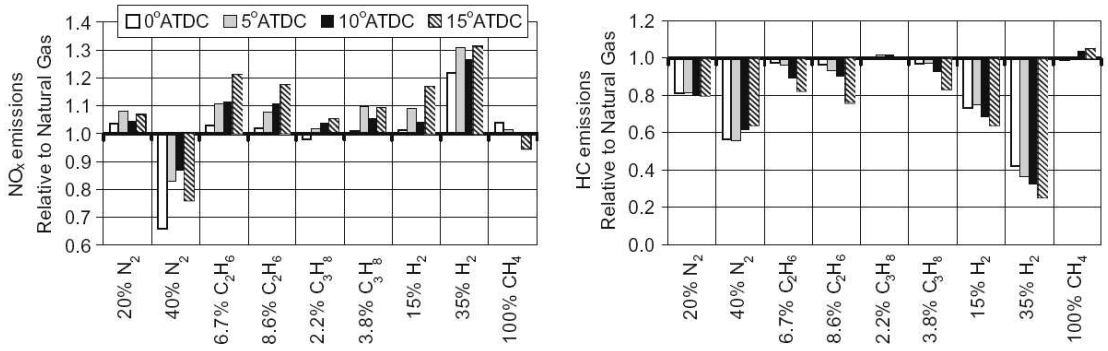


Figure 2.28 Fuel additives effect (relative to NG) on NOx and HC emissions for different combustion timings corresponding to occurrence of 50%IHR at 0, 5, 10, and 15º ATDC. Adapted from [80].

Figure 2.28 also demonstrates that all additives reduced HC emissions (predominantly unburned methane). However, the mechanisms for the reduction in HC emissions vary for different fuel additives. For instance, the wider flammability limits and the increased radical concentrations with the H_2 additive resulted in a more complete combustion and hence HC emissions were reduced [81]. In opposition, the improved late-cycle mixing with N_2 addition was the reason behind consuming more of the fuel that did not react in initial combustion event; reducing HC [79]. With ethane and propane, on the other hand, it was suggested that these heavy hydrocarbons may be helping to delay the onset of bulk quenching (occurring as the in-cylinder temperature and pressure fall during the expansion stroke). The increased burn duration with heavy hydrocarbons (complex C-H bonds) hold over the onset of bulk quenching; involving more fuel in combustion process prior to the reactions being extinguished by this fall in temperature and hence reducing HC emissions. With different fuel additives, all in all, it is likely that all effects are independent of combustion timing.

The reported results concerning CO emissions are not consistent with those of HC; the authors suggested that there are different formation routes for these harmful products. While this agrees with the interpretation that HC emissions are primarily unreacted fuel

while CO is a by-product of partial combustion, the specific nature of these effects are unclear. With regard to particulate matter (PM), the authors found that the addition of N_2 or H_2 to the fuel virtually eliminates black-carbon (BC). On the other hand, adding ethane or propane to the fuel increases total PM mass, with both the BC and the volatile emissions increase. This is consistent with the high carbon-to-hydrogen (C/H) ratio of the heavy hydrocarbons. The authors developed an interesting relationship between the change of the specific heat ratio of the fuel ($\gamma=C_p/C_v$) and the PM emissions; 1% change in (γ) brings about 50% change in the PM. Similar to the situation with NOx emissions, all of these effects depend significantly on combustion timing.

2.5 Conclusions

In this chapters, previous studies of pilot-ignited NG-diesel engines (PINGDEs) were reviewed. Combustion and emissions characteristics of these engines were covered, and the effects of different parameters on combustion and emissions were also considered. Some of the key findings are:

- DF engines suffer increased BSFC and elevated HC and CO emissions at part load; mainly because of the weak mixture strength, the poor fuel utilization, and the slow-burning rate of NG at these conditions. Lower cylinder temperature results in lower NOx emissions compared with diesel operation. At high load, the increased mixture strength promotes combustion; reducing HC and CO emissions yet increases NOx.
- A drastic reduction in soot emissions is achieved under DF strategy, regardless of the engine operating conditions, as NG has a very small tendency to produce soot. Also, CO_2 emission is always lower due to lower C/H of NG compared with diesel.
- The practical substitution levels of NG with diesel fuel are restricted at low load by factors like cyclic variability, limited combustion efficiency, and elevated HC and CO emissions; and at high loads by the exhaust gas temperature limits.
- PINGDEs with NG introduced to the intake manifold can maintain stable operation with as much as 86% NG energy substitution. This could be achieved at low speeds for the entire load range, but higher engine speeds and loads are restricted to lower NG substitution levels; to avoid severe knock.

- Pilot size should be quantified such that it keeps dual-fuel operation feasible and maintains stable operation at low loads, and avoids knock at high loads.
- Advancing pilot injection timing for fixed equivalence ratio provides better overall combustion and reduces HC and CO emissions, yet increases NOx emissions. Too much advance, however, could lead to spray impingement, increased emissions, and erratic engine operation. Optimized injection timing could result in two-stage auto-ignition that improves poor performance and emissions of DF engines at part load.
- Increasing pilot injection pressure provides better atomization and jet penetration. This creates more ignition nuclei and improves flame propagation. The influence of NG port injection pressure on engine performance and emissions is marginal.
- NG composition strongly influences combustion and emissions of DF engines. The presence of heavy hydrocarbons enhances mixture ignitability and increases flame propagation rate. Lean combustion limit is extended and HC emissions are reduced yet NOx emissions increases as T_{ad} increases.
- Large divergence in gaseous fuel composition from the average levels considerably affects pollutant emissions that it may require readjusting the engine management system to offset these emissions via controlling other parameters (injection timing, injection pressure, or EGR levels).

CHAPTER THREE

FUTURE DIRECTIONS OF NG-DIESEL DUAL-FUEL ENGINES

3 Future Directions of NG-Diesel Dual-Fuel Engines

3.1 Introduction

The overview provided by the literature review in Chapter 2 discussed the concept and challenges of operating CI engines on NG-diesel dual-fuelling mode and examined the progress that has been made in recent years. In this chapter, the focus is on the research topics that require further work. As illustrated by Fig. 3.1, the broad categories of the research in the filed could be grouped into fuel delivery or charge composition studies; where each category is directly linked to either the NG or the pilot fuel. While some of these topics have been lengthily studied, others are yet to be investigated. These include pilot split-injection, DI of NG into the engine cylinder, increasing the injection pressure of the two fuels, using alternative high-cetane pilot fuels, and the use of additives. Each of these is discussed in this chapter to assess its potentials, and pilot split-injection, in particular, will be further explored, experimentally, in Chapter 6.

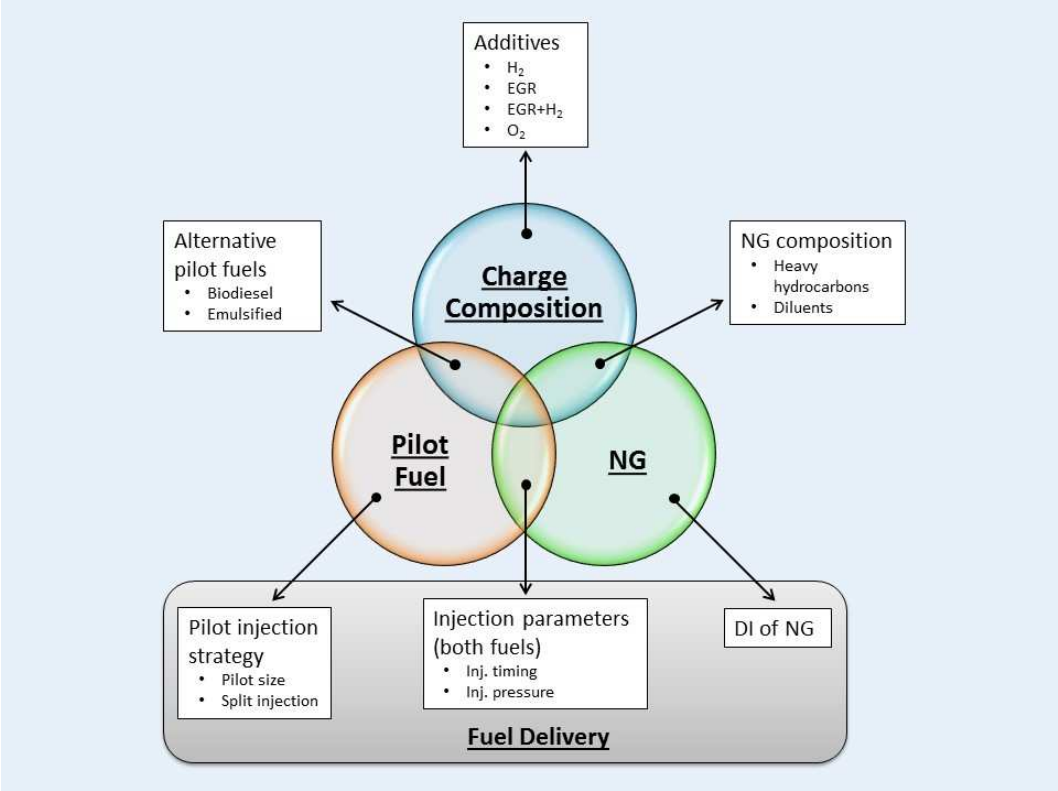


Figure 3.1 NG-diesel dual-fuel engine research topics.

3.2 Splitting the Diesel Pilot into Pre-Injection and Main-Injection

As discussed in Chapter 2, combustion process in DF engines characteristically depends on the pilot fuel injection strategy and its subsequent ignition mode [64]. The shift from the mechanically-governed fuel injection systems into the high-pressure common rail (HPCR) systems becomes essential to the demand for a better fuel economy and lower emissions [83]. The modern generation of high-pressure common rail (HPCR) injection systems incorporates piezo-electric injectors that can perform a very rapid switching. Hence, shorter injection durations, smaller injection quantities, and multiple injections per cycle all become possible [84]. While this is already proven beneficial for diesel engines performance and emissions, the advanced injection techniques also bring many novel ideas to DF engines [85]. Pilot injection strategy plays the key role in changing the combustion mode, from the conventional diesel dual fuel (DDF) combustion into other novel modes [37]. DDF combustion mode is attained by using a single injection of the diesel pilot, late in the compression stroke, to act as an ignition source for the premixed gaseous fuel-air mixture. In this mode, the combustion starts with a classical diesel auto-ignition in the pilot region, together with some of the methane-air mixture entrained in the pilot fuel jet and in its immediate vicinity, and then flame propagates throughout the rest of methane-air mixture [19]. Yet, within the short time available, flame propagation from the pilot region might not proceed throughout the entire charge, especially at part loads [86]. This increases the CO and HC emissions, while the intense combustion of the centralized pilot promotes NOx formation [37]. To overcome these issues, homogeneous charge compression ignition (HCCI) combustion was proposed. This mode is attained in dual fuel engines through using a very early injection of the diesel fuel during the intake stroke; easily achievable by using the HPCR system. The early injection of diesel will form a homogeneous mixture in the methane-air charge. If the mixture is perfectly homogeneous, the rise of the pressure and temperature during the compression stroke will lead to a spontaneous ignition, differs from the classical diesel auto-ignition process in the sense that it does not occur at a specific place in the spray, but simultaneously across the chamber [67]. Reactions in HCCI engines involve a two-stage process; the low temperature and high-temperature reactions (LTR; HTR) [66]. For dual-fuel HCCI combustion, the two-stage process is different from those of diesel-like or gasoline-like fuel HCCI combustion and still unclear, but the general

features are analogous [64]. While the absence of a centralized ignition source and the nonexistence of any rich fuel pockets reduces NOx and PM substantially, HCCI combustion is very difficult to control as it is ultimately governed by the chemical kinetics. It also has a relatively large cyclic variability due to the very lean mixture.

For a better, more direct control of combustion phasing without the need for a closed-loop control, partially premixed compression ignition (PPCI) combustion is put forward [87]. In this mode, diesel pilot is split into two injections; an early pre-injection of a comparatively small portion of the pilot, followed by a late injection of the main pilot. The accurate control of the injection timing and quantity is fulfilled using the advanced HPCR system. The pre-injection part of the pilot acts as an ignition improver as it has a relatively long mixing period with the methane-air mixture at moderate temperature and pressure. The LTR of the diesel fuel at these conditions and the associated radicals promotes the combustion [88]. The main pilot injection then initiates the combustion that further propagates throughout the cylinder charge, and hence it provides a direct control of combustion timing and phasing. The strengthened, yet smoother, combustion yields lower noise levels, improved fuel economy, and lower levels of emissions [88]. Employing a pilot-split technique with the pre-injection part becomes largely premixed, this novel mode will be referred to as partially premixed dual fuel (PPDF) combustion. Figure 3.2 gives a graphical representation of the different dual fuel combustion modes; DDF, HCCI, and PPDF in contrast with the conventional diesel combustion.

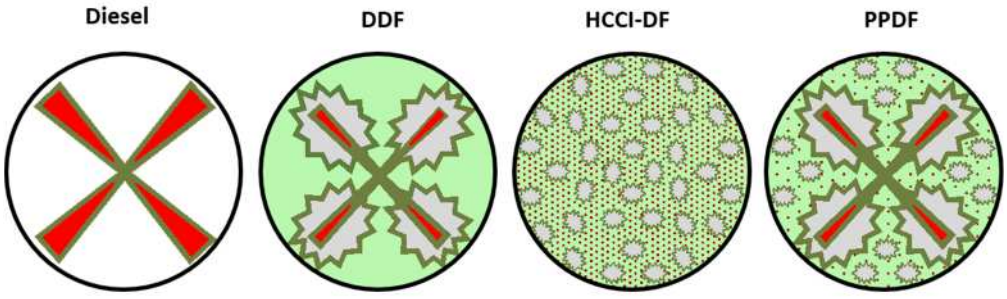


Figure 3.2 **Graphical representation of different DF combustion modes; compared with conventional diesel operation. The red triangles present the diesel main injection close to the TDC. Charge is air only with diesel (white), premixed NG-air with DDF (green), premixed NG-air-diesel vapor with HCCI and PPDF (green seeded with red dots). The large grey flickers present the combustion of the main injection and the entrained NG; small ones present the spontaneous auto-ignition of distributed diesel particles.**

Compared with DDF, PPDF combustion mode can yield an improved fuel economy and reduced emissions [89]. The pre-injection part of the pilot diffuses throughout the charge; improving mixture flammability by introducing a high reactivity fuel into a low reactivity fuel-air mixture. The pockets of the highly reactive fuel also allow for more ignition sites to occur; where the non-uniform local equivalence ratios drive differences in chemical kinetic reaction rates [89]. The enhanced combustion occurs over a shorter duration without flame quenching. More gaseous fuel experience complete combustion; combustion efficiency with PPDF could exceed 98%. The most praised aspect of PPDF combustion is therefore its ability to reduce CH_4 slip and CO emissions; compared with DDF [89]. The lower heat transfer losses bring about less ISFC at all load conditions, while NOx emissions are reduced as long as the same EGR levels are maintained [89]. The benefits of pilot split-injection in PPDF engines are best observed at medium loads, where there are favorable cylinder conditions (temperature, pressure, and equivalence ratio) for combustion imitation and development, with no restrictions on the pilot split. At high loads, the amount of the pre-injection part of the pilot has to be kept at a certain level in order to remain within the permissible limits for the cylinder pressure as well as the maximum ROPR. At light loads, the potentials of PPDF combustion are reduced by the encountered flammability issues of methane under the lean, low temperature and pressure conditions [89]. In addition, the mass of the pre-injection part of the pilot could be significantly small; potentially losing its effect. Researches in this area are limited and in need for further efforts. Chapter 6 in this study is dedicated to investigating PPDF combustion mode under light load operating conditions, with a focus on the influence of pilot pre-injection mass.

3.3 Direct Injection of NG inside the Engine Cylinder

The majority of NG-diesel dual-fuel engine studies to date have been conducted on conventional diesel engines modified to suit dual-fuel operation, where NG is inducted or injected into the intake manifold to mix uniformly with air; while maintaining the original in-cylinder injector for pilot fuel injection. The advantage of this technique is its simple adaptation, but the main disadvantage is that good substitution levels are only obtained at medium loads. This is because at low loads, diesel fuel injectors still require a substantial fuel delivery to operate efficiently, while at high load the extended ignition

delay and mixed fuel in the end zone aggravate both Diesel and SI types knock [90]. In addition, as the NG displaces some of the air in the intake manifold, a reduction in volumetric efficiency occurs, which leads to a proportional reduction in power output; as per Equation 3.1) (derived following the procedure outlined in Appendix B):

$$\dot{W} = \eta_{th}.\phi.FAR^{stoic}.\left(\eta_v.\rho_a.V_d.k.N\right).LHV_f \quad (3.1)$$

where (η_v) is the overall volumetric efficiency based on ambient conditions at intake manifold where (ρ_a) is the density of air, (V_d) is the engine displacement, (k) is the number of suction strokes per engine revolution (i.e. $k=1/2$ for four-stroke engine), and (N) is the engine speed.

Moreover, the gas mixers and venturis installed in the intake pipe to mix the NG with the intake air may offer a further restriction to the air flow; increasing the negative impact on volumetric efficiency and the associated horsepower [91]. The effect is larger as the engine speed increases, due to the increased degree of flow restrictions when a larger amount of air is admitted [91]. One proposed alternative option to minimize the volumetric efficiency penalty of NG induction or injection in the intake manifold is via keeping the NG supply separated from the air until very close to the intake valve [69]. In such a technique, NG is admitted via a small pipe in the intake manifold near the intake valve. The resultant volumetric efficiency is reduced by only 2-4%. As a result, power output levels are fairly maintained; particularly at low and intermediate speeds. Maximum engine speed in this configuration, nevertheless, is limited by the amount of gaseous fuel that can be inducted (via the intake manifold) into the cylinder per cycle, where fuel starvation occurs at high speed [95]. To overcome this limitation, NG supply must be independent of the engine speed; i.e. by injection rather than by induction. This is advantageous in controlling the amount of NG introduced independently of engine speed, and also beneficial in approaching in-cylinder charge stratification [93]. Charge stratification results in an efficient combustion and improves the lean-burn capability of NG [94]. Nonetheless, the optimum distribution of the gaseous fuel-to-air ratio inside the engine cylinder is still not achieved.

To maintain the air mass flow entering the cylinder (and consequently the volumetric efficiency) to the highest possible value, and for improved charge scarification leading to an optimum distribution of the gaseous fuel and air, direct injection of NG into the combustion chamber has been proposed. Preliminary work in this field, however, was characterized by some practical complications, due to the necessity of a high-pressure supply and to the problem of positioning another injector into the cylinder head. In recent years, a state-of-the-art HPDI multi-fuel injector (called concentric-needle multi-fuel injector) was used in the place of the original diesel injector, to directly inject both the diesel pilot and the NG inside the engine cylinder [95]. This HPDI injector has two solenoid-controlled valves to precisely control the injection timing and the metering of each fuel to the combustion chamber; where the diesel fuel comes from the original common rail of the engine, while the NG is supplied through an additional parallel rail. Both fuels are being injected (shortly before the end of the compression stroke) at a high pressure of the order of 20-30 MPa, where the bulk of the energy (up to 95%) is supplied by the NG injection, preceded by pilot diesel injections (via separate nozzle holes) as small as 5% of the total energy supplied [96]. A photo of the typical injector used, along with a schematic diagram of the injector tip assembly and the sequence of injection is illustrated in Fig. 3.3 [97]. While the load in this technique is controlled by controlling the amount of NG injected, some researches [95] achieved pilot percentage as low as 2.4% at full load conditions (100%), while that percentage raised up to 9% when the load was brought down to 20%. Following the pilot injection, it auto-ignites; generating multiple ignition sources that ignite NG jets. NG burns in a predominantly non-premixed combustion event very similar to that takes place in conventional diesel engines; hence offering high fuel-conversion efficiency [96]. That is, dual-fuel engines with HPDI of NG maintain power output and thermal efficiency levels compared with conventional non-dual-fuel diesel engines. While conventional DI diesel engines with high-pressure injection systems offer better tradeoff between NOx and PM [98], dual-fuel engines with HPDI of NG provide reduced NOx emissions by approximately 40%, thanks to the lower adiabatic flame temperature of NG, and up to 65% reduction in PM; owing to the lower carbon content of the gaseous fuel [99]. It has also been reported that optimizing the gas injection timing and pressure at different operating conditions could yield highest NOx reduction without a large impact on thermal efficiency [95].

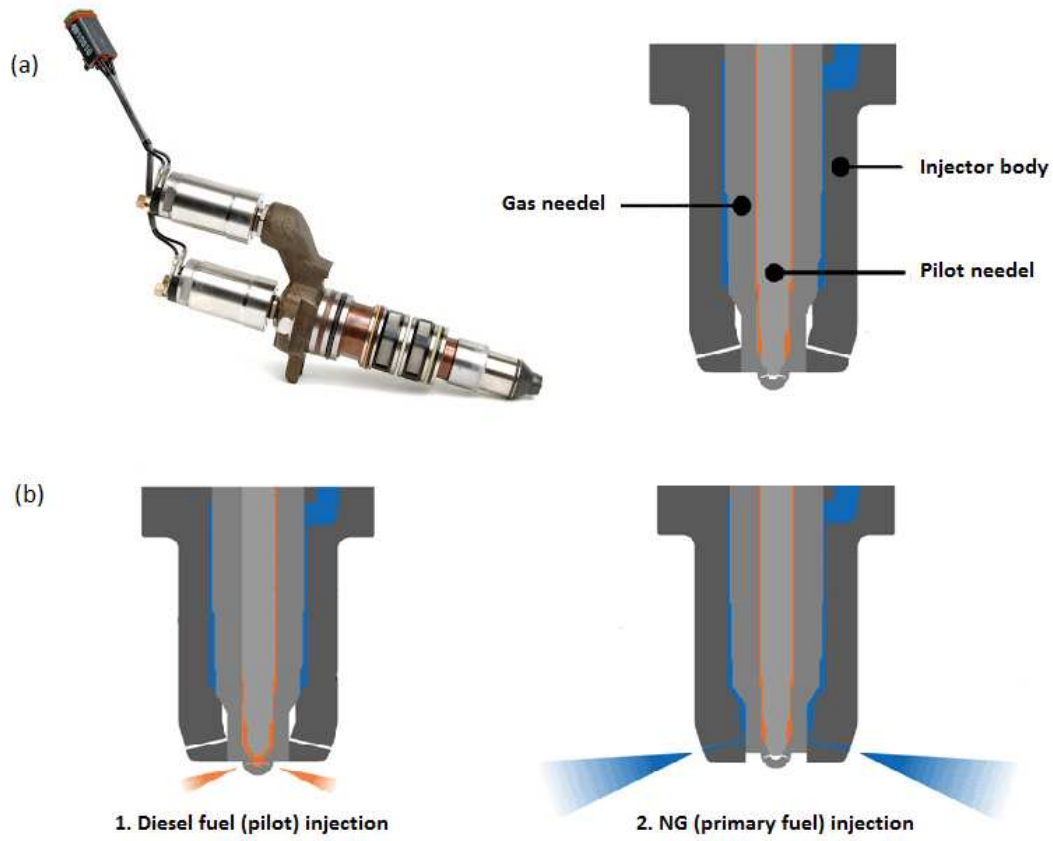


Figure 3.3 **(a) A photograph of the typical injector used in HPDI technique (left) along with a schematic of the injector tip assembly (right); and (b) the sequence of injection for the two fuels showing the separate nozzle used. Adapted from [83].**

Opposing other NG fuelling technologies that rely on fumigation, in the HPDI engines NG is not premixed in the combustion chamber, and therefore emissions of unburned fuel are significantly lower than conventional dual-fuel engines with gas mixers and even those employ manifold injection [100]. With the non-premixed air-fuel mixture in HPDI engines, end-gas knock becomes not a concern; and hence the high compression ratio can be maintained. The global air-to-fuel ratio remains quite similar to that of an equivalent diesel engine, with comparable sensitivity to the EGR as well [96]. Charge dilution of HPDI NG engines with nitrogen can produce a further reduction in exhaust emissions, characteristically NOx, PM, HC, and CO, without having a negative effect on engine performance and thermal efficiency [79]. Further, stratified combustion with very lean burn capability could be realized with DI NG, where the optimum distribution of the gaseous fuel-to-air ratio inside the cylinder is highly achievable [94].

However, it should be taken into consideration that the direct injection of NG requires gas pressures up to 30 MPa, while the NG is frequently stored in vessels at 20 MPa. Onboard compression of NG from 20 MPa and atmospheric temperature to 30 MPa requires work input equal to about 0.1% of the enthalpy of combustion of NG, and more in terms of exergy content. This work (exergy) expenditures for the compression of NG should be taken into account in the well-to-wheel assessment [20]. However, it has been reported that up to 20% reduction in tank-to-wheel greenhouse gases (GHGs) emissions could be obtained when HPDI system is optimized for efficiency; compared to an equivalent diesel engine. All in all, direct injection of NG inside the engine cylinders is understood to be very potent and subjected to further development. A decade ago [100], it was concluded that substantial further research is required before such an engine can be developed for commercial heavy-duty on-road applications. In 2015 [96], it has been reported that the HPDI technique already came to service in commercial heavy-duty applications is North America as well as Australia.

3.4 Increasing the Injection Pressure of the Two Fuels

Further improvement in NG-diesel dual-fuelled CI engines can be obtained by varying the injection pressure of the natural gas jet and the diesel pilot fuel. For conventional non-dual-fuel CI engines, increasing the injection pressure improves fuel atomization and air entrainment; leading to better fuel-air mixing rates [39]. This is attributed to the improved spray properties with increasing the injection pressure. Fuel atomization is caused by the collision of the turbulent jet of fuel with the air inside the combustion chamber. Therefore, the higher the relative velocity between fuel and air, and the higher the density of the air, the more finely the fuel is atomized [84]. The atomization quality of a certain fuel is influenced by microscopic and macroscopic spray properties [101] (microscopic properties include spray tip penetration, spray cone angle, on top of their derivatives; while macroscopic properties include droplet velocity and size, distribution and air-fuel ratio [102]). It was found that spray penetration length increases with higher injection pressure and low ambient density, while spray angle increases with increase in ambient density [103]. The speed and extent to which fuel penetration occurs inside the combustion chamber decide the air utilization and the fuel-air mixing rate [104]. Accordingly, with the increased injection pressure, the combustion process is improved

while soot is reduced and NOx emissions are increased [105]. The primary outcome of increasing injection pressure on diesel ignition process is the reduction of the ignition delay, particularly the physical part, as a direct consequence of better mixing achieved [106]. In most cases, injection pressures range from 200 bar with mechanical injection systems up to ≈2000 bar with HPCR systems [84]. Recently, an exceptionally higher pressure level of 3200 bar was achieved; where the combination of such pressure level with optimized nozzle geometry demonstrated high potential to comply with EURO-VI emissions standards, without exhaust aftertreatment measures [107].

In a similar way with direct NG-injection dual-fuel engines, increasing the injection pressure of both diesel pilot and NG increases the mass flux of fuel into the combustion chamber and increases the degree of turbulence inside the engine cylinder. The fuel-air mixing process is highly enhanced, and the delay period is shortened. In addition, high-pressure pilot fuel injection can provide more ignition points distributed more widely throughout the NG-air charge; which improves the combustion intensity [108]. Higher combustion-progress rates are recorded; bringing about shorter overall combustion duration. NOx emissions are increased slightly with increased injection pressure, while CO and PM emissions are reduced. The change of HC emissions with injection pressure is insignificant. Once more, these emission trends are caused by better levels of mixing between the pilot fuel, NG, and air, in addition to the faster combustion-progress rates. Increasing injection pressure slightly alters SFC, but the associated effect on thermal efficiency levels remains marginal [108]. It has also been demonstrated that the faster combustion of NG as a result of increased injection pressure of the diesel pilot increases the in-cylinder pressure considerably, which is beneficial for performance. In addition, for the same amount of pilot fuel, increasing the number of nozzle holes while reducing their diameter results in a better atomization, and a larger number of ignition centers are dispersed more widely all over the charge. This improves the combustion efficiency [109]. Optimized distribution of the gaseous fuel and air through proper stratification of the cylinder charge improves light load operation. With manifold NG-injection, on the other hand, the effect of NG injection pressure tends to be insignificant [61]; it is the NG injection timing that plays the key role in this configuration, as it has proved the capability of achieving some degree of charge stratification inside the cylinder [72].

With regard to direct injection of the gaseous fuel, researchers conducted on constant volume chamber for different pressure ratios demonstrated that the jet tip penetration of NG increases for higher injection pressure and decreases for the higher pressure of the chamber [110]. On the contrary, the jet cone angle decreases with higher injection pressure and increases with increasing the chamber pressure [110]. It was reported that the improvement of the diesel-NG jet characteristics (such as jet tip penetration and jet cone angle) improves diesel-NG DF combustion process and the associated formation of pollutants [102]. In general, higher injection pressure leads to improved entrainment between the NG and the air; i.e. results in better mixing [102].

In HDPI engines, most recent studies investigated the direct injection of NG into the combustion chamber at elevated injection pressures as high as 600 bar [96]. Compared with the values obtained at 300 bar that was used previously with HPDI engines [99], up to 7% increase in the efficiency as well as 20% increase in the engine power could be achieved when the NG injection pressure was doubled to 600 bar. The effect was more voluminous at high engine speeds; where the combustion process is injection rate-limited at conventional pressures [96]. Up to 90% reduction in engine-out PM at peak torque could also be achieved. Also, the faster combustion resulting from the increased injection pressure allowed earlier combustion phasing to take place without exceeding the peak pressures. Yet, the benefits of increased injection pressure were attainable only at high load conditions. That is, below 75% of engine full load, no significant benefits from higher pressure were accomplished [96]. As far as the drawbacks are considered, increased injection pressure resulted in harsher combustion with higher noise levels. However, this could be mitigated by regulating the flow through reducing the nozzle hole. While the harsh combustion results in increased NOx emissions, higher injection pressure combined with increased EGR level was effective in keeping NOx emissions constant diameter [96]. Researches in this field are subjected to further investigation.

3.5 Utilization of Alternative High-Cetane Pilot Fuels

While conventional diesel fuel is used as a pilot fuel in the majority of NG-diesel dual-fuel engines at the moment, the utilization of alternative high-cetane fuels as pilot fuels is promising. It is not only convenient from the perspective of reducing the dependence on petroleum diesel fuel (i.e. towards a more sustainable transport) but also beneficial for improving some of the combustion and emissions characteristics of NG dual-fuelled engine compared with petrodiesel pilot. A variety of alternative high-cetane pilot fuels may be used:

3.5.1 Biodiesel fuels

Biodiesel fuels have great potential as alternative fuels, either for conventional mono-fuel compression ignition engines or for NG-diesel dual fuel engines as a pilot; due to its properties that are similar to diesel fuel [111]. Biodiesel is defined as "fuel comprised of mono-alkyl esters of long-chain fatty acids derived from vegetable oils or animal fats", and it is designated "B100" as formulated in the biodiesel standard ASTM D6751 [112], with European biodiesel standard EN 14214 [113] referring to fatty acid methyl esters (FAME) as the fuel. This fuel, obtained from an oil or fat by a transesterification reaction with glycerol as co-product, has a chain length of C_{14} to C_{22}, a cetane number higher than petrodiesel (the minimum cetane number of biodiesel is 47 [112] compared to only 40 with petrodiesel [114]), and a relatively high LHV around 40 MJ/kg [115]. It is also easy to handle because its boiling point is higher than that of diesel fuel, and it is an environmentally friendly fuel with low smoke and PM emissions as it contains up to 10% oxygen (volume basis). In view of that, it is considered a promising candidate as a pilot fuel for dual fuel operation with NG. It is worth mentioning that the word "biodiesel" should not be mixed up with the expression "renewable diesel"; where the latter stands for the product that can be obtained from a lipid feedstock (oil or fat) by hydrodeoxygenation reaction at elevated temperature and pressure in the presence of a catalyst, as the produced fuel in this case resembles the composition and properties of petroleum-derived diesel fuel (petrodiesel) [116]. Figure 3.4 presents a simplified flow diagram for biodiesel and renewable diesel; from transformation to engine combustion. Transformation techniques and co-products of the processes are also shown [116].

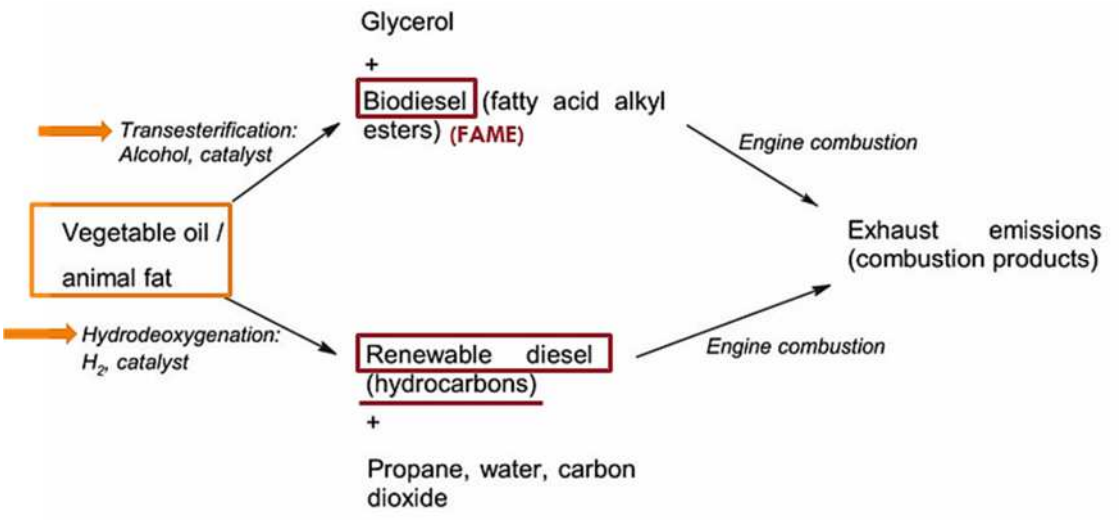


Figure 3.4 Simplified flow diagram for biodiesel and renewable diesel; from transformation to engine combustion. Ref [116].

Recent studies [117, 118] on vegetable (edible frying) oil as a pilot fuel for a common rail DI diesel engine dual fuelled with NG exhibited analogous results to that obtained with petrodiesel (or simply diesel) pilot. The IMEP was slightly greater with diesel-NG compared with biodiesel-NG. While the relatively higher LHV of diesel stands behind the increased peak pressure, it is also believed that biodiesel has a higher power loss because of its higher kinematic viscosity compared with petrodiesel [112, 114], as the power consumption of the common rail pump driven by the engine differs as a result of the variation of fuel properties (and amounts); even at the same injection pressure [119]. Cylinder pressure traces and HRR trends were analogous in both cases; i.e. diesel-NG and biodiesel-NG, at the same operating conditions. However, the direct use of straight vegetable oil implicates some problems such as lube oil dilution, high carbon deposits, ring sticking, scuffing of the engine liner, and injection nozzle failure [120]. Chemical modification (such as transesterification and pyrolysis) are therefore essential [121]. Rapeseed methyl ester (RME), a product of methanol transesterification of rapeseed oil and marketed as biodiesel in Europe, is also a very popular candidate since it performs very closely to diesel fuel as a pilot in terms of performance and thermal efficiency. It also exhibits very similar ignition delay and peak cylinder pressure levels [122]. This is a result of the similar physical properties (such as cetane number - CN) and chemical properties (such as carbon-to-hydrogen ratio) of the two fuels. At the same time, oxygen

molecules contained in the RME chemical composition provides a higher degree of fuel oxidation thus compensates for its relatively lower LHV (36.7-40.5 MJ/kg) compared with petrodiesel (42.5 MJ/kg) [122]. A congruent study [123] also demonstrated similar overall trends of the exhaust gas emissions, but with a slight increase in NOx emissions and corresponding reductions in CO and HC emissions primarily because of the oxygen content of the RME that leads to a more complete combustion at higher temperatures. Nevertheless, issues related to the sustainability of RME as a first-generation biodiesel (competition for land with food crops) and effects of long-term use in engines (such as cylinder deposits, cold weather suitability, solidification, and biodegradation) remain; especially with the vehicular applications where additional care and more regularity in maintenance and periodic services of the engine will be required [124, 125].

Other biodiesel fuels have also been investigated. For instance, the use of jojoba-(seed) methyl ester as a diesel fuel substitute, with a significantly higher cetane number of 63, results in lower rates of combustion pressure rise, reducing noise and knock tendency [126]. It also provides comparable power levels and BSFC values relative to the diesel pilot, but higher CO and HC emissions [127]. The issue with high viscosity could be addressed via preheating the fuel, upstream the injection pump [128]. One study [129] on eucalyptus oil (has a cetane number of 53) revealed improved combustion stability and higher peak cylinder pressure over the entire load range. The ignition delay with eucalyptus biodiesel pilot was shorter than the petrodiesel; due to higher cetane number, but the BSFC was higher due to the comparatively lower LHV. Yet, NG DF operation with both pilot fuels (eucalyptus biodiesel and conventional petrodiesel) showed similar emissions trends [129]. Another one [130] used pongamia pinnata methyl ester (PPME) as pilot fuel for NG dual-fuelled CI engine showed better performance and emissions characteristics of the engine. Although it has lower LHV than petrodiesel, the use of PPME as a pilot resulted in improved brake thermal efficiency and reduced BSFC; principally owing to its rich oxygen content that improves the oxidation process upon thermal decomposition and helps in attaining a better combustion reaction. Also, the associated higher in-cylinder temperature with PPME results in reduced CO and HC levels but increased NOx emissions [130]. Other work [131] considered the addition of diethyl ether (DEE) to pilot at volumetric ratios as small as 5 and 10%, where this was found to bring about improvement in brake thermal efficiency and in specific energy

consumption. This is owing to the high cetane number of DEE and its oxygen content, and hence combustion process is improved. DEE evaporates rapidly and mixes with air easily; forming a homogeneous mixture [132]. Moreover, its high heat of evaporation results in overall lower temperature and hence NOx emissions were reduced [131].

In recent years, Dimethyl ether (DME) started to attract increasing attention as a clean alternative fuel; two decades ago it was considered as a fuel for the 21st century from the perspectives of environmental conservation as well as energy security [133]. DME is produced by the conversion of various feedstocks such as NG, coal, oil residues and biomass, where the particular feedstock is used to generate syngas that is first converted to methanol, then the methanol is dehydrated to yield the Dimethyl-ether [134]. Figure 3.5 presents a simplified flowchart of the process.



Figure 3.5 Simplified flowchart for the process of producing DME from feedstock.

DME maintains gaseous under standard atmospheric conditions (0.1 MPa at 298 K), but when it is pressurized above 0.5 MPa, it condenses to the liquid phase. Gaseous DME is denser than air while liquid DME has a density two-thirds that of water [135]. As a fuel, DME is considered a potent replacement for the conventional petrodiesel; due to its superior auto-ignition characteristics [136]. It has an elevated cetane number that exceeds 55, and a corresponding auto-ignition temperature as low as 235ºC [137]. It also has higher oxygen content than conventional fossil fuels (about 35%), and no direct carbon-to-carbon (C-C) bond and hence it produces lower emissions, particularly PM and HC, than conventional fuels [138]. Still, it suffers from low viscosity and lacks good lubricating characteristics, which may cause fuel leakage through the fuel supply system (which relies on small clearances for sealing), and also it could cause intensified surface wear of moving parts in fuel injection system [139]. It has been suggested the use of lubricity additives such as Lubrizol (539N), HiTEC additives 4140 (H4140), and other biodiesel fuels to improve DME viscosity and lubricity [140]. Another drawback

of DME is its lower heating value (about 28.4 MJ/kg), and hence it requires almost the double amount of fuel injected per cycle in order maintain similar engine power output [141]. Also, the low boiling point of DME and its fast evaporation necessitate keeping it stored under constant pressure in order to maintain it in the liquid phase and avoid evaporation [142]. The features of the fuel injection system also differ from those of petrodiesel one due to the different physical and chemical properties, and hence some modifications have to be made appropriately [135]. This adds more complexity to the process, particularly in vehicular applications. To use DME fuel in automotive vehicles, injector design, fuel feed pump, and the high-pressure pump have to be modified [143]. While the very early works investigated neat DME as a replacement of the petrodiesel in a mono-fuel operation of CI engines [144, 145], other work examined its blends with diesel to improve its properties [146], and recently to attain novel combustion modes such as premixed charge compression ignition (PCCI) [147]. Moreover, the potentials of DME as an alternative pilot fuel for the dual-fuel operation with NG have also been investigated [148]. Compared with biodiesel fuels, such as RME, it was found that the use of DME as a pilot fuel for NG-fuelled CI engines produces lower peak in-cylinder pressure; where this was attributed to the lower combustion enthalpy of the DME [148]. Table 3.1 presents some of the chemical and physical properties of DME as well as RME; in comparison with Diesel [148].

Table 3.1 Some of the chemical and physical properties of DME, RME and Diesel fuel. Adapted from [148].

Property	DME	RME	Diesel fuel
Chemical formula	C_2H_6O	$C_{21}H_{38}O_2$	$C_nH_{1.8n}$
Density (kg/m^3)	668 (liquid)	880	827-840
Lower heating value (MJ/kg)	28.4	36.7-40.5	42.5
Cetane number	>55	≈54	52
Stoichiometric air/fuel ratio (kg/kg)	9.0	12.6	14.5
Auto-ignition temperature (°C)	235	170	250

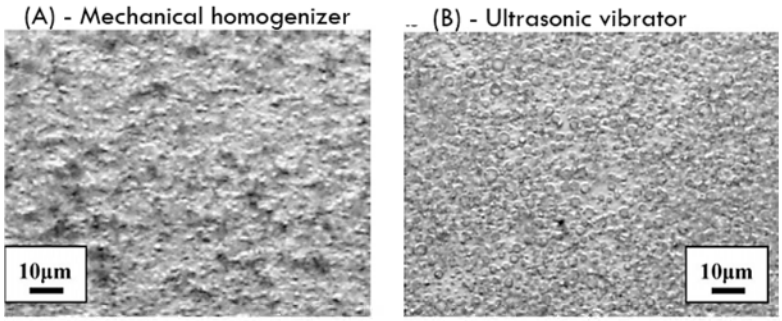
The thermal efficiency of NG engines with pilot DME is consistently lower than those with RME pilot throughout the entire load range; also due to the lower LHV [148]. On the other side, DME evaporates instantaneously when injected into the cylinder; and

hence mixes uniformly with the NG-air mixture. This results in a noticeably smoother combustion process [149]; combustion of DME is therefore known for generating lower levels of noise than conventional petrodiesel [150]. The evaporation of the DME as it is injected into the combustion chamber also cools the charge. When this cooling effect is combined with the comparatively slow flame propagation and the lower temperature (associated with lower pressure), the result is a significate reduction in NOx emissions; particularly at part loads [148]. Conversely, the slow flame propagation generated by the DME pilot coupled with its cooling effect could bring about higher CO as well as HC levels at low and intermediate equivalence ratios; compared with RME [148]. The undisputed advantage of the DME, nevertheless, stands as the almost zero smoke levels. When used as a pilot fuel for NG engines, no smoke readings (in units of Bosch smoke number) could be detected [148].

3.5.2 Emulsified fuels

Emulsified fuels, aka water-in-fuel emulsions, are typically petrodiesel or biodiesel fuel mixed with varying concentrations of water; and they are used as fuels for regular diesel engines [151]. The physical and chemical properties of water-in-fuel emulsions depend significantly on the way by which the emulsions are prepared [148]; several approaches are employed to produce the emulsion. For instance, one study [152] used a mechanical emulsifier made of an electric motor driving a chopper blade inside a mixing chamber. Another one [153] used an ultrasonic vibration machine. Different emulsifying methods employed can produce water-in-fuel emulsions with comparatively varied properties; where the most influential ones are density, viscosity, and bulk modulus of elasticity [154]. These properties are reflected on the emulsification characteristics, such as the water droplets dispersion-and-separation rates and the emulsion stability; thus affecting engine combustion and emission characteristics [155]. Water-in-oil (W/O) emulsions prepared using ultrasonic vibrators have more favorable emulsification characteristics than emulsions produced using mechanical homogenizers [155]. Better characteristics include smaller mean droplet size and larger number of droplets, better distribution and more homogeneous emulsion, stronger intermolecular bonds, and friction forces, and higher emulsification stability and lower separation rate. Figure 3.6 shows microscopic photographs of two emulsions prepared with the two different methods and compares

their properties with neat diesel fuel. Regardless of the preparation method, chemical mixing agents or surfactants such as Span 80 (Sorbitan monooleate) and also Tween 80 (Polyoxyethylene Sorbitan monooleate) could be used to stabilize the emulsions [156].



Item	Neat diesel fuel	W/O emulsion A	W/O emulsion B
Viscosity (cst)	3.17	4.60	4.73
Specific gravity	0.83	0.84	0.84
Mean particle size of water phase (μm)	–	2.6	2.1
Separating rate (remain motionless for 7 days)	–	12.0%	10.7%

Figure 3.6 Microscopic photographs of W/O emulsions prepared by (A) mechanical homogenizer and (B) ultrasonic vibrator; and a comparison of their properties with neat diesel fuel. Adapted from [155].

The use of stabilized emulsions in DI diesel engine in the place of the conventional diesel fuel results in an improved air-fuel mixing process. One reason for this is the additional momentum in jet behavior due to the water entrained in fuel molecules [157]. Nevertheless, the prime reason stands as a phenomenon called “micro-explosion” in which the emulsified fuel droplets explode violently during combustion as a result of vaporization of the entrained water; allowing more ignition points to be distributed throughout the entire charge [158]. Droplet group micro-explosions in emulsion sprays is induced by the volatility difference between the water and the fuel [156], and it occurs on a turbulence eddy scale near the outer layer and the spray head. These explosions possess enough energy to eject torn droplets to a distance several millimeters away from the spray boundary, improving atomization, evaporation, and air-fuel mixing processes [159]. The concept of the micro-explosion phenomenon is graphically illustrated in Fig. 3.7 [160]. Since the physical processes of the liquid fuel combustion take much longer

time than the chemical reaction, micro-explosions can speed up flame propagation and combustion rate [159]. It has also been reported that diesel emulsion exhibits improved combustion efficiency. The engine torque, power, and brake thermal efficiency increase as the water percentage in the emulsion increases [161].

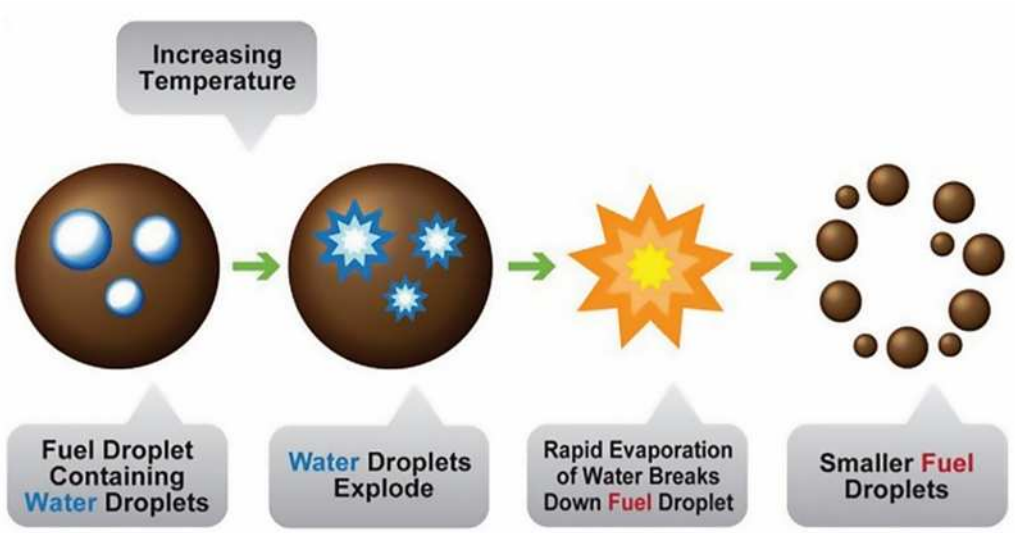


Figure 3.7 The concept of the micro-explosion phenomenon. Ref [160].

As far as the use of W/O emulsions as a pilot for NG dual-fuelled engines is considered, it has been shown that RME emulsion as a pilot is beneficial for engine combustion and emissions [152]. This has been observed with different compositions of water-in-RME emulsions (i.e. 5% as well as 10% water-in-RME emulsions) [148]. The water content in the pilot emulsion plays two different roles. From one side, the micro-explosion phenomenon of the water droplets entrained in the emulsion results in a better mixing process, which eventually leads to higher thermal efficiency, particularly at low engine speeds. From the other side, the vaporization of the water droplets absorbs energy from the surrounding air; hence lowering the in-cylinder temperature. It was found that the rate of pressure rise with the 10% emulsified pilot fuel is higher than that associated with the 5% emulsified pilot fuel; suggesting that the micro-explosion phenomenon and the consequential better distribution of the fuel across the combustion chamber are the governing factors in this condition. With regard to the peak in-cylinder pressure, in the same way, 10% emulsion exhibited a higher value of peak cylinder pressure compared with the 5% one [148]. Both emulsions, though, produced lower peak pressure values compared with the neat RME pilot; owing to the cooling effect of the water content

evaporation. For the same reason, ignition delay was always longer with the emulsions relative to the neat RMR pilot [152]. However, some inconsistencies could be noticed in the results reported with regard to the effect of percentage of water content. That is, the results reported by [152] reveal that ignition delay will always be shorter with higher water content of the emulsion; at all engine speeds, while in the work presented in [148] this was the case only at low engine speed (1000 rpm), while at higher speed (1500 rpm) 5% emulsified pilot fuel exhibited shorter ignition delay that the 10% one. The authors [148] attributed the difference in trends at different speeds to the quality of the emulsions themselves. In their setup, they had a measuring flask in which the emulsion would stay undisturbed as the engine consumed them as pilot fuel, and then it would travel down a fairly long fuel line before entering the engine fuelling system [148]. As a result, there was separated water in the fuel line during operation, and hence it cannot be guaranteed that the appropriate amount of water remained in the injected volume of the emulsion during the injection period. The anticipated separation of the emulsion along the fuel line might also be the reason behind the engine stalling at high loads; as reported by the authors [148, 152]. Regarding exhaust emissions, it was found that the emulsified pilot fuels produced lower amounts of NOx than neat RME, especially at lower equivalence ratios. This was attributed to the cooling effect of the water content evaporation, which lowers the combustion temperature. At higher equivalence ratios, nevertheless, the micro-explosion phenomenon and the resulting improved distribution of fuel droplets improves the combustion process. Accordingly, NOx emissions of the emulsified fuel increased to approach that of neat RME [148]. The case is reversed with CO and HC emissions, where the same reasons now affect in the opposite way. Lower combustion temperature (due to water evaporation effect) leads to higher CO and HC emissions, while improved mixing and droplet distribution (because of micro-explosion phenomenon) reduces CO and HC emissions [148]. The water content of the emulsions also brings about a different effect on PM. The better mixing can prevent the formation of locally rich pockets that could form soot; however, the cooling effect could prevent the oxidation of the already-formed soot particles [148, 152]. To conclude, smoke levels were, in general, slightly lower with emulsified pilot fuels when compared with dual-fuel operation with neat pilot fuels [152].

3.6 Utilization of Various Additives

Whereas the effect of NG composition on combustion process and exhaust emissions characteristics has been addressed in some researches [80] and discussed in Chapter 2, the fact that several additives may be introduced to the cylinder of NG-diesel dual-fuel engines calls for more research in this field. Additives could be influential upon engine performance and combustion stability in addition to exhaust emissions characteristics and knock tendency, yet not of all their effects are well known and they do need more careful study. Some of these additives are highlighted hereinbelow.

3.6.1 Addition of H_2

Hydrogen as a fuel has extraordinary combustion characteristics. Its unique properties compared to conventional liquid fuels like gasoline, as well as gaseous fuels like NG, makes it a challenging yet promising fuel for ICEs; Table 3.2 lists some properties of hydrogen compared with methane and iso-octane (chosen to represent NG and gasoline, respectively, as it is more accurate to define the properties of single-component fuels) [162]. There has been some continued progress in the development of hydrogen-fuelled internal combustion engines (H_2ICEs) in the last two decades [163, 164]. Most recent reviews, such as [165], also exhibited a particular interest in H_2 addition to the efficient CI engines. However, some limitations still hinder its widespread application as engine mono-fuel, where those are related to its production, storage, portability, transport, and purity [166].

Table 3.2 Hydrogen properties compared with methane and iso-octane. Data given at 300 k and 1 atm. Adapted from [162].

Property	Hydrogen	Methane	Iso-Octane
Molecular weight (g/mol)	2.016	16.043	114.236
Density (kg/m^3)	0.08	0.65	692
Mass diffusivity in air (cm^2/s)	0.61	0.16	~ 0.07
Minimum ignition energy (mJ)	0.02	0.28	0.28
Minimum quenching distance (mm)	0.64	2.03	3.5
Flammability limits in air (vol%)	4-75	5-15	1.1-6
Flammability limits (ϕ)	0.1-7.1	0.5-1.67	0.66-3.85
Lower heating value (MJ/kg)	120	50	44.3
Stoichiometric air/fuel ratio (kg/kg)	34.2	17.1	15.0

There has been a continuous research work considering NG-H_2 blends as fuels in ICEs as these blends are attracting an increasing attention [167-169]. Taking advantage of the existing infrastructure of NG; it has been reported that H_2 could be introduced in increasing proportions up to 20% to the existing NG pipelines with no modifications necessary [169]. The addition of H_2, in small percentages, to the cylinder charge of NG-diesel DF engines presents a potential solution for mitigating some of the drawbacks of these engines; especially at part loads. H_2 has wide flammability limits, low minimum ignition energy, and high laminar burning velocity, and hence it enhances the limited lean-burn capabilities of NG at low loads where the mixture strength is considerably weak, increases the engine stability, and reduces the coefficient of variation (COV_{IMEP}) [170, 171]. The addition of H_2 to NG is useful to the ignition of the air-fuel mixture and the subsequent initial flame kernel establishment and development, which also results in increased HRR and thermal efficiency [172]. It has been reported that the total BSFC was considerably reduced when H_2 was added in small percentages to NG-diesel dual fuel engine, where this drop was accompanying a decrease in CO and HC emissions; revealing an improvement in gaseous fuel combustion [173]. The increased flame speed and the associated higher peak cylinder pressure with hydrogen addition result in a more efficient expansion work; further improving the thermal efficiency [174]. Hydrogen-enrichment becomes even more influential at higher air-fuel ratios, where the unstable and incomplete combustion leads to high emissions and poor performance [81]. While NG (predominantly composed of methane) has one of the lowest carbon-to-hydrogen ratios among hydrocarbon, hydrogen is a free-carbon fuel and hence enriching NG with H_2 brings about lower CO_2 emissions. It should yet be taken into consideration that H_2 addition leads to the conversion of a considerable portion of CO into CO_2 as a result of attaining a more complete combustion of the gaseous fuel. Furthermore, the improved combustion process and the associated higher cylinder temperature generate more NOx emissions for the same air-fuel ratio [173]. Nevertheless, the addition of H_2 extends the lean combustion limits and allows NG-diesel dual-fuel engines to operate at higher air-fuel ratios; i.e. with leaner mixtures. As the combustion temperature decreases with the reduced mixture strength, combining hydrogen addition with higher air-fuel ratios can lead to a net reduction in NOx emissions [81].

It is evident from the literature that the majority of the works related to these blends are considering their usage in SI engines, while the studies related to enriching NG with H_2 in CI engines with pilot diesel fuel are very limited.

3.6.2 Addition of EGR

Exhaust gas recirculation (EGR) may be used to improve combustion and emissions characteristics of NG-diesel dual fuel engines; particularly at low to intermediate loads. At such load conditions, the engine suffers from lower thermal efficiency and higher CO and HC emissions; owing to the weak mixture strength and the associated poor fuel utilization efficiency [175]. When employing EGR, a portion of the unburned gas in the exhaust from the previous cycle is recirculated, and expected to possibly re-burn in the succeeding cycle; resulting in a reduction in the unburned fuel and an improvement in thermal efficiency, while also reducing CO emission [176]. At engine half load, using 20% EGR (defined on mass basis as the percent of total intake mixture that is recycled exhaust [39]) can increase the brake thermal efficiency of a DF engine by 2% [30]. At high loads, however, the amount of NG introduced into the cylinder is increased, and hence the amount of oxygen available for combustion decreases. The presence of EGR further aggravates the problem and the combustion process is deteriorated. The brake thermal efficiency is therefore reduced with EGR at these conditions [175].

Besides, the dilution effect of EGR (the reduced oxygen concentration as the EGR replaces some of the fresh intake charge [177]) increases the mixture heat capacity and lowers the in-cylinder temperature; and hence NOx emissions are reduced substantially [178]. The higher the percentage of EGR is employed, the larger the reduction of NOx is achieved. It was reported that more than 60% reduction in NOx emissions of a dual-fuel engine at half load conditions could be achieved by employing 20% EGR (mass basis) [30]. However, PM is increased as NOx is reduced; where this is attributed to the lowered oxygen concentration. When EGR is further increased, the engine reaches operation zones with higher instabilities, increased carbonaceous emissions, and power losses [175]. Nevertheless, the use of EGR is effective to reduce the combustion noise (as represented by the maximum rate of pressure rise) [179]. The use of EGR in NG-diesel dual-fuel engines also reduces the in-cylinder peak pressure and hence extends the engine life. The effect gets more visible with the increase of EGR percentage. At

engine half load, for instance, it was more than 8% reduction in the in-cylinder peak pressure of a plain DF engine is possible when employing 20% EGR (mass basis) [30]. While there has been some notable research work with regard to studying the effect of utilization of EGR in NG-diesel DF engines, some uncertainties still do exist. Those, in particular, are related to the optimum EGR percentage to attain large reduction of NOx emissions without compromising the thermal efficiency. This value is expected to vary significantly with the operating conditions; where high load involves the use of a larger amount of NG on the account of air. Reduced air concentration makes high EGR ratios unachievable, although NOx emissions are naturally elevated in these conditions due to high temperatures. Another topic is related to the stationary applications where EGR temperature could be controlled independently of the engine cooling circuit. Additional studies are required to look into the compromise between using cooled EGR (to attain more reduction in NOx as well as combustion noise) and hot EGR (to improve thermal efficiency) still need to be tailored properly to suit specific operating demands.

3.6.3 Simultaneous addition of EGR and H_2

In the conditions where large reduction of NOx is required, higher levels of EGR ought to be employed. With elevated EGR levels, nevertheless, combustion process highly deteriorates due to the large dilution of the charge with the exhaust gas [180], and consequently, CO, HC, and PM emissions increase substantially [181]. One proposed solution that could maximize the potential benefits of using large amount EGR is to use a fuel additive to enhance combustion stability; where hydrogen is believed to be the best candidate that has been studied for NG-fuelled engines [81]. With exceedingly unstable operating conditions of the engine represented by low-load, low-speed, as well as elevated EGR ratios as high as 40% (volume basis - calculated as the percentage of CO_2 concentration in the intake to that in the exhaust; according to [40]), the addition of H_2 to the charge (23% volume basis) significantly enhances the overall combustion event, improves the engine stability and reduces the COV_{IMEP} [182]. The addition of H_2 does increase the reactivity of the gaseous fuel and hence tends to counterbalance the slow mixing and combustion rates commonly encountered with the utilization of high EGR amounts [81]. Besides, engine-out GHG are noticeably reduced with H_2 addition; where the CO_2 emissions are reduced due to the lowered carbon-to-hydrogen ratio of

the blended gaseous fuel, while CH_4 emissions are reduced as a result of the enhanced overall combustion. At part loads, a 10% increase in hydrogen in the fuel could reduce the GHG emissions by 5% [182]. Besides, the presence of H_2 in the combustion zone increases the concentrations of active radicals; typically, H, OH, and O, where these highly reactive molecules are helping to provide more rapid oxidation of the unburned fuel and partial-combustion species; including CO and HC [183]. Generally, HC and CO emissions were reduced by 15%-20% for every 10% increment in H_2 concentration in the fuel, mainly due to the improved combustion stability. PM emissions, in turn, were reduced by 10% for the same increment, where this was attributed to reductions in the black-carbon content of the PM. Sufficiently high concentrations of hydrogen in the fuel can virtually eliminate emissions of BC particulate [182]. However, the higher reactivity of fuel associated with the increase of hydrogen concentration also increases NOx emissions. That is, the increase in NOx emissions could be attributed to both the increased combustion intensity and in-cylinder temperatures, and the increased prompt-NO formation due to increased OH radical concentrations [183]. However, operating at higher EGR fractions could offset these increases in NOx while maintaining good combustion stability and low levels of CO, HC, and PM emissions [182].

It appears clearly that further research on this particular topic is essentially required as only limited studies have considered that issue; while heavy-duty CI engines (the main target of this approach) usually involve the use of EGR. One potent approach is the use of exhaust gas fuel reforming, to produce a hydrogen-rich combustible gas that is then fed to the engine. This will be discussed in Chapter 7 as a potent way to improve the light load operation of DF engines.

3.6.4 Addition of O_2

The addition of oxygen to combustion air, aka oxygen-enriched combustion (OEC), has been shown to reduce overall fuel consumption [184]. In NG-diesel dual fuel engines, oxygen enrichment improves the combustion process at low loads and reduces knock tendency at high loads [185]. At low load conditions where NG-diesel dual fuel engines suffer from noticeably lean mixtures, the addition of oxygen improves the combustion stability and prevents misfiring as the partial oxidation reactions are accelerated [186]. The promoted combustion and the increased reaction activity enable a larger portion of

gaseous fuel to be entrained in the oxidation process; reducing the BSEC. About 7% reduction in BSFC could be obtained in NG-diesel dual-fuel engines at part load; should the oxygen concentration of the cylinder is increased from 21% (i.e. normal air) to 30% [185]. At high loads, the utilization of large amount of NG leads to a prolonged ignition delay [175], and hence allows more time for heat transfer to the end gas; which results in a tendency to knock [187]. Oxygen addition counteracts that effect; it decreases the ignition delay and shortens the combustion duration, and thereby lowers the tendency to knock. It was reported that more than 18% reduction in the maximum ROPR can be attained if the oxygen concentration of the cylinder is increased from 21% to 25% [185]. As far as exhaust emissions are considered, OEC is considered advantageous from some perspective. The variation of HC in the exhaust gas is consistent with the quality of the combustion process, while the rate of CO formation is a function of the unburned fuel availability and the mixture temperature [25]. Oxygen-enrichment improves the overall combustion process and flame propagation, increases the in-cylinder temperature, and enhances the oxidation process of crevice and deposit-layer hydrocarbon. In addition, the reduced ignition delay as a result of oxygen-enrichment eliminates the diesel pilot spray over-penetration; preventing the unwanted fuel impingement on the cylinder walls. It also reduces the amount of fuel mixed beyond the lean flammability limit that is not able to auto-ignite or sustain a fast reaction front [188]. Consequently, both HC and CO emissions are considerably reduced. About 28% reduction in brake specific HC and CO emissions can be attained at medium load when the oxygen concentration of the cylinder is increased to 30% [185]. OEC also exhibits a substantial drop in the diesel pilot smoke levels; where high oxygen-enrichment ratios at high load conditions may lead eventually to almost zero soot [185]. However, the increase of NOx emissions is a key issue for this technique, since the cylinder temperature increases with the increased oxygen content. Still, this can be moderated by the utilization of water-emulsified diesel along with the oxygen enrichment [189]. Nevertheless, while the emissions trends with oxygen enrichment are quite predictable, there are yet some uncertainties relating to the knocking behavior of NG-diesel DF engines. For instance, excessive oxygen addition at high load conditions may lead to severe knock. This is attributed to the increase in laminar flame speed, which causes the burned mixture to rapidly expand and compress the unburned NG-air mixture; leading to a knocking condition [185]. The elevated peak

cylinder pressure with OEC [190] should be dealt with care not to cause damage to engine structure. All in all, OEC in NG-diesel dual-fuel engines needs further works in order to assess its validity for different conditions.

3.7 Conclusions

In this chapter, the areas that require further work on the topic of NG-diesel DF engines were identified and discussed. Some of the key conclusions are:

- Splitting the diesel pilot into a pre-injection followed by the main injection has the capacity to change the combustion mode from conventional diesel dual fuel (DDF) mode into novel, two-stage, partially premixed dual fuel (PPDF) combustion.
- Compared with DDF, PPDF combustion shows the ability to improve fuel economy and reduce emissions. Combustion efficiency with PPDF mode could exceed 98%, with a minimal slip of CH_4.
- The benefits of PPDF mode are best observed at medium loads. At high loads, the mass of the pre-injection part of the pilot is limited by the maximum peak pressure and ROPR, while at light loads it could be too small and potentially lose it effect.
- Direct injection of NG inside the engine cylinder maintains the maximum air mass flow entering the cylinder, and provides a high degree of charge stratification. This extends the lean flammability limits and allows the engine to run on less diesel and more gaseous fuel. A special centrally-located HPDI multi-fuel injector is used to directly inject both fuels inside the cylinder. Pilot diesel could be as low as ≈2% with this technique.
- DF engines with HPDI of NG maintain comparable power output and brake thermal efficiency levels to those attained with conventional diesel engines, but with up to 40% and 65% reduction in NOx and PM; respectively. However, this technology is expensive and adds more complexity and less flexibility to the system.
- Common rail fuel systems with pressures up to 3200 bar improve the performance of DF engines. Increasing NG injection pressure increases the mass flux of the fuel and the degree of turbulence inside the cylinder; highly enhancing the combustion event. More improvement is achieved if advanced injectors with a larger number of nozzle holes of smaller diameters are used.

- The use of alternative high-cetane pilot fuels reduces the dependence on petrodiesel and potentially improves some combustion and emissions characteristics. Biodiesel and emulsified fuels are amongst the most promising ones. The high oxygen content of biodiesel (up to 10% v/v) provides better oxidation and lower smoke and PM.
- The water content of emulsified fuels lowers the combustion temperatures and NOx emissions, while the “micro-explosion” phenomenon produces more ignition points throughout the entire charge. However, the effects of biodiesels and their emulsions on long-term use in engines (such as cylinder deposits, cold weather suitability, and biodegradation) are questioned.
- Hydrogen-enrichment mitigates some of the DF engines drawbacks, particularly at part loads. It enhances the limited lean burn capabilities of NG, increases the engine stability, and reduces the COV_{IMEP}. Total BSFC is considerably reduced, while CO and HC emissions become lower. However, higher cylinder temperature generates more NOx emissions. The combination of EGR and hydrogen could be used in the conditions where large reduction of NOx is required without sacrificing the engine performance.
- Oxygen enrichment of NG-diesel DF engines improves combustion stability at low loads and decreases knock tendency at high loads. The more complete combustion reduces CO and HC emissions and substantially lowers smoke levels; yet increases NOx emissions.

CHAPTER FOUR

EXPERIMENTAL FACILITIES AND DATA PROCESSING

4 Experimental Facilities and Data Processing

4.1 Introduction

This chapter provides a detailed description of the experimental facilities used in this study. This covers the two test engines, the test bed facilities and auxiliary systems, the fueling system, the data acquisition system and instrumentations, and the software and control measures. The procedures of data collection and processing are then presented. These include the methodology to determine the top dead center of the piston position, the synchronization of cylinder pressure data with the corresponding crank angle degree values, and the data post-processing to filter any noise interference in the signal. The zero-dimensional single-zone combustion model used in the heat release calculations is then considered. Finally, indicated work determination and the engine stability criteria are discussed.

4.2 Experimental Facilities and Setup

4.2.1 Engines and test bed

The first part of the experimental work in the present study has been carried out on a Ford Puma (ZSD 424 Range) four-cylinder, 2.4 liters, turbocharged intercooled direct injection diesel engine. The main specifications of this engine are listed in Table 4.1. The engine has a mechanical injection system, in which a chain-driven rotary distributor fuel injection pump supplies the diesel fuel to the mechanical injectors. The quantity and timing of injection are controlled by the Engine Control Unit (ECU). This engine is referred to throughout the thesis as the distributor pump (DP) engine. The engine was mounted on the test bed, and tested and commissioned by some former researchers; including [191]. Figure 4.1 shows general view of the DP-Engine mounting on the test bed. In the present contribution, this engine has been used only under diesel operation, as a part of the investigations aiming at the influence of FIE on combustion and heat release characteristics in CI engines. The details of this study are given in Appendix A.

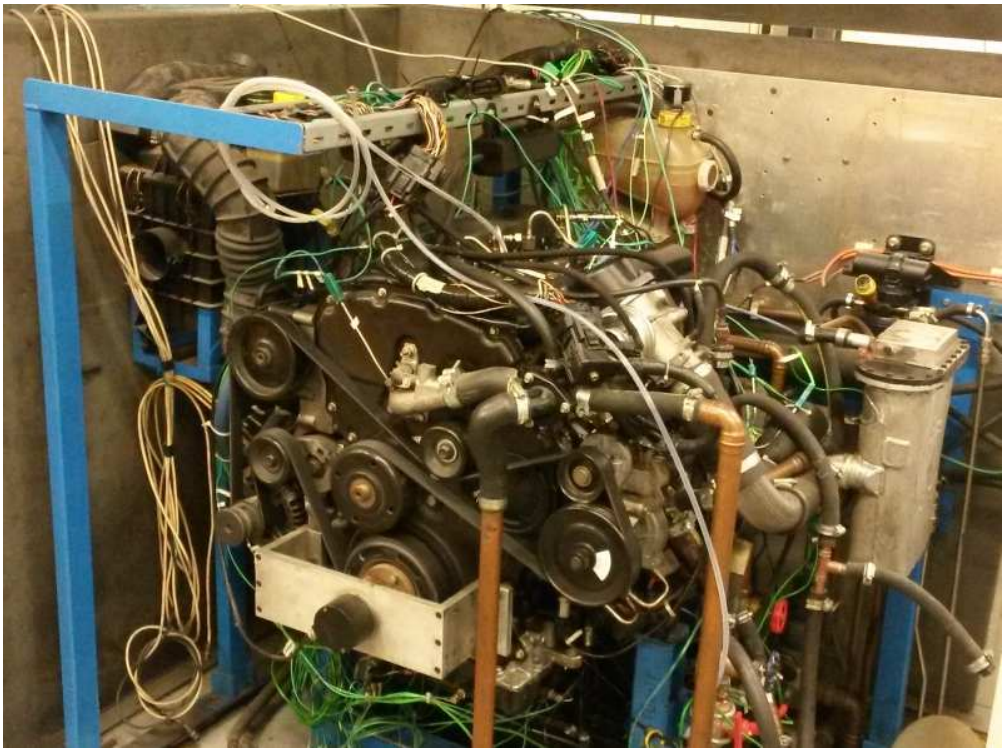


Figure 4.1 Ford Puma (ZSD 424) 2.4 liters DP-Engine mounted on the test bed.

Table 4.1 Main specifications of the DP-Engine used in the present work

Model	Ford Puma (ZSD 424 Range)
No. of cylinders	4
Capacity	2.4 litres
Cooling system	Water cooled
Induction system	Exhaust Gas Turbocharged, Intercooled
EGR system	Electronically controlled EGR system
Bore	89.9 mm
Stroke	94.6 mm
Con. rod length	149.8 mm
Compression ratio	18.4:1
Rated power	88 kW @ 4000 rpm
Maximum torque	240 Nm @ 2300 rpm
Fuel injection system	Direct injection, Rotary distributor pump, Mechanical injectors
Fuel injector opening pressure	200 bar
Induction System	Turbocharged, Intercooled
Combustion system	Bowl in piston
Valves per cylinder	2 intake; 2 exhaust

The second and main part of the experimental work in the present study has been carried out on a Ford Puma (Duratorq ZSD 422 Range) four cylinder, 2.2 liters, turbocharged intercooled direct injection (DI) diesel engine. The specification of this engine is given in Table 4.2. This engine has a high-pressure common-rail fuel injection system; where the injection pressure could be controlled independently of the engine speed or injected fuel quantity, and is generated by a high-pressure pump develops a pressure as high as 1800 bar. This engine is referred to as the common rail (CR) engine. The high-pressure pump is electronically controlled via the Engine Control Unit (ECU). Figure 4.2 shows general view of the CR-Engine. This engine has been first tested under diesel operation to complement the studies regarding the effect of FIE, then it has been converted to dual-fuel (DF) operation using methane and diesel fuel. The studies of DF operation are presented in Chapters 5 and 6.

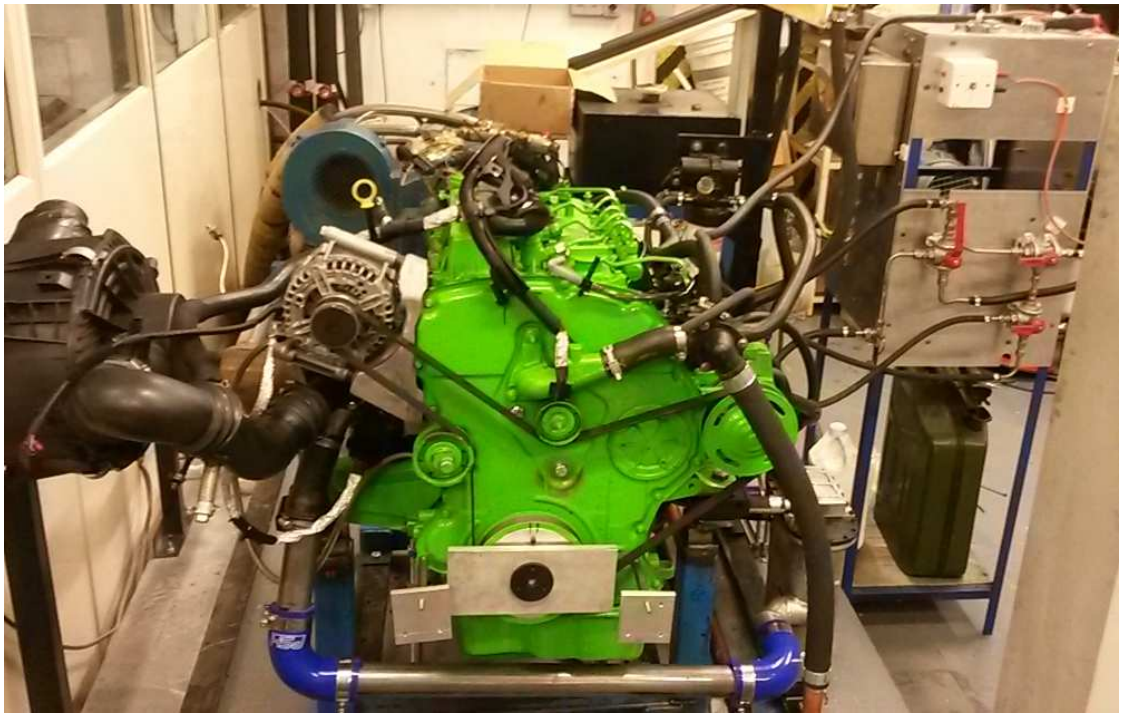


Figure 4.2 Ford Puma (ZSD 422) 2.2 liters CR-Engine mounted on the test bed.

Table 4.2 Main specifications of the CR-Engine used in the present work

Model	Ford Puma (ZSD 422 Range)
No. of cylinders	4
Capacity	2.2 litres
Cooling system	Water cooled
Induction system	Turbocharged, Intercooled
EGR system	Electronically controlled EGR system
Bore	86.0 mm
Stroke	94.6 mm
Con. rod length	149.8 mm
Compression ratio	15.7:1
Rated power	110 kW @ 3500 rpm
Maximum torque	380 Nm @ 2000 rpm
Fuel injection system	High-pressure common-rail (HPCR)
Common rail pressure	1800 bar
Combustion system	Bowl in piston
Valves per cylinder	2 intake; 2 exhaust

When installed, the engine under test has been directly coupled to a David McClure DC electric motor regenerator dynamometer through a modified version of the standard gearbox; where the internal gears were removed and replaced with a linking propeller shaft. The alignment process of the coupling and shaft has been carried out carefully to reduce any changes over the long-term operation [192]. The dynamometer has a rated power of 90 kW and a maximum speed of 4000 rpm, and it is controlled by a DC drive unit that maintains steady speed motoring/absorbing operation against varying torque. Some modifications were necessary to allow test bed usage. The engine alternator was run unloaded, and the standard battery used was charged through the mains via a battery power pack. The battery has been used to power the DP-Engine electronics, but a set of main power suppliers have been used with the CR-Engine instead. For both engines, the glow-plugs were removed and replaced by pressure transducers to measure the in-cylinder pressure. Further, for the DP-Engine, in particular, the standard power steering pump originally fitted have been kept only for the convenience of running the accessory belt, while its high-pressure outlet has been routed back, via a finned cooling tube, to the fluid reservoir.

Both engines have external high-pressure loop Exhaust gas recirculation (EGR); where the EGR, after passing through a coolant-fed heat exchanger for cooling, is introduced into the intake pipe downstream the compressor and the intercooler. Figure 4.3 provides a schematic diagram of the engine induction and exhaust systems.

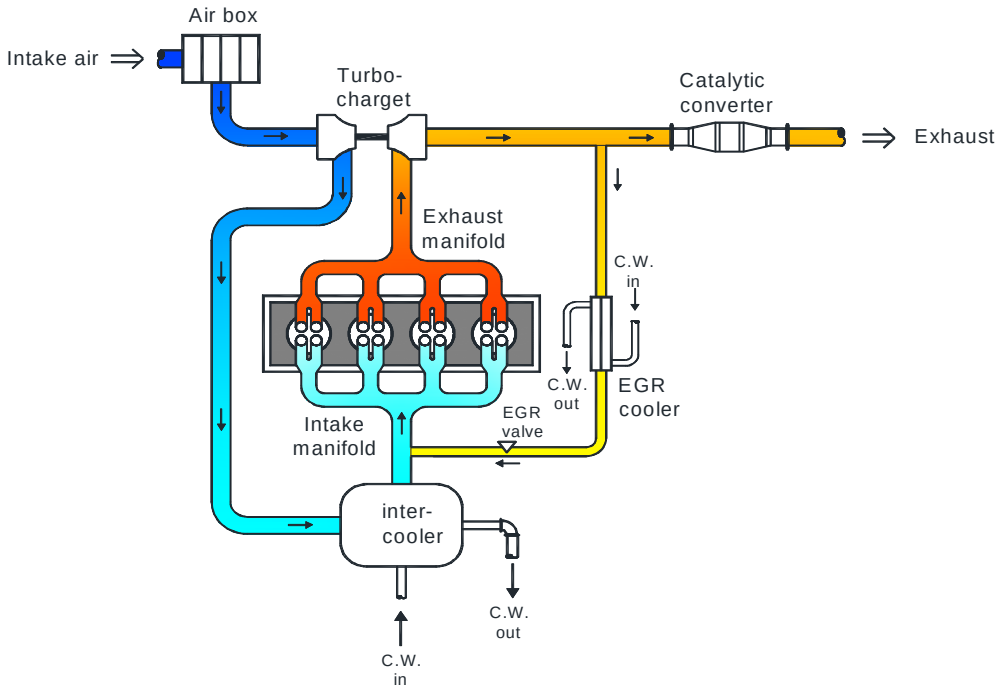


Figure 4.3 Schematic diagram of the engine induction and exhaust systems.

The radiator of the coolant system was replaced with a counter-flow shell-and-tube heat exchanger, which rejected the heat to cooling water pumped from the cooling plant of the laboratory. A water-to-air intercooler has been used in the place of the original air-to-air intercooler with an independent cooling circuit for the intercooler coolant. The standard EGR cooler and Oil cooler have been retained. Figure 4.4 presents a schematic diagram of the test bed cooling circuits; for the engine, the intercooler, the EGR cooler, and the Oil cooler.

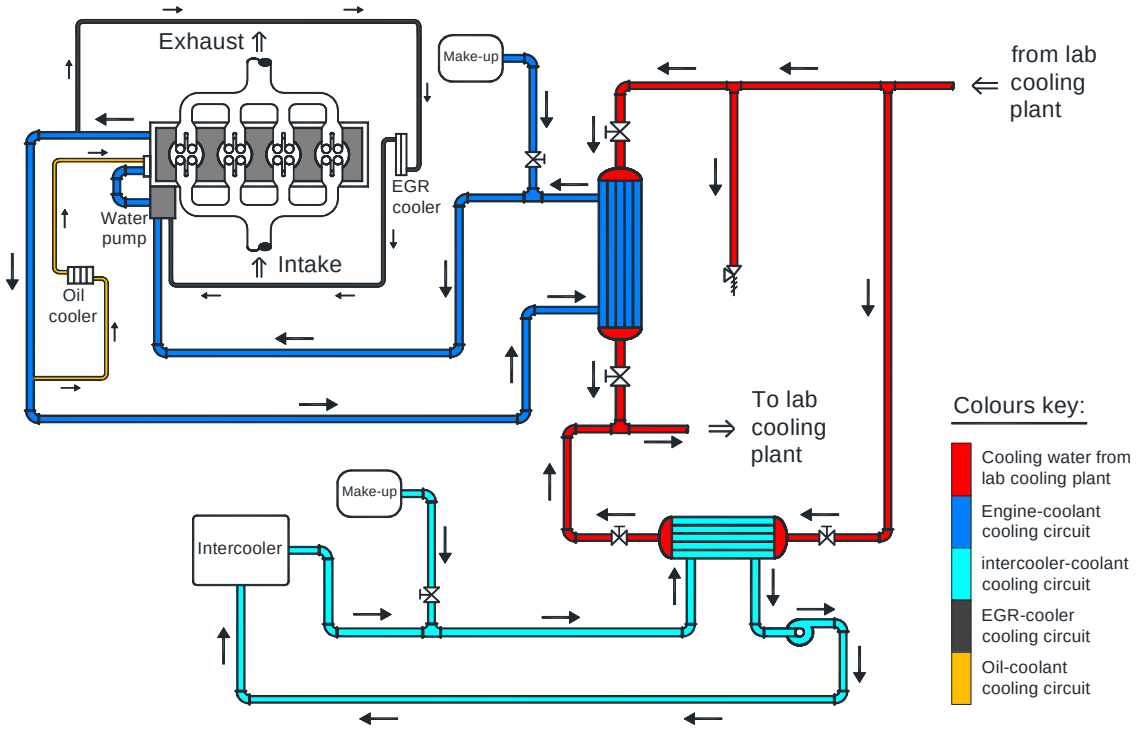
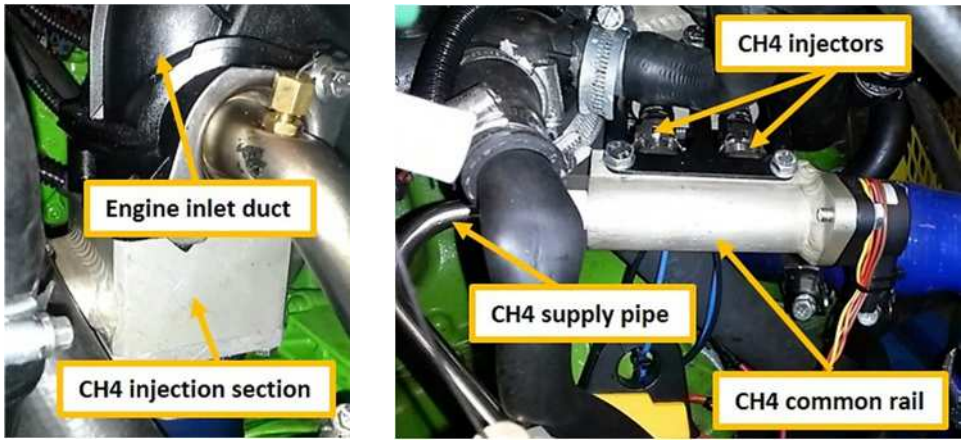


Figure 4.4 **Schematic diagram of the test bed cooling circuits. Arrows show the potential directions of the flow. Colours are for clarification only. Not to scale.**

The standard fuelling system in both engines is originally controlled via the ECU using a drive-by-wire electronic accelerator pedal position (APP) sensor. For test bed purpose with the DP-Engine, fuelling quantity was preset using a potentiometer mounted in the main control panel. With CR-Engine, the pedal outputs 2 signals inversely proportional to each other, and fuelling quantity was controlled via a homemade pot-box comprises a set of two 10-turns potentiometers oppositely attached to the center of rotation of the control wheel. With both engines, the speed was made independent of fuelling quantity and controlled through regulating the dynamometer speed.

For methane-diesel DF tests on CR-Engine, the intake manifold was modified to allow for gaseous fuel utilization. The modification involves attaching a special gas injection system, comprising a gaseous fuel rail and mixing section, where the gaseous fuel is injected and mixed with the intake stream before being admitted to the engine. This section is fitted with a thermal fuse that melts if the temperature goes higher than a 120ºC; indicating the incidence of flame flashback in the intake manifold. As the fuse melts, it cuts the power to the gas injectors immediately. Figure 4.5 shows a photograph of the gaseous fuel injection section as attached to the intake manifold.



(a) **(b)**

Figure 4.5 Gaseous fuel injection system; (a) General view of the setup within the intake manifold, and (b) the arrangement of gas supply line, gas rail, and injectors.

A dedicated gaseous fuel supply system was designed and executed by the author of the present work. All system parts in contact with the gaseous fuel are made from 316L Stainless Steel. Gaseous fuel (99.95% CH_4) was supplied from commercial compressed gas bottles of 50L capacity. The gas pressure is first reduced from the bottle pressure of 200 bar to 15 bar via a single-stage high-pressure (HP) regulator. The gas then flows through an arrangement of seamless and flexible tubes by to a single-stage low-pressure (LP) regulator; where the pressure is brought down to the injectors working pressure of 6 bar. The gas then passes through a thermal mass flow meter before being fed into the gas injection rail. That is, the gas flow rate was measured as it is being injected into the intake manifold; no provision was made to measure the actual amount of gas entering to each individual cylinder. Measuring the gas flow rate on global basis has the problem of encountering a variation of the gas amount from cylinder-to-cylinder. Reasons for that could be any possible lag in the electric signal fed to the injector solenoid, the non uniformity of low inside the intake manifold, and any difference in the valve timing due to non-matching of the cam profile. All of these variations do exist but they are very difficult to account for. This is not expected to largely influence the present work as any potential error remains marginal. The complete system has been fitted with several safety measures, including a pressure relief valve, isolation valves, on top of flashback arrestors. The details about the safety measures can be found in Appendix C.

Figure 4.6 presents a schematic diagram of the gaseous fuel system, and a descriptive photograph of gas system piping and control measures is presented in Fig. 4.7.

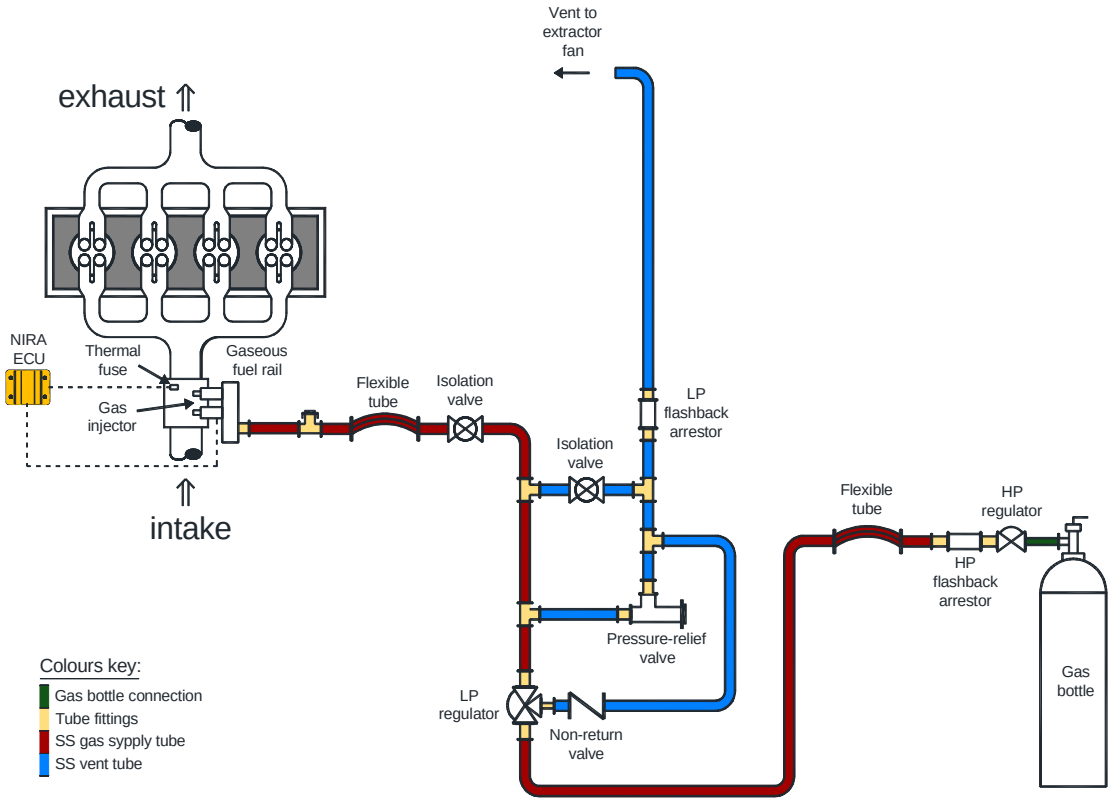
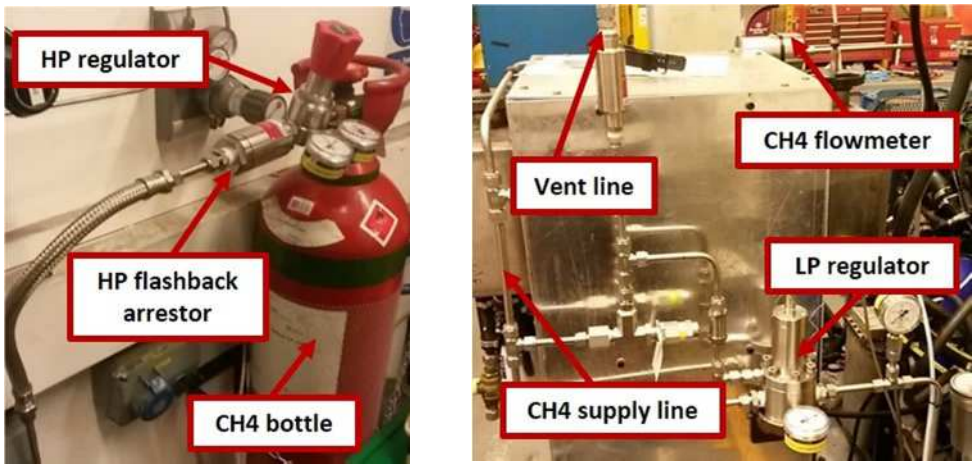


Figure 4.6 Schematic diagram of the gaseous fuel system. Not to scale.



(a) **(b)**

Figure 4.7 Gaseous fuel piping system; (a) the compressed gas cylinder complete with the HP regulator and the FB arrestor, and (b) the LP side comprises LP regulator, supply line fitted with gas flow meter, and venting system complete with FB arrestor.

4.2.2 Data acquisition and instrumentation

Experimental data were acquired to a PC through an integrated data acquisition system and control programs. Although the basic structure of the setup is almost the same, the hardware and software arrangement used differ between DP-Engine and CR-Engine in some aspects. With DP-Engine, two categories of parameters were measured. Those are the engine standard variables and the additional measurements. Standard variables are those measured in vehicles via the ECU, such as the fuel demand and injection timing. In the experimental setup, those variables were still measured via the ECU. The output of the ECU was to a network hub connected directly to the PC through a USB. This hub is the main interface to the software, namely ATI Vision, installed on the PC to collect the signals from the ECU and from other external sources. It is also be used to program the ECU and perform a real-time calibration. Figure 4.8 shows a screen-shot for the ATI user interface for the project file used in the present work.

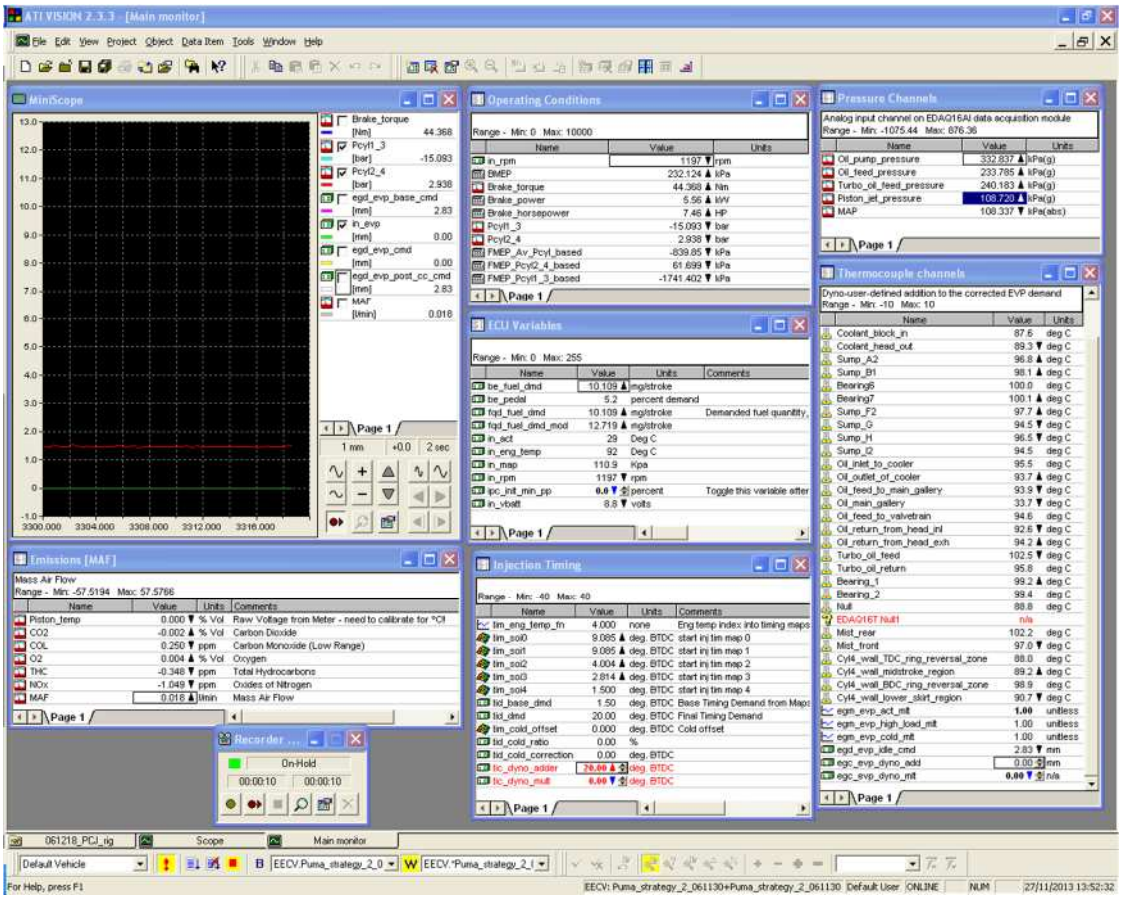


Figure 4.8 A screen-shot of the ATI user interface.

Other than engine variables, several additional measurements were taken to fulfill the test requirements. Type-K thermocouples were fitted throughout to measure the coolant temperatures, oil temperatures, intake and exhaust manifolds temperatures, and fuel line temperature. The signals generated were then fed to external data acquisition (EDAQ) modules for thermocouples; by ATI. The output of those modules was routed to the network hub then to the PC; to be read and processed by the ATI Vision software.

A set of Kulite PT-2054 non-amplified pressure sensors and Kulite PT-2028 amplified pressure sensors were used to measure oil pressure, intake Manifold Absolute Pressure (MAP), and exhaust manifold pressure. A Horiba MEXA-7000 Exhaust Gas Analyzer was used to measure the concentrations of CO_2 in both the intake and exhaust manifold so the actual EGR percentage can be determined; as per equation (5.1). The produced analog signals were then fed to an EDAQ module of analog inputs; by ATI. The output of the EDAQ analog input module was routed to the network hub then to the PC; to be read and processed by the ATI Vision software.

Two Kistler 6055C piezoelectric non-cooled combustion pressure sensors were used to measure the in-cylinder pressure in cylinders 2 and 4. The output signal of each pressure transducer was fed to a Kistler 5011 charge amplifier comprising a high-gain inverting voltage amplifier with a MOSFET input for high insulation resistance. A Hohner W-series, model W2D11R, incremental optical encoder was used to monitor the crankshaft position. The encoder was attached to the free end of the crankshaft via a mounting bracket and flexible coupling. This encoder is suitable for a rotational speed up to 6000 rpm, and it has two output signals; a repetitive pulse every half degree of crankshaft rotation (i.e. 720 pulses pre revolution), and a reference pulse every complete revolution (360^o). The repetitive pulse signal is referred to as “Index-A” signal, or the clock signal, while the reference signal is referred to as “Index-Z” signal, or the encoder TDC marker. The two signals, along with the output voltage signal from the charge amplifier, were routed to a National Instrument (NI) PCI-MIO-16E4 high-speed (250 kHz) 12-bit resolution ADC card installed on the PC for data acquisition process. To obtain crank angle-synchronized cylinder pressure data, a dedicated program has been written in LabVIEW environment, in which the data acquisition process has been triggered by the encoder’s Index-Z signal and clocked (timed) by the encoder’s Index-A signal.

Figure 4.9 shows a schematic diagram of measurement circuits for different variables for DP-Engine.

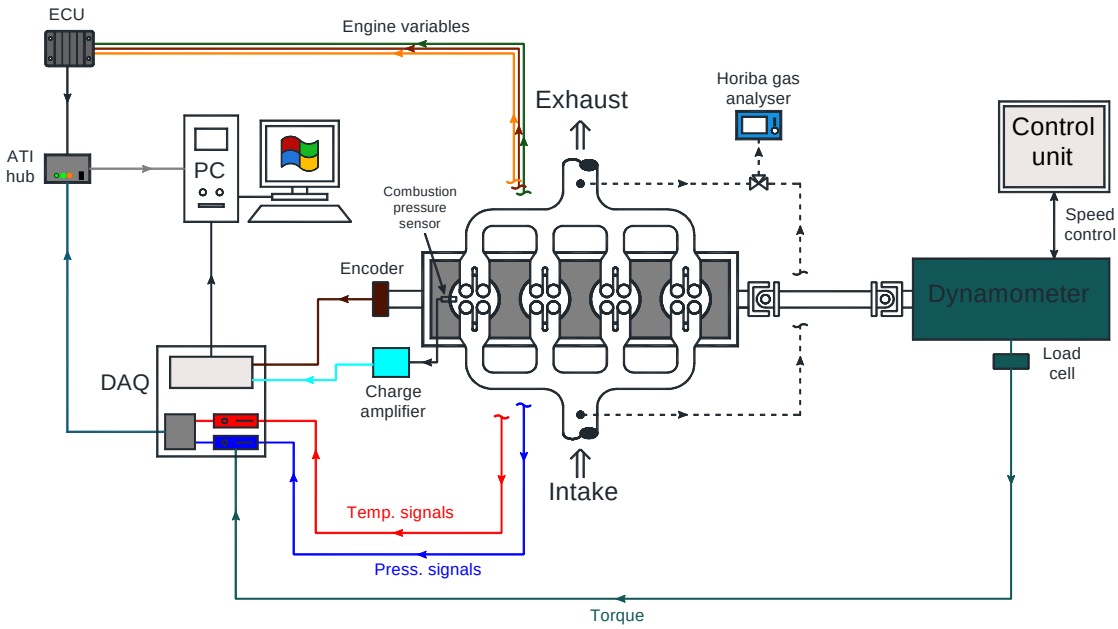


Figure 4.9 Schematic diagram of the test rig instrumentations and measurement circuits for DP-Engine. Not to scale.

With the CR-Engine, advanced NIRA common rail diesel engine management system was used. The system comprises a NIRA-i7r engine control unit complete with NIRA-rk application tool for loading the software program, tuning the engine data, monitoring etc. NIRA-i7r ECU is connected to the PC, where NIRA-rk application tool is installed, through a dedicated dongle. Engine standard variables, including diesel fuel injection parameters (mode, timing, and quantity) were measured and controlled by this system, while the gaseous fuel consumption in dual-fuel experiments was measured through a thermal mass flow meter, model F-113AI by Bronkhorst, then imported into a dedicated software. The gas injection quantity and duration were controlled through the NIRA-rk software. Figures 4.10 shows a screen-shot of the NIRA-rk user interface.

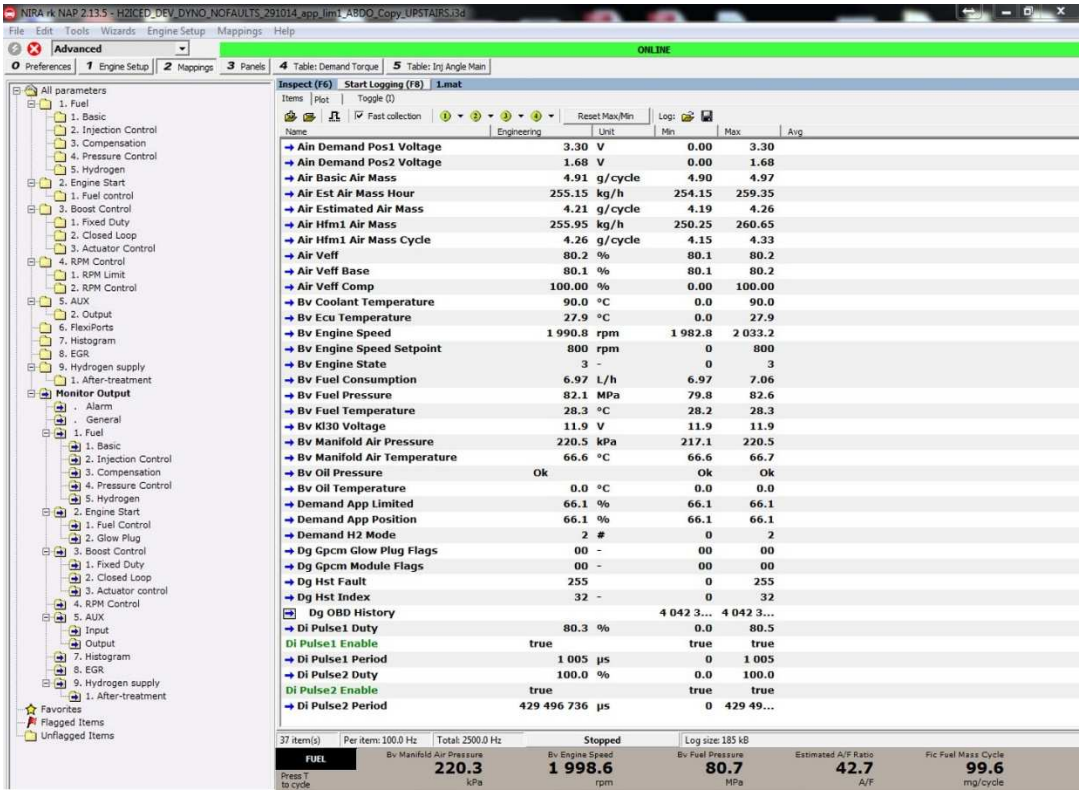


Figure 4.10 A screen-shot of the NIRA-rk user interface.

Type-k thermocouple signals were acquired by a NI-9213 thermocouple module on a cDAQ-9171 Compact DAQ chassis connected directly to the PC through a USB cable. The signals were monitored and recorded in LabVIEW environment. The same set of Kulite PT-2054 and Kulite PT-2028 pressure sensors were used to acquire the different pressure values throughout, but the output signals were fed to X-Series NI USB-6351 16 AIs, high-speed (1 MS/s multichannel), 16-bit resolution ADC card; connected directly to the PC through a USB cable. The signals have been monitored and recorded using LabVIEW. Also, the same arrangement of Kistler 6055C piezoelectric pressure sensors and Kistler 5011 charge amplifiers were used to measure and manipulate the in-cylinder pressure data from cylinders 1 and 3. Likewise, the same W2D11R Hohner incremental optical shaft encoder has been used to monitor the crankshaft position. The output signals have been fed to the X-Series NI USB-6351 high-speed card and then to the PC to obtain the crank angle-synchronized in-cylinder pressure data in LabVIEW. Figure 4.11 illustrates a schematic diagram of the measurement circuits for the different variables of CR-Engine.

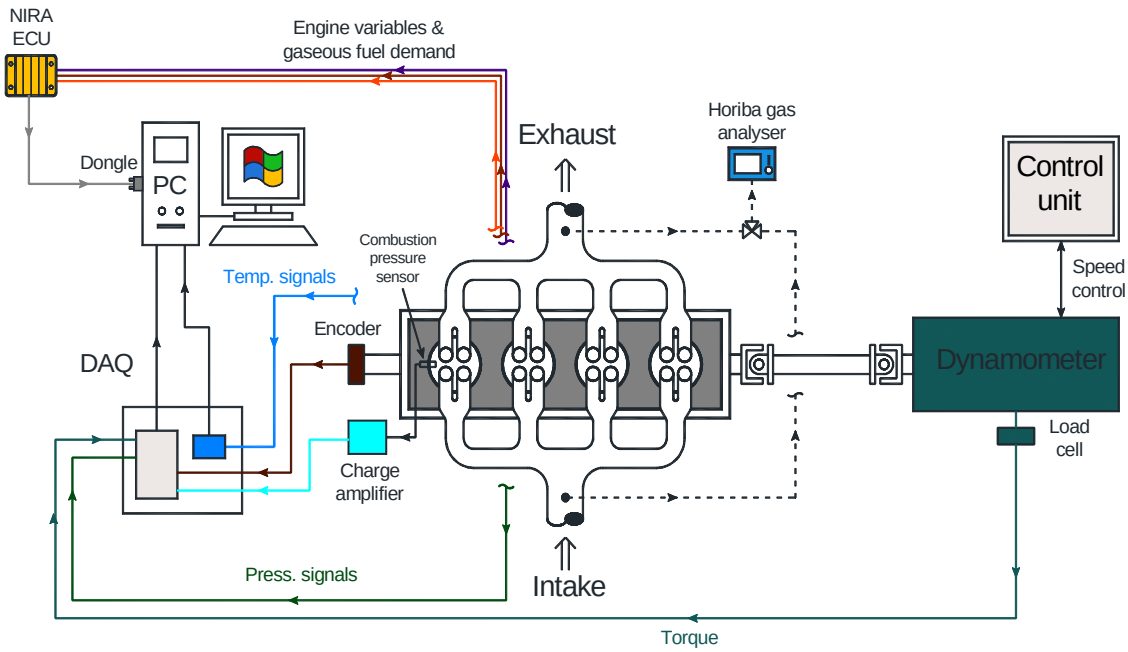


Figure 4.11 Schematic diagram of the test rig instrumentations and measurement circuits for CR-Engine. Not to scale.

4.3 Data Collection and Processing

4.3.1 Determination of the top dead center (TDC)

The accuracy of the volume calculation primarily depends on the accuracy of both the clearance volume measurement and the crank angle determination [193]. The accuracy indicated work and indicated mean effective pressure (IMEP) calculations relies on the accurate alignment of the measured pressure and the corresponding change in volume [39]. This alignment depends on the shaft encoder's TDC marker pulse, i.e. the "Index-Z" signal, being very carefully aligned to the engine's true cylinder 1 TDC point.

To obtain a first "rough" alignment, the true TDC of cylinder 1 is checked using a DTI gauge riding on the number 1 piston through the injector hole as shown in Fig. 4.12 (a). It is highly recommended that this procedure is applied to cylinder 1 in particular as it is the one immediately next to the shaft encoder, and hence any potential errors in the TDC determination caused by torsional vibrations are avoided [194]. Once this point is visually found, the shaft encoder is turned to its TDC pulse position then locked to the crankshaft pulley via an adapting hub. This process, referred to as "static determination of TDC", is accurate to no less than one crank angle degree. This could be insufficient

for IMEP measurement accuracy; it has been reported that each one degree offset of the crank angle position from the actual TDC results in 5% error in the corresponding value of IMEP [195]. In view of that, a dynamic TDC, i.e. actual TDC that takes into account piston stretch and crankshaft twist, has to be found. This is carried out by using "OT-Sensor-428" capacitive TDC probe, by AVL, to measure any phase difference between encoder's TDC pulse and piston's actual TDC point with the engine running. As shown in Fig. 4.12 (b), the probe is inserted into the injector hole of cylinder 1 through a special adapter, then fixed with its end very close to the piston at the TDC. This proximity probe outputs a voltage signal proportional to the closeness of the piston crown and the probe end. The engine is then motored through the dynamometer at an arbitrary speed around 1000 rpm, while the probe signal as well as the encoder TDC marker pulse, i.e. "Index-Z" signal, are acquired together then processed through a dedicated LabVIEW program. The software then processes the two signals then outputs the phase difference between the dynamic TDC of cylinder 1, and the falling edge of the shaft encoder TDC pulse (as this was the triggering instant of the data acquisition process). This phase difference was found to be 1.7 CA degrees after the true TDC. This was subsequently accounted for in data presentation and processing.



(a) **(b)**

Figure 4.12 The determination of the TDC; (a) the use of a DTI gauge for a rough estimation of the TDC, and (b) fining the true TDC using the AVL capacitive probe.

4.3.2 Synchronization of in-cylinder pressure and crank angle data

- *Align the in-cylinder pressure traces.*

In order to synchronize the cylinder pressure data with the crank angle (and hence with the corresponding cylinder volume), it is essential to determine exactly at what point in the engine thermodynamic cycle data acquisition process has started. As mentioned in section 4.2.2, the shaft encoder's TDC pulse (the "Index-Z" signal) was used to trigger the data acquisition. This has the disadvantage that the recorded data may begin at either compression TDC or exhaust TDC. Therefore, it is first required to determine at which TDC the data acquisition process has started. To accomplish this, the 1st data point (that corresponds to angle zero) is compared to the 720th point (that corresponds to the angle 360 as the encoder resolution is 0.5º CAD). The pressure value is greater at compression TDC than that at exhaust TDC as the valves are closed. Consequently, if the pressure value at the 1st point is greater than that at the 720th point, the triggering signal is taking place at the compression TDC. If the opposite is correct, it is the exhaust TDC that the triggering signal was occurring at. It is preferred to start acquisition from the exhaust TDC, so the presented data will show the complete engine thermodynamic cycle from the beginning, i.e. from the intake stroke, with the peak pressure value around the 360º CA and not at the start or the end of the cycle.

For the four-cylinder engines, it is desirable to align the four-cylinder pressure traces with each other rather than plotting them with the 180º phase shift. The LabVIEW code has been developed to automatically account for that phase shift every cycle. If the comparison between the 1st and the 720th data points of the cyl-1 pressure trace yielded that the acquisition has been triggered at its exhaust TDC, the code will automatically acquire the four-stroke pressure data of cyl-1 from angle zero to angle 720, while it will acquire that of cyl-3 from angle 180 to angle 900 (180º shift), and so on (for the firing order 1-3-4-2). Alternatively, if the comparison has yielded that the acquisition has been triggered at cyl-1 compression TDC, the firing order dictates that it is cyl-4 that is at it exhaust TDC, and hence the acquisition process starts with that cylinder; followed by the others in accordance with the firing order (again; with the 180º shift). The alinement process has been done in real-time automatically through the LabVIEW code so to yield the aligned data. The code has also been designed such that the triggering process is

repeated at every individual cycle. That is, each full thermodynamic cycle for the four cylinders has been triggered with a reset encoder's TDC pulse (or "Index-Z" signal); independently of the preceding cycles. This is because in real-time acquisition there is a chance that a noise spike or spurious electrical pulse might be counted as a sample clock (or "Index-A" signal). If this happens, then the recorded crank angle (and hence the calculated cylinder volume) will be out-of-synchronization with the pressure traces. If the data acquisition process relies solely on the first TDC signal at the very beginning, then any of these spurious events could build up over the subsequent engine cycles, and the measurement could become progressively out of synchronization.

- *Referencing the in-cylinder pressure to an absolute value.*

Piezoelectric transducers produce an electrical output only when a change in state is experienced; that is, they cannot perform true static measurements [195]. This type of transduces suffers various types of drifts and outputs a charge relative to the change in pressure levels, and not an absolute value. To obtain the absolute value of the cylinder pressure, the data has to be referenced to a known pressure at some point in the engine cycle. This process is known as "pressure pegging". While several methods for pressure pegging have been studied [196, 197], one most common approach that was employed in the present study is to set a point within the engine cycle to a known (or estimated) pressure. It has been found that referencing the in-cylinder pressure at the intake bottom dead center (BDC) to the intake MAP gives best results [198]. This method is quick and simple, yet it is only accurate for engines with unturned intake systems while it yields inaccuracies with engines having tuned-intake systems [199]. Alternatively, the in-cylinder pressure at the exhaust top dead center (TDC) may be referenced to the exhaust pressure (in absolute). The developed LabVIEW code automatically applies the referencing process on the acquired pressure data and enables the user to determine whether it is requested to refer to the MAP or the exhaust manifold pressure, and based on the selection it refers to the corresponding data point of the complete thermodynamic cycle. That is, if the in-cylinder pressure is requested to be referenced to the MAP, then the code sets the value of the in-cylinder pressure at the intake BDC (i.e. the 360^{th} data point) to be equal to the MAP at the same instant. When it requested to reference to the exhaust manifold, instead, it is the exhaust TDC (i.e. the 1440^{th} point) that is set to be

equal to the exhaust pressure at that time. To eliminate the inertia effects of the charge entering the cylinder at the end of the intake stroke (or leaving it at the end of the exhaust stroke) as well as the effect of any fluctuation in the manifold pressure signal, the code has a controllable referencing window, through which it is possible to take the average of a certain number of points, taken equally on the two sides of either the intake BDC or exhaust TDC; rather than taking only the central point. There is a provision by the LabVIEW code used in this work for concatenating two complete thermodynamic cycles, to accommodate the cases where the referencing window lies at the end of any particular cycle.

Referencing the cylinder pressure to an absolute value on a cycle-to-cycle basis is also useful in overcoming inherit nature of piezoelectric transducers to drift. Drift is defined as any undesirable change in the output signal over the time that is not a function of the measured variable [200]. This could lead to a considerable error of the measured signal over the course of time. This type of drift, aka inter-cycle drift [199], can be eliminated by short-term pegging (every cycle) of the cylinder pressure to the reference pressure. Yet, another type of drift, which is the drift that occurs between the beginning and the end of each cycle (aka the intra-cycle drift [199]) still exist, but has been found of tiny effect with the transducer used in the present work. One major source of piezoelectric pressure transducer drift is what is referred to in the literature as the “thermal shock”; a phenomenon in which the cyclic exposure of the transducer to the combustion event in IC engine results in contraction and expansion of its diaphragm as a result of the large temperature variation during each cycle [201]. This causes the force acting on the quartz to be different from that applied actually by the cylinder pressure alone for a particular part of the cycle. A number of ways have been proposed to reduce the effect of thermal shock; e.g. the use of water cooling, heat shields, and coating the transducer membrane [202]. Other sources of transducer drift include the vibration that may cause the quartz element to yield a measurement error, and the infinitesimal deformation of the cylinder during the engine working cycle that could result in a corresponding deformation in the transducer itself [203]. However, as these are very difficult to account for, the present work has only relied on the real-time pegging to eliminate the inter-cycle drift.

4.3.3 In-Cylinder pressure data post-processing

The processing of cylinder pressure data gives insights into several parameters; such as the indicated mean effective pressure (IMEP), rate of pressure rise (ROPR), heat release rate (HRR), ignition delay (ID), start of combustion (SOC), and many others [204]. The challenge here is to first obtain the cylinder pressure data with high accuracy, eliminate any undesirable pulsations, and characterize the unaccounted noise on a cycle-to-cycle basis [205]. Flow processes inside the engine cylinder are turbulent and there are local fluctuations in the flow field; resulting in cycle-to-cycle variation in the mean flow of cylinder [39]. Also, the manufacture and operation of individual fuel injectors are not identical, and there is a slight variation in fuel mass injected from cylinder-to-cylinder and from cycle-to-cycle [39]. Test-to-test analysis has been conducted to determine the number of consecutive cycles required to attain a stabilized average for the in-cylinder pressure data. A total number of 50 cycles has been found to achieve this for different test conditions examined with good repeatability. The position of the mean average of the 50 cycles relative to all cycles recorded is shown in Fig. 4.13.

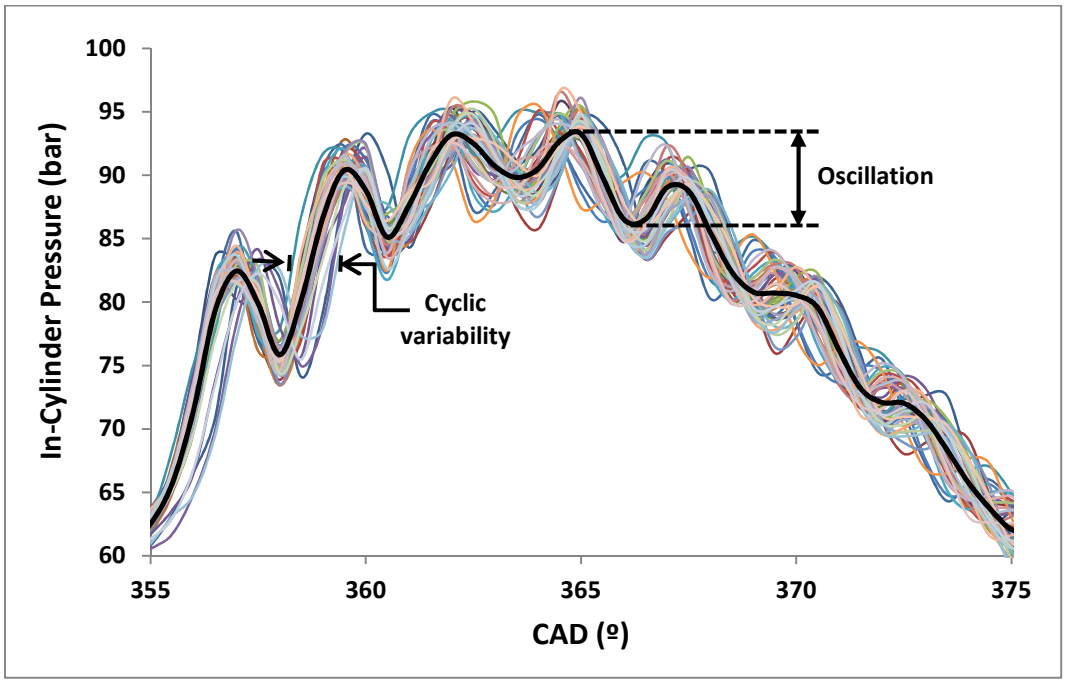


Figure 4.13 **Cyclic variability for diesel fuel operation; at 2000 rpm and 4 bar BMEP. A total number of 50 consecutive cycles are presented; the thick black line represents the mean average. Oscillation in the pressure wave is also shown.**

The figure shows that the maximum cyclic variability is of the order of 1º CA; meaning a maximum error of 0.5º CA on either side of the mean average cycle. In addition to the cyclic variability, an oscillation of cylinder pressure traces can be clearly observed in Fig. 4.13. This is attributed to the incidence of an abrupt pressure rise after the SOC which induces transient vibrations as it excites the natural resonance of some of the hardware components in the measurement system. This phenomenon was encountered with both engines tested in the present work, which suggests that it is related to the configuration of the pressure transducer mounting [206] rather than to the combustion chamber cavity [207]. It is recommended to mount the transducer such that its tip is as flush as possible with the cylinder head (the combustion chamber); full flush mounting is not practical as it will totally expose the measuring diaphragm to the very harsh environment, unless a thermos-protection shield is used [208]. However, if it is not possible to machine the cylinder head to flush-mount the pressure transducer, a special adapter in the shape of glow plug is generally used to provide access to the combustion chamber and also to support the transducer. With a typical glow-plug size abound 4mm diameter, the small pressure transducer cannot be flush mounted in most cases; instead, there will be a short passage between combustion chamber boundary and the transducer tip. The concept is illustrated by the schematic diagram in Fig. 4.14. This has been the case with the present work; Fig. 4.15 presents a photo of the transducer alongside the glow plug adapter used, and how they fit together as per manufacturer's standards [209]. Non-flush-mounting of pressure transducers is commonly associated with the incidence of resonant waves in the narrow access passage between and the combustion chamber and the transducer tip; if the natural frequency of the passage is less than the maximum desired frequency of interest of the transducer [205]. This introduces undesirable noise to the signal that highly hinders obtaining meaningful heat release rate (HRR) data from the recorded cylinder pressure signal. As shown by equation (4.10), heat release rate term involves a derivative of the pressure term, and thus any error or high-frequency noise in the pressure data results in a massive distortion in the heat release rate data. Figure 4.16 illustrates an example of the effect of the presence of noise in the pressure signal on heat release rate.

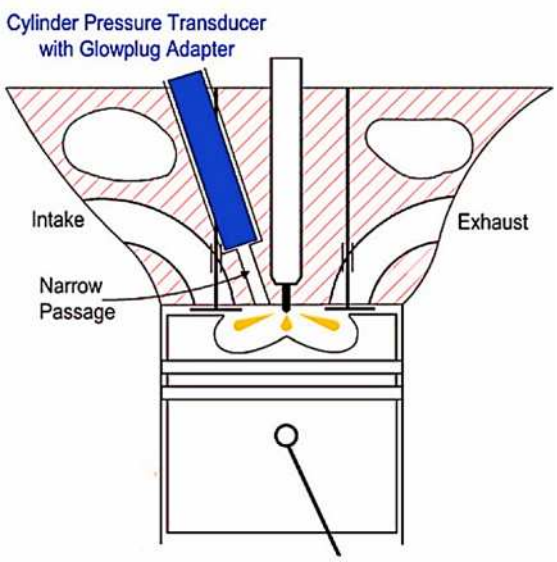


Figure 4.14 A schematic shows the layout of fitting the pressure transducer into the glow plug adapter. The small diameter of the adapter at its end forms a narrow passage between the combustion chamber and transducer tip. Adapted from [206].

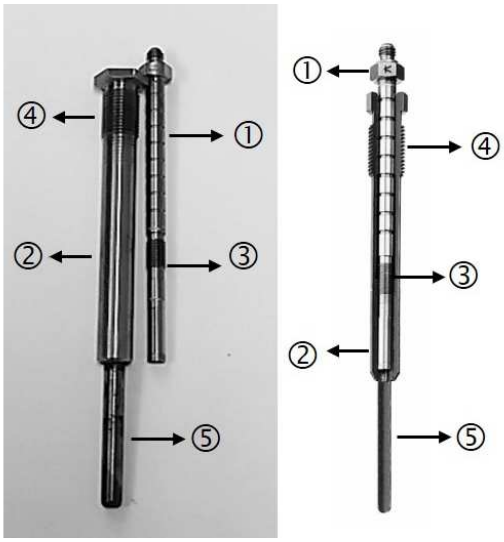


Figure 4.15 A photo of the transducer used in the present work (#1), along with the glow plug adapter (#2). They join together by a thread (#3) while the adapter holds to the cylinder head via external thread (#4). The narrow passage is (#5). Cross-sectional drawing is adapted from [209].

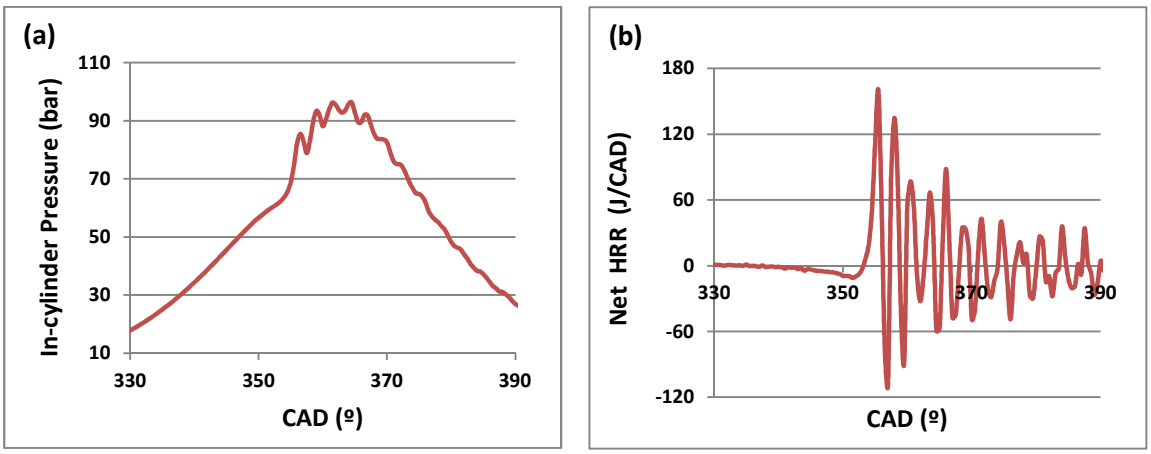


Figure 4.16 (a) Noisy pressure data; for diesel fuel operation at 2000 rpm and 4 bar BMEP, and (b) the derived heat release rate (HRR).

The fundamental resonant frequency for the access passage is given as [206]:

$$f_n = \frac{c}{4L} \tag{4.1}$$

where (f_n) is the passage resonant frequency; (Hz),

(c) is the speed of sound of the gas at noise incidence conditions; (m/s),

(L) is the length of the access passage; (m),

The speed of sound for gas is estimated from the equation:

$$c = \sqrt{\frac{\gamma \bar{R} T}{M}} \tag{4.2}$$

where (γ) is the specific heat ratio of the gas,

$(\bar{R})$ is the universal gas constant; (J/kg.k),

(T) is the gas absolute temperature; (k),

(M) is the apparent molar mass of the gas; (kg/kmol).

For the cases examined in the present work, the speed of sound of the in-cylinder gas at noise incidence conditions has been around 640 m/s for an absolute gas temperature of around 1100 k. The measured length of the access passage is 36.9 mm. From Eq. (4.1), the estimated value of the fundamental resonant frequency of the access passage is around 4.35 kHz. When there is no mass exchange between the combustion chamber and the access passage, gas temperature is about 420 K, which yields a speed of sound ≈400 m/s and a wave frequency of about 2.72 kHz.

An attempt has been made to correlate the frequency of the sound waves generated due to access passage resonance with the peak noise frequency that actually appears on the recorded pressure signal. This has been done by analyzing the recorded pressure signal in the frequency domain using a Fast Fourier Transform (FFT) algorithm in a MATLAB environment. Power spectral density (PSD) curve is constructed for the pressure signal to have an insight into the frequency components of the signal. It has been found that the peak noise frequency of the pressure signal is around 4.3 kHz, which almost equals the resonate frequency of the access passage. However, the noise component starts to dominate over the pressure signal itself at fairly lower frequency [205].

To eliminate the undesired noise components from the signal, a filtering algorithm has been developed in MATLAB environment. The filter parameters; such as the filter type, the pass-band characteristics, the order of the filter, and the cut-off frequency have been carefully selected. A Butterworth filter has been selected as it has the flattest pass-band response [210]. Since most of the noise, as well as resonant frequency components, are predominantly in the high-frequency zone [202], a low-pass filter was employed. To attain high rates of noise attenuation without increasing the complexity of the process, the filter was set to be of the third order. The cut-off frequency has been determined as

the frequency corresponding to the incidence of fluctuation in the PSD; particularly an increase in the slope of the decreasing curve, as this implied that the noise component began to dominate over the combustion frequency component [211]. Figure 4.17 shows the PSD of the pressure signal presented in Fig. 4.16 (a), the methodology of specifying the cut-off frequency (≈2.7 kHz), and the peak noise frequency (≈4.3 kHz).

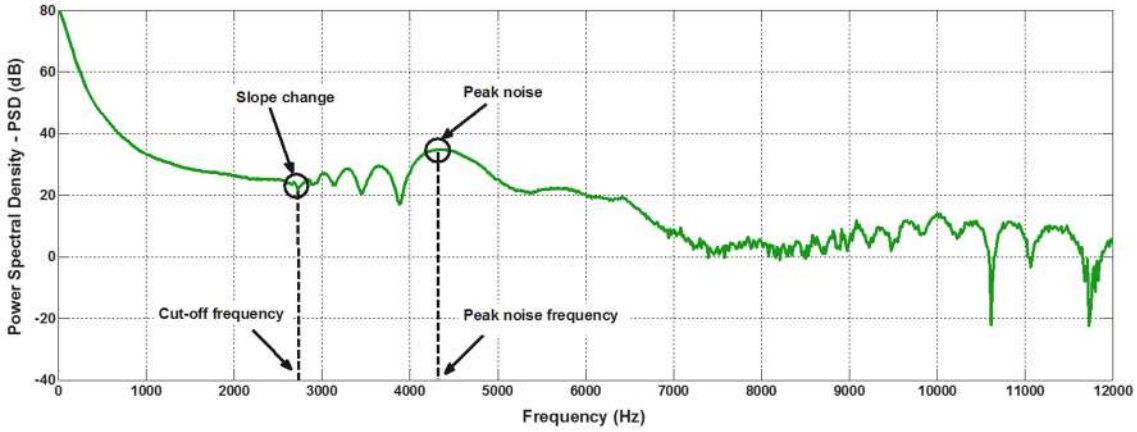


Figure 4.17 **Power spectral densities (PSD) of the noisy pressure signal, the methodology of the determination of the cut-off frequency, and the peak noise frequency.**

Following this assessment, the proposed filter has been applied to the noisy pressure data to attenuate the high-frequency noise. Subsequent post-processing of the filtered pressure data was proved to yield meaningful HRR data; as shown in Fig. 4.18.

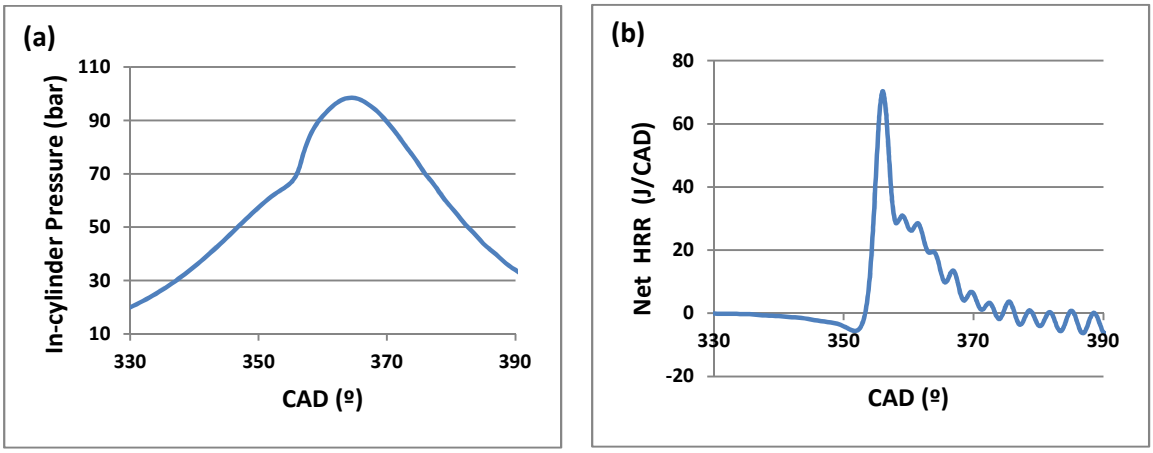


Figure 4.18 **(a) Filtered pressure data; for diesel fuel operation at 2000 rpm and 4 bar BMEP, and (b) the derived heat release rate (HRR).**

4.3.4 Heat release rate (HRR) analysis

Heat release rate (HRR) analysis has been the main combustion diagnostic used in the present work. Thermodynamic-based zero-dimensional single-zone combustion model has been employed. The calculations are mostly taken and adapted from Heywood [39]. The measured cylinder pressure data has been used to tune the model. This particular type of models was employed as it is fairly simple meanwhile it gives consistent results with reasonable accuracy [30].

HRR analysis computes how much heat would have to be added to the cylinder content, in order to produce the observed pressure variation [40]. In-cylinder pressure changes with crank angle as a result of cylinder volume change, combustion of fuel, heat transfer to the chamber walls, flow into and out of crevice regions, and leakage; where the first two of these effects are the largest [39].

If the first law of thermodynamics is applied to the cylinder content, the fuel's chemical energy released by combustion is given by:

$$\delta Q_{ch} = dU + \delta W + \delta Q_{ht} + \sum_i \dot{dm}_i \, h_i \tag{4.3}$$

where (δQ_{ht}) is the heat transfer to the cylinder walls, and $(\dot{dm}_i)$ and (h_i) are the mass flux flowing into or out of the system and the enthalpy of that flux; respectively.

Omitting the crevice flows and blow-by effects for simplicity, and considering that the sensible enthalpy of injected fuel is negligible compared to the sensible internal energy of the cylinder charge, equation (4.3) may be written as:

$$\delta Q_{ch} = dU + \delta W + \delta Q_{ht} \tag{4.4}$$

The change in internal energy can be calculated from:

$$dU = mc_v dT \tag{4.5}$$

From the equation of state $(pV=mRT)$, it yields:

$$mdT = \frac{1}{R}(pdV + Vdp) \tag{4.6}$$

Substituting equation (4.6) into equation (4.5) gives:

$$dU = \frac{c_v}{R}(pdV + Vdp) \tag{4.7}$$

Substituting equation (4.7) into equation (4.4); noting that the work exerted is expressed by *(δW=pdV)*, the heat released by combustion of the fuel is given on an incremental angle basis as:

$$\frac{dQ_{ch}}{d\theta} = \frac{c_v}{R}\left(p\frac{dV}{d\theta} + V\frac{dp}{d\theta}\right) + p\frac{dV}{d\theta} + \frac{dQ_{ht}}{d\theta} \tag{4.8}$$

which is also known as the gross heat release rate ($\frac{dQ_{gross}}{d\theta}$). If semi-perfect gas behavior is assumed; such that ($c_p - c_v = R$) and ($\frac{c_p}{c_v} = \gamma$), then equation (4.8) may be written as:

$$\frac{dQ_{gross}}{d\theta} - \frac{dQ_{ht}}{d\theta} = \frac{1}{\gamma-1}\left(p\frac{dV}{d\theta} + V\frac{dp}{d\theta}\right) + p\frac{dV}{d\theta} \tag{4.9}$$

or:

$$\frac{dQ_{net}}{d\theta} = \frac{\gamma}{\gamma-1}p\frac{dV}{d\theta} + \frac{1}{\gamma-1}V\frac{dp}{d\theta} \tag{4.10}$$

where:

($\frac{dQ_{net}}{d\theta}$) is the net heat release rate; (Joule/CAD),

(θ) is the crank angle in degrees (CAD),

(p) is the in-cylinder pressure at that angle; (Pa),

(V) is the gas volume at that angle; (m^3),

(γ) is the specific heat ratio.

Based on the basic geometric properties of reciprocating engines [39], the gas volume *(V)* at a certain piston position is determined from [212]:

$$V = A_p \,.S + V_c \tag{4.11}$$

where:

(A_p) is the top area of the piston (m^2); $A_p = \frac{\pi}{4}.B^2$; where *(B)* is the cylinder bore; (m)

(V_c) is the clearance volume (m^3); $V_c = \frac{A_p.l}{r-1}$; where *(l)* is the stroke length; (m) , and *(r)* is the compression ratio,

(S) is the piston displacement from the TDC (m).

The piston displacement is calculated from [212]:

$$S = R[1 - \cos(\theta_{rad})] + L\left\{1 - \sqrt{1 - \left[\frac{\sin(\theta_{rad})}{\frac{L}{R}}\right]^2}\right\} \tag{4.12}$$

where:

(R) is the radius to crank pin; (m),

(L) is the connecting rod length; (m),

(θ_{rad}) is the argument of trigonometric function; (radians).

Precise alignment between the encoder TDC and the piston TDC is a prerequisite for accurate heat release determinations. If the two TDCs are misaligned; i.e. shifted, by a phase angle degrees, then the value of *(θ_{rad})* is determined from:

$$\theta_{rad} = \frac{\pi(\theta - 360 + \theta_{phase})}{180} \tag{4.13}$$

where

(θ) is the crank angle; (degrees),

(θ_{phase}) is the phase shift angle; (degrees).

The specific heat ratio *(γ)* varies with the variation of gas temperature, and it can be calculated from the following equation:

$$\gamma = \left(1 - \frac{R}{C_p}\right)^{-1} \tag{4.14}$$

where *(C_p)* is the specific heat of the gas at constant pressure; (J/kg.k). The value of $\left(\frac{R}{C_p}\right)$ can be calculated from:

$$\frac{R}{C_p} = (A_0 + A_1 T + A_2 T^2 + A_3 T^3 + A_4 T^4)^{-1} \tag{4.15}$$

where *(T)* is the absolute bulk gas temperature; calculated from the equation of state, and *(A_0)*, *(A_1)*, *(A_2)*, *(A_3)*, and *(A_4)* are constants; where their values are [212]:

A_0 =3.04473; A_1 =1.33805e^{-3}; A_2 = –4.88256e^{-7}; A_3 =8.55475e^{-11}; A_4 = –5.70132e^{-15}

Following the sequence of equations highlighted above, the net heat release rate can be directly obtained from equation (4.10). If the gross heat release rate is required, two separate models for the heat transfer to cylinder walls and the crevice flows should be added to the net heat release rate calculations. Principally, the present work employed the net heat release analysis, as opposed to the gross heat release analysis, to investigate the in-cylinder behavior; since the former is based upon fewer assumptions and it has less complexity. However, an approximated gross heat release analysis was conducted for selective cases to illustrate some basic concepts. In such analysis, only the heat transfer to the cylinder walls was calculated, as it accounts for about 10 to 25% of the

total heat release; while the crevice flows were neglected as they only account for 1 to 2% of the total heat release [39].

Heat transfer process in engine cylinder takes place through a combination of different modes; conduction, convection, and radiation. However, heat transfer from the cylinder charge to the wall is mainly by convection [39].

The rate of convection heat transfer is calculated, based on Newton's law of cooling [213], from the equation [39]:

$$\frac{dQ_{ht}}{dt} = h_c . A_w . (T - T_w) \tag{4.16}$$

where *(h_c)* is the convection heat transfer coefficient; (J/s.m^2.k),

(A_w) is the combustion chamber wall area (m^2); $A_w = 2A_p + \pi B.S$,

(T_w) is the effective wall temperature; (K). A value of T_w=485 K was found to give satisfactory results [212].

Heat transfer in reciprocating engines is a non-uniform and unsteady phenomenon since heat fluxes between fluids and metal surfaces vary during the engine operating cycle in time and space. In-cylinder heat fluxes vary between few MW/m^2 during combustion and near zero or even negative values during the intake stroke [214]. Several empirical correlations have been developed to estimate heat fluxes in engine cylinder, where these correlations provide a heat transfer coefficient representing a spatially-averaged value for the cylinder, and consequently, they are commonly referred to as global heat transfer models [215, 216]. The most known ones were inventoried by Borman and Nishiwaki [217]; among which those developed by Eichelberg [218], Annand [219], Woschni [220], and Hohenberg [221] are commonly used. In the present work, Eichelberg correlation [218] was employed as it only depends on the cylinder pressure, gas bulk temperature, and mean piston speed; while it is free from any other variant coefficients. The Eichelberg correlation for the heat transfer coefficient is:

$$h_c = 7.67 \times 10^{-3} . S_p^{(1/3)} . (P.T)^{(1/2)} \tag{4.17}$$

where *(S_p)* is the mean piston speed (m/s); $S_P = \frac{2R.\omega}{\pi}$, where (ω) is the crankshaft speed; (rad/s), or equivalently, $S_P = \frac{2l.N}{\pi 60}$, where (N) is the engine speed; (rpm).

The heat transfer to the cylinder wall can then be calculated on an incremental angle basis; i.e. in units of Joule/CAD, from:

$$\frac{dQ_{ht}}{d\theta} = \frac{h_c.A_w.(T-T_w).\ 60}{360N} \tag{4.18}$$

Combining the results of equations (4.10) and (4.18), approximated gross heat release rate is obtained on incremental angle basis; i.e. Joule/CAD. The two instantaneous rates of heat release; i.e. the net and the gross, are calculated and plotted at each incremental crank angle degree throughout the engine cycle. Meanwhile, the cumulative heat release profiles are made by integrating the instantaneous rates over the complete combustion process. The ultimate value of the cumulative gross heat release should equal, within a few percent only, the mass of fuel injected times the fuel lower heating value [39]. That is:

$$Q_{gross} = \int_{\theta_{c,s}}^{\theta_{c,e}} \frac{dQ_{gross}}{d\theta} d\theta \approx m_f \times LHV_f \tag{4.19}$$

The difference between the two values is owing to the combustion inefficiency, which is usually less than 2% in diesel engines [39]. The present analysis demonstrated good consistency between the two values, but with difference slightly higher than 2%; where this was attributed to the omitting of the crevice flows and fuel vaporization and heat-up effects in the employed model.

Figure 4.19 (a) shows an example of the two instantaneous rates of heat release; i.e. the net and the gross, while (b) presents the corresponding cumulative heat release curves. The characteristics of the heat release profile are discussed in details in the next chapter.

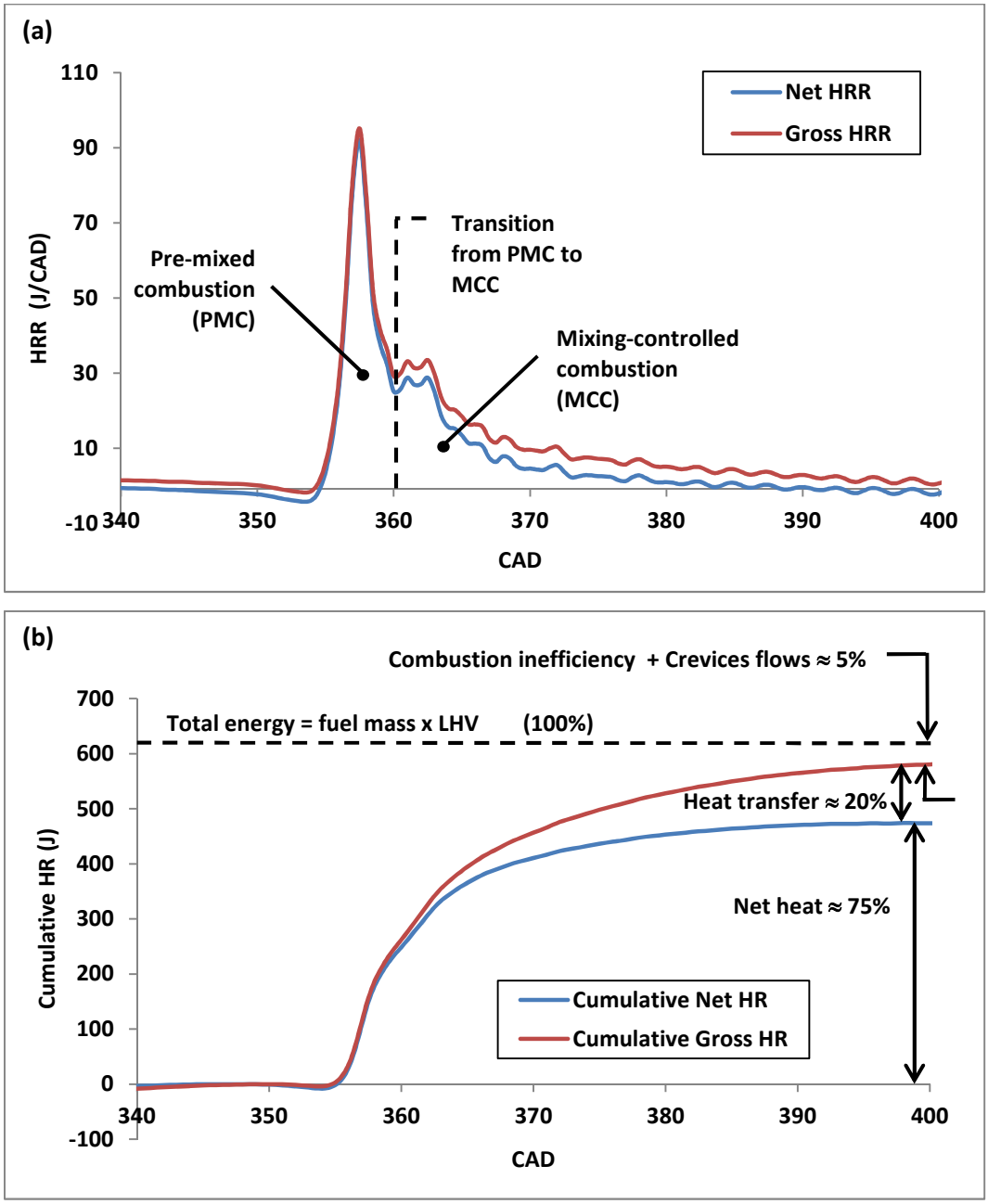


Figure 4.19 **(a) A plot of the instantaneous rates of HR; the net and the gross, and (b) the corresponding cumulative HR curves; illustrating the relative magnitudes (approx.) of the net HR, the heat transfer to the wall, and the combustion inefficiency and crevices flows; with respect to the fuel's chemical energy. Data presented is for diesel fuel operation at 1500 rpm and 3 bar BMEP.**

The accuracy of the heat release model employed was verified through applying the equations to the pressure trace obtained at engine motoring conditions. In the absence of combustion, the instantaneous rate of gross heat release should equal zero throughout the engine cycle. This has been shown to be the case in the present work, with negligible

error; as demonstrated by Fig. 4.20. The difference in magnitude between the gross and the net HRR shown in the figure stands for the heat transfer to the cylinder wall, caused by the elevated temperature of charge as a result of the polytropic compression process with a polytropic exponent of 1.3 (±0.05%) [39].

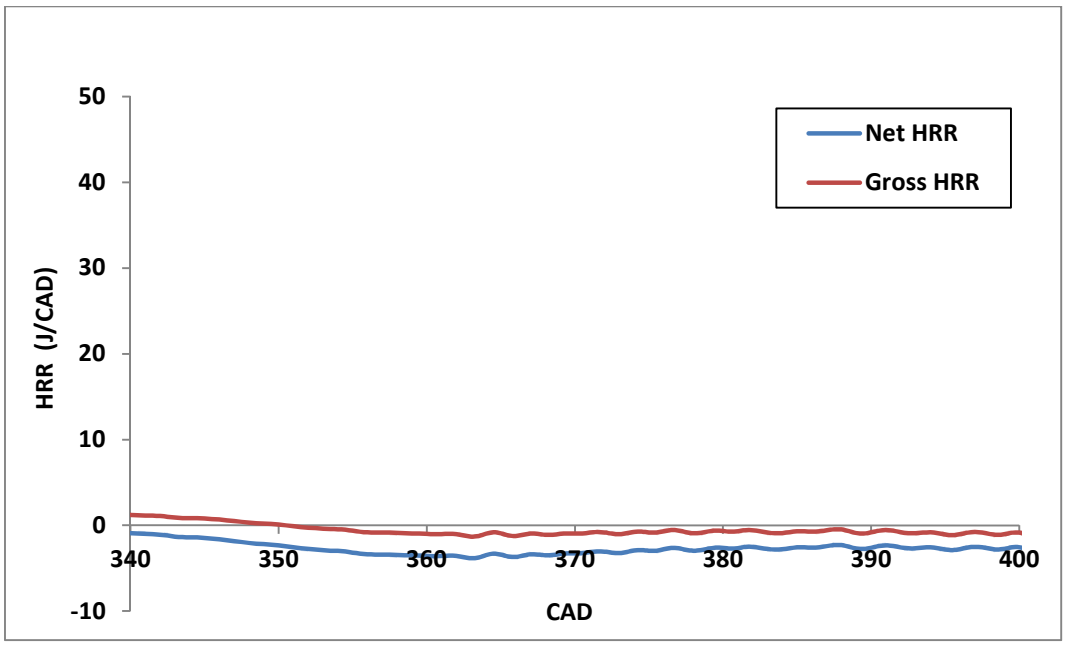


Figure 4.20 **A plot of the instantaneous rates of HR; the net and the gross, at engine motoring conditions. The difference in magnitude between the two curves stands for the heat transfer to the cylinder wall caused by the elevated temperature of the charge as a result of the polytropic compression. Data presented is for engine motoring at 1500 rpm.**

The variation of heat release profile with operating conditions reveals vital information on the change of combustion phasing, burning rate, and effectiveness of fuel conversion processes with operating conditions [222]. Examples of heat release rate (HRR) profiles for selective cases at low, intermediate, and high load conditions at fixed engine speed and injection timing are given in Figures 4.21, 4.22, and 4.23, respectively. It could be seen that the overall combustion process in CI engines is characterized by the presence of four stages; typically, the ignition delay (ID), pre-mixed combustion (PMC), mixing-controlled combustion (MCC), and late combustion. Each stage is usually recognized on the HRR profile, although different stages vary significantly in relative magnitudes, duration, and overall shape with operating conditions [39, 40].

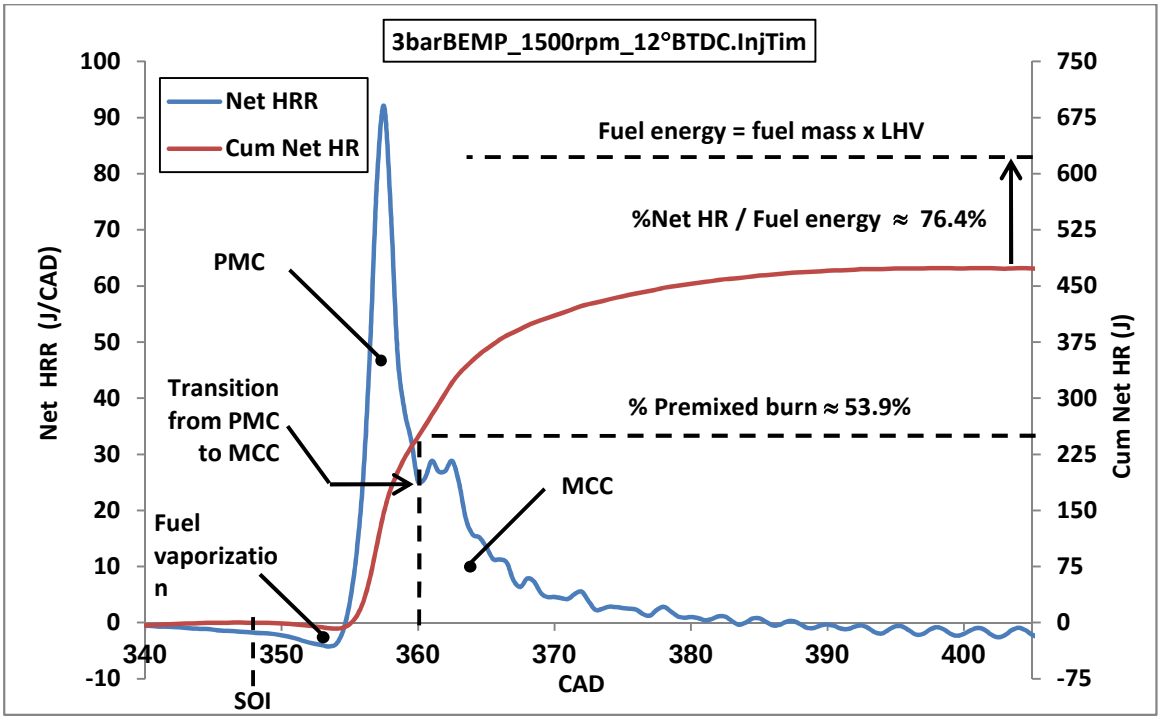


Figure 4.21 An example of net HRR and cumulative net HR curves at low load conditions; illustrating the key phases of HR profile. Data obtained from DP-Engine.

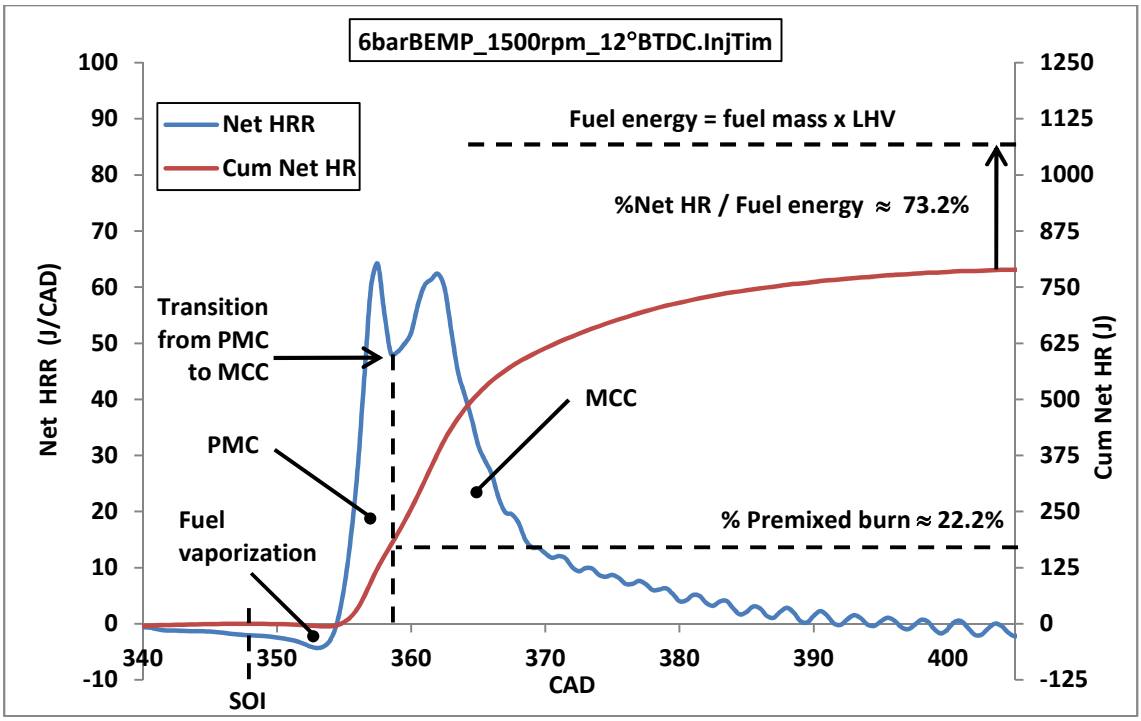


Figure 4.22 An example of net HRR and cumulative net HR curves at medium load conditions; illustrating the key phases of HR profile. Data obtained from DP-Engine.

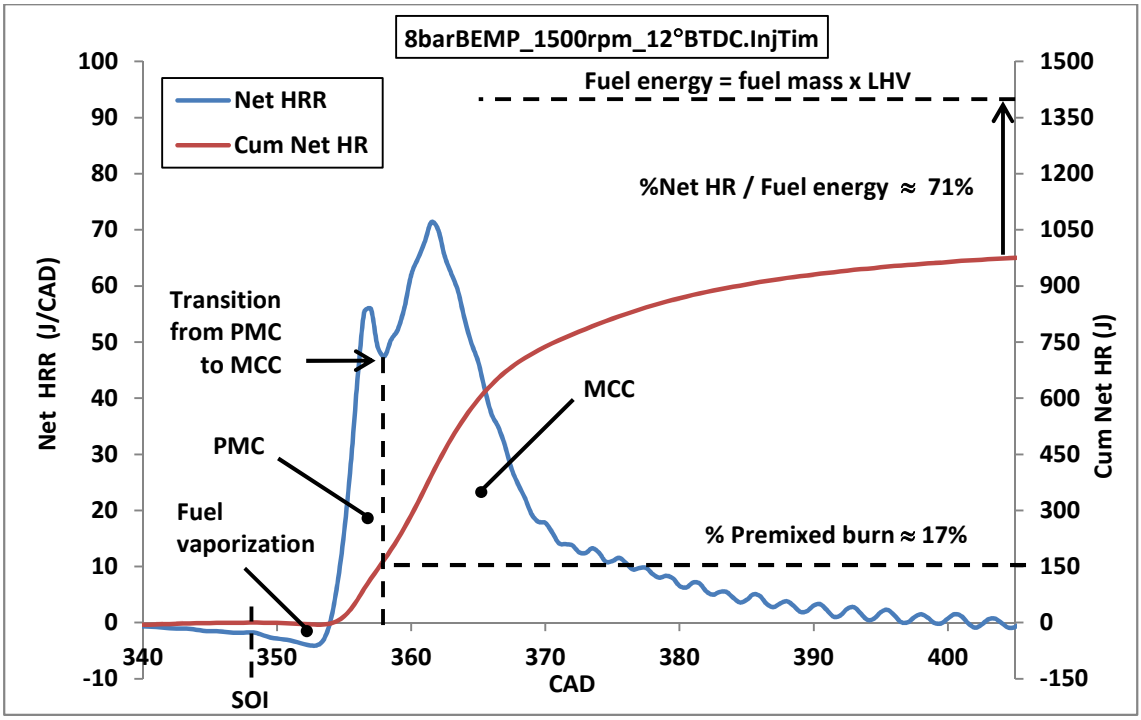


Figure 4.23 An example of net HRR and cumulative net HR curves at high load conditions; illustrating the key phases of HR profile. Data obtained from DP-Engine.

It can be seen that the net HRR curve falls below zero at the late stages of compression before introducing the fuel into the cylinder. This is attributed to the heat transfer to the cylinder wall, caused by the elevated temperature of the charge following the polytropic compression process. Ignition delay (ID) period begins with the start of injection (SOI). Shortly after SOI, a further drop in the net HRR curve is remarkable where this negative heat release stands for fuel vaporization and heating up. The enthalpy of vaporization of diesel fuel is about 1% of its heating value, while the energy change associated with heating up the fuel vapor from the injection temperature to the typical compression air temperature goes around 3% of the fuel heating value [39]. The heated-up fuel vapor mixes with air, and the fuel/air mixture within flammability limits auto-ignites; where the start of combustion (SOC) indicates the end of the ignition delay and the beginning of what is so-called the pre-mixed combustion (PMC) phase. The SOC was determined in the present work as the CAD at which net HRR reaches 2 J/CAD. This criterion was employed previously in an analogous recent work [223] and demonstrated consistent results.

In the PMC phase, combustion of the fuel/air mixture formed during the ignition delay period takes place rapidly in a few crank angle degrees. When this burning mixture combines with the fuel that becomes ready for burning and burns, indeed, in this phase, inevitable result is the high rates of HR that characterize this phase of combustion [39]. The relative magnitude of this phase varies significantly with operating conditions. For instance, PMC phase is dominant at low load conditions as illustrated by Fig. 4.21. This is attributable to the relatively lower in-cylinder temperature at such conditions and the associated longer ignition delay; which results in the availability of a larger fraction of injected fuel ready for burning when the delay period ends. On the contrary, the shorter ignition delay as the load is increased results in a reduced amount of fuel available for combustion as the delay period ends, and hence the PMC phase is reduced in magnitude and duration, as shown in Figures 4.22 and 4.23 for medium and high load conditions; respectively, with the effect being more pronounced in the latter.

Following the PMC phase comes the mixing-controlled combustion (MCC) phase. The transition from PMC to MCC is defined as the incidence of gradient inflection in the net HRR curve after the PMC spike [223, 224]. In the MCC phase, the burning rate is controlled by the rate at which new fuel/air mixture becomes available for combustion. The relative magnitude of the MCC phase sizably changes with operating conditions. The factors that tend to increase the PMC phase are likely to decrease the MCC phase; and vice versa. Thus, the shorter ignition delay at high and medium loads and the larger amount of fuel used result in the majority of the fuel to be burned in the MCC phase, which becomes the dominant phase of combustion, as shown in Figures 4.22 and 4.23. By the end of this phase, most of the fuel would been burned. The remaining fraction of fuel that has not been burned, and any fraction of energy presented in soot and fuel-rich combustion products, burn in what is called late combustion, in which final burnout processes occurs at lower rates as the temperature decreases during expansion [39].

The premixed burn fraction of total heat release can be estimated from the heat release profile; as the ratio of the cumulative sum of the heat release from the SOC till the point of transition from PMC to MCC, to the total cumulative sum of the heat release until the end of combustion (EOC). The methodology of estimating this value is illustrated in Figures 4.21, 4.22, and 4.23. Also, the percentage of net HR to the total energy supplied to the engine is calculated as the ratio of the ultimate value of cumulative net

HR to the fuel chemical energy; where the difference between the two quantities stands primarily for the heat transfer to the cylinder wall, in addition to the crevice losses and combustion inefficiency. It can be seen that this ratio reduces as the engine load is increased; where this is attributed to the increased heat transfer to the cylinder wall as a result of the elevated temperature inside the combustion chamber at higher loads.

The HRR results above were obtained from the DP-Engine, while the diesel fuel was injected into the cylinder at one. When it comes to the CR-Engine, it is acknowledged that one of the most important characteristics of the high-pressure common-rail (HPCR) is the ability to use multiple injections per cycle. Splitting the diesel fuel injection into a pre-injection succeeded by the main injection could bring several benefits to the engine performance and emissions [224]. This was investigated to assess the potentials of applying such a technique in the gas-diesel dual-fuel engine operation in the later stages of the work. To examine the influence of pre-injection, the engine was run at steady state of constant speed and load of 1500 rpm and 3 bar BMEP, respectively, with two injection strategies. The first one introduces the total diesel fuel injected at once at 12° BTDC, while in the other strategy the fuel injection is split into a pre-injection (presents 10% of the total fuel), followed by the main injection. The injection timing of the main injection was held at 12° BTDC, while the interval between the two injections was set to 12°. Figure 4.24 shows the net HRR profiles for both injection strategies.

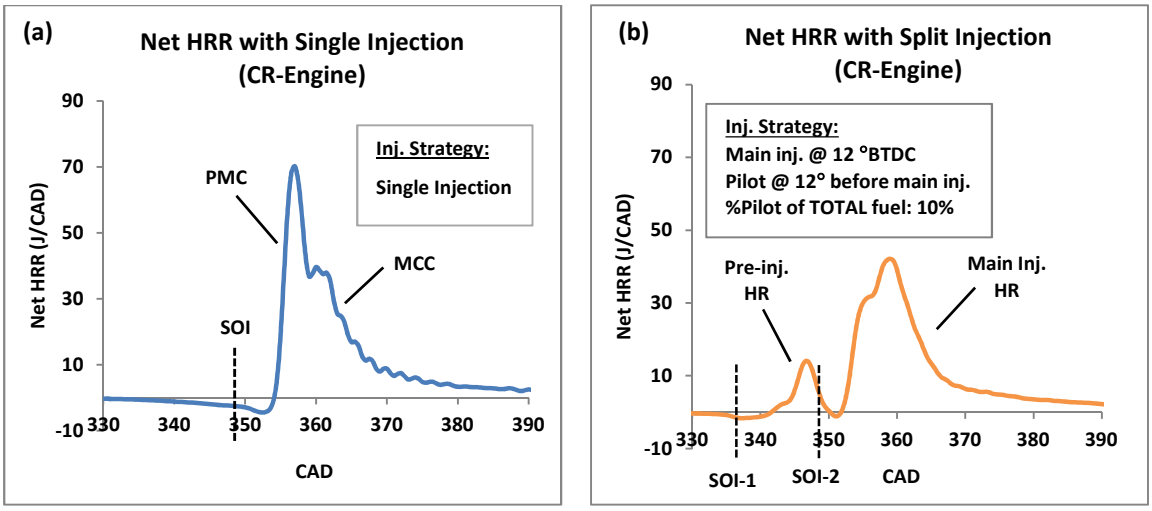


Figure 4.24 **Net HRR data for CR-Engine with different injection strategies; (a) single injection @ 12º BTDC, and (b) split injection, with the main injection @ 12º BTDC preceded by a 10% pre-injection mass 12º earlier. Data at 1500 rpm and 30bar BMEP.**

In single injection strategy as shown in Fig. 4.24 (a), the heat release process takes place at once but over two phases, the PMC and the MCC as discussed in details earlier. With split injection strategy, the heat release process takes place over two separate stages; as illustrated by Fig. 4.24 (b). The pre-injection HR is preceded by only a small drop in the HR accounts for the evaporation and heat up of the pre-injection part (only 10% of the total diesel fuel supplied). Combustion process starts with the pre-injection part that is fully consumed, owing to its small size, before the main combustion begins. That is, split injection strategy involves two ignition delay periods; one for the pre-injection and another for the main injection. Figure 4.25 shows the ignition delay for both injections; compared with the single injection strategy. It could be seen that the pre-injection part exhibits longer ignition delay than the single injection strategy, where this is attributed to the comparatively lower cylinder pressure and temperature at the SOI. The relatively long ignition delay could produce some cool flame reactions of the diesel fuel vapour that have high degree of reactivity [67]. This is partially evident in Fig. 4.24 (b) by the small hump in the HRR curve following the fuel evaporation drop and before the pre-injection combustion commences. On the other hand, the main injection exhibits much shorter ignition delay, as it is injected into the high temperature and pressure resulting from the pre-injection combustion. This shorter ignition delay means the PMC part of the main injection will be considerably small, and the majority of the injection will be consumed through MCC. That is, combustion process with split injection strategy starts with smaller amount of fuel, and with less premixed size. This largely reduces the rate of pressure rise (ROPR), combustion noise, and also NOx emissions [224]. Figure 4.26 illustrates the maximum ROPR with both injection strategy. It could be seen that more than 50% reduction in the maximum ROPR could be achieved using the split injection strategy. The reduced combustion noise is also evident by the absence of any ringing in the late stages of the HRR with split injection strategy as shown in Fig. 4.24 (b). It could be seen from Fig. 4.24 (a) that this ringing accompanies the HRR with a single injection. This combustion noise originates from the high rates of pressure rise during the initial rapid combustion owing to the injection of a large amount of fuel at once [40].

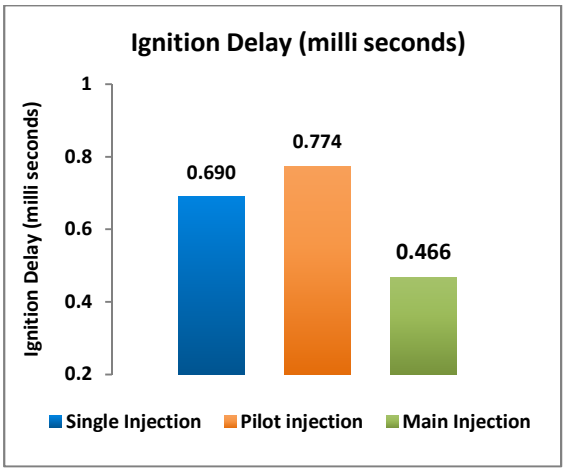


Figure 4.25 Iignition delay for single injection vs. split injection (pilot & main). Data for 1500 rpm and 3 bar BMEP. Injection timing of 12° BTDC for single injection is also held for the main injection, while the pre-injection is 12° before the main.

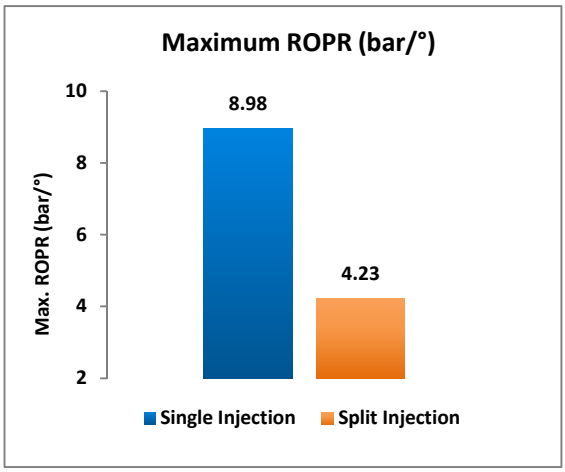


Figure 4.26 Maximum ROPR value for single injection vs. split injection (pilot & main). Data for 1500 rpm and 3 bar BMEP. Injection timing of 12° BTDC for single injection is also held for the main injection, while the pre-injection is 12° before the main.

Reduced noise through avoiding too much fuel being burnt at the end of ignition delay via using pre-injection is effective in improving fuel economy [40]. The reduced brake specific fuel consumption (BSFC) with this strategy could be inferred from the higher brake thermal efficiency (BTE), compared with single injection strategy, as illustrated by Fig. 4.27. The figure shows that more than 5% absolute improvement in the BTE could be achieved in the current setup using split injection strategy. Also, starting the main combustion at higher temperature and pressure (resulting from the HR of the pre-injection) generates higher cylinder pressure levels following the ignition of the main injection. The higher cylinder pressure values combined with lower fuel consumption bring about ≈15% less gross indicated specific fuel consumption (ISFC), as shown in Fig. 4.28.

On top of its large influence on combustion phasing, noise, and engine performance, the use of pre-injection also affects NOx, HC, and PM emissions [40]. Moreover, it was demonstrated that the control of injection parameters could transit the combustion mode from the conventional diesel combustion mode to novel combustion modes [64]. This could be very advantageous to dual-fuel operation, and the potentials of this technique are investigated in more details in Chapter 6.

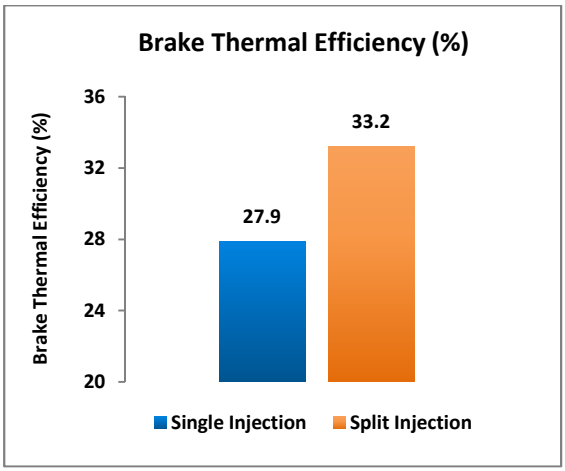


Figure 4.27 Brake thermal efficiency (%) for single injection vs. split injection (pilot & main). Data for 1500 rpm and 3 bar BMEP. Injection timing of 12° BTDC for single injection is also held for the main injection, while the pre-injection is 12° before the main.

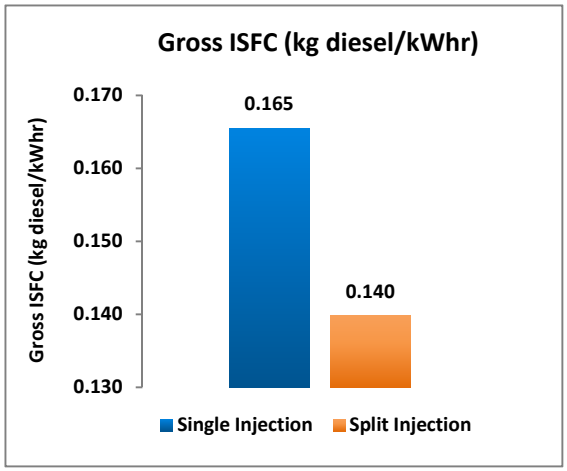


Figure 4.28 Gross ISFC for single injection vs. split injection (pilot & main). Data for 1500 rpm and 3 bar BMEP. Injection timing of 12° BTDC for single injection is also held for the main injection, while the pre-injection is 12° before the main.

4.3.5 Indicated work and engine stability indicator

Indicated work is the work transferred to the piston from the gases contained inside the engine cylinder [39].This work can be obtained from engine cylinder pressure data over the operating cycle; that is:

$$W_{ind} = \oint pdV \tag{4.20}$$

If the integration is carried out over the compression and expansion strokes only, where the overall work flow is essentially from the gases to the piston, the output is known as the “gross indicated work”; always positive quantity. Alternatively, if the integration is carried out over the intake and exhaust strokes, the result is called the “pumping work”. Pumping work is the work exerted to draw the fresh charge through the intake system and into the cylinder, as well as to eject the burned gases from the cylinder and out of the exhaust system; and consequently, it is a negative quantity for naturally aspirated engines, but could be positive quantity for turbocharged engines [225]. Integrating over the entire engine cycle yields, therefore, the net work delivered to the piston per cycle; and hence it is called the “net indicated work”. That is:

$$W_{ind,net} = W_{ind,gross} - W_{pumping} \tag{4.21}$$

Not all of the net indicated work is available at the drive shaft as a useful output (brake work). Instead, part of this work is disspated in the mechanical friction and the engine parasitic loads; such as water pump, oil pump, fuel pump, etc. That is:

$$W_{brake} = W_{ind,net} - W_{friction} \tag{4.22}$$

The friction work is a sufficiently large fraction of the indicated work; it varies from about 10% at full load and up to100% at idle or no load, and it also increases with the increase of engine speed [39].

It is convenient to discuss the difference between the indicated and the brake power output in terms of mean effective pressure (MEP). It is defined as the work per cycle per unit displaced volume; as [39]:

$$MEP = \frac{W_{cycle}}{V_{disp}} \tag{4.23}$$

The resulting unit is force per unit area; i.e. pressure units. MEP is a very useful relative engine performance measure that could be used with the terms “indicated”, “brake”, and “friction”. However, only when applied to the indicated work value does the MEP (in this case it will be referred to as IMEP) have some physical meaning, as in this case, it relates to the average pressure in the cylinder acting on the piston over an engine cycle [226]. It still applies to the other measures of work (e.g. Brake and Frictional) but only on the basis of providing a comparison to the Indicated value.

Similar to the case with indicated work, IMEP has two definitions common in use; the gross IMEP which represents the work delivered to the piston over the compression and expansion strokes per cycle per unit displaced volume, and the net IMEP which is the work delivered to the piston over the entire four strokes of the cycle per unit displaced volume. $IMEP_{gross}$ rather than $IMEP_{net}$ is most commonly used as a measure of the work produced. It represents the sum of the useful work available at the shaft and the work required to overcome all the engine losses [39]. Also, by using $IMEP_{gross}$, any potential cycle-by-cycle fluctuations in pumping work due to external conditions, such as wave motion in the intake and exhaust ducting, is eliminated. In some recent work, however, the trends in net and gross IMEP data were very similar [227].

From the $IMEP_{gross}$ data recorded over the 50 consecutive pressure cycles (as discussed in Section 4.3.3), another very important parameter is derived, which is the coefficient of variation in gross indicated mean effective pressure ($COV_{IMEPgross}$). This parameter is used to define the cyclic variability as a measure of engine stability and it is calculated as:

$$COV_{IMEPgross} = \frac{\sigma_{IMEPg}}{\overline{IMEPg}} \times 100\% \tag{4.24}$$

where (σ_{IMEPg}) is the standard deviation and ($\overline{IMEPg}$) is the mean value of the gross IMEP over the recorded cycles.

While conventional diesel operation is mostly free of any high levels of combustion instability under fully-warm, normal operating conditions, this parameter is very critical in the operation of dual-fuel (DF) engines at light loads. These operating conditions are most challenging, due to the very lean mixture that is expected to result in poor flame propagation and increased engine instability. Excessive $COV_{IMEPgross}$ (~ 10%) results in very unstable running of the engine and serious drivability problems of the vehicle [39]. This parameter will be assessed and evaluated when it comes to dual-fuel operation of the engine, as discussed in the following chapters.

CHAPTER FIVE

COMBUSTION PROCESS IN METHANE-DIESEL DUAL-FUEL ENGINES AT LIGHT LOAD CONDITIONS

5 Combustion Process in Methane-Diesel Dual-Fuel Engines at Light Load Conditions

5.1 Introduction

In this chapter, experimental results for dual fuelling of the engine with high-pressure common rail (HPCR) injection, at light load conditions are presented and analyzed. The area of interest is the change of heat release characteristics with methane substitution for diesel fuel, and what gives rise to these changes. The purpose is to provide a better understanding of combustion process in methane-diesel dual-fuel engines, and how the variation of gas substitution ratio would affect the rates and mechanisms of the energy release. Following the knowledge gained from heat release analysis of diesel operation in Chapter 4, the work in this chapter identifies the different stages of combustion in methane-diesel DF engines. A wide range up to 80% of methane substitution for diesel fuel was examined at quarter load (25%) conditions for engine speed of 1600 rpm. The maximum possible methane substitution for diesel fuel is then investigated at near-idle low-load (5%) conditions. The amount of minimum diesel fuel injected by the FIE was also investigated. Any other restrictions on methane substitution were also examined. Combustion characteristics were assessed and evaluated throughout.

5.2 Overview and Method

In port injected gas-diesel DF engines, the use of two independent fuelling systems for the diesel pilot and the gaseous fuel provides a high level of control over cylinder charge preparation and the subsequent combustion process. Varying the relative quantities of the two fuels and altering the injection strategy can yield a wide spectrum of mixture conditions in DF engines. Accordingly, different combustion mechanisms are expected to dominate the ensuing fuel conversion processes [228].

An overall classic examination of the combustion process in a DE engine can be made through the apparent heat release rate (HRR) variation; derived from the corresponding cylinder pressure variation with time [229]. The process of fuel oxidation is considered to be made up of three overlapping major energy release processes; combustion of the diesel fuel pilot, combustion of the gaseous fuel in the immediate vicinity of the ignition

and combustion centers of the pilot, and any pre-ignition reaction activity and ensuing turbulent flame propagation within the overall lean mixture of mainly gaseous fuel and air [229]. The characteristics of each identified combustion stage depend on the relative quantities of the two fuels, and on the total equivalence ratio; defined as [58]:

$$\phi_{tot} = \frac{AFR_{CH4}^{stoic} \times \dot{m}_{CH4} + AFR_{D}^{stoic} \times \dot{m}_{D}}{\dot{m}_{air}} \quad (5.1)$$

where (AFR_{CH4}^{stoic}) and (AFR_{D}^{stoic}) are the stoichiometric air-fuel ratios of methane and diesel, and $(\dot{m}_{CH4})$, $(\dot{m}_{D})$, and $(\dot{m}_{air})$ are the mass flow rates of methane, diesel, and intake air; respectively. The resulting combustion mechanism in any particular stage is mainly governed by the dominant fuel in this stage. The general features of combustion process, HRR, and emissions formation are expected to changes with the change of substitution ratio of methane for diesel fuel; defined on energy basis as [71]:

$$\%\mathrm{CH}_4 = \frac{\dot{m}_{CH4} \times LHV_{CH4}}{\dot{m}_{D} \times LHV_{D} + \dot{m}_{CH4} \times LHV_{CH4}} \quad (5.2)$$

where (LHV_{CH4}) and (LHV_{D}) are the lower heating values of methane and diesel. This parameter is also known as the percentage of energy substitution (PES) [230].

For a given test condition, the HRR data for dual-fuel operation is obtained from the recorded in-cylinder pressure data, as per the procedure outlined in Chapter 4. After DF data was recorded, the engine was switched into conventional diesel mode via cutting the methane supply to the engine, while keeping other parameters unchanged. Diesel-only measurements were then recorded, and from that, the corresponding HRR values were obtained via the same procedure.

The apparent HRR data for the CH_4-only condition was calculated as the arithmetic difference between dual-fuel HRR and diesel-only HRR, at any given crank angle; i.e.:

$$\mathrm{HRR}_{CH4,apparent}|_{\theta} = \mathrm{HRR}_{dual-fuel}|_{\theta} - \mathrm{HRR}_{Diesel}|_{\theta} \quad (5.3)$$

5.3 Influence of Methane Substitution Ratio on DF Engine Combustion

The variation of HRR data was analyzed for three different %CH_4 ratios; 30%, 60%, and 80%, at quarter load (25%) conditions for engine speed of 1600 rpm. For each case examined, the HRR data were constructed for DF operation, diesel-only operation, and apparent CH_4-only as described in Section 5.2. Figures 5.1, 5.2, and 5.3 demonstrates the data corresponding to the three test cases; respectively. The first derivative of HRR data for DF operation was also found to be of a valuable assist in the determination of combustion stages, and thus it is also presented (as a normalized value) on a secondary axis of each figure.

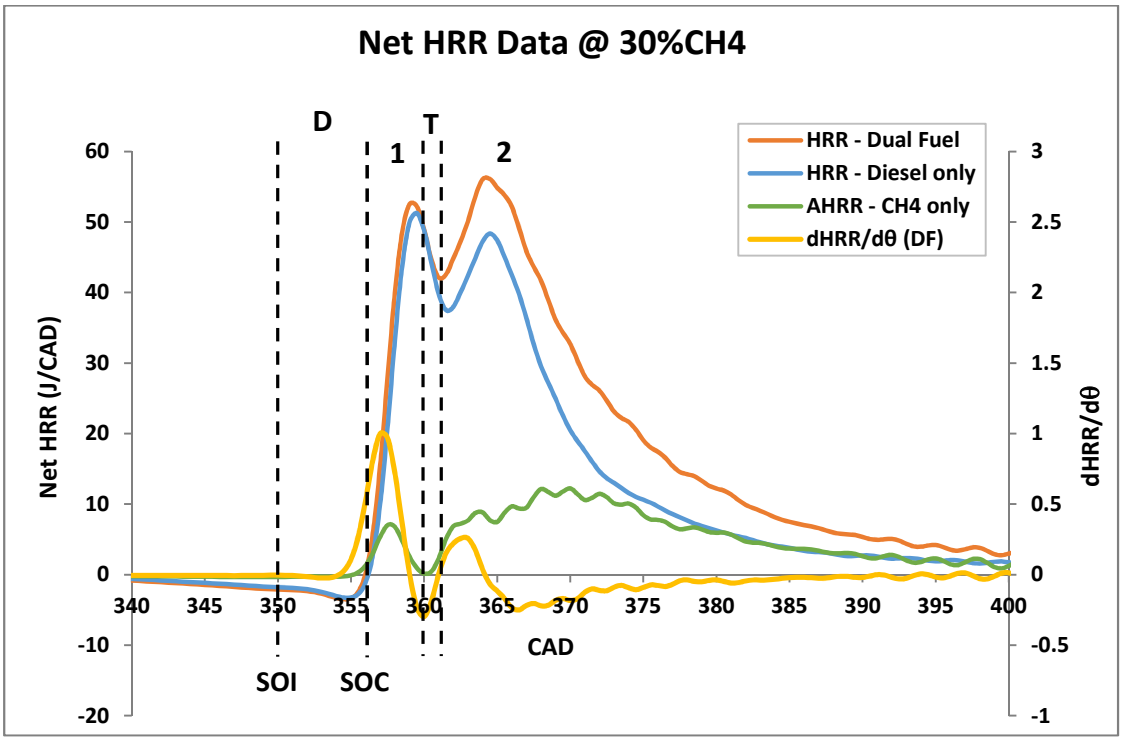


Figure 5.1 **Net HRR data for different components of DF combustion (Apparent w/ CH4) with 30% CH_4 substitution ratio. Data is for 25% engine load @ 1600 rpm.**

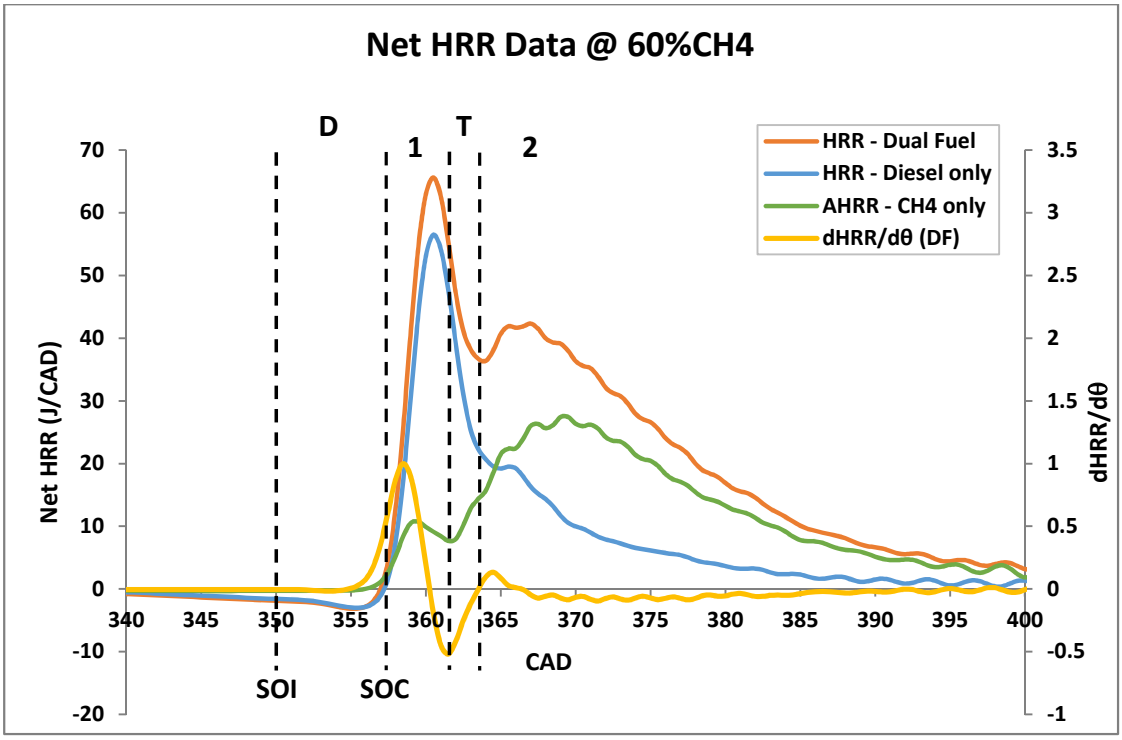


Figure 5.2 **Net HRR data for different components of DF combustion (Apparent w/ CH4) with 60% CH_4 substitution ratio. Data is for 25% engine load @ 1600 rpm.**

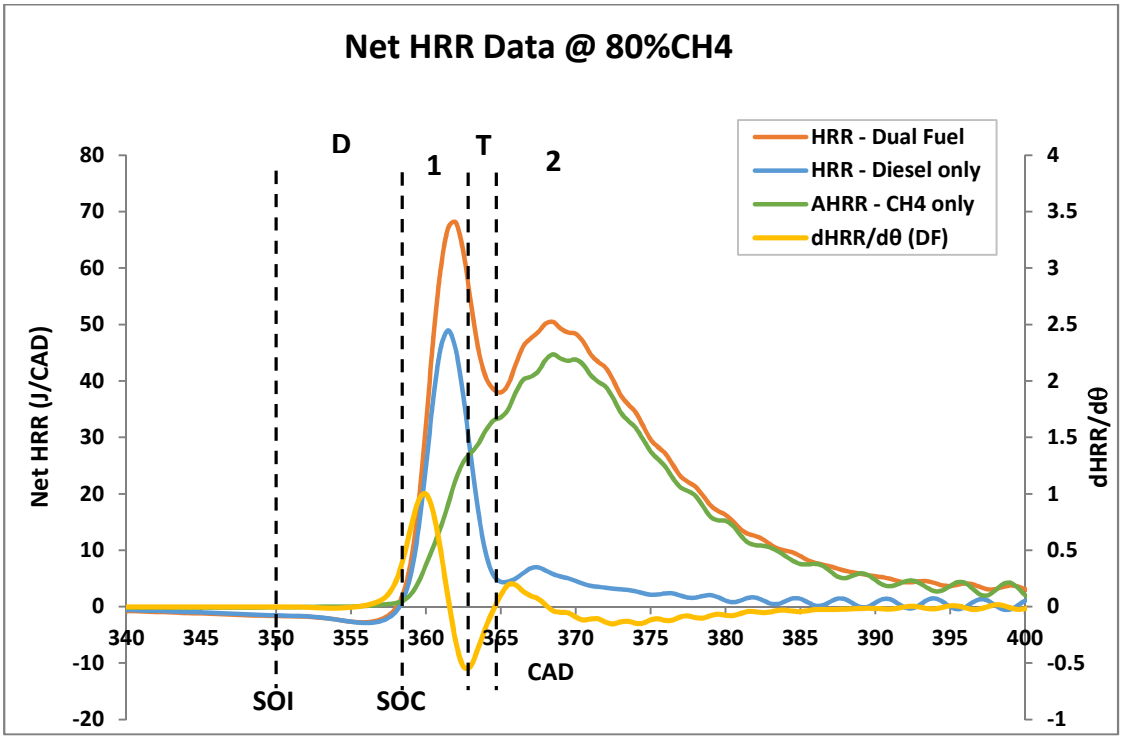


Figure 5.3 **Net HRR data for different components of DF combustion (Apparent w/ CH4) with 80% CH_4 substitution ratio. Data is for 25% engine load @ 1600 rpm.**

The figures indicate that the net HRR data for DF operation is similar to those of diesel-only operation in the early stages prior to combustion. As discussed in Chapter 4, the net HRR data demonstrates a slight drop below zero at the late stages of compression before diesel fuel injection, where this is attributed to the heat transfer to cylinder walls as the charge temperature increases during the polytropic compression process. The start of injection (SOI) of the diesel pilot, set to 10° BTDC in the test cases presented, is succeeded by a further drop in the net HRR, due to diesel fuel evaporation and heat up. It could be seen from the figures that this drop becomes less concave as the $\%CH_4$ is increased; unambiguously due to the reduced diesel fuel amounts at these conditions. Like diesel-only operating conditions, ignition delay (ID) period of dual-fuel operation is identified as the period between the SOI and the start of combustion (SOC); identified in the present work as the point at which the net HRR reaches 2 Joule/CAD. As noticed in Figures 5.1, 5.2, and 5.3, and further illustrated by Fig. 5.4, the increase in $\%CH_4$ substitution elongates the ignition delay (denoted D) of DF operation in the test cases examined. This is attributed to several interrelating effects; including, reduced oxygen partial pressure (due to air displacement by CH_4), as well as reduced temperature and pressure during the initiation of ignition as methane has a higher heat capacity than air (aka cooling effect of CH_4 admission) [231]. Also, the incidence of pre-ignition reaction activities between CH_4 and air may affect those between diesel and air (i.e. competition of active radicals between diesel fuel and CH_4 [232]); increasing the ignition delay.

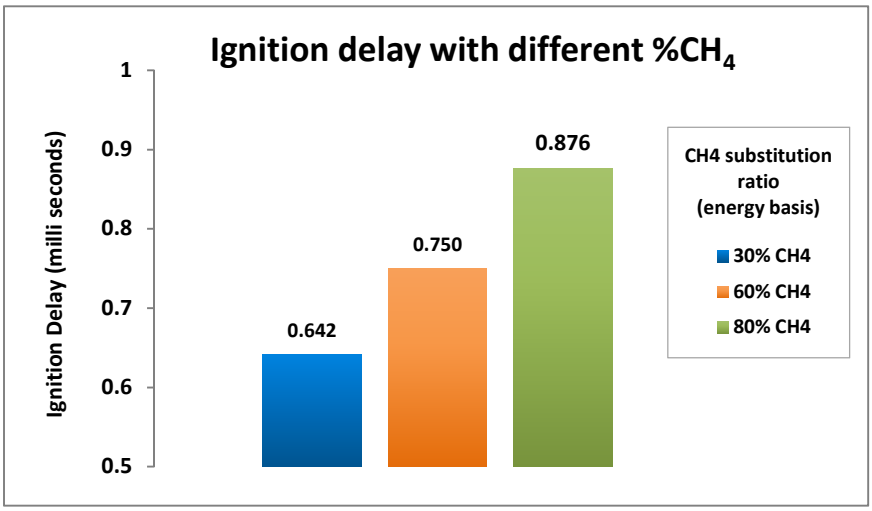


Figure 5.4 **Ignition delay for DF operation with different % CH_4 substitution ratios. Data is for 25% engine load @ 1600 rpm, SOI @10°BTDC.**

Advancing the classical definition of DF combustion process outlined in Section 5.2, a more expressive description could be inferred from observing the development of the process with the increase of $\%CH_4$, as illustrated by Figs. 5.1, 5.2, and 5.3. Combustion process is considered to be formed of two main distinctive stages (denoted 1 and 2), separated by a transient stage (denoted T). SOC defines the commencement of stage-1 combustion. This stage is characterized by a sharp rise in the HRR curve as a result of the combustion of a large amount of fuel after the ignition delay ends. Regardless of the amount of CH_4 used, stage-1 is dominated by the ignition and rapid combustion of the premixed part of the pilot, where this part (relative to the total size of the diesel fuel used) is increased with the increase of the $\%CH_4$, because of the relatively long ignition delays at these conditions. Figure 5.5 illustrates the diesel pilot premixed burn fraction, relative to the total diesel fuel amount; as estimated from the corresponding cumulative net HR profiles. With $\%CH_4$ as high as 80%, it could be seen that almost three-quarters of the pilot diesel fuel burns in a premixed combustion (PMC); due to the long mixing period between the end of injection and the start of combustion.

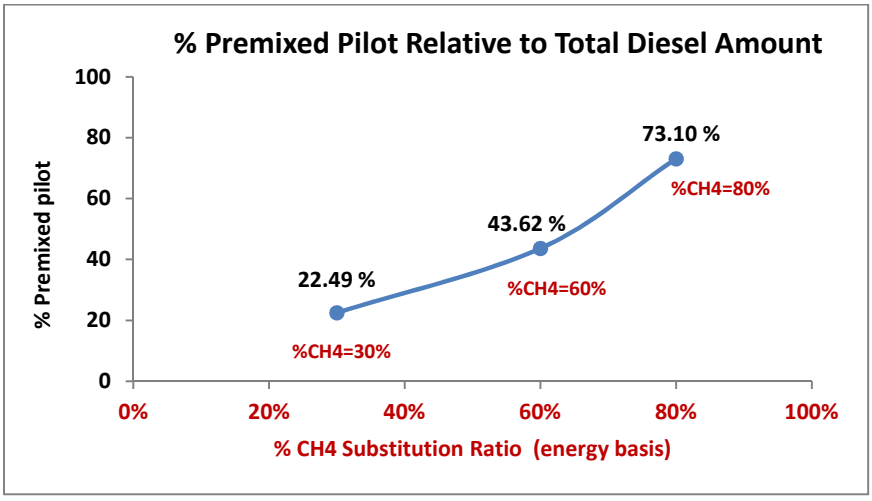


Figure 5.5 **Pilot premixed burn fraction relative to the total diesel fuel amount, at different %CH4 substitution ratios. Values estimated from the corresponding cumulative net HR profiles. Data is for 25% engine load @ 1600 rpm, SOI @10°BTDC.**

In contrast with the description given in [233], the present work demonstrates that the combustion of the gaseous fuel in the immediate vicinity of the ignition sources of the pilot is not sequential to the pilot combustion. Instead, there is an evident entrainment

of some of the gaseous fuel into the pilot combustion, and the contribution of CH_4 to stage-1 combustion is clearly visible on Figs. 5.1, 5.2, and 5.3. The level of entrainment of CH_4 into the premixed combustion increases with the increase of $\%CH_4$ on the account of diesel injection size; indicating that this entrainment is more affected by the mixture strength than by the jet properties. Figure 5.6 illustrates the percentage of CH_4 contribution to stage-1 combustion as estimated from the corresponding cumulative net HR profiles. It could be seen from the figure that with $\%CH_4$ as high as 80%, almost one-third of the HR in the premixed combustion comes from the gaseous fuel. The peak value of HRR rate is therefore considerably influenced by the gaseous fuel combustion, and accordingly, it is believed that it is not only the diesel pilot that most influences NOx emissions formation at these conditions; gaseous fuel also plays a notable role.

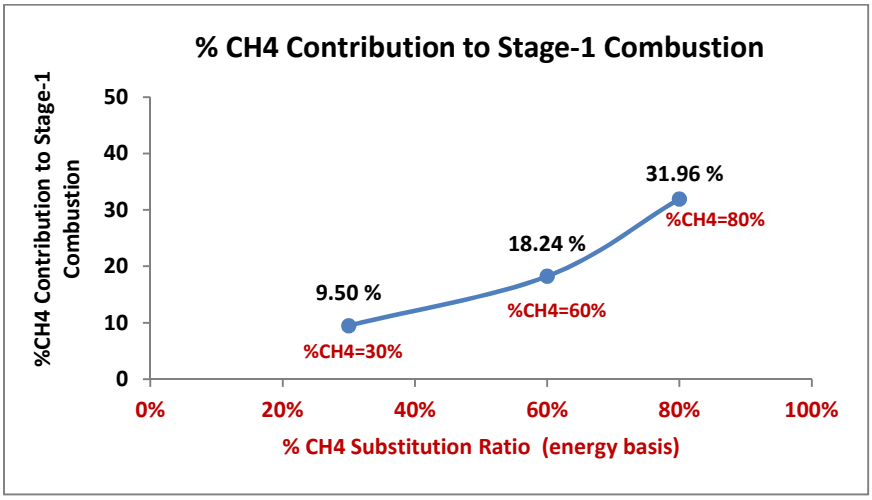


Figure 5.6 **Percentage of CH4 contribution to stage-1 combustion, at different %CH4 substitution ratios. Values estimated from corresponding cumulative net HR profiles Data is for 25% engine load @ 1600 rpm, SOI @10°BTDC.**

Stage-1 combustion terminates as a minimum local value of the derivative of the HRR (dHRR/dθ) occurs after the peak value of HRR is attained; that is:

$$\theta_{E1} = \theta\,|_{\min(\frac{dHRR}{d\theta})} \tag{5.4}$$

where (θ_{E1}) is the crank angle at which stage-1 combustion terminates. The increase in the reaction rate past this value is interpreted as the onset of a new, different combustion mechanism. For that reason, this point was identified as the end of stage-1 combustion.

Following stage-1 comes a new stage of combustion that presents the transition from the auto-ignition of premixed diesel vapor along with the entrained gaseous fuel, into the regime in which the majority of the gaseous fuel is expected to burn. This transient stage (denoted T) lasts for a very short interval and is not characterized by the presence of a certain dominate combustion mechanism. Instead, it is composed of the combustion of the premixed diesel fraction left after stage-1 terminates, along with a corresponding small part of methane that is responsible for the increase in the reaction rate illustrated by the (dHRR/dθ) diagram. The transient stage terminates when the DF HRR starts to increase again following the drop that takes place after the first peak. This is identified as the crank angle at which the first derivative of the net HRR (dHRR/dθ) equals zero;

$$\theta_{ET} = \theta \,|_{\left(\frac{dHRR}{d\theta}\right)=0} \tag{5.5}$$

where (θ_{ET}) is the crank angle at which transient combustion stage terminates.

The termination of the transient stage indicates the beginning of stage-2 combustion, in which the bulk of gaseous fuel-air mixture away from the influence of diesel pilot zone is expected to burn; mostly in a turbulent flame propagation event [233]. Nevertheless, the dominant combustion mechanism in this stage is largely determined by the relative magnitudes of the diesel pilot and gaseous fuel available for combustion at this stage. Figure 5.7 shows the contribution of turbulent flame propagation ensuing from gaseous fuel combustion to the total heat release during stage-2 combustion; as estimated from the corresponding cumulative HR profiles. Similar to the results presented in [228], a linear correlation between the gaseous fuel amount and the incidence of turbulent flame propagation in stage-2 combustion is established. Mixtures with methane equivalence ratio (ϕ_{CH4}) greater than 0.35 are capable of sustaining a stable flame-propagation. With low $\%CH_4$ ratios, the mixing-controlled combustion of the diesel pilot rules over the flame propagation of the gaseous fuel, as shown in Fig. 5.1. As the $\%CH_4$ increases, the contribution of gaseous fuel combustion to stage-2 becomes prominent, and flame propagation mechanism starts to dominate, as illustrated by Fig. 5.2. With high $\%CH_4$ as in Fig. 5.3, stage-2 combustion becomes almost entirely composed of turbulent flame propagation of the gaseous fuel (provided that a bulk auto-ignition or knock does not take place). In view of that, it is expected that the dominant combustion mechanism in this stage will affect the formation of CO and HC emissions more substantially. It is to

the point here to highlight that with some other research work [228], a low-intensity tail on the HRR was observed to extend far into the expansion stroke, with no additional HRR peak visible. This stage of combustion is characterized by much lower HRR levels as well as longer combustion durations than the previous stages of combustion. While this was not encountered in the present work, it is believed that the low-intensity stage could be associated with a large amount of HC emissions; especially when considering the inherent nature of diesel engines converted to dual-fuel operation to emit large HC emissions at part load, owing to their large crevices volume [234]. This stage could be thought of as a late burn-out of the remaining fuel in the cylinder, in keeping with the classic description of premixed charge combustion [40].

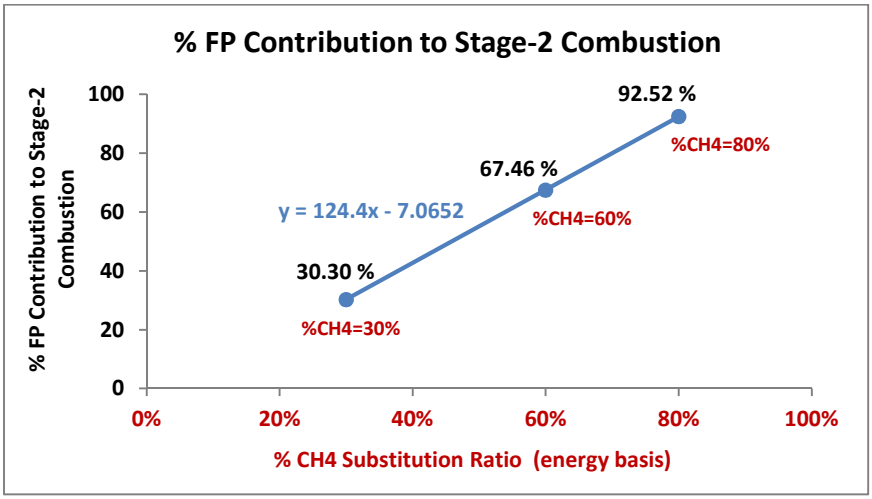


Figure 5.7 **Percentage of flame propagation contribution to stage-2 combustion, at different % CH4 substitution ratios. Values estimated from the corresponding cumulative net HR profiles. Data is for 25% engine load @ 1600 rpm SOI @10°BTDC.**

It should be taken into consideration that the experimental results were obtained using methane as the gaseous fuel. If NG is used instead, the variation of the gas composition will alter engine combustion and emissions characteristics. As discussed in Chapter 2, the presence of heavy hydrocarbons (e.g. ethane, propane) in NG enhances the mixture ignitability and increases flame propagation rate, relative to pure methane [80]. Ignition delay becomes shorter, relative to pure methane operation, and hence pilot fuel injection timing has to be slightly retarded. Lean combustion limit is extended and HC emissions are reduced with NG, compared with methane combustion, yet NOx emissions increase as T_{ad} increases [77]. In opposition, NG with large CO_2 content will dilute the mixture

and slows the reaction rates, yet reduces NOx [19]. In all cases, the lower LHV of NG compared with methane means larger amount of the gaseous fuel is required to supply the engine with the same energy level [19]. This involves a corresponding change in the pilot fuel amount as well. To conclude, pilot fuel mass and its injection timing may require readjusting should the gaseous fuel used changes from methane to NG [80].

5.4 Investigating Maximum Possible Methane Substitution for Diesel Fuel

The most challenging operating conditions for gas-diesel DF engines are those at very low loads with high gaseous fuel substitution ratios. Using very lean mixtures and small amounts of liquid fuel at these conditions, the engine suffers slow flame propagation and even quenching. The flames originated from the pilot ignition regions cannot fully propagate far enough within the time available to consume the entire fuel-lean mixture [235]. This will leave some of the gaseous fuel unconverted or only partially oxidized; as revealed by the increased CO emissions and unconverted methane in the exhaust gas [236]. Although a notable feature of engine operation at these conditions is its inferior performance, as demonstrated by the increased specific energy consumption, the engine could still operate and produce consistent firing cycles. However, this lasts only until a certain value of gaseous fuel substitution is met where a severe combustion instability, misfiring, and excessive COV_{IMEP} levels are encountered [237].

To investigate the value of maximum possible methane substitution for diesel fuel at near-idle conditions, the engine was first run on conventional diesel operation at 5% of its rated load at the particular speed. Methane was then introduced on the account of diesel fuel and gradually increased until the first engine misfire/uncontrollable running takes place, as noticed by the engine operator. Methane substitution ratio ($\%CH_4$) was continuously monitored and recorded throughout; where the tests were conducted at four engine speeds of 1600, 1500, 1400, and 1300 rpm. It is to the point here to mention that for the current experimental setup, the test case 5% load @ 1300 rpm was the lowest achievable conditions (load-speed) for a steady running, free of undesirable vibrations and/or load fluctuation.

The trends of different parameters investigated at different speeds demonstrated a high degree of analogy. In view of that and for space convenience, only the test results with an engine speed of 1600 rpm are individually discussed, then the results with all speeds

will be collectively presented. Figure 5.8 shows the HRR data for the entire range of methane substitution ratios for diesel fuel up to the maximum achievable value, at 5% engine load and 1600 rpm.

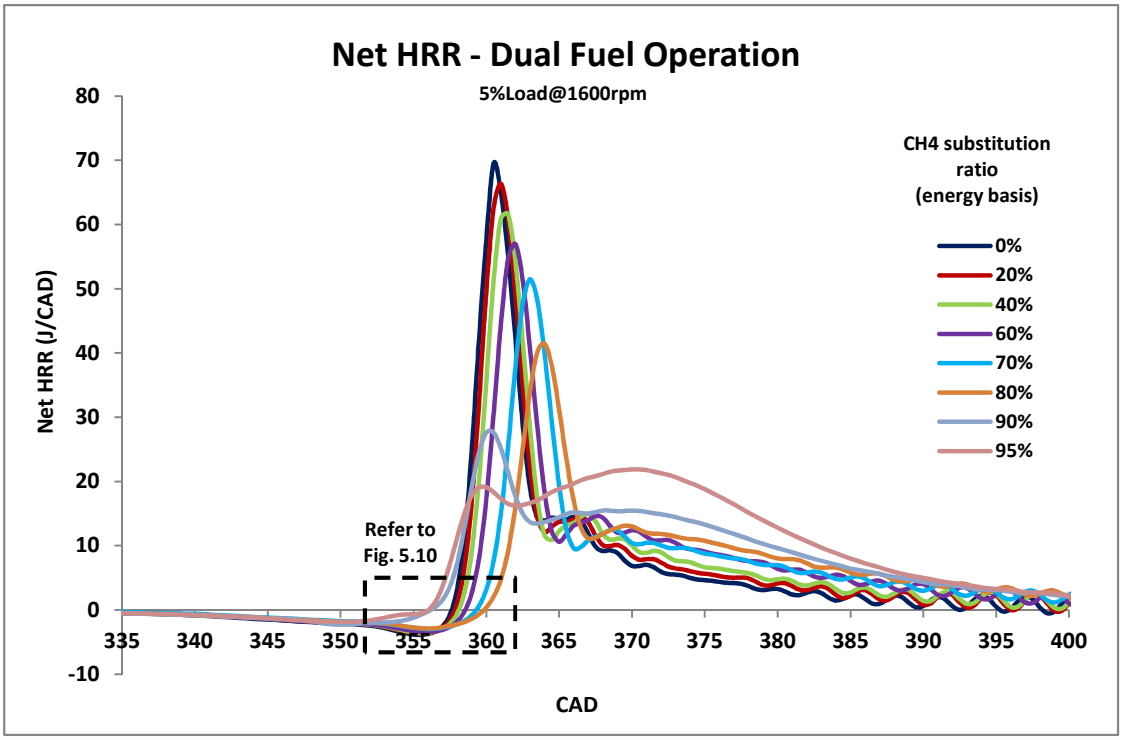


Figure 5.8 **Net HRR data for DF operation with different % CH_4 substitution ratios. Data is for 5% engine load @ 1600 rpm. Injection timing is set @ 10°BTDC.**

At low load operating conditions where the amount of fuel is effectively small, stage-1 combustion is always dominated by the ignition and rapid combustion of the premixed part of the diesel pilot. Following a very narrow transient stage, gaseous fuel conversion in stage-2 combustion takes place in a non-flame propagation combustion event, as the low ϕ_{CH4} (below 0.3) at these conditions is not sufficient enough to propagate a stable flame [228]. The absence of a profound correlation between the mean value of the heat released during stage-2 combustion (as an indirect measure of the turbulent flame speed [228]) and the value of ϕ_{CH4} supports this theory. Gaseous fuel conversion process under these conditions is, therefore, expected to follow a different mechanism other than the flame propagation [228]. Stage-2 combustion here is categorized as “pilot-dominant”, owing to the major contribution of the pilot (particularly at low-to-intermediate %CH_4 levels); despite any involvement of the gaseous fuel.

An approximation of the pilot contribution to DF combustion process could be inferred from Fig. 5.9 that shows HRR trends for diesel-only operation using the same amount of diesel fuel used as a pilot in the DF mode, at different %CH4 substitution ratios. It could be seen that most of diesel combustion is characteristically a premixed, while the second stage of combustion gradually declines as the injected fuel mass is reduced (as discussed in Chapter 4). The trend of stage-2 combustion under dual-fuel operation is the opposite, where the increased methane admission on the account of diesel increases the heat release, but at slower rates, as shown in Fig. 5.8. The low-intensity combustion of methane is expected to strongly contribute to the unburned HC emissions; especially at high %CH_4 ratios where the small pilot amount is mostly consumed during the early stage of combustion [236]. Figure 5.8 shows that increasing methane on the account of diesel fuel slows down the reaction rate and shifts the whole combustion process further down in the expansion stroke. This should not be confused with the change in ignition delay behavior observed in Fig. 5.9, as the latter is explicitly due to the change in load conditions as diesel fuel quantity changes, as discussed in Chapter 4.

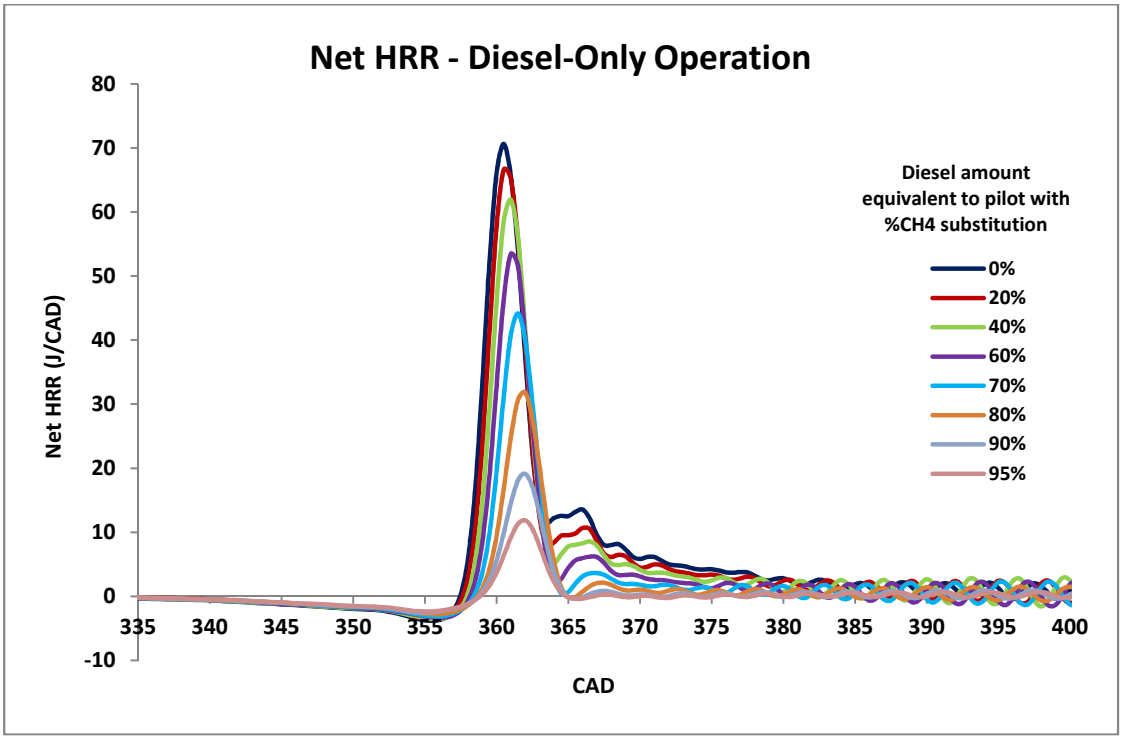


Figure 5.9 **Net HRR data for diesel-only operation using the same amount of diesel fuel used as a pilot in the DF mode at different %CH4 substitution ratios at 5% engine load @ 1600 rpm. Injection timing is set @ 10°BTDC.**

At high %CH_4 substitution levels, it could be seen from Fig. 5.8 that there is a threshold point at which the net HRR pattern drastically changes; indicating a definite change in combustion mechanism. In this case (5% load @1600rpm), this phenomenon occurred at about 80% CH_4 substitution and was characterized, on top of the notable change of the HRR pattern, by the occurrence of pre-ignition reactions and reduced ignition delay. The incident pre-ignition reactions are evident in Fig. 5.8 as a small release of energy after the SOI (@ 10°BTDC) and before the SOC (net HRR reaches 2 J/°). Figure 5.10 shows a magnification of the inset outlined in Fig. 5.8, where the direct proportionality of the ignition delay with %CH_4 before the threshold and the reverse after the threshold are clearly visible. The figure also shows the diminishment of the negative HR as %CH_4 increases, since the increased substitution level means there is a lesser amount of diesel fuel to be evaporated and heated up. The values of ignition delay (in milliseconds) with different %CH_4 substitution ratios are presented in Fig. 5.11.

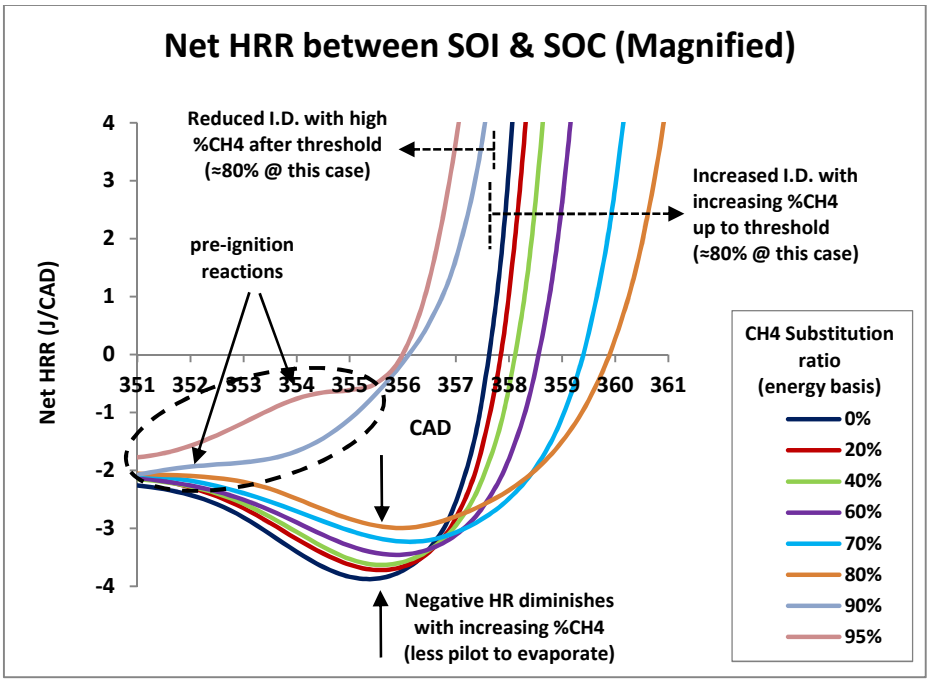


Figure 5.10 **Magnified part of net HRR data between SOI and SOC (refer to Fig. 5.8) for DF operation with different % CH_4 substitution ratios. Data is for 5% engine load @ 1600 rpm. Injection timing (SOI) is set @ 10°BTDC.**

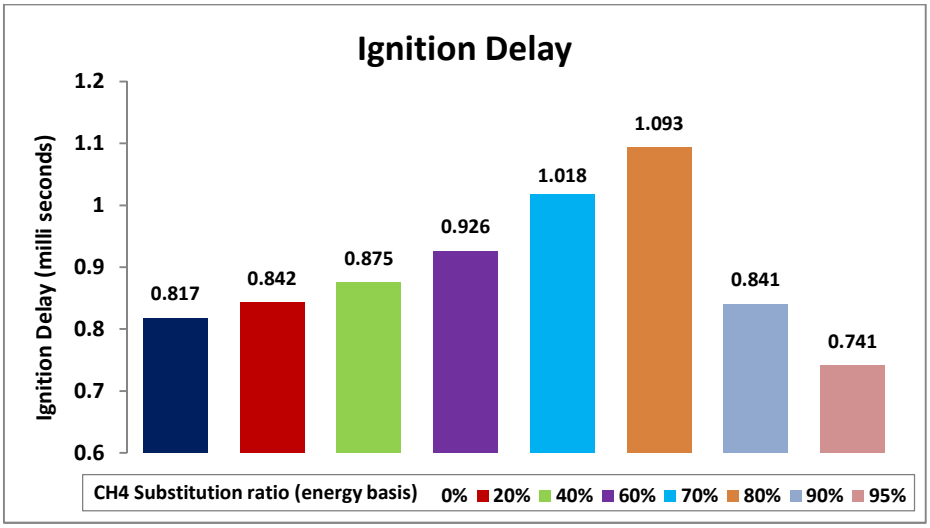


Figure 5.11 Ignition delay for DF operation with different % CH_4 substitution ratios. Data is for 5% engine load @ 1600 rpm. Injection timing is set @ 10°BTDC.

At low load with high %CH_4 substitution ratios, the pilot injection mass is sufficiently small that it could possibly evaporate completely [238], then locally intermix with the very lean gaseous fuel-air mixture. It was found in some study [239] that the presence of small concentrations of n-heptane vapor (to an extent of a fraction of 1%) can bring about a substantial acceleration of the oxidation reaction of methane in air. Therefore, it is believed that the presence of a small amount of higher hydrocarbon vapor, such as the vapor produced from the diesel fuel pilot, can significantly enhance the combustion initiation in dual-fuel engines, even without necessarily making a substantial change in temperature or composition. Based on the phenomenological model for the combustion of successive pilot-injections in diesel-only combustion [238], the ensuing combustion mechanism following the threshold is an oxidation reaction of a diesel vapor-methane-air mixture surrounding the ignition sites and predominantly governed by the chemical kinetics [239]. This resembles the reactivity controlled compression ignition (RCCI) combustion with methane as the low reactivity fuel and diesel fuel as the high reactivity one [240]. The change in mechanism principally targets stage-2 combustion, although it also influences stage-1 combustion. This could be inferred from comparing the values of the first peak of the HRR data in Figs. 5.8 and 5.9 following the threshold. As shown in Fig. 5.10, the pre-ignition reactions become more visible at the highest %CH_4 where minimal pilot mass used is likely to experience a complete evaporation. The resulting enhanced combustion is reflected as a notable reduction in the ignition delay, as shown

in Fig. 5.11, and also as a reduction in the duration of combustion (DOC) following the threshold point (≈ 80% CH_4 substitution), as shown in Fig. 5.12. While the changes in the combustion mechanism and HRR pattern following the threshold are evident, the change in combustion phasing, as represented by the center of heat release (COHR), or the CA50, is relatively small; despite the large change in the ignition delay. This is due to the increased HR in stage-2 combustion, while the HR in stage-1 becomes smaller. However, CA50 shifts back towards the TDC after reaching its farthest position at the threshold point; Fig. 5.13 shows the absolute positions of CA50 in crank angle degrees.

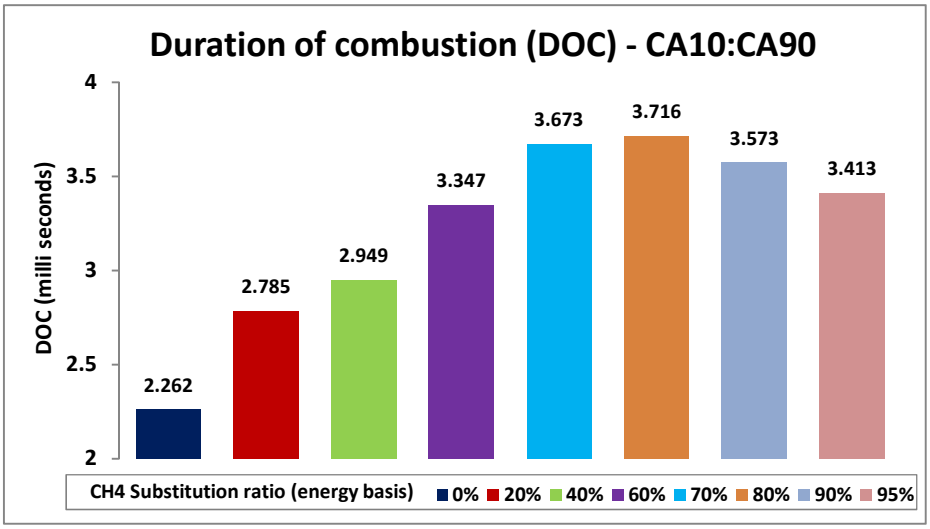


Figure 5.12 **Duration of combustion (CA10:CA90) for DF operation with different %CH_4 substitution ratios. Data is for 5% engine load @ 1600 rpm, SOI @ 10°BTDC.**

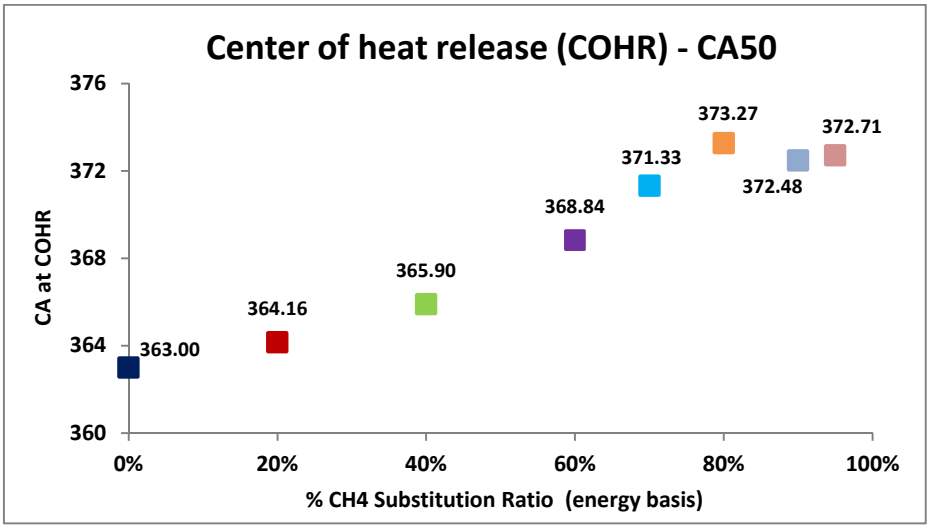


Figure 5.13 **Center of heat release - COHR (CA50) for DF operation with different %CH_4 substitution ratios. Data is for 5% engine load @ 1600 rpm, SOI@ 10°BTDC.**

The maximum possible methane substitution for diesel fuel in the current setup was as high as 95%; as demonstrated above. This value largely exceeds that of 86% achieved in another study using gaseous fuel induction into the intake manifold [58]. This proves that the use of gaseous fuel injection into the intake, rather than induction using simple venturis or gas mixers, is an effective way to extend gaseous fuel substitution limits in dual-fuel engines. The pilot diesel injected mass corresponding to the 95% substitution level at this operating condition was as low as 0.8 mg/stroke. In the current setup, this is the minimum limiting value of the FIE used, below which the piezoelectric injectors no longer delivers any fuel, as the engine ECU drops the signal automatically. That is, the limiting factor in this condition is a system-limitation. Yet, at this point, the engine is likely to be on the verge of uncontrollable running, where a high degree of instability was encountered. The high level of cyclic variability (as represented by $COV_{IMEPgross}$) at high $\%CH_4$ ratios is shown in Fig. 5.14. The engine potentially experiences misfiring cycles beyond this limiting point. The increased engine instability, combined with the lower cylinder pressure and slow burning rate result in a retarded engine performance; as indicated by the very low break thermal efficiency shown in Fig. 5.15. This indicates that large part of the weak gaseous fuel-air mixture escapes the combustion process; emitting significant HC emissions.

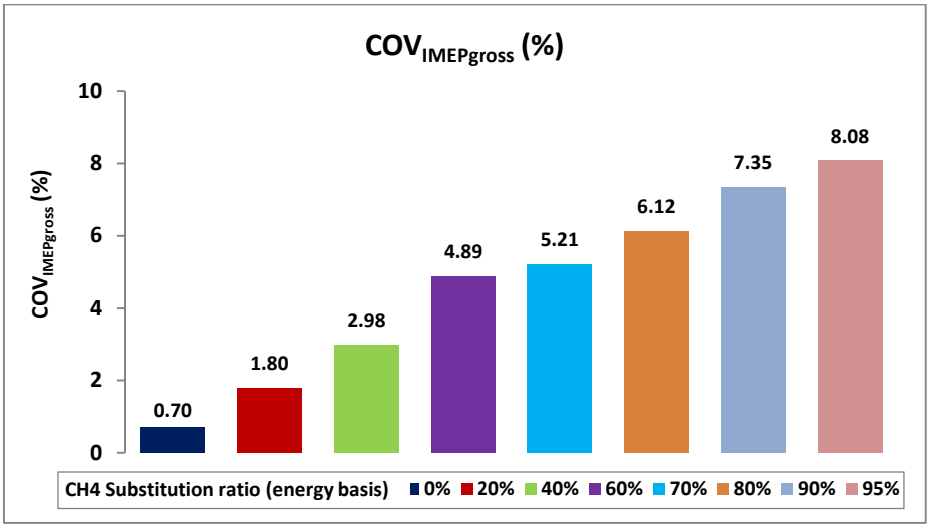


Figure 5.14 COV of gross IMEP for DF operation with different $\%CH_4$ substitution ratios. Data is for 5% engine load @ 1600 rpm, SOI @ 10°BTDC.

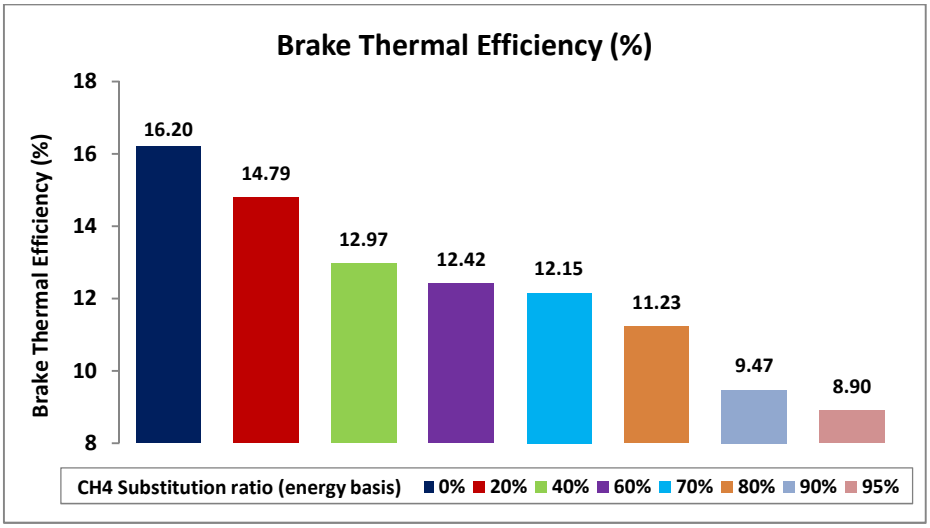


Figure 5.15 Break thermal efficiency for DF operation with different %CH_4 substitution ratios. Data is for 5% engine load @ 1600 rpm, SOI @ 10°BTDC.

While these detailed results were obtained at an engine speed of 1600 rpm, very similar trends were obtained at the same load level (5% of the engine rated load) at other speeds investigated. Figures 5.16, 5.17, and 5.18 show the HRR data for the entire range of achievable %CH_4 substitution ratios at 1500, 1400, and 1300 rpm; respectively. It could be seen that the phenomena regarding the changes in HRR pattern and ignition delay behavior are consistently encountered at different speeds. This supports the theory of undergoing a change in the combustion mechanism at some specific %CH_4 substitution value; depending on the fuelling settings. As illustrated by Fig. 5.19, ignition delay (in milliseconds) increases at all speeds as the %CH_4 increases, but only up to the specific threshold values, then decreases afterward. This reveals the incident change from the low intensity-pilot dominant mechanism into a combustion of diesel vapor-methane-air mixture that resembles the RCCI. At any given %CH_4, ignition delay increases as the engine speed decrease; only in the pilot-dominant regime where the physical parameters (i.e. temperature and pressure) inside the cylinder are the governing factors. This agrees with the behavior of diesel-only operation as discussed in Chapter 4. %CH_4 substitution ratio of 40% is an example of this case, as shown in Fig. 5.19.

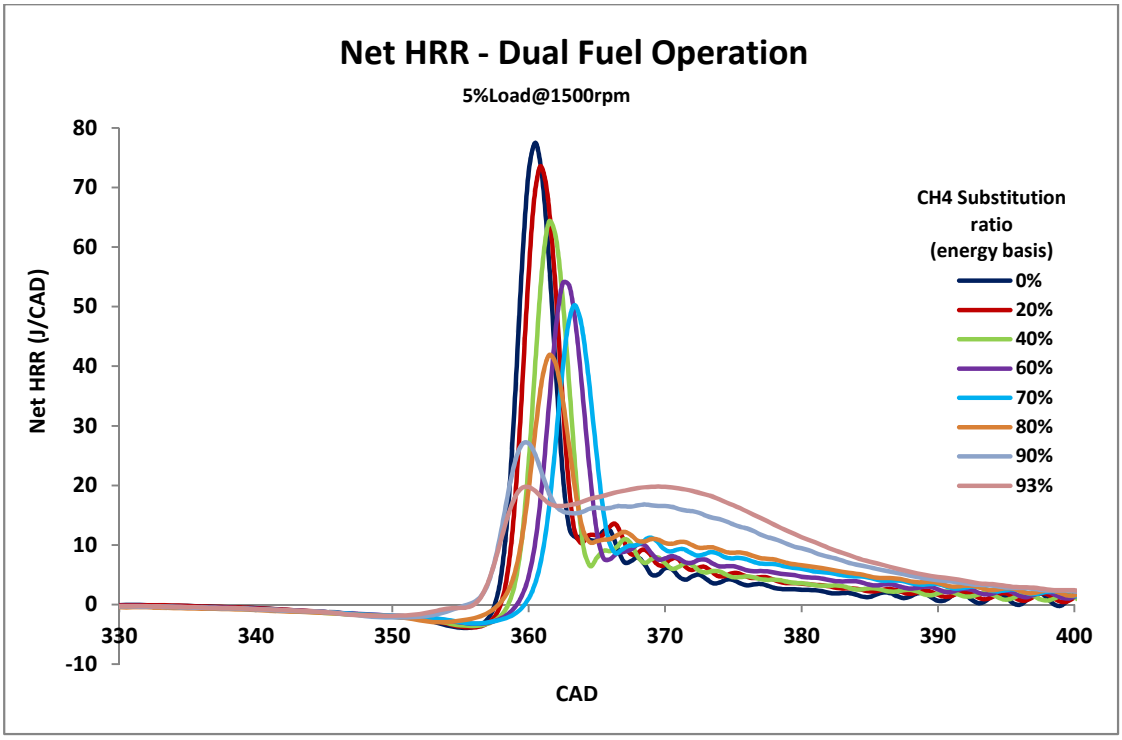


Figure 5.16 **Net HRR data for DF operation with different % CH_4 substitution ratios. Data is for 5% engine load @ 1500 rpm. Injection timing is set @ 10°BTDC.**

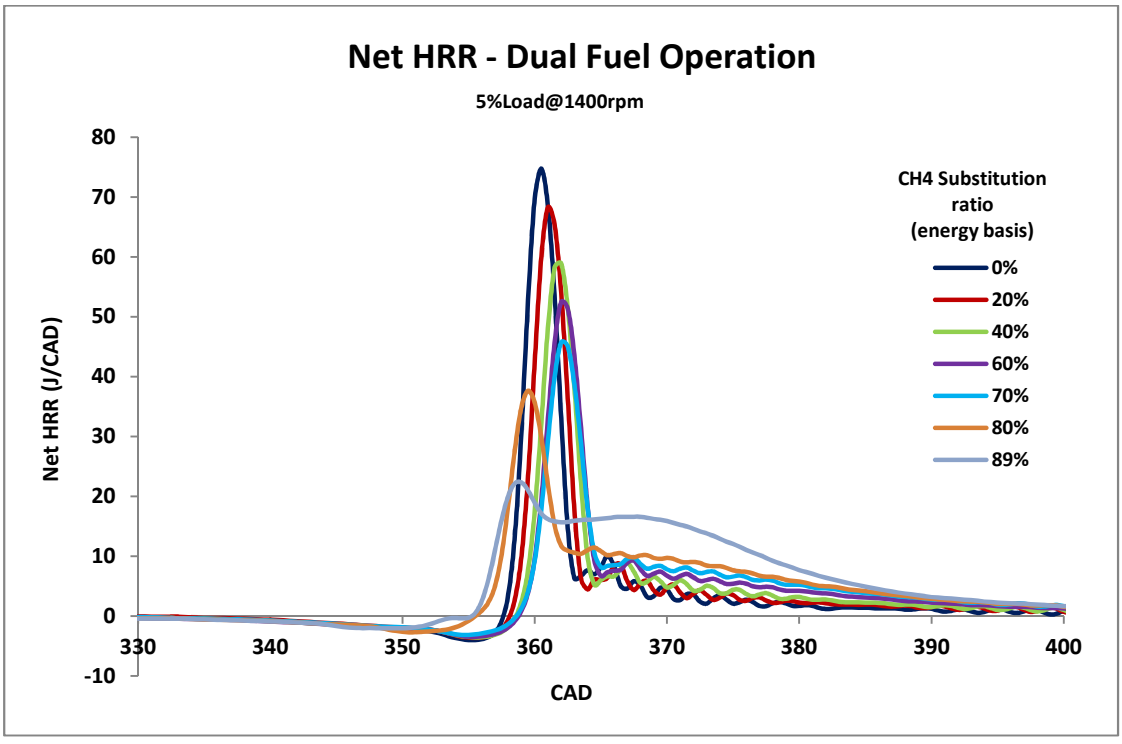


Figure 5.17 **Net HRR data for DF operation with different % CH_4 substitution ratios. Data is for 5% engine load @ 1400 rpm. Injection timing is set @ 10°BTDC.**

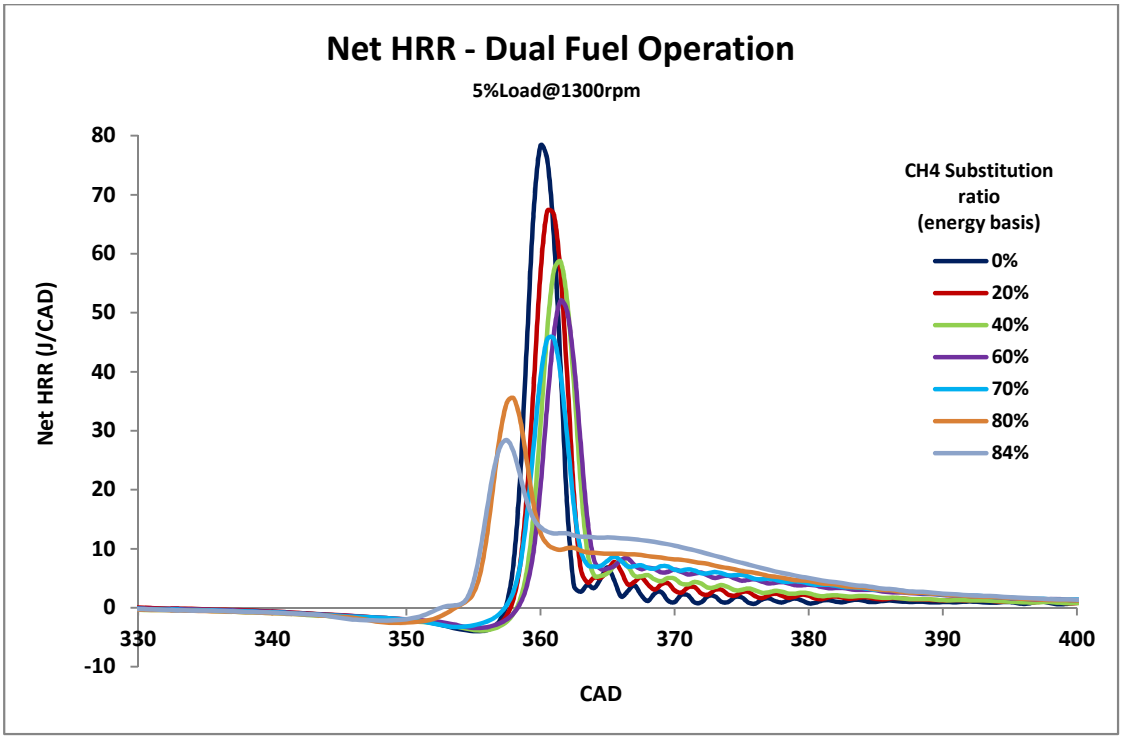


Figure 5.18 Net HRR data for DF operation with different % CH_4 substitution ratios. Data is for 5% engine load @ 1300 rpm. Injection timing is set @ 10°BTDC.

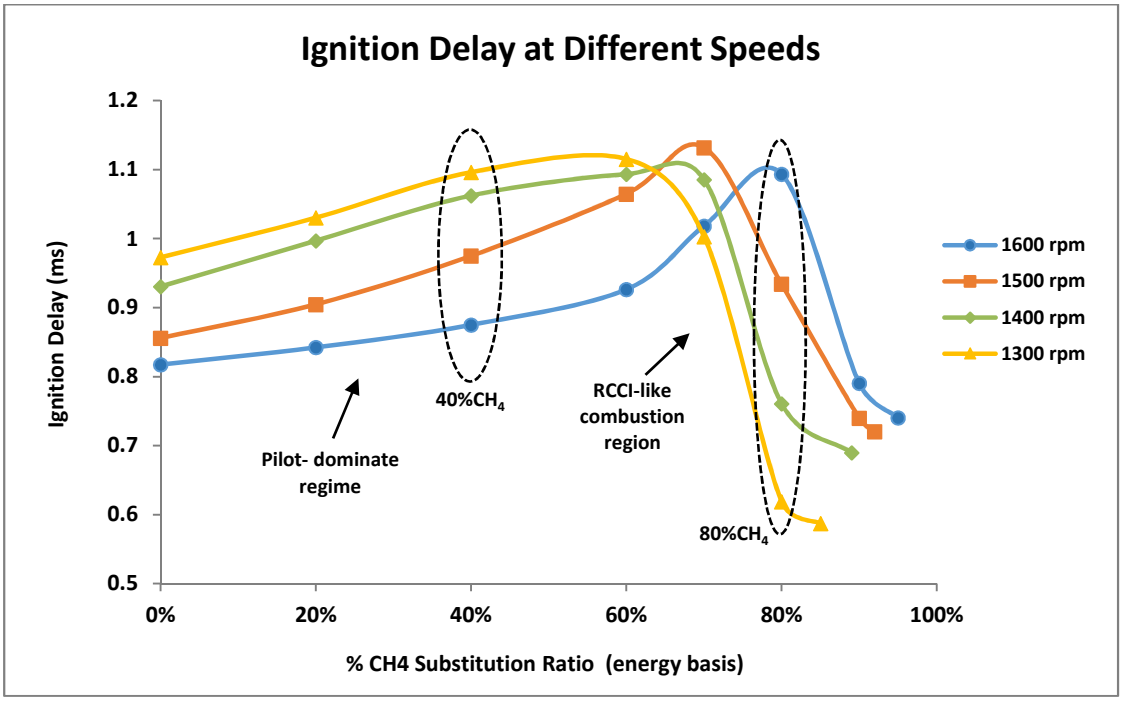


Figure 5.19 Ignition delay at different engine speeds with different % CH_4 substitution ratios. The two distinctive combustion mechanisms are revealed by the change in trend. Data is for 5% engine load, SOI @ 10°BTDC.

As the combustion mechanism change, chemical kinetics of the oxidation reactions of the fuel vapor-gaseous fuel-air mixture plays the key role [229]. Since the transition takes place at less %CH_4 substitution levels as the engine speed decreases; lower speeds demonstrate shorter ignition delay following their transition, as higher speeds are yet to undergo a complete transition into the RCCI-like mechanism. 80% CH_4 is an example of this condition; as shown in Fig. 5.19. The decisive criterion that discloses the change in combustion mechanism is, therefore, considered to be the ignition delay behavior, even if the change is yet to be visible on HRR trends. Figure 5.20 illustrates a simplified two-dimensional map for the %CH_4 substitution threshold values at which the transition of combustion mechanism takes place, at different engine speeds. It could be seen that this value drops from ≈80% at 1600 rpm to ≈70%, ≈65%, and ≈60% at 1500, 1400, and 1300 rpm respectively. Reduced CH_4-air mixture strength as the engine speed decreases requires more concentration of higher hydrocarbon vapor [239], and hence larger pilot quantities are required to initiate the transition at lower speeds. The dotted curved lines represent the constant speed contours on which other operating conditions for different %CH_4 ratios should appear on the $\dot{m}_{diesel}$ -ϕ_{CH4} space; but they were omitted from the figure for clarity. It is evident that the threshold values strongly depend on both $\dot{m}_{diesel}$ and ϕ_{CH4}, where a relationship between the two parameters is established throughout the range of speeds examined. At any given engine speed, the points above the line of transition are characterized as pilot-dominate combustion regime, where $\dot{m}_{diesel}$ rules. Alternatively, the points below the line experience the RCCI-like combustion that is largely affected by ϕ_{CH4}. It should be noted that this correlation is valid only for the current setup as obtained from the test cases examined, and any other fuel combinations or operating conditions (different load, EGR, injection timing, *etc*) might be subjected to a different boundary. The linear trend of the boundary in this test condition could be attributed to the close range of speeds investigated.

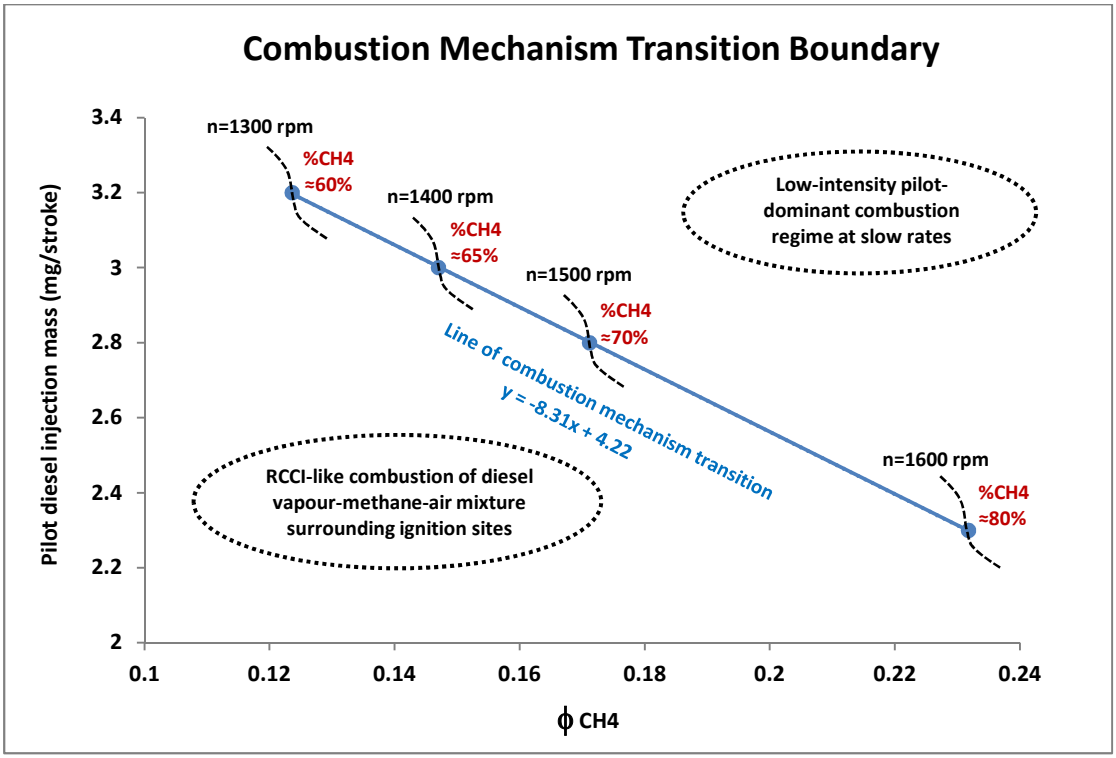


Figure 5.20 **Simplified two-dimensional map of combustion mechanism transition boundary at different engine speeds. Threshold values of $\%CH_4$ are highlighted in red (Substitution ratio axis is not represented in this map). The dotted curved lines represent the constant speed contours (omitted for figure clarity). Data is for 5% engine load, SOI @ 10°BTDC.**

The increased in-cylinder reactivity as the higher hydrocarbon vapor participates in the oxidation process, following the transition threshold, is also reflected as an accelerated combustion at a shorter duration. Figure 5.21 shows the duration of combustion (DOC) at different $\%CH_4$ substitution ratios; for different engine speeds. It could be seen that DOC increases with the $\%CH_4$, but only up to the threshold, then decreases afterward. The dotted line illustrates the trend for the 1300 rpm data. Contrasting the case with the ignition delay, DOC is always shorter with higher engine speeds at any given $\%CH_4$; regardless of the dominant combustion mechanism. This is attributed to the increased degree of turbulence inside the engine cylinder that enhances the combustion process under these conditions [58]. The absolute position of the center of heat release (CA50) observes the opposite trend, as it largely depends on the amount of the fuel. Figure 5.22 shows that at any given $\%CH_4$, CA50 position at higher engine speeds is always further in the expansion stroke relative to that at the lower speed. At all speeds, however, CA50 shifts back towards the TDC after reaching its farthest position at the threshold point.

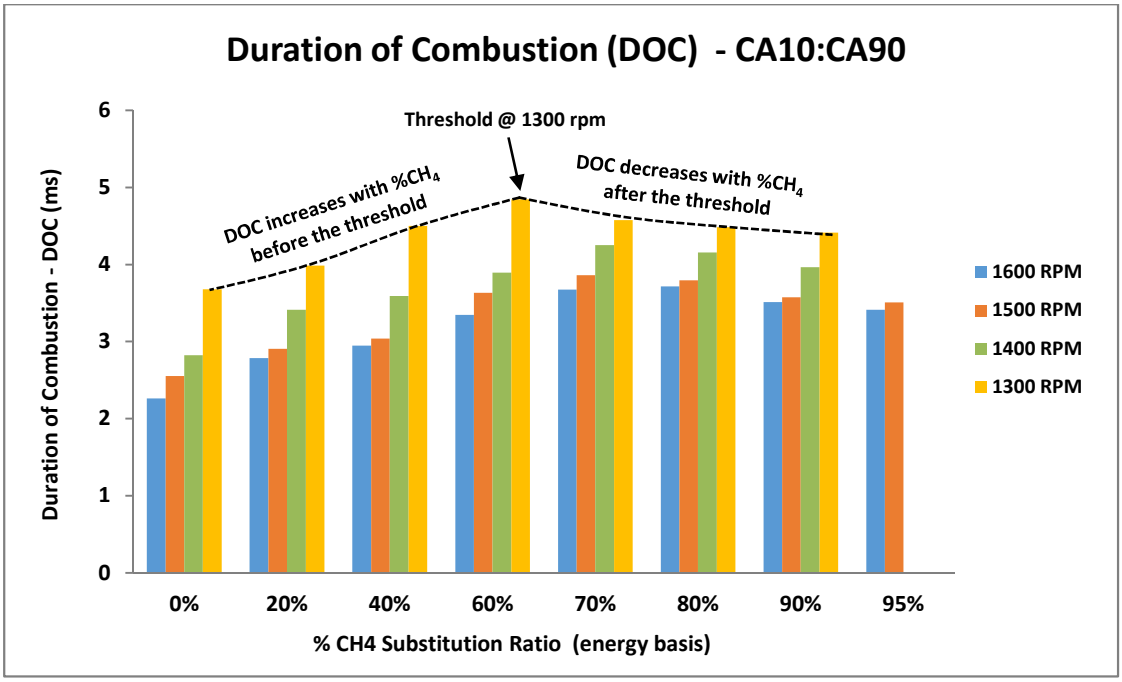


Figure 5.21 **Duration of combustion (CA10:CA90) at different speeds with different %CH_4 substitution ratios. X-Axis values are based on the %CH_4 substitution @ 1600 rpm. Max. %CH_4 substitutions are 84%, 89%, and 93% at 1300, 1400, and 1500 rpm. Data is for 5% engine load, SOI @10°BTDC.**

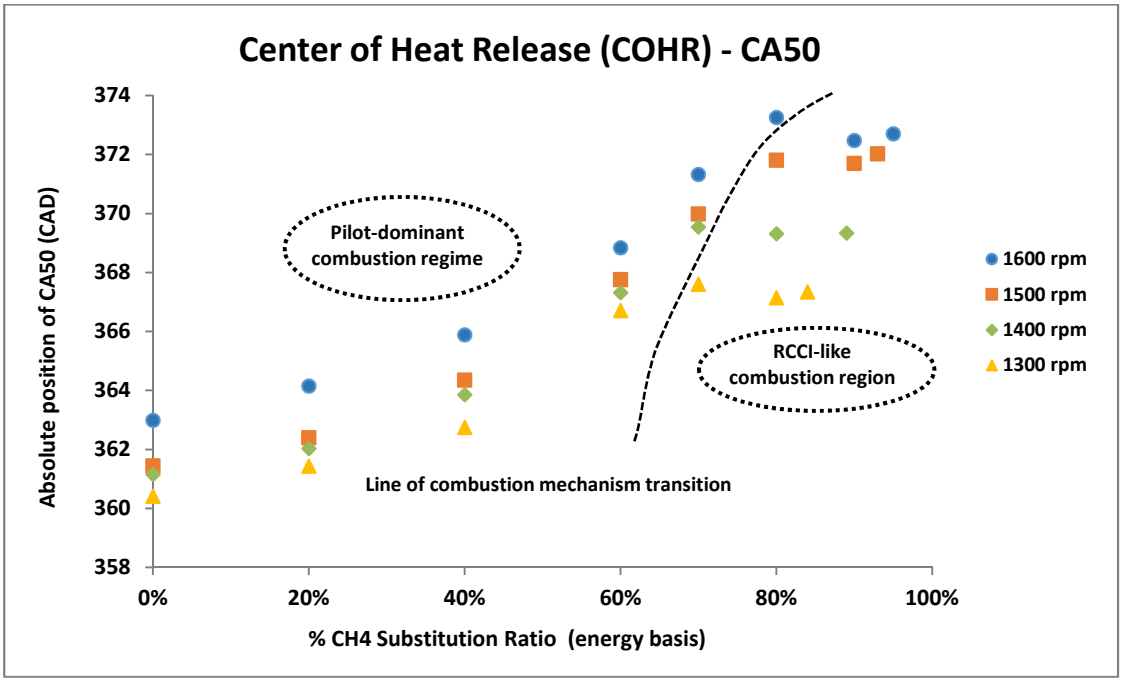


Figure 5.22 **Center of heat release (CA50) at different speeds with different %CH_4 substitution ratios. The two distinctive combustion mechanisms are revealed by the change in trend. Line of transition is not to scale and used for graphical representation only. Data is for 5% engine load, SOI @10°BTDC.**

The maximum possible methane substitution for diesel fuel in the test cases examined drops from ≈95% at 1600 rpm to ≈93%, ≈89%, and ≈84% at 1500, 1400, and 1300 rpm; respectively. The corresponding values of diesel pilot injection mass at these last three points were 0.9, 1.1, and 1.4 mg/stroke, respectively, which are greater than the limiting minimum value of the FIE used (0.8 mg/stroke). Larger pilot masses imply an increased degree of the in-cylinder reactivity; this is revealed by a larger amount of pre-ignition heat release as illustrated in Fig. 5.23.

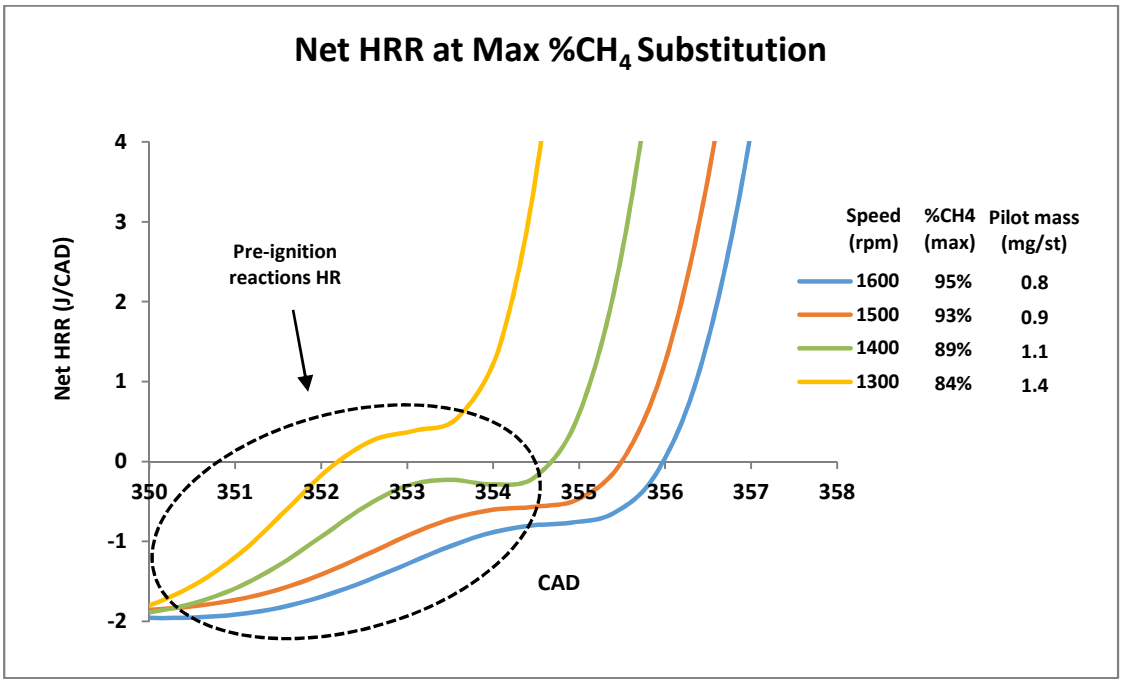


Figure 5.23 **Magnified part of the net HRR at the maximum %CH4 substitution for different engine speeds. Pre-ignition reactions are more voluminous at lower speeds due to larger pilot mass. Data is for 5% load, SOI @ 10°BTDC.**

The fact that pilot masses exceed the FIE limiting value suggests that the restriction on methane substitution under these conditions is not caused by a system-limitation. Figure 5.24 shows a two-dimensional map of the maximum possible methane substitution, in $\dot{m}_{diesel}$ - ϕ_{CH4} space. Constant speed contours (on which other fuelling settings should be plot) are partially represented by the dotted curves. At a given speed, any $\%CH_4$ value higher than the upper limit, i.e. below the line, sets the engine at high level of instability, uncontrollable running, and misfiring. This is evident by the elevated levels of engine cyclic variability (represented by $COV_{IMEPgross}$), as shown by Fig. 5.25. The restriction on methane substitution at these conditions is considered as an operation-limitation.

In opposition, the engine stability at any lower %CH4 substitution levels, i.e. above the line, remains in the range with a $COV_{IMEPgross}$ value less than 8%. The engine observes a stable RCCI-like combustion in diesel vapor-CH_4-air mixture in this region, but only within a certain boundary beyond which the combustion mechanism change into pilot-dominant, as presented in Fig. 5.20. Figure 5.24 shows a linear correlation governing the $\dot{m}_{diesel}$ - ϕ_{CH4} relationship at the maximum %CH_4 substitution, for different engine speeds investigated. This linear trend is observed until the line of the minimum diesel injection amount is met. Any further increase in ϕ_{CH4} after this point takes place at the minimum $\dot{m}_{diesel}$ amount, until the engine operation is limited by the $COV_{IMEPgross}$ value. This supports the earlier observation found with engine speed of 1600 rpm, where a combination of FIE limitation on fuel injection mass and high $COV_{IMEPgross}$ was met. Once more, this correlation is valid only for this setup and test conditions, and might change with different configuration.

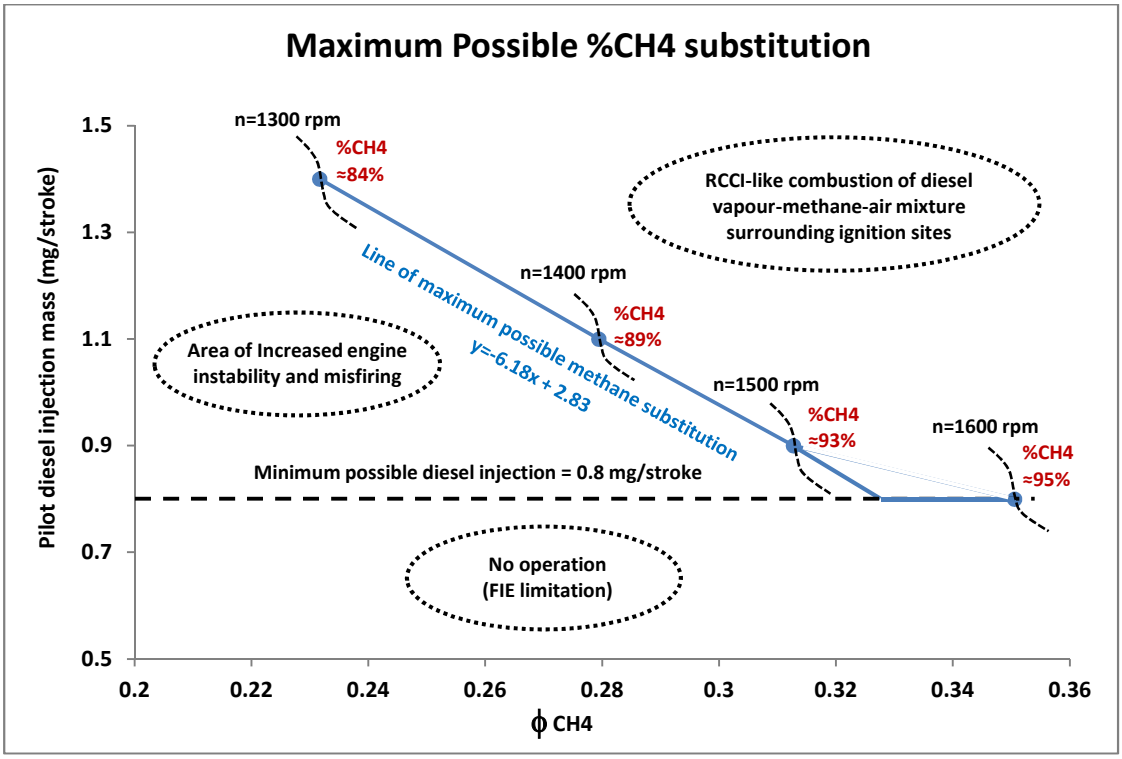


Figure 5.24 **Simplified two-dimensional map of maximum possible methane substitution for diesel fuel at different engine speeds. The values of Maximum %CH_4 are highlighted in red (Substitution ratio axis is not represented in this map). The dotted curved lines represent the constant speed contours (omitted for figure clarity). Data is for 5% engine load. Injection timing is set @ 10°BTDC.**

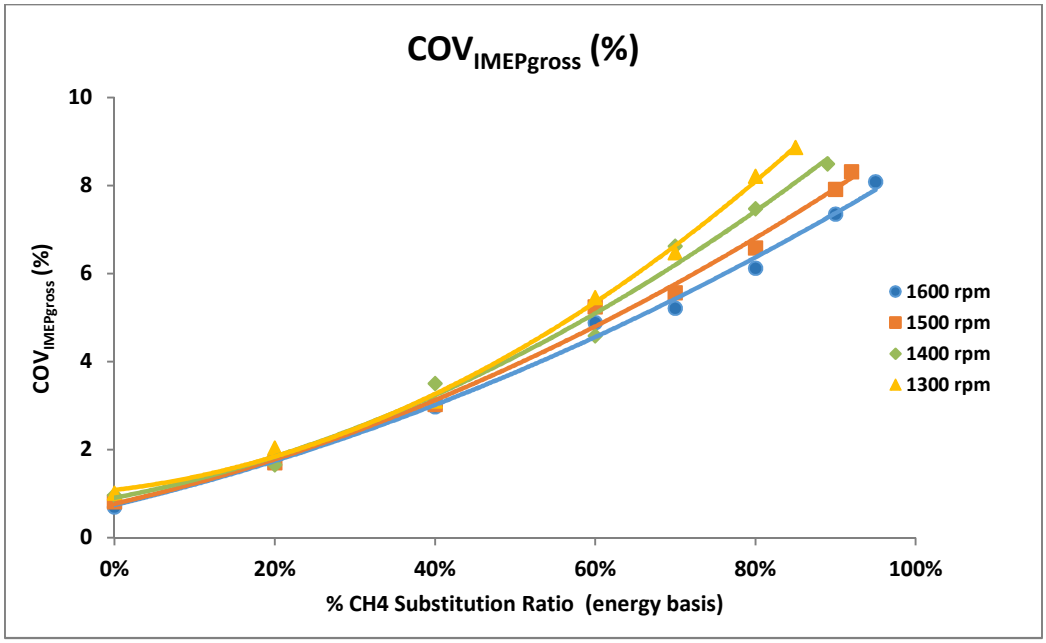


Figure 5.25 **COV of gross IMEP at different engine speeds with different %CH_4 substitution ratios. Data is for 5% load. Injection timing is set @ 10°BTDC.**

It could be seen from Fig. 5.25 that for the same power level (speed and load), engine stability deteriorates as the gas substitution ratio increases. This is mainly attributed to the variation of the burning rate of methane in the weak mixture (ϕ_{CH4}<0.3). Partial burn cycles appear more frequently as the substitution ratio increases until complete misfire takes place at the ultimate $COV_{IMEPgross}$ value (~9%). The criterion on acceptable engine stability levels under DF operation is usually considered as $COV_{IMEPgross}$ ≈5% [19]. This value is attained at higher substitution ratios as the engine power increases. The use of larger pilot size enables the use of larger amount of gaseous fuel at higher substitution ratio, where the engine load increases while the stability is maintained. Table 5.1 lists the numeric values of two tests cases maintaining $COV_{IMEPgross}$ ≈3%, at constant engine speed of 1600 rpm. Engine load increases as a consequence of increasing both fuels.

Table 5.1 **Impact of pilot fuel size on gaseous fuel amount and substitution ratio at the same engine stability level ($COV_{IMEPgross}$ ≈3%), at constant speed of 1600 rpm.**

Pilot size (mg/stroke)	Gas admission @ COV_{IMEP}≈ 3% (m3n/hr)	Substitution ratio (%CH4)	Engine load (% rated load)
5.8	0.9	40%	5%
6.7	3.4	70%	25%

The operation of dual-fuel engines at low load conditions is characterized by poor fuel conversion efficiency. While lower engine speeds exhibit a slightly better fuel economy as they encounter less friction, DF operation remains much inferior to conventional diesel one; especially at high %CH_4 substitution ratios. The diminished performance is attributed to the poor fuel utilization as large part of the weak CH_4-air mixture escapes the combustion process, the slow burning rates, the lower cylinder pressure values, and the increased engine instability. Figure 5.26 shows the brake thermal efficiency trends for dual-fuel operation at different engine speeds, throughout the entire range of %CH_4 substitution ratio investigated.

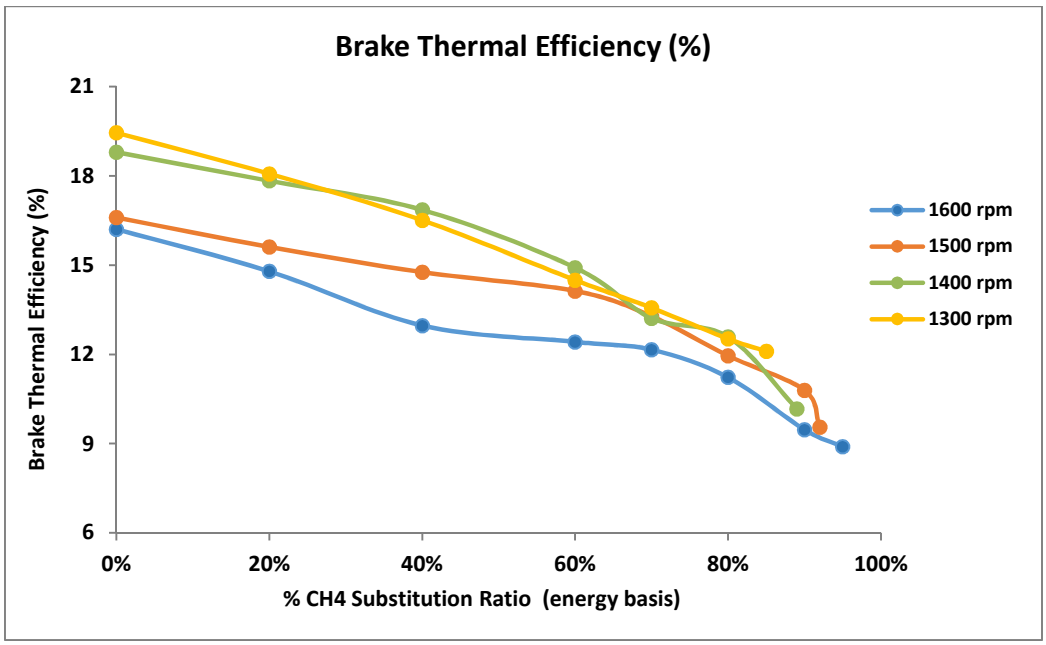


Figure 5.26 Brake thermal efficiency at different engine speeds with different % CH_4 substitution ratios. Data is for 5% load. Injection timing is set @ 10°BTDC.

5.5 Conclusions

In this chapter, combustion process in methane-diesel DF engines was experimentally studied at light load (25%) with different substitution ratios (up to 80%). The maximum substitution ratio of methane for diesel fuel at near-idle low-load conditions (5% of the rated load) was investigated. The focus of the study was the heat release characteristics. Some of the key findings are:

- Typical heat release diagram for gaseous fuel-diesel dual-fuel engines is made of the following stages:
  - Ignition delay: the period between the start of injection (SOI) of the diesel fuel into the cylinder, and the start of combustion (SOC); identified in the present work as the point at which the net HRR reaches 2 Joule/CAD.
  - Stage-1 combustion: this stage is characterized by a sharp rise in the HRR curve due to the combustion of a large amount of diesel fuel after the ignition delay ends. There is an evident entrainment of some of the gaseous fuel into this stage; particularly the part in the immediate vicinity of the pilot ignition sources.
  - Transient stage: a very shorts stage presents the transition from the auto-ignition of premixed diesel vapor along with the entrained gaseous fuel, into the regime in which the majority of gaseous fuel is expected to burn.
  - Stage-2 combustion: in which the bulk of the gaseous fuel-air mixture distant from the influence of diesel pilot zone is expected to burn; mostly in a turbulent flame propagation event (for gaseous fuel equivalence ratio $\phi_{CH4} > 0.35$).
- Stage-1 combustion is always dominated by the ignition and rapid combustion of the premixed part of the diesel pilot; regardless of the amount of gaseous fuel used. However, the level of gaseous fuel entrainment increase with the substitution ratio; indicating that it is more affected by the mixture strength than by the jet properties.
- The dominant combustion mechanism in stage-2 combustion is largely determined by the relative magnitudes of diesel pilot and gaseous fuel available for combustion at this stage. At low gaseous fuel concentration ($\phi_{CH4} < 0.3$), the ensuing combustion is categorized as a “pilot-dominant”, where the gaseous fuel conversion takes place in a low-intensity non-flame propagation event.

- At very low load and high substitution ratios, the pilot injection mass is sufficiently small that it can evaporate then locally intermix with the very lean gaseous fuel-air mixture; increasing the charge reactivity. This yields an RCCI-like combustion in diesel vapor-methane-air mixture surrounding ignition sites. Complete evaporation occurs at pilot masses as low as 1.6 mg/stroke, however, the combustion mechanism starts to change at as much as twice this value.
- The substitution ratio threshold at which the combustion mechanism changes from the low intensity-pilot dominant into the RCCI-like combustion reduces from ≈80% at 1600 rpm to ≈70%, ≈65%, and ≈60% at 1500, 1400, and 1300 rpm; respectively. The reason behind this is the need for a larger pilot mass (i.e. more diesel vapor) to initiate the transition with weaker methane-air mixtures.
- At all speeds, ignition delay period increases with the increase of substitution ratio; but only up to the threshold. The behavior is reversed following the threshold due to the increased degree of reactivity inside the cylinder.
- The minimum amount of pilot injection mass with the current FIE used is 0.8 mg/ stroke. This presents a system-limitation on maximum achievable substitution ratio.
- The maximum gas substitution ratio achieved was as high as 95% at 1600 rpm. This value decreases to 93%, 89% and 84% at 1500, 1400, and 1300 rpm; respectively. Methane substitution beyond these limits is restricted by the ultimate value of the $COV_{IMEPgross}$ value for a stable running (≈8% − 9%); i.e operation-limitation.
- The use of larger diesel pilot injected mass allows for the use of a larger amount of the gaseous fuel; without exceeding the stability criterion ($COV_{IMEPgross}$ ~ 5%).

CHAPTER SIX

EFFECT OF PILOT PRE-INJECTION ON DUAL-FUEL ENGINES COMBUSTION

6 Effect of Pilot Pre-Injection on Dual-Fuel Engines Combustion

6.1 Introduction

In Chapter 4, it was proven that the use of split injection (i.e. pre-injection followed by main injection) in HPCR diesel engines improves fuel economy and reduces the rates of pressure rise. Chapter 5 revealed that the evaporation and mixing of a small diesel fuel amount in the lean gaseous fuel-air mixture improves the combustion initiation and changes the combustion mode. These findings complement the outcome of Chapter 3, where it was shown that the use of pilot-split injection in dual-fuel engines changes the combustion mode from the conventional diesel dual fuel (DDF) combustion to a novel two-stage partially premixed dual fuel (PPDF) combustion that has several advantages to engine combustion and emissions.

The aim of this chapter is to investigate the effect of pilot pre-injection on DF engines combustion. The optimum injection strategy to attain PPDF combustion is determined, and the influence of pilot pre-injection mass on the combustion process is examined. The focus of the work is the light load operating conditions (25% of rated load), at wide ranges of engine speeds and substitution ratios of methane for diesel fuel.

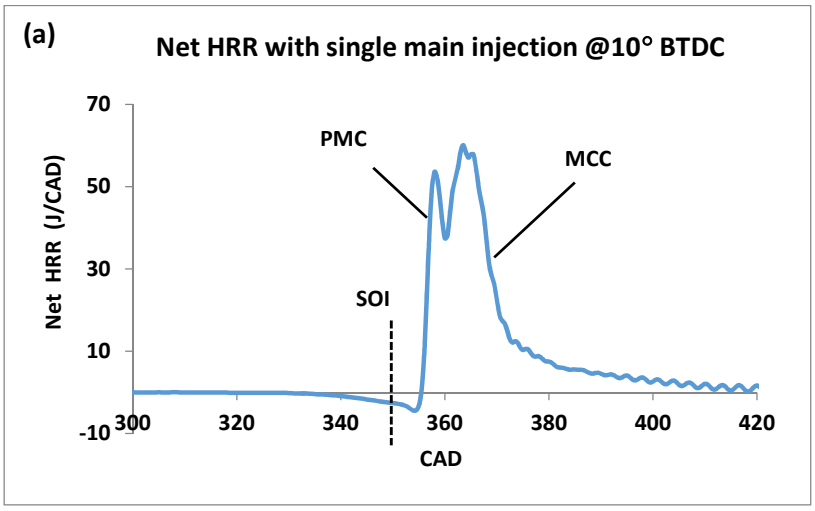
6.2 Overview and Method

As discussed in Chapter 3, the key to combustion mode change in dual-fuel engines is the pilot fuel injection strategy [37]. Table 6.1 summarizes the differences in the pilot injection strategy between DDF, HCCI-DF, and PPDF combustion modes.

Table 6.1 Summary of the pilot injection strategy in different DF combustion modes.

Combustion Mode	Pilot Injection Strategy	Theory
Conventional DDF	Single injection; late in the compression stroke.	To act as an ignition source for the premixed CH4-air mixture.
HCCI-DF	Single injection; early in the intake stroke.	To form a lean homogeneous mixture of diesel with the CH4-air mixture.
PPDF	Two injections; an early pre-injection part (small size), followed by a late injection of the main part of the pilot.	The pre-injection part acts as an ignition improver; the main pilot injection then initiates the combustion that further propagates throughout.

To approach PPDF combustion, the pre-injection part of the pilot should be optimized in timing and quantity. With regard to timing, it should be noted that too early injection will cause spray impingement and poor atomization of fuel, while too late injection will lead to the incidence of classical diesel ignition [241]. To assess the optimum timing with the current setup, a sweep of different pre-injection timings (ranging from 20° to 80° BTDC) was investigated under conventional diesel operation at 1600 rpm and 25% load, with the main injection fixed at 10° BTDC. Any significant changes in the diesel combustion mode would essentially be reflected on the subsequent combustion of the gaseous fuel-air mixture [64]. To avoid any possible high rates of pressure rise with the early injection timings, the pre-injection quantity was kept at 10% of the total diesel fuel supplied to the engine. The resulting HRR curves when pre-injection is used were compared with that obtained from the single injection of diesel fuel (set at 10° BTDC). Figure 6.1 (a-d) show the resulting HRR curves for some selective test cases.



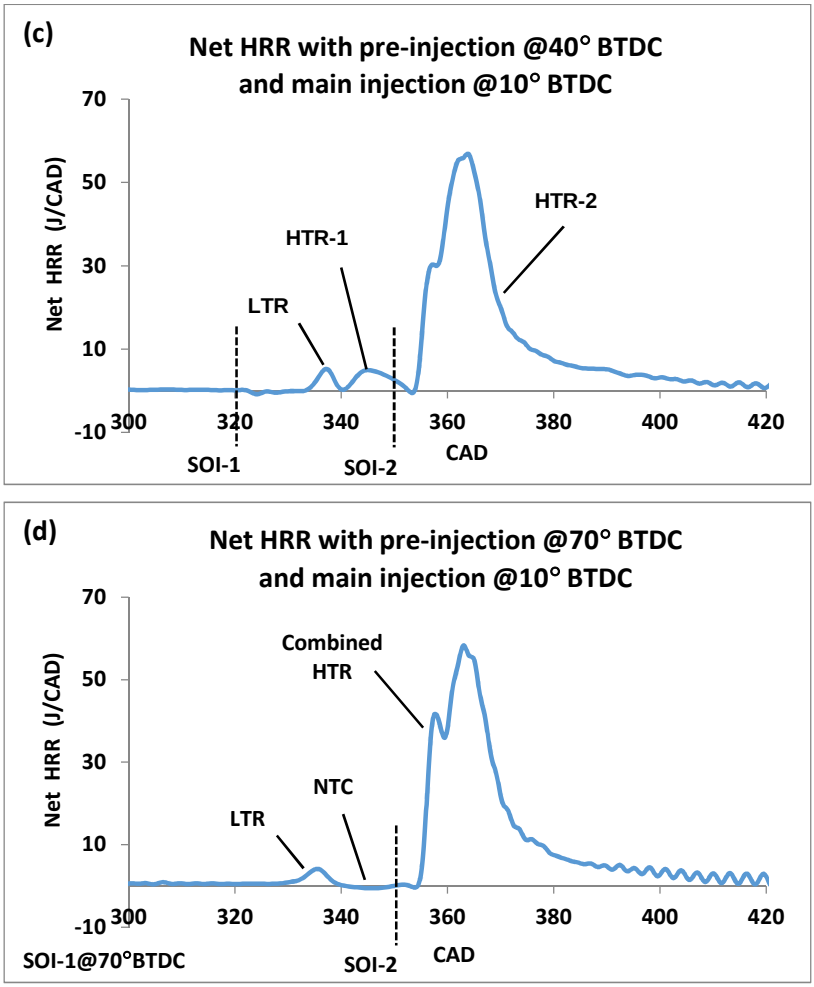


Figure 6.1 **The influence of diesel injection strategy on the net HRR and combustion mode; (a) with single main injection of diesel @10° BTDC; (b), (c), (d) with two split injections with the main injection fixed @10° BTDC and the pre-injected set to 25°, 40°, and 70° BTDC; respectively. Data for conventional diesel operation at 1600 rpm and 25% load.**

It can be seen from Fig. 6.1 (b) that the relatively late injection timing @ 25° BTDC of the pre-injection will result in the characteristic CI spray combustion mode (i.e. that distinguishes diesel engines) of that pilot. This is attributed to the elevated high pressure and temperature inside the engine cylinder upon injection, and hence as soon as the ignition delay (ID) of that part of injection ends, it burns immediately. Nevertheless, in contrast with the classical diesel combustion that is characterized by the presence of two phases; premixed combustion (PMC) and mixing-controlled combustion (MCC) as shown in Fig. 6.1 (a) and described in Chapter 4, the combustion of the relatively late pre-injection will take place over only one stage, due to its limited quantity. This stage (referred to as HTR-1) is predominantly a high-temperature reaction that increases the

cylinder temperature significantly. Accordingly, the main part of the fuel subsequently injected experiences a very short ID, after which it will burn in a second HTR (referred to as HTR-2) with much less premixed fraction and lower noise levels; as discussed in Chapter 4.

When the pre-injection timing is advanced, its ignition mode changes from the classical diesel combustion mode into a two-stage combustion mode. As shown in Figs. 6.1 (c) and (d), this mode is characterized by the presence of a low-temperature reaction (LTR), or a cool flame zone, that has a high degree of reactivity due to a high level of radicals [67]. In an ideal HCCI two-stage combustion, a negative temperature coefficient (NTC) zone separates the LTR and the HTR regimes without any other heat release processes [67]. Nevertheless, with an average advance of the pre-injection timing, e.g. 40° BTDC as shown in Fig. 6.1 (c), in-cylinder conditions (pressure and temperature) are relatively high and favor combustion. As a result, the LTR at these conditions could be followed by a HTR of some part of the pre-injection (referred to as HTR-1), and the NTC is not realized. Any unburned fraction of the pilot pre-injection will then burn in the main combustion event (HTR-2) that takes place after the auto-ignition of the main injection. With further advance of the pre-injection timing, e.g. 70° BTDC as illustrated in Fig. 6.1 (d), the NTC zone becomes recognizable after the LTR zone, while the HTR-1 no longer exists. Instead, a combined HTR regime for the pre-injection along with the main injection occurs, with a larger premixed part compared with the retarded per-injection timings, and at higher rates of heat release. But in both cases, as long as the two-stage ignition mode is attained, the LTR zone always occurs at a specific position; about 20-25°BTDC [67].

In view of that, it was concluded that an optimum pre-injection timing for the current setup would be around 50° BTDC with the main injection timing set to 10° BTDC. This would bring about a two-stage ignition mode of the pilot that promotes the combustion of the main injection that subsequently burns at acceptable rates of heat release.

As far as the optimum quantity of the pre-injection part of the pilot is considered, it is noted that too large pre-injections may cause high rates of pressure rise (ROPR) beyond the acceptable levels. Too small quantities, on the other hand, might not be capable of producing the desired cool flame reactions and active radicals. Another critical factor

that has to be considered is the limitation on the minimum amount of fuel that could be injected through a given FIE, as discussed in Chapter 5. In conventional diesel engines with split injection strategy, the pre-injection part is usually set to a certain percentage of the total diesel fuel used at the particular operating condition. This procedure was preliminary used in the current work, to quantify the size of the pre-injection part of the pilot; i.e.:

$$\%\ \mathrm{FR}_{Pre} = \frac{\dot{m}_{Pre}}{\dot{m}_D} \times 100\% \tag{6.1}$$

where ($\%FR_{Pre}$) is the size of the pre-injection, as a fixed ratio (percentage) of the total diesel fuel supplied to the engine (inclusive of the pre-injection), ($\dot{m}_{Pre}$) is the mass flow rate of the pre-injection, and ($\dot{m}_D$) is the total mass flow of the diesel fuel.

To set a solid base of comparison, the value of $\%FR_{Pre}$ should be kept constant for all test cases examined. To assess the value that could be maintained throughout the entire range, a sweep of different pre-injection masses (ranging from 5% to 25% FR_{Pre}) was investigated under conventional diesel operation at 1600 rpm and 25% load. The sweep tests were conducted at the optimum pre-injection timing of 50°BTDC (as determined earlier) and main injection timing of 10°BTDC. Figure 6.2 shows the Net HRR data for pre-injection masses of 10% and 20%FR_{Pre}. It could be seen from the figure that the quantity of pre-injection does not affect the position of the LTR zone (it appears at 20-25° BTDC as highlighted above), but it slightly affects its magnitude. This is attributed to the availability of large amount of fuel with larger pre-injection masses to go through the cool flame reactions. It is the relative magnitudes of the HTR zones that experience the more apparent change, where the larger $\%FR_{Pre}$ leads to the release of larger amount of active radicals that promotes the combustion of some of the pre-injection part; owing to the relatively high cylinder temperature at these conditions. For that reason, the HTR-1 zone becomes more distinguished in Fig. 6.2 (b) as more fuel experiences combustion. The HTR-2 at these conditions exhibits a smaller premixed part, because of the reduced contribution of the pre-injection from one side, in addition to the reduced ID of the main injection from the other side (shorter ID reduces the premixed fraction, as discussed in Chapter 4). It should be taken into consideration that the designated $\%FR_{Pre}$ has to be achievable at all $\%CH_4$ substitution ratios investigated, to solidify a base of comparison.

As the current work involves CH4 substitution ratios as high as 80%, it was found that a value of 20% FR_{Pre} would be the optimum pre-injection ratio that could consistently be realized without compromising the cool flame effect or the ROPR.

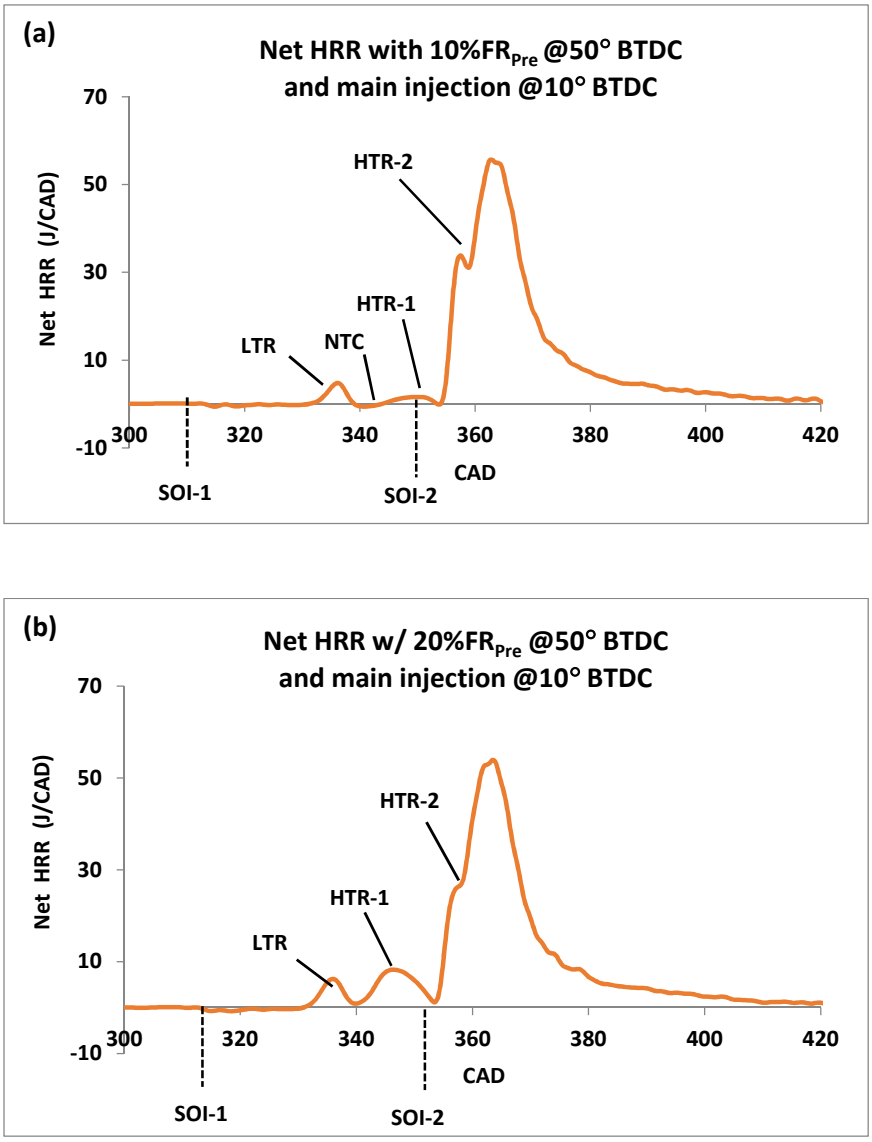


Figure 6.2 **The influence of pre-injection ratio (%FR_{Pre}) on the net HRR at optimum injection timing of 50° BTDC; (a) 10% FR_{Pre}, and (b) 20% FR_{Pre}. The quantity of the main injection varies accordingly, but its timing is always set @10° BTDC. Data is for conventional diesel operation at 1600 rpm and 25% load.**

6.3 PPDF Combustion vs. Conventional DDF Combustion

The outcome of the sweep tests reveals that the sought-after change in the pilot ignition mode could be achieved by employing a pilot pre-injection quantity of 20% of the total diesel fuel (i.e. 20%FR_{Pre}) injected at 50° BTDC, while the main injection is kept at 10° BTDC. This injection strategy will be employed in dual fuel operation in an attempt to attain the PPDF combustion modes. The results of PPDF tests are then compared with those obtained from conventional DDF operation (with single injection @10°BTDC), at the same operating conditions. The focus of the study is the light load conditions that prevail in city traffic. Therefore, the experiments were conducted at 25% of the engine rated load at a wide range of speed from 2000 rpm down to 1400 rpm, with different substitution ratios of methane for the diesel fuel (from 20 to 80% on energy basis).

Figure 6.3 (a) and (b) show the in-cylinder pressure traces and the associated values of maximum ROPR for DDF and PPDF combustion modes at different CH_4 substitution ratios. From the figure, it can be seen that PPDF mode exhibits higher cylinder pressure values compared with conventional DDF mode; particularly at high %CH_4. The reason behind this is the earlier start of combustion associated with the use of pre-injection in PPDF, as the presence of active radicals from the LTR zone promotes the combustion process. The earlier start of the intensified combustion yields higher cylinder pressure values [242]. The effect is more voluminous at high %CH_4, as DDF combustion itself at these conditions exhibits prolonged combustion duration, as discussed in Chapter 5, which results in lower cylinder pressure values. Above and beyond, the use of pilot pre-injection in PPDF means that the combustion process will start with an auto-ignition of a less amount of the diesel fuel, and hence the maximum ROPR values are much less compared with DDF. The average reduction in maximum ROPR with PPDF is as high as 17%. This is advantageous to engine combustion noise, fuel economy, and NOx and PM emissions [40].

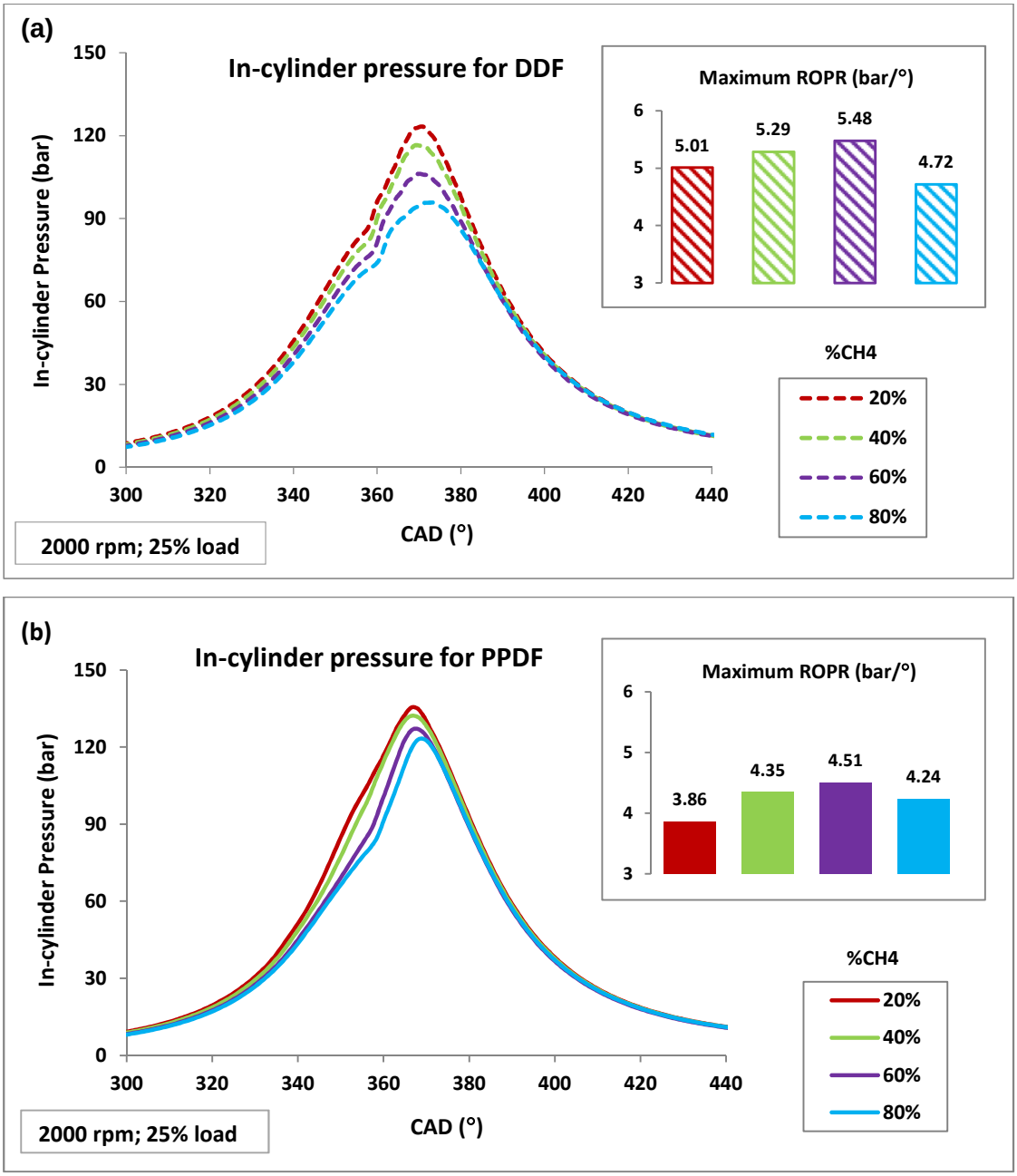


Figure 6.3 **In-cylinder pressure and the associated maximum ROPR (in the inset), for (a) conventional DDF operation with single pilot injection @10° BTDC, and (b) PPDF operation with 20%FR_{Pre} @50° BTDC and main injection @10° BTDC. Data is for 25% load at 2000 rpm, for 20, 40, 60 and 80% CH_4 substitution ratio.**

Figure 6.4 (a) and (b) show the net HRR traces, along with the corresponding positions of the occurrence of CA50; for both DDF and PPDF modes at different CH_4 substitution ratios. The LTR zone could be observed with PPDF combustion as already discussed, although its magnitude notably decreases with the increase of % CH_4. This is the natural consequence of the decrease in the pre-injection mass, as the total diesel fuel injected

decreases according to Equation (6.1) above. However, it is believed that the small pre-injection is still capable of increasing the degree of reactivity inside the engine cylinder and promoting combustion. This is evident by the enhanced burning rates and reduced combustion duration at all %CH_4 ratios; in contrast with DDF [89]. Yet, HTR-1 zone decreases as the %CH_4 increases; owing to the reduced pre-injection quantity.

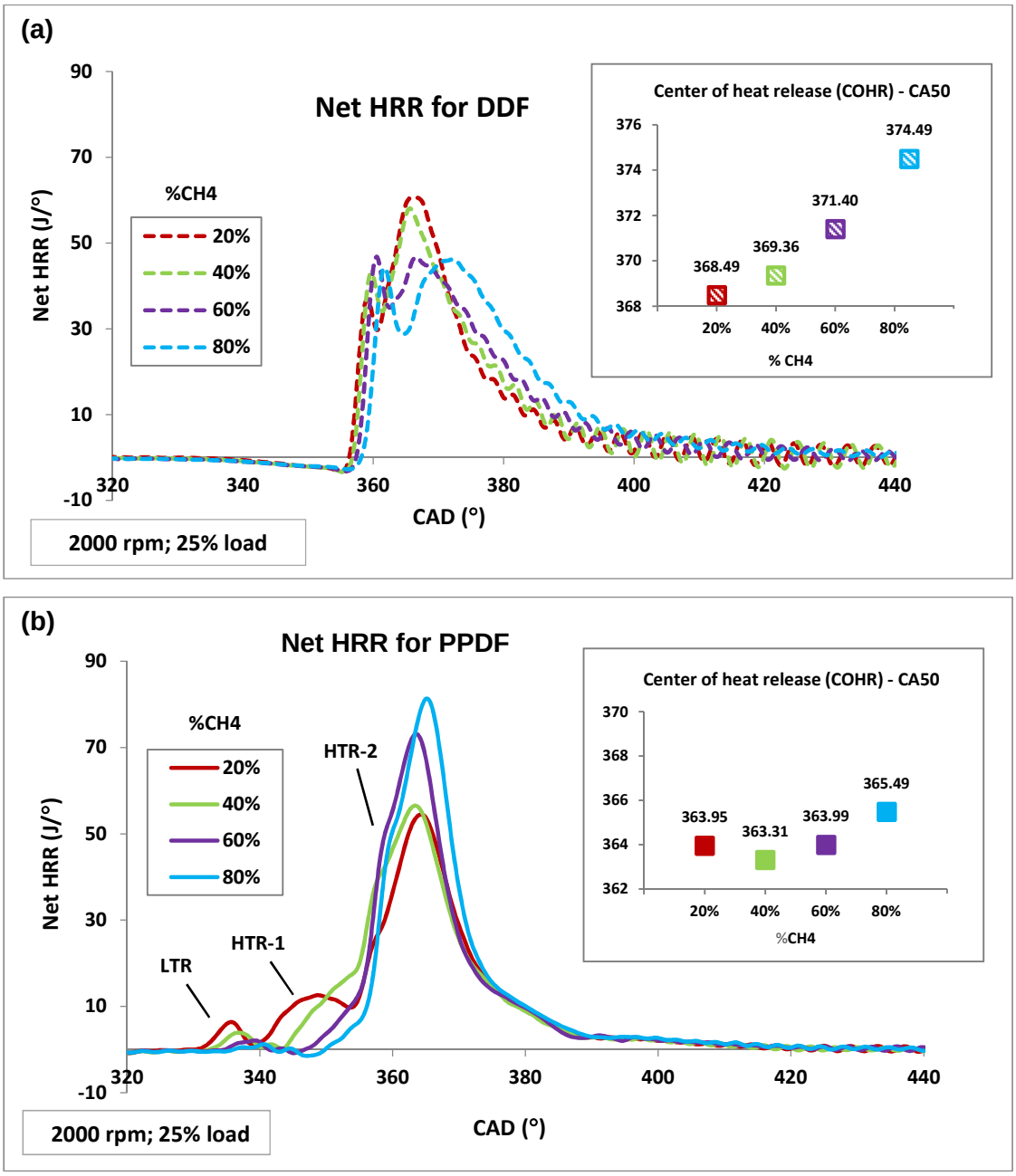


Figure 6.4 **Net HRR data and the corresponding positions of the occurrence of CA50 (inset), for (a) conventional DDF operation with single pilot injection @10° BTDC, and (b) PPDF operation with 20%FR_{Pre} @50° BTDC and main injection @10° BTDC. Data is for 25% load at 2000 rpm, for 20, 40, 60 and 80% CH_4 substitution ratio.**

Combustion phasing, as represented by CA50, is much improved with PPDF, where the major part of the heat release takes place closer to the TDC; producing a more useful work [243]. The late stages of heat release with PPDF are also free of any ringing visible (unlike DDF); demonstrating the reduction of combustion noise.

The effect of pre-injection on engine stability and performance is illustrated in Figs. 6.5 and 6.6, respectively. It could be noticed from Fig. 6.5 that the use of pre-injection in PPDF mode maintains the engine cyclic variability (as represented by $COV_{IMEPgross}$) at acceptable levels (2-3%) throughout the entire range of $\%CH_4$. This is attributed to the intensified combustion in the PPDF mode that provides better engine stability [242]. With DDF, on the contrary, the use of high $\%CH_4$ ratios is always associated with high cyclic variability, particularly at part load, owing to flame propagation problems [244]. This has been demonstrated in Chapter 5, where the increased COV_{IMEP} was even found to set and operating-limit on the conventional DDF operation at high $\%CH_4$ substitution ratios. Above and beyond, Fig. 6.6 shows that more than 5% improvement in the engine performance, as represented by the brake thermal efficiency, could be achieved when the engine is switched from DDF to PPDF operation. This improved performance is the consequence of the combination of many factors; including increased cylinder pressure, reduced ROPR, enhanced combustion intensity, faster burning rate, better combustion phasing, and increased engine stability.

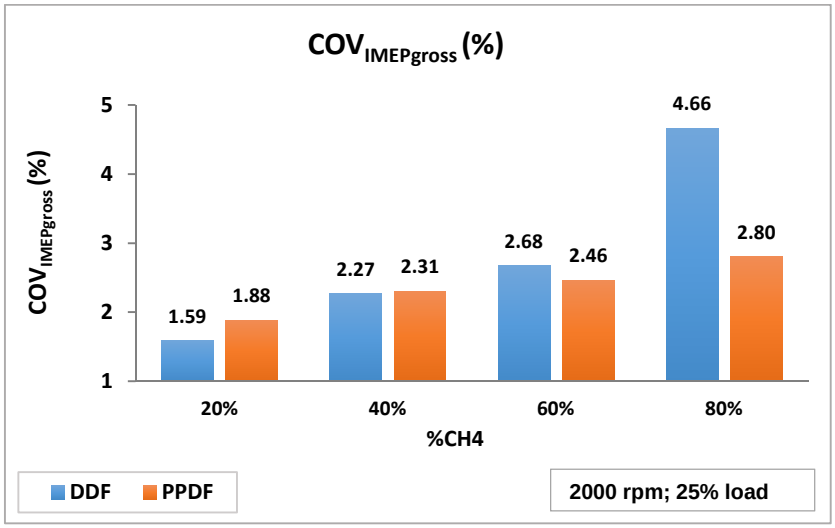


Figure 6.5 Coefficient of variation ($COV_{IMEPgross}$); for both DDF and PPDF modes.

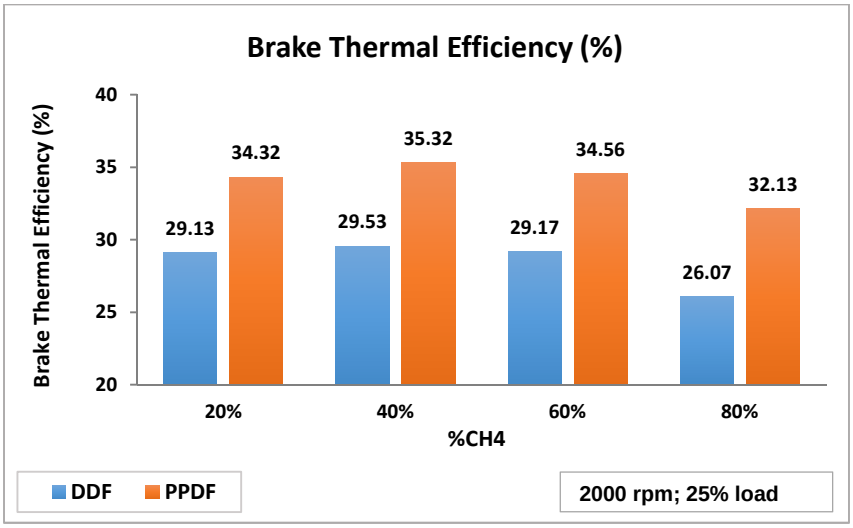


Figure 6.6 Brake thermal efficiency (%); for both DDF and PPDF modes.

The improved fuel economy with PPDF mode means that the engine will work at lower total equivalence ratio (ϕ_{tot}) compared with DDF; as illustrated by Fig. 6.7. The reduced total equivalence ratio involves the reduction of both fuels; $(\dot{m}_D)$and$(\dot{m}_{CH4})$, as implied by Equation (5.1). That is, the lean operating limit of the engine could be extended. In addition, the reduced $(\dot{m}_D)$ with PPDF, as shown by Fig. 6.8, implies a corresponding reduction in the PM emissions originated from the diesel fuel pilot. This effect is more influential at low % CH_4 substitution ratio where the diesel pilot size is more significant, and hence the reduction in the PM emissions becomes more tangible.

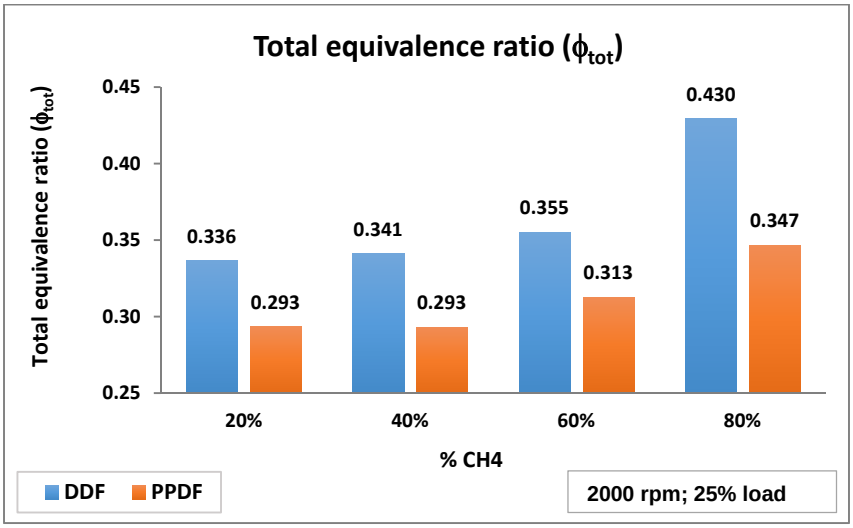


Figure 6.7 Total equivalence ratio (ϕ_{tot}); for both DDF and PPDF modes.

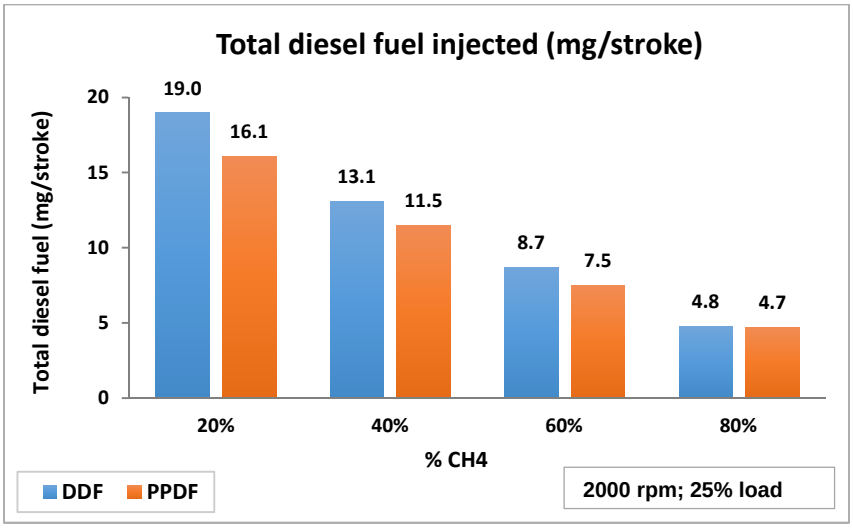


Figure 6.8 Total diesel fuel injected (mg/stroke); for both DDF and PPDF modes.

6.4 Influence of Pre-Injection Mass on PPDF Combustion

The quantification of the pre-injection part of the pilot as a fixed ratio (FR) of the total diesel fuel supplied to the engine, as per Equation (6.1), does not present any hurdle to the mono-fuel operation of diesel engines with split injection. Nevertheless, it could be challenging to dual-fuel operation, where the relative proportions of gaseous fuel and diesel could change at the same power level produced. With high levels of gaseous fuel substitution, the total diesel fuel mass becomes considerably small, and as a result, the mass of the pre-injection part of the pilot could substantially drop; potentially losing its effect. To examine the influence of pilot pre-injection mass on PPDF combustion, an alternative way of quantifying the size of the pre-injection was developed. In this new approach, referred to as fixed mass (FM) strategy, the mass of the pre-injection is held constant at a certain value, and any gaseous fuel addition will take place on the account of the main injection part of the pilot. As already discussed in Section 6.2, the optimum value of the %FR that was achievable with the current fuel injection equipment (FIE) system throughout the range of test cases, without substantially affecting the cool flame reactions or the ROPR, was found to be 20%. In view of that, it was decided to set the base value of fixed mass strategy (%FM) to be 20% of the total mass of the diesel fuel used to operate the engine under conventional diesel operation at the specified operating conditions. This value (3.2 mg/stroke) was held constant throughout all the $\%CH_4$ used,

and any change in the total diesel fuel quantity (as a result of a corresponding change in gaseous fuel) was solely addressed by changing the main injection part of the pilot. It is to the point here to highlight that fuel flow rates were measured on a global basis; i.e. as a total amount supplied to the engine rather than to each individual cylinder. As discussed in Chapter 4, this could possibly lead to some errors due to the potential lag in the electrical signal to the injector from cycle-to-cycle, and any difference to valve timing. Again, these errors are difficult to account for but they remain marginal.

The impact of pilot pre-injection mass on PPDF combustion becomes more voluminous at the operating conditions where limited quantity of diesel fuel is used. In view of that, it was decided to deliver a comparative study between PPDF with FR pre-injection (will be referred to as FR-PPDF) and with FM pre-injection (will be referred to as FM-PPDF) at the lowest test speed of 1400 rpm; at 25% engine load. For both strategies, the timings of the pre-injection and the main injection were kept @ 50° and 10° BTDC respectively, in keeping with the results of the sweep tests as concluded in Section 6.2 above. Figure 6.9 (a) and (b) show the cylinder pressure traces and the associated values of maximum ROPR at each combustion mode; for different CH_4 substitution ratios. It can be seen from Fig. 6.9 (a) that the in-cylinder pressure with FR-PPDF combustion considerably drops as the $\%CH_4$ increases; while FM-PPDF combustion always maintains the high levels of cylinder pressure as shown in Fig. 6.9 (b). This could reveal that with FR pre-injection, the decrease of the pre-injection mass as the $\%CH_4$ substitution ratio increases eventually causes the pre-injection to lose its effect in promoting the combustion. As a consequence, the ignition delay (ID) of the main part of the diesel gets prolonged as the $\%CH_4$ increases [51]. The late start of combustion (SOC) means that the peak cylinder pressure will be attained at a later position relative to the TDC; i.e. at lower value. With FM pre-injection, on the other hand, the presence of active radicals from the LTR zone promote the combustion process. The earlier start of that intensified combustion yields higher cylinder pressure values [242]. In addition, since the increase in the $\%CH_4$ takes place on the account of the main injection, the main combustion event will start with the auto-ignition of a less amount of diesel fuel, and hence the maximum ROPR values become much less; the average reduction in the maximum ROPR exceeds 8%. This is advantageous to combustion noise, fuel economy, and NOx and PM emissions [40].

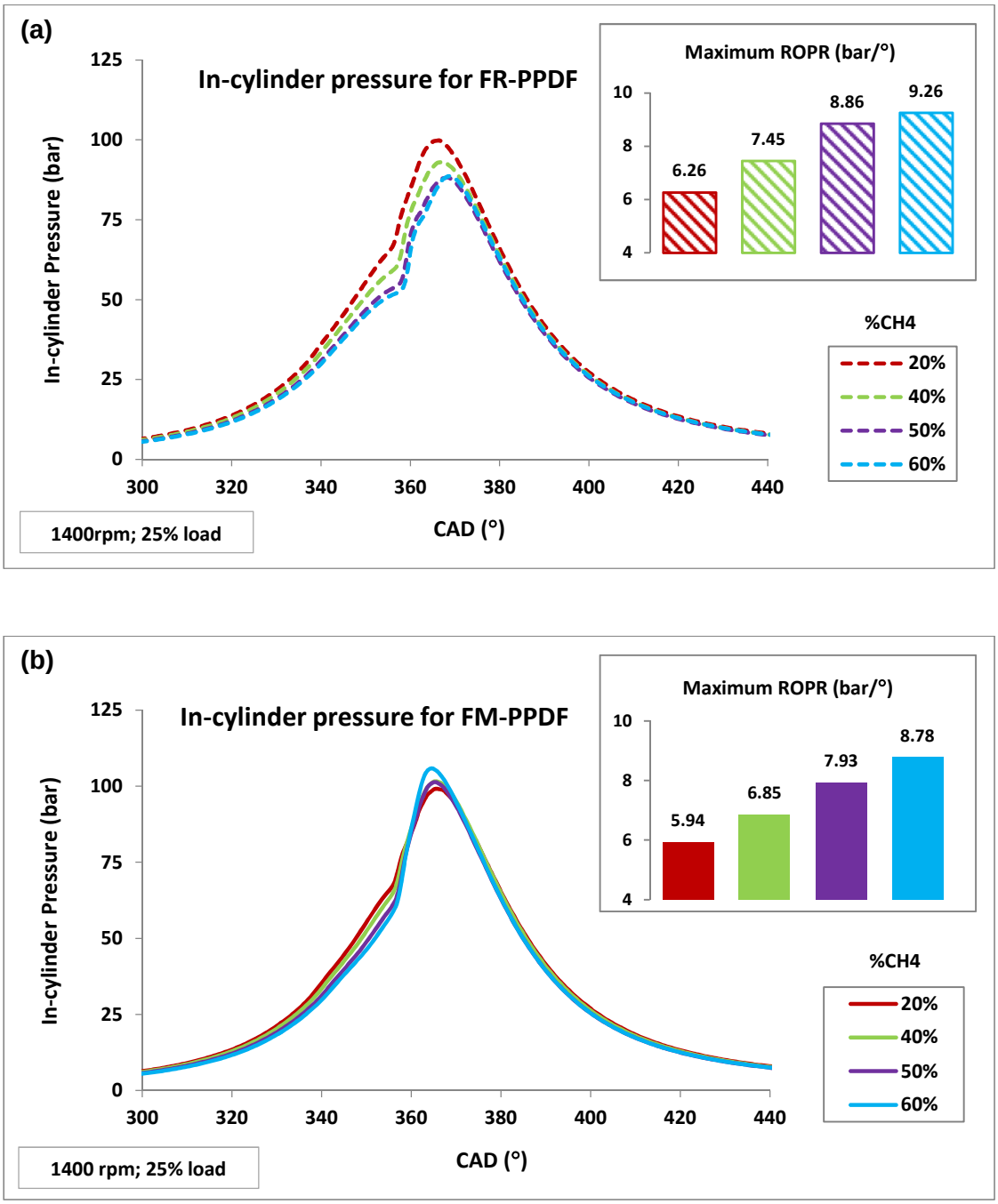


Figure 6.9 **In-cylinder pressure and the associated maximum ROPR (in the inset); for (a) 20% fixed ratio (FR) PPDF combustion, and (b) 20% fixed mass (FM) PPDF combustion. For both cases, pre-injection and main injection timings are kept @50° BTDC and @10° BTDC, respectively. Data is for 25% load at 1400 rpm, for 20, 40, 50 and 60% CH_4 substitution ratio.**

Figure 6.10 (a) and (b) show the net HRR traces, along with the corresponding positions of the occurrence of CA50 for FR-PPDF and FM-PPDF combustion modes; at different CH_4 substitution ratios. The influence of the reduction of the FR pre-injection mass as the $\%CH_4$ is increased could be clearly noticed in Fig. 6.10 (a), where the reduction in the pre-injection mass results in a decay in the LTR zone; reducing the amount of active radicals that promote the combustion. Consequently, the ability of the pre-injection to sustain a reaction (HTR-1) that leads to the entrainment of some of the methane in this stage becomes very limited; especially with high substitution ratios. The resulting main combustion (HTR-2) therefore much resembles that of conventional DDF, where the ignition delay and combustion duration both increase with the increase of $\%CH_4$. With FM pre-injection, it is evident from Fig. 6.10 (b) that the magnitude of the LTR zone is almost the same, while it shows a slight shift towards the TDC as $\%CH_4$ increases. This could be attributed to the incidence of some chemical interactions between the methane and the diesel fuel vapor [51]. In general, the increased reactivity due to the cool flame reactions leads to the entrainment of some of the methane in the combustion of the pre-injection part of the pilot. This is demonstrated by the increased magnitude of the HTR-1 stage prior to the commencement of the main combustion (identified as the sharp rise of the HRR curve) and the subsequent increase in the cylinder temperature and pressure [245].

The distinctive aspect of the process with FM-PPDF combustion at these conditions is the ignition delay behavior. The value of ID almost remains unchanged with all $\%CH_4$ employed; in contrast with FR-PPDF. Similarly, the duration of combustion is almost unchanged for all $\%CH_4$ ratios. In view of that, it could be postulated that the effects of the increase of $\%CH_4$ on elongating the ignition delay and combustion duration could be excluded if a certain degree of charge reactivity is attained through using a sufficient per-injection mass. The ensuing intensified combustion takes place very rapidly during a few CADs [89], with the improved flame propagation at high %CH4 brings the CA50 closer to the TDC. The case was reversed with the FR-PPDF, where the increased substitution ratio leads to the occurrence of the CA50 further away from the TDC; again due to the decay of the influence of the pre-injection as its mass get significantly small. It is to the point here to highlight that for adiabatic engines, the optimal CA50 is attained just right at the TDC [243].

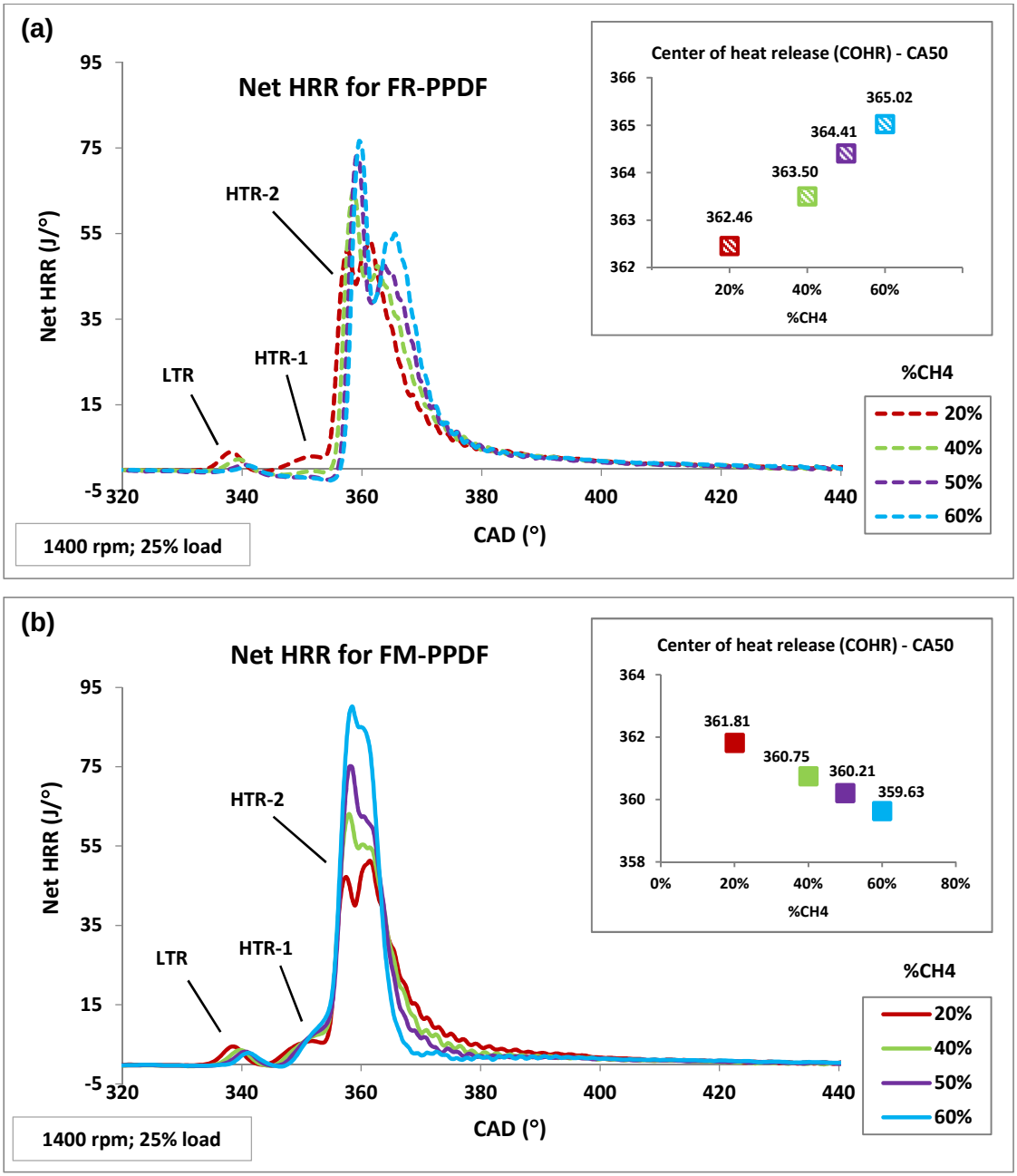


Figure 6.10 **Net HRR data and the corresponding positions of the occurrence of CA50 (in the inset); for (a) fixed ratio (FR) PPDF combustion, and (b) fixed mass (FM) PPDF combustion. For both cases, pre-injection and main injection timings are kept @50° BTDC and @10° BTDC, respectively. Data is for 25% load at 1400 rpm, for 20, 40, 50 and 60% CH_4 substitution ratio.**

As far as the engine stability and fuel economy are considered, it could be seen from Fig. 6.11 that FM-PPDF exhibits a slightly better engine stability (represented by the lower value of $COV_{IMEPgross}$), while Fig. 6.12 demonstrates that this mode also yields a slightly higher brake thermal efficiency compared with FR-PPDF combustion mode.

This slight improvement in BTE could be attributed to the higher in-cylinder pressure levels at the early stages of the expansion stroke, along with the reduced ROPR levels. Nevertheless, the values obtained with FR-PPDF are still very comparable.

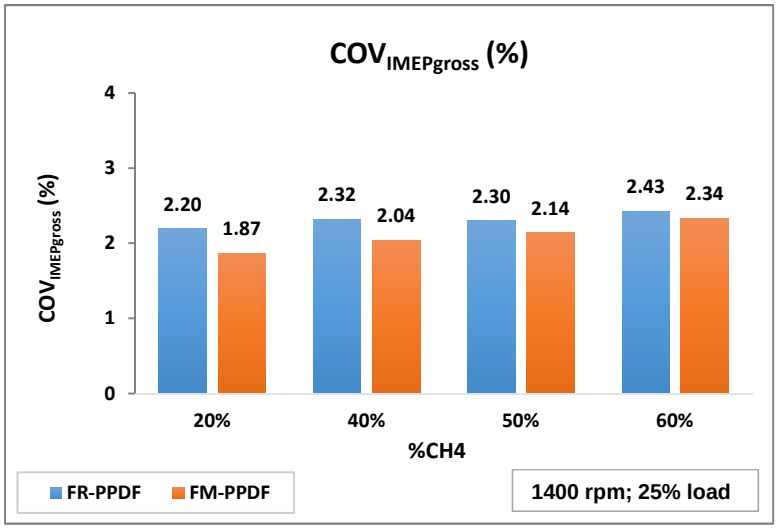


Figure 6.11 Coefficient of variation ($COV_{IMEPgross}$); for both FR-PPDF and FM-PPDF modes.

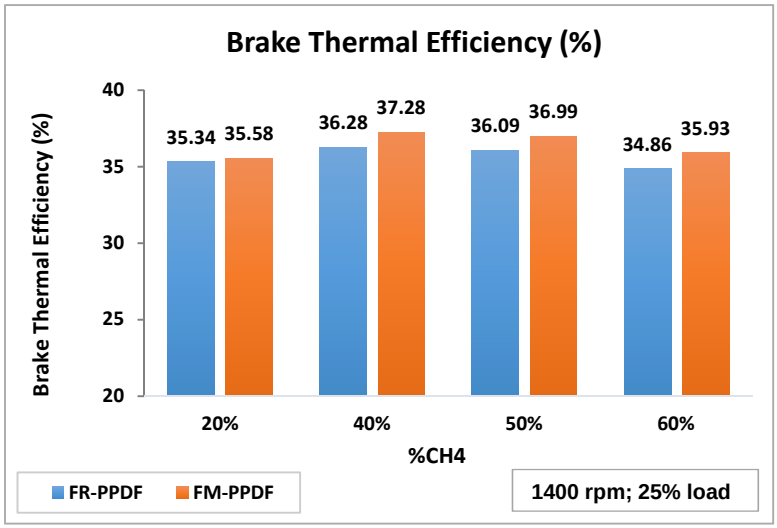


Figure 6.12 Brake thermal efficiency (%); for both FR-PPDF and FM-PPDF modes.

The slight improvement in engine performance could be further demonstrated by Figs. 6.13 and 6.14 that present the values of the total equivalence ratio (ϕ_{tot}) and the total diesel fuel mass, respectively, for both injection strategies. The figures reveal that only minor reductions in both the (ϕ_{tot}) and the total fuel mass are attained with FM-PPDF

strategy compared with FR-PPDF strategy. In view of that, it is expected to experience a corresponding minor change in the PM emissions; yet the larger pre-injection mass is expected to increase the global mixture strength and reduce CO and HC emissions [37]. The reduced size of the main injection part implies a corresponding reduction in the spray-cone rich mixture zone; potentially reducing NOx emissions in some measure [39]. Any elimination of the hot and rich zones inside the cylinder with less diffusion flame is effective in reducing NOx [246].

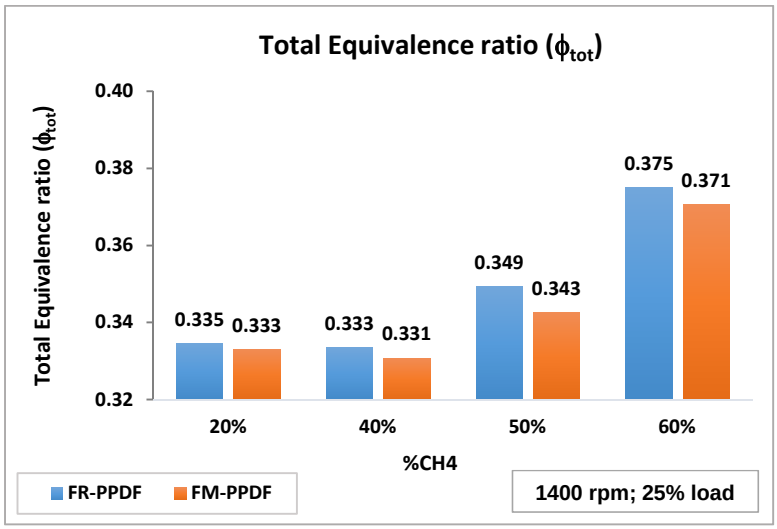


Figure 6.13 Total equivalence ratio (ϕ_{tot}); for both FR-PPDF and FM-PPDF modes.

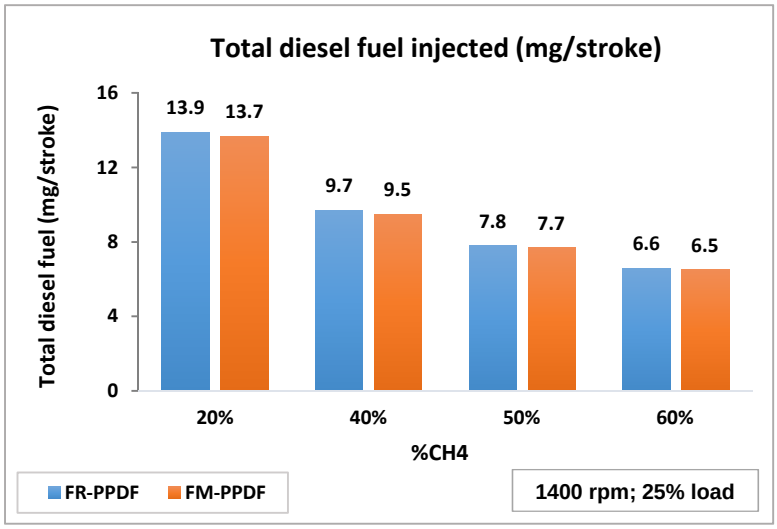


Figure 6.14 Total diesel fuel injected (mg/stroke); for both FR-PPDF and FM-PPDF modes.

6.5 Conclusions

In this chapter, the effect of pilot pre-injection, as well as the influence of its mass on DF engine combustion were investigated and analyzed. The study covered a wide range of engine speeds (from 1400 to 2000 rpm) at 25% load, with different substitution ratios of methane for diesel fuel (ranging from 20 to 80% on energy basis). Some of the key findings are:

- The use of pilot pre-injection changes the combustion mode from the conventional diesel dual fuel (DDF) combustion into the two-stage partially premixed dual fuel (PPDF); if the pre-injection timing and quantity are optimized.
- PPDF combustion is attained with pre-injection timings between 40 and 80° BTDC, and quantities between 10% and 20% of the total diesel fuel. In this work, the values of 50° BTDC and 20% gave the optimum results, with the main injection timing set at 10° BTDC.
- The high level of active radicals with PPDF combustion results in a more intensified yet smoother combustion, with faster burning rate and better combustion phasing.
- About 17% reduction in the maximum ROPR and 5% increase in the brake thermal efficiency could be obtained with PPDF combustion, while maintaining the engine stability at acceptable levels (2-3%); even with high $\%CH_4$ substitution levels.
- The total equivalence ratio with PPDF is less than that with DDF, meaning that the engine lean operating limit could be extended; increasing the practicality.
- The pre-injection mass has to be kept a certain level to remain capable of changing the combustion mode. This approach is referred to as the fixed mass (FM) PPDF, as opposed to the fixed ratio (FR) PPDF. This value is 3.2 mg/stroke for this work.
- FM-PPDF strategy maintains high cylinder pressure values with high $\%CH_4$ levels, and at the same time provides about 8% reduction in the maximum ROPR. It also offers a slight improvement in engine stability and performance.
- Unlike conventional DDF or FR-PPDF modes, the commencement and duration of the main combustion event in FM-PPDF mode are both not influenced by the level of $\%CH_4$ substitution. It is the degree of charge reactivity that plays the key role.

CHAPTER SEVEN

DISCUSSION AND CONCLUSIONS

7 Discussion and Conclusions

7.1 Introduction

The work presented in this thesis has been undertaken to provide a better understanding of combustion initiation and development in light-duty common rail diesel engines dual fuelled with methane. The aim was to establish how the heat release characteristic and work output of these engines depend on the pilot injection strategy and the percentage of energy substitution of methane. The focus of the study was the light load operating conditions. This chapter serves to provide the overall discussion of the work presented in the thesis as well as the key findings. The suggestions of future work that complement the present contribution are also highlighted. Finally, the main conclusions of the thesis are presented.

7.2 Discussion

The research on gas-diesel dual fuel (DDF) engines is derived by the imperative need to reduce the dependence on diesel fuel as a finite energy source and reduce the harmful pollutant emissions from diesel engines [247]. In DDF engines with gas port-injection, the use of two independent fuelling systems for diesel pilot and gaseous fuel provides a high level of control over the charge preparation and hence on the ensuing combustion process [228].

To obtain a better insight into the combustion process in DFF engines, the present work has developed a simple yet very effective technique through the resolving the HRR data of DF operation into its component; i.e. diesel and methane contributions to the energy release process. The study covered a wide range of methane substitution for diesel fuel; ranging from 30% up to 80%, at quarter load (25%) conditions for engine speed of 1600 rpm. The diesel contribution in each case has been estimated from the conversion of the engine into the diesel-only operation using the exact amount of diesel fuel used as a pilot in the specific DF operating condition. The apparent contribution of methane has been approximated as the arithmetic difference between dual-fuel HRR and diesel-only HRR at any given crank angle as per Equation (5.3). Data analysis has revealed that the main fuel conversion processes in DF operation take place over two stages, referred to

in the present work as Stage-1 and Stage-2, where the dominant combustion mechanism in each stage is essentially determined by the relative quantities of the two fuels.
Stage-1 is always dominated by the ignition and rapid combustion of the premixed part of the diesel pilot; regardless of the amount of methane used. Contrasting what has been reported in other studies [233], the present work has demonstrated that the combustion of the gaseous fuel in the immediate vicinity of the ignition sources of the pilot is not sequential to the pilot combustion itself. There has been an evident entrainment of some of the gaseous fuel into the pilot combustion in this stage, where this part increases with the increase of the gas substitution ratio. This behavior indicates that this entrainment is more affected by the mixture strength than by the jet properties. With $\%CH_4$ as high as 80%, almost one-third the HR in Stage-1 combustion has been produced from CH_4 combustion. The premixed peak of HRR rate is considerably influenced by the presence of methane; revealing that it is not only the diesel pilot that influences NOx emissions formation at these conditions [236].

Unlike the classical diesel combustion where the MCC commences immediately after the PMC, DDF combustion is characterized by the presence of a transient stage between the diesel auto ignition and the gas bulk combustion. This stage lasts for a very limited time and is not characterized by any dominate combustion mechanism. The role of this stage in emissions formation is ambiguous and difficult to expect. Stage-2 experiences the combustion of the bulk of gaseous fuel-air mixture away from the influence of diesel pilot zone. It is therefore responsible for the formation of HC (mostly composed of CH_4 in this condition; that is why the phenomenon is usually referred to as “methane-slip” [37]) and CO more substantially [228]. The dominant combustion mechanism in Stage-2 is largely determined by the relative magnitudes of diesel pilot and methane available for combustion. For high CH_4 concentrations ($\phi_{CH4} > 0.35$), this stage is characterized by the incidence of turbulent flame propagation event, while for weak mixture strength ($\phi_{CH4} < 0.3$), gaseous fuel conversion occurs in a low-intensity non-flame propagation event, categorized as a “pilot-dominant” combustion. This slow combustion reaction is expected to produce a large amount of unburned products [228].

The increased substitution ratio also results in an increase in the ignition delay; in most operating conditions. This is the consequence of combined factors; comprising reduced oxygen partial pressure (as methane replaces some of the air), reduced temperature (due to the increased specific heat of the mixture; aka cooling effect of methane admission) [231], and the competition for active radicals between diesel fuel and methane [232]. This has been found to be the case in all test conditions examined; unless there has been a global change in the combustion mode. As discussed in Chapter 5, this change could take place if the pilot mass is sufficiently small that it could fully evaporate then locally intermix with the very lean methane-air mixture. The presence of a small concentration of the higher-hydrocarbon vapor enhances the combustion initiation in DDF engines and reduces the ignition delay. The ensuing combustion mechanism is predominantly governed by the chemical kinetics, and it can be described as an RCCI-like combustion with methane as the low reactivity fuel and diesel fuel as the high reactivity one [240]. This phenomenon has been encountered in the present study at the very low loads (5%) with high substitution ratios. It has been proved that the degree of cylinder reactivity increases with the increased amount of diesel fuel vapor. Complete evaporation of the diesel pilot has taken place at injection masses as low as 1.6 mg/stroke; despite the fact that the combustion mechanism may start to change at as much as twice this value. The substitution ratio at which the combustion mechanism changes (referred to as threshold value) essentially varies with fuelling conditions (as governed by engine power level). It has been found that weaker methane-air mixture requires more concentration of the higher-hydrocarbon vapor, i.e. larger pilot, to create a combustion mode change. The duration of combustion (DOC) follows the same trend as the ignition delay; it increases with methane substitution up to the threshold value, and then decreases afterward. All in all, it could be concluded that employing novel combustion modes in DDF engines has the potential to speed up the slow combustion process under light load conditions. Whilst the RCCI-like combustion in the present work has been encountered at the very low load conditions, its potential benefits could be more realized under a wide range of operating conditions if the change in combustion mechanism has been attained through employing advanced injection strategy. This is further discussed later in this section.

There have been several factors affecting the maximum possible methane substitution for diesel fuel; some of them are identified as “system-limitations” while the others are viewed as “operation-limitations”. The most prominent system-limitation is one related to the minimum limiting value of the FIE used, as this value determines the maximum substitution ratio attainable at a given power level. In the current setup, this value has been found to be 0.8 mg/stroke, where it has yielded a maximum substitution ratio of 95%. With recent development of FIEs, this value has been pushed further down to as low as 0.3 mg/stroke [248], where some studies achieved a substitution ratio as high as 97% to 98% [249]. Regardless of the FIE of diesel fuel used, the use of gaseous fuel injection into the intake, rather than induction using simple venturis or gas mixers, is an effective way to extend the gaseous fuel substitution limits in DDF engines. Another limitation on the maximum possible methane substitution for diesel fuel has been found to be the limiting value of the COV_{IMEP} for engine stable running. This value has been experimentally identified in the present work as 8% – 9%. Beyond this level, the engine has suffered high degree of instability, uncontrollable running, and even misfiring. For that reason, no further admissions of CH_4 were possible if this operation-limitation have been reached.

There are some other operation-limitations on the maximum possible $\%CH_4$ that have not been investigated in the present work; yet they do exist. For instance, the maximum allowable cylinder pressure values, as well as the maximum ROPR, put constraints on the amount of gaseous fuel used at high loads where the burning rate becomes very fast [247]. The maximum permissible exhaust gas temperature is another limitation at these conditions (exhaust manifold and turbocharger material constraint) [54]. The requested reduction in NOx emissions might also be compromised with high $\%CH_4$ at high load conditions [247]. Elevated HC and CO emissions, on the other hand, as well as retarded engine performance characterize high $\%CH_4$ ratios at low load conditions, even if the limiting $COV_{IMEPgross}$ is yet to be met [19].

It has been found possible to tackle many of the negative aspects accompanying light load operation of DDF engines through the use of pilot split-injection strategy. This has been proven effective to change the combustion mode into a novel two-stage partially-premixed dual fuel (PPDF) combustion [250]. In this mode, the diesel pilot is split into

two injections; an early pre-injection of a comparatively small part of the pilot, followed by a late injection of the main pilot. The pre-injection part acts as an ignition improver in a low-temperature reaction (LTR) regime of high degree of reactivity, while the main injection then initiates the high-temperature reaction (HTR) combustion throughout the cylinder charge [87]. That is, the combustion mode change is attained in a controllable manner through the pre-injection, and combustion initiation is accurately timed by the main injection and not ultimately governed by the chemical kinetics (unlike DF-HCCI combustion) [88].

For a successful application of PPDF combustion in DF engines, the pre-injection part of the pilot should be optimized in timing and quantity. Too early injection timing must be avoided not to cause spray impingement, while too late timings will not be effective in changing the combustion mode. Also, large pre-injections may result in unacceptable ROPR values, while too small injections might not be capable of producing the desired cool flame reactions and active radicals. In the present study, the desirable change in the pilot ignition (and subsequent combustion) mode has been achieved by employing a pilot pre-injection quantity of 20% of the total diesel fuel injected at 50° BTDC, while the main injection is kept at 10° BTDC (for 25% load at wide range of speeds).

The results of the comparative study between conventional DDF combustion and PPDF mode have demonstrated that PPDF exhibits higher cylinder pressure values compared with conventional DDF mode; at all %CH4 ratios. This has been attributed to the effect of active radicals in promoting the combustion process [242]. The implication of that is the ability of the engine to produce more useful power output, should the combustion phasing has been carefully adjusted. Also, up to 17% reduction in the maximum ROPR has been attained with PPDF as the main combustion event begins with less amount of diesel fuel, compared with DDF. This is advantageous to engine combustion noise, fuel economy, and NOx and PM emissions [40]. PPDF combustion has also demonstrated a better combustion phasing, as represented by CA50, and a better engine stability, as represented by $COV_{IMEPgross}$, compared with DDF. With PPDF, it has been possible to have the major part of the heat release takes place closer to the TDC while keeping the $COV_{IMEPgross}$ at acceptable levels (2-3%) throughout the entire range of $\%CH_4$. PPDF is therefore believed to be a very successful strategy to maintain a stable engine running with high methane substitution at light load condition.

The combined influence of higher cylinder pressure with low ROPR, faster burning rate with better phasing, and increased stability with reduced noise produces as high as 5% improvement in the engine brake thermal efficiency under PPDF mode; compared with conventional DDF operation. The improved fuel economy means that the engine works at lower total equivalence ratio; i.e. the lean operating limit has been extended [251]. The lower total equivalence ratio also implies a reduction in the diesel fuel pilot mass; resulting in a reduction in the PM emissions.

The mass of the pre-injection part of the pilot has been found to be very influential on PPDF combustion mode; particularly at light load operation with high levels of methane substitution [252]. In these circumstances where the total pilot size becomes small, the quantification of the pre-injection part as a ratio of the pilot is perhaps inadequate as its mass could be too small to cause the desired change in the combustion mode. A detailed analysis of the influence of pre-injection mass on PPDF combustion has been presented in Chapter 6. Contrasting the fixed ratio (FR) quantification of the pilot, an alternative way has been introduced in which the pre-injection size was set as a fixed mass (FM), while any gaseous fuel addition takes place on the account of the pilot main injection. The optimum value of the fixed mass pre-injection has been found as 20% of the total mass of the diesel fuel used to run the engine at the specified operating conditions under conventional diesel operation. It has been found that FM-PPDF operation maintains the high cylinder pressure values at high $\%CH_4$ ratios where FR-PPDF has failed to do so; indicating that the small pre-injection mass with the latter has potentially lost its effect in promoting combustion. Also, the maximum ROPR with FM-PPDF has exhibited 8% reduction compared with FR-PPDF, since the main combustion event with the former starts with less amount of diesel fuel. Once more, this is beneficial to engine noise level, fuel economy, and emissions [40].

Under the test cases examined, it has been found that the values of ignition delay and duration of combustion remain unchanged with all $\%CH_4$ levels under FM-PPDF mode. This reveals that the influence of increased gaseous fuel concentration on these two parameters could be excluded if a certain degree of charge reactivity is attained through using a sufficient per-injection mass. More intense study of this phenomenon could lead to developing a method for an accurate control over the commencement and duration

of combustion process in DF engines regardless of the level of gaseous fuel substitution. There has been only slight improvement in engine stability and fuel economy with FM-PPDF compared with FR-PPDF mode. Also, FM-PPDF is expected to have lower levels of CO and HC emissions owing to the increased mixture strength with using larger pre-injection, and less NOx emissions due to the reduced spray size of the main injection [37, 39].

7.3 Further Work to Complement This Thesis

The work presented in this thesis has provided important information with regard to the combustion and performance of methane-diesel DF engines at light load operation, and answered some critical questions on the topic. It could be complemented by some other additional efforts:

7.3.1 Exhaust emissions analysis

While dual-fuelling of diesel engines with methane is an effective way to reduce CO_2 and PM emissions, owing to the low carbon-to-hydrogen ratio of methane and its simple molecular structure, NOx and HC emissions remain an issue regardless of engine load conditions. Based on the detailed HRR analysis presented in Chapter 5, it is understood that formation of NOx emissions largely takes place in the first stage of DF combustion, while HC emission formation dominates the second stage. NOx formation is primarily associated with the pilot combustion zone, where the local temperature is very high and there is a sufficient time for the oxygen-nitrogen reactions to proceed [30]. This will be amalgamated with further NOx formation (to a lesser degree) from the heated mixture zone entrained in pilot combustion and in its immediate vicinity; it has been established in Chapter 5 that there is an evident entrainment of the gaseous fuel in the first stage of combustion. Only marginal NOx formation is expected afterward from the combustion of the overall lean mixture, while flame propagation plays a large role in NOx formation from richer mixtures [253]. Generally, NOx formation in DDF engines largely depends on both the pilot fuel size and the total equivalence ratio [19]. The relationship is very complex where several mechanisms do exist [37], and it needs more investigation. HC emissions in DDF engines are predominantly composed of methane, where there are

two major sources contribute to HC formation; combustion chamber crevices and flame quenching [254]. It has been found that with very lean operation of DDF engines, flame quenching is the major source of HC emissions, while the contribution of crevices, in particular from the top land, as a source of HC formation, becomes more influential as the mixture strength increases [37]. It has been found that the top land crevice remains the major source of HC emissions as long as the combustion of the bulk gas is efficient [254]. In view of that, a modification to the standard piston could be made so as to attain a less top land crevice volume, where a possible, simple yet efficient, way to achieve that is via machining a 45° chamfer around the top edge of the piston [37].
As deliberated in Chapter 6, PPDF combustion mode is expected to provide improved emissions characteristics relative to the conventional DDF mode; especially with large pre-injections. The pre-injection part of the pilot will intermix with the gaseous fuel-air mixture; increasing its strength and reactivity. The enhanced combustion process will result in less HC emissions. Additionally, the reduced size of the main pilot injection will reduce the size of the high-temperature zone; effectively reducing NOx emissions.

It has not been possible to perform the exhaust emissions tests during the present work, but these are highly recommended to be part of any complementary study that follows the lead of this thesis.

7.3.2 Test rig development

The experimental setup used in the present work have fulfilled the aims and objectives of this thesis to a high degree of completion. However, some suggestions for a further development of the test rig are highlighted herein below:

- The diesel fuel system was not equipped with a liquid fuel flow meter. The quantity of fuel used at any particular test case has been identified to be equal to the demand value, set by the user, as processed by the ECU. This has been considered acceptable given the fact that the original OEM fuel calibration maps have been kept without any change, while the engine has been calibrated by the supplier before the project commenced. The fuel chemical energy was also compared to the cumulative value of the heat release, and the results were comparable (taking into account the crevices loss and combustion inefficiency). Repeatability tests were done at regular intervals

during the work to ensure that there was no drift. While this has been sufficient, a highly recommended upgrade of the test rig is the inclusion of a liquid fuel flow meter to measure the actual flow rate independently of the ECU and engine original calibration. This will also allow for a full control over the fuel injection parameters regardless of the fuelling quantity; providing an extra degree of freedom.

- The gaseous fuel system comprised two manually-controlled pressure regulators, to bring down the gaseous fuel pressure from the supply bottle pressure to the injectors working pressure. The use of manual regulator means that the gaseous fuel injection pressure would be the same regardless of the intake manifold pressure. Whereas the level of boost noticeably changes with the operating condition owing to the use of VGT turbocharger, fixing the injection pressure while the intake manifold pressure change means that the effective injection pressure will not be constant. In view of that, it is suggested to use an automatic pressure regulator to maintain the gaseous fuel injection pressure at a certain level above the intake manifold pressure. This will facilitate the study of the influence of gaseous fuel manifold injection pressure on charge stratification if the timing is optimized, as discussed in Chapter 2.
- If the exhaust emissions analysis is to be done, the phenomenon of “methane-slip” would be at the core of this investigation. As discussed in Section 7.3.1, the top land crevices are the main source of HC emissions, and hence it is recommended to have a special set of engine pistons machined with a 45° chamfer around the top edge of the piston, to evaluate the effectiveness of this technique in reducing HC emissions.
- As discussed in Section 7.4.2, a prospective topic of future research is the influence of injector tip temperature on the phenomenon of nozzle hole coking. If this is to be investigated, a special set of injectors has to be manufactured, such that they allow for the inclusion of a Type-K thermocouple as close as possible to the injector tip. Another set of injectors manufactured as above is also required to be fitted with a copper sleeve enclosing the tip as a measure of cooling, so the influence of nozzle tip temperature could be assessed.

7.4 Suggestions for Future Research

7.4.1 Improving light load operation

The main focus of the present work has been the light load operation of DF engines, where the weak mixture strength and the associated slow flame propagation bring about several problems to engine combustion, performance, and emissions. In this study, the use of pilot split-injection strategy has been proven successful in improving DF engine operation under these conditions. Some other remedial measures could also be proposed for future investigation:

- Increasing the overall fuel reactivity. This will yield improved combustion initiation and development [240]. There are three approaches to apply this concept; the most classical one is the use of a larger amount of the high reactivity fuel; i.e. the pilot. The use of relatively larger pilot fuel sizes with optimum injection parameters; i.e. lower injection pressure (to avoid spray wall-impingement) and advanced injection timing (to provide longer mixing period) is considered remedial [255]. Larger pilot size can offer higher ignition energy and shorter ignition delay, while the larger diffusivity of the higher-hydrocarbon vapor throughout the weak gaseous fuel-air mixture provides better oxidation process and enhanced flame propagation [239]. Increasing the pilot size has been proven more effective in reducing the incomplete combustion products than the increase of gaseous fuel-air mixture strength [228], but possibly on the expense of NOx emissions. Another way to increase the overall fuel reactivity is the addition of a small amount (less than 1% vol.) of cetane number (CN) improver to the diesel fuel pilot. This has been found a very effective way to increase the fuel reactivity and reduce the ignition delay [256], hence overcoming the slow burning rate of the weak gaseous fuel-air mixture. The use of CN improver has been proven effective in increasing the cylinder pressure and fuel economy while reducing CO and HC emissions; with no significant effect on NOx emissions [257]. Finally, the use of alternative high-cetane pilot fuels also results in improved fuel reactivity, and it could yield improved engine combustion and emissions [258]. Nevertheless, this approach could have some implications over the engine hardware and FIE, as discussed in Chapter 3.

- Intake charge preheating. While only a slight increase in the temperature is required, this could be done through the use of a simple gas-to-gas heat exchanger with the exhaust, or a liquid-to-gas heat exchanger with the water jacket. The increased inlet temperature brings about higher mixture temperature at the end of the compression stroke and during the pilot injection period; enhancing the flame propagation and reducing the HC emissions [37]. The increased temperature reduces the minimum ignition energy from one side [25], while it widens the flammability limits from the other side [259]; meaning that the mixture becomes more capable of maintaining a sustainable flame at the same equivalence ratio. However, excessive increase of the inlet temperature increases the tendency to knock and pre-ignition [253].
- Partial reduction of the amount of the intake air supplied to the engine, to produce an effectively richer mixture. This can be implemented either by applying a physical restriction to the intake air flow; i.e. the use of throttling, or by reducing the effective mass of air charge through using a large amount of external EGR, or by trapping a large amount of combustion products inside the engine cylinder through the use of large negative valve overlap. The use of throttling is a simple procedure that needs a slight modification to the intake system so as to restrict only the air flow (before the induction/injection of the gaseous fuel. This approach has been proven effective in improving combustion process, reducing HC and CO emissions, and providing a better specific energy consumption [260]. The downsides of this procedure are the increased pumping losses and the possibility of undermining pilot ignition process if the throttling was excessive; unless an accurate lambda-control, similar to the one used with modern SI engines, is used [37]. Using a large amount of EGR, instead, is a potent strategy to approach near stoichiometric conditions while minimizing the throttling loss. It is also very beneficial in reducing NOx emissions while enabling a very cost-effective aftertreatment system using three-way-catalysts [261]. While the EGR tolerance in CI engines is much large compared with SI engines due to the strong ignition source, the use of high EGR levels might cause a deterioration in the combustion process, due to the large dilution of the charge. This could be mitigated by the use of a suitable auxiliary fuel as an additive, such as hydrogen, as discussed in Chapter 3. The use of internal EGR through employing a negative valve overlap (NVO) is also an effective way of increasing the effective mixture strength without

large pumping loss [262]. The increased temperature promotes the combustion and partial oxidation of methane and largely reduces HC emissions [263]. However, the variable valve timing (VVT) technique is yet to make its way into production diesel engines, which could limit the application of this strategy in DDF engines.

- The implementation of cylinder deactivation (CDA) in multi-cylinder engines. This technique has been established as an effective way to provide a better fuel economy and reduced emissions in throttled engines due to the reduced pumping loss and the lower heat transfer [264]. It could be accomplished either through fuel cut-off to the particular cylinder, or valves cut-off (keeping the intake and exhaust valves of the particular cylinder closed) [265]. The former approach is used with DF engines with HPDI of the gaseous fuel, while the second is used with gas port-injection engines. This technique in its ultimate form is referred to as dynamic skip fire (DSF), and it could vary the firings and skips continuously with the load demand [266]. The use of this technique at light loads mean that the engine cylinders other than the deactivated one operate with effectively richer gaseous fuel-air mixture, as the total amount of fuel is distributed over a less number of cylinders. The increased mixture strength results in improved engine combustion and emissions. DSF technique has the capacity to improve noise, vibration, and harshness (NVH) levels [267], but it requires a very accurate control of the operating variables; adding more complexity to the system.
- The attainment of a proper degree of stratification between the gaseous fuel and the air inside the engine cylinder. As discussed in Chapter 3, this could be achieved by keeping the gaseous fuel supply separated from the air until very close to the intake valve; especially using injection rather than induction [93]. This could improve light load operation as the formation of a stratified rich mixture in the vicinity of the pilot injection results in a more satiable flame that could propagate further through much of the remaining leaner mixture. The use of HPDI of gaseous fuel inside the engine cylinder has been proven much effective in achieving a stratified combustion with very lean burn capability [247]. Yet again, this system is complex is expensive, and it potentially reduces the degree of fuel flexibility compared with conventional DDF engines with manifold injection [37].

- Exhaust gas fuel reforming. In this technique, part of the fuel is catalytically reacted with hot engine exhaust gas to produce a hydrogen-rich combustible gas that is then fed to the engine [268]. The presence of a small amount of H_2 is proven effective at increasing the reactivity of the gaseous fuel and accelerating the combustion rates [81]. The application of exhaust gas reforming in diesel and homogeneous charge compression ignition (HCCI) engines improves the fuel economy and reduces NOx levels [269]. This technique has the advantage of producing the high-octane fuel on board with no need to include additional fuelling system [270]. One recent study [271] on the use of exhaust gas fuel reforming with biogas-diesel dual-fuel engines demonstrated the effectiveness of this technique in improving the fuel economy and reducing CO and HC emissions, relative to the DF operation without reforming [271]. Researches on the use of exhaust fuel reforming to improve methane-diesel dual-fuel engine light load operation where the conditions are not favourable for an efficient gaseous fuel oxidation are in need for further effort.

7.4.2 Limitations on methane substitution at high loads

The present work has examined the various limitations on maximum possible methane substitution for diesel fuel at light loads. Limitations under high loads are expected to result from totally different reasons than those encountered at light loads. These could be proposed for a future study.

With recent development in FIEs, nozzle hole diameter of modern diesel fuel injectors has become smaller. While this is beneficial to spray characteristics, it means the nozzle becomes more susceptible to the formation of deposits within and around its holes. This phenomenon, known as “nozzle coking”, results in spray deterioration and flow loss as a result of the reduction in the hydraulic diameter [272]. In view of that, the lower-than-demanded injection quantity brings about power loss, increased emissions, and even misfire. The case is aggravated at low injection pressures as the reduced shear forces and cavitation in the nozzle holes limit the process of deposit removal [272]. Injector nozzle coking is a critical issue potentially facing DDF engines under medium and high load operation with large methane substitution (i.e. small diesel fuel pilot). Under these conditions, the injection pressure is low, and the amount of diesel fuel flowing through the nozzle is considerably small that it could not be sufficient enough to cool down the

nozzle tip. High nozzle tip temperature is very influential on deposit formation through the thermal condensation and cracking reactions [273]. It has been found that a nozzle tip temperatures exceeding 300° C may produce substantial coking [274]. This could imply a restriction on the maximum possible methane substitution at high power levels where a certain amount of diesel fuel would be required to cool down the nozzle below the limiting temperature. This value fundamentally varies with the fuel composition and the nozzle hole geometry, and it has to be assessed for the particular test setup.
One possible way to cool down the nozzle tip, thereby extending the substitution ratio range, without imposing a limitation on the engine operation, is through encapsulating the nozzle tip with copper sleeve [275]. This will increase the thermal conductivity and enhance the heat transfer through the tip to the rest of the injector and the cylinder head; eventually to the water jacket.
The studies with regard to the role of nozzle tip temperature and the risk of coking on setting a limit on the maximum methane substitution for diesel fuel in DDF engines are very limited. This topic is therefore suggested to supplement the present contribution.

Another limitation of substitution ratio at high load conditions is due to the incidence of knock. This has been deliberated lengthy in the literature, as discussed in Chapter 2. It could be, however, an integral part of any future work considering high load operation of DDF engines.

7.5 Conclusions

This study has considered the combustion process of a methane-diesel dual-fuel engine under light load operating conditions, and how heat release characteristics and engine stability depend on the ratio of the two fuels and the pilot injection strategy. The main conclusions of this thesis are:

7.5.1 Dual-fuel operation at light load

- Fuel conversion process under dual-fuel operation takes place over two main stages, where the dominant combustion mechanism in each stage is dictated by the relative quantities of the two fuels. Only the mixtures with methane equivalence ratio (ϕ_{CH4}) greater than 0.35 are capable of sustaining flame-propagation.
- Pilot combustion dominates in weaker mixtures (ϕ_{CH4} below 0.3). The mechanism changes to an RCCI-like combustion in diesel vapor-methane-air mixture if the pilot mass is small enough to evaporate and locally intermix in the charge.
- The limits of FIE on the injection quantity dictate the minimum pilot fuel size used under dual-fuel operation. This value is 0.8 mg/stroke for the test engine used.
- The maximum possible methane substitution under fully-warm near-idle low-load operating condition is 95%. The value of $COV_{IMEPgross}$ at this condition exceeds 8%, and the engine becomes on the verge of uncontrollable running.
- For a constant power level (speed and load), engine stability deteriorates as the gas substitution ratio increases. Increasing diesel pilot injected mass allows for the use of a larger amount of gaseous fuel without exceeding the engine stability criterion ($COV_{IMEPgross}$ ~ 5%).
- Dual-fuel operation at light load conditions exhibits poor fuel economy, especially with high substitution ratio of gaseous fuel. The use of sufficiently large pilot size is a remedial measure, although the brake thermal efficiency remains inferior to that under 100% diesel operation.

7.5.2 Pilot injection strategy

- Pilot injection strategy dictates the combustion mode under DF operation. Splitting the pilot into a small pre-injection (~20% of the total diesel fuel used) followed by the main injection could change the combustion mode from the conventional diesel dual fuel (DDF) combustion into the two-stage partially premixed dual fuel (PPDF) combustion, depending on the injection timing.
- The pilot main injection should be injected close to the TDC for best fuel economy. The pre-injection timing should be in the range between 80° and 40° BTDC. Later pre-injection timings lead to the incidence of a single-stage diesel combustion.
- At the same operating conditions (speed, load, and gaseous fuel substitution ratio), PPDF combustion mode provides ~17% reduction in the maximum ROPR and ~5% increase in the brake thermal efficiency relative to conventional DDF combustion, while maintain the engine stability at acceptable levels ($COV_{IMEPgross}$ ~ 2-3%).
- The total equivalence ratio with PPDF combustion is less than that with DDF at the same power levels, meaning the engine lean operating limit can be extended.
- The mass of the pre-injection has to be kept at a certain level not to lose its capability of changing the combustion mode. This value is 3.2 mg/stroke in the present work.
- The commencement and duration of the main combustion event in PPDF mode are more influenced by the pre-injection mass than by the gas substitution ratio.

REFERENCES

[1] British Petroleum. BP Statistical Review of World Energy. 66th ed. June 2017.

[2] United Nations, Department of Economic and Social Affairs, Population Division. World Population Prospects: The 2017 Revision, Key Findings and Advance Tables. Working Paper No. ESA/P/WP/278. 2017.

[3] International Energy Outlook 2017 (IEO2017). U.S. Energy Information Administration (EIA), September 2017.

[4] Oil Market Report. International Energy Agency (IEA), October 2015.

[5] ExxonMobil. The outlook for energy: a view to 2040. 2015.

[6] Kalghatgi GT. The outlook for fuels for internal combustion engines. Int J Engine Res 2014;15(4):383-398.

[7] Kalghatgi GT. Developments in internal combustion engines and implications for combustion science and future transport fuels. Proc Combust Inst 2015;35(4):101-115.

[8] U.S. Energy Information Administration. Glossary. Available on: http://www.eia.gov/tools/glossary/index.cfm (accessed 31 July 2015).

[9] U.S. Energy Information Administration. Refinery Yield. Available on: http://www.eia.gov/dnav/pet/pet_pnp_pct_dc_nus_pct_a.htm (accessed 31 July 2015).

[10] The European Parliament and the Council of the European Union. Regulation (EC) No 715/2007 of the European parliament and of the council of 20 June 2007 on type approval of motor vehicles with respect to emissions from light passenger and commercial vehicles (Euro 5 and Euro 6) and on access to vehicle repair and maintenance information. Official Journal of the European Union; OJEU, 29.6.2007, L 171/1.

[11] Transport, Energy and CO_2: Moving Towards Sustainability. International Energy Agency (IEA), 2009.

[12] Advanced Combustion Engine Research and Development: Annual progress report, Vehicles Technology Office. US Department of Energy, 2013.

[13] Advances in Internal Combustion Engines and Fuel Technologies. In: Ng HK, editors. Rijeka, Croatia: InTech; 2013.

[14] Ward-Jones RS. Environmentally Friendly Cars: Promoting and increasing their use in the UK. Earth Environ 2008;3:282-317.

[15] Brownstein AM. Renewable Motor Fuels: The Past, The present and the Uncertain Future. Oxford, UK: Butterworth-Heinemann; 2015.

[16] The international Council on Clean Transportation (ICCT). European Vehicle Market Statistics. Pocketbook 2016/17 Edition.

[17] Production Costs of Alternative Transportation Fuels - Influence of Crude Oil Price and Technology Maturity. International Energy Agency (IEA), 2013.

[18] Gajendra Babu MK, Subramanian KA. Alternative Transportation Fuels: Utilization in Combustion Engines. Boca Raton, USA: CRC Press; 2013.

[19] Karim GA. Dual-Fuel Diesel Engines. Boca Raton, USA: CRC Press; 2015.

[20] Mokhatab S, Poe WA, Mak JY. Handbook of Natural Gas Transmission and Processing. 3rd ed. Oxford, UK: GPP Elsevier. 2015.

[21] Korakianitis T, Namasivayam AM, Crookes RJ. Natural-gas fueled spark-ignition (SI) and compression-ignition (CI) engine performance and emissions. Prog Energy Combust Sci 2011;37:89-112.

[22] Rutz D, Janssen R, BioFuel Technology Handbook, WIP Renewable Energies, Germany, 2007.

[23] Abbasi T, Tauseef SM, Abbasi SA. Biogas Energy. New York, USA: Springer; 2011.

[24] Semin, Abu Bakar R. A technical review of compressed natural gas as an alternative fuel for internal combustion engines. Am J Eng Appl Sci 2008;1(4):302-311.

[25] Turns SR. An Introduction to Combustion: Concepts and Applications. 2nd ed. New York, USA: McGraw-Hill; 2000.

[26] Alternative Fuels Data Centre. U.S. Department of Energy. Available on: http://www.afdc.energy.gov/fuels/fuel_properties.php (accessed 31 July 2015).

[27] Cho HM, He BQ. Spark ignition natural gas engines - A review. Energy Convers Manage 2007;48:608-618.

[28] Sahoo BB, Sahoo N, Saha UK. Effect of engine parameters and type of gaseous fuel on the performance of dual-fuel gas diesel engines - A critical review. Renewable Sustainable Energy Revs 2009;13:1151-1184.

[29] U.S. Department of Energy. Clean Cities Alternative Fuel Price Report. July 2015.

[30] Hegab AH. Utilization of EGR in pilot ignited natural gas diesel engines. MSc thesis, Cairo, Egypt: Department of Mechanical Engineering, Al-Azhar University; 2011.

[31] Namasivayam AM. Combustion, Performance and Emissions Characteristics of Compression-Ignition Engines Fuelled by Sustainable Fuels. PhD thesis, London, UK: School of Engineering and Material Sciences, Queen Marty University of London; 2011.

[32] Demirbas A. Fuel properties of hydrogen, liquefied petroleum gas (LPG), and compressed natural gas (CNG) for transportation. Energy Sources 2002;24:601-610.

[33] International Gas Union (IGU). World LNG Report - 2013 Edition.

[34] Ma L, Geng J, Li W, Liu P, Li Z. The development of natural gas as an automotive fuel in China. Eergy Policy 2013;62:531-539.

[35] The GVR - Gas Vehicles Report. NGV Journal. No.168; January 2016.

[36] Natural & bio Gas Vehicle Association (NGVA) Europe, Worldwide NGV Statistics, Worldwide NGV shares in Total Vehicle Market, September 2015. Available on: http://www.ngvaeurope.eu/worldwide-ngv-statistics (accessed 31 Jan. 2016).

[37] Königsson F. On combustion in the CNG-diesel dual fuel engine. PhD thesis, Stockholm, Sweden: Dept. Mach. Des., Royal Institute of Technology; 2014.

[38] Papagiannakis RG, Hountalas DT, Rakopoulos CD. Theoretical study of the effects of pilot fuel quantity and its injection timing on the performance and emissions of a dual fuel diesel engine. Energy Convers Manage 2007;48: 2951-2961.

[39] Heywood JB. Internal Combustion Engine Fundamentals. New York, USA: McGraw-Hill; 1988.

[40] Stone R. Introduction to Internal Combustion Engines. 3rd ed. Oxford, UK: Macmillan; 1999.

[41] Karim GA. A review of combustion processes in the dual fuel engine - The gas diesel engine. Prog Energy Combust Sci 1980;6:277-285.

[42] Nwafor OM. Combustion characteristics of dual-fuel diesel engine using pilot injection ignition. Inst of Eng J 2003;84:22-25.

[43] Papagiannakis RG, Hountalas DT. Combustion and exhaust emission characteristics of a dual fuel compression ignition engine operated with pilot diesel fuel and natural gas. Energy Convers Manage 2004;45:2971-2987.

[44] Wei L, Geng P. A review on natural gas/diesel dual fuel combustion, emissions and performance. Fuel Process. Technol. 2016;142:264-278.

[45] Lounici MS, Loubar K, Tarabet L, Balistrou M, Niculescu D, Tazerout M. Towards improvement of natural gas-diesel dual fuel mode: An experimental investigation on performance and exhaust emissions. Energy 2014;64:200-211.

[46] Selim MYE. Pressure-time characteristics in diesel engine fuelled with natural gas. Renew Energy 2001;22(4):473-489.

[47] Ibrahim A, Bari S. Optimization of a natural gas SI engine employing EGR strategy using a two-zone combustion model. Fuel 2008;87:1824-1834.

[48] Lapuerta M, Armas O, Rodríguez-Fernández J. Effect of biodiesel fuels on diesel engine emissions. Prog Energy Combust Sci 2008;34:198-223.

[49] Musculus MPB. Measurements of the influence of soot radiation on in-cylinder temperatures and exhaust NOx in a heavy-duty DI diesel engine. SAE tech pap 2005-01-0925; 2005.

[50] Shenghua L, Ziyan W, R. Jiang R. Development of compressed natural gas/diesel dual-fuel turbocharged compression ignition engine. Proc Instn Mech Engrs, Part D: J Automob Eng 2003;217(9):839-845.

[51] Liu Z, Karim GA. An examination of the ignition delay period in gas-fueled diesel engines. J Eng Gas Turbines Power, 1998;120(1):225-231.

[52] Mittal M, Donahue R, Winnie P, Gillette A. Exhaust emissions characteristics of a multi-cylinder 18.1-L diesel engine converted to fueled with natural gas and diesel pilot. J Energy Inst 2015;88:275-283.

[53] Mittal M, Donahue R, Winnie P, Gillette A. Combustion and gaseous emissions characteristics of a six-cylinder diesel engine operating within wide range of natural gas substitutions at different operating conditions for generator application, SAE tech pap 2014-01-1312; 2014.

[54] Karnik AY, Shelby MH. Effect of exhaust gas temperature limits on the peak power performance of a turbocharged gasoline engine. J Eng Gas Turbines Power, 2010;132 (11):112801-1-112801-7.

[55] Weaver C, Turner S. Dual fuel natural gas/diesel engines: Technology, performance, and emissions. SAE tech pap 940548; 1994.

[56] Wang X, Huang Z, Kuti OA, Zhang W, Nishida K. Experimental and analytical study on biodiesel and diesel spray characteristics under ultra-high injection pressure. Int J Heat Fluid Flow, 2010;31(4):659-666.

[57] Kim JK, Park SH, Lee CS. A study on the macroscopic spray behavior and atomization characteristics of biodiesel and dimethyl ether sprays under increased ambient pressure. Fuel Process Technol 2010;91(3)354-363.

[58] Mbarawa M, Milton BE. An examination of the maximum possible natural gas substitution for diesel fuel in a direct injected diesel engine. R&D J, Inc SA Mech Eng 2005;21(1):3-9.

[59] Abd-Alla GH, Soliman HA, Badr OA, Abd-Rabbo MF. Effect of pilot fuel quantity on the performance of a dual fuel engine, Energy Convers Manage 2000;41:559-572.

[60] Imran S, Emberson DR, Ihracska B, Wen DS, Crookes RJ, Korakianitis T. Effect of pilot fuel quantity and type on performance and emissions of natural gas and hydrogen based combustion in a compression ignition engine. Int. J. Hydrogen Energy 2014;39:5163-5175.

[61] Carlucci AP, De Risi A, Laforgia D, Naccarato F. Experimental investigation and combustion analysis of a direct injection dual-fuel diesel-natural gas engine. Energy 2008;33:256-263.

[62] Mousavi SM, Saray RK, Poorghasemi K, Maghbouli A. A numerical investigation on combustion and emission characteristics of a dual fuel engine at part load condition. Fuel 2016;166:309-319.

[63] Abd-Alla GH, Soliman HA, Badr OA, Abd-Rabbo MF. Effect of injection timing on the performance of a dual fuel engine. Energy Convers Manage 2002;43:269-277.

[64] Wang Z, Zhao Z, Wang D, Tan M, Han Y, Liu Z, Dou H. Impact of pilot diesel ignition mode on combustion and emissions characteristics of a diesel/natural gas dual fuel heavy-duty engine. Fuel 2016;167:248-256.

[65] Colliou T, Tilagone R, Martin B. Adapting the NADI^{TM} Concept to Heavy Duty Engines. Oil Gas Sci Technol 2006;61(1):73-84.

[66] Tanaka S, Ayala F, Keck JC, Heywood JB. Two-stage ignition in HCCI combustion and HCCI control by fuels and additives. Combust Flame 2003;132:219-239.

[67] Yao M, Zheng, Z, Liu H. Progress and recent trends in homogeneous charge compression ignition (HCCI) engines. Prog Energy Combust Sci 2009;35:398-437.

[68] Mitakos DA. Experimental investigations for phenomenological modelling of two-stage auto-ignition under HCCI conditions. Dr. sc. ETH Zurich thesis, Zurich, Switzerland: ETH Zurich; 2014.

[69] Carlucci AP, Laforgia D, Saracino R, Toto G. Combustion and emissions control in diesel-methane dual fuel engines: The effects of methane supply method combined with variable in-cylinder charge bulk motion. Energy Convers Manage 2011;52:3004-3017.

[70] Huang Z, Shiga S, Ueda T, Nakamura H, Ishima T, Obokata T, Tsue M, Kono M. Effect of fuel injection timing relative to ignition timing on the natural-gas direct-injection combustion. J Eng Gas Turbines Power 2003;125(3):783-790.

[71] Yang B, Xi C, Wei X, Zeng K, Lai MC. Parametric investigation of natural gas port injection and diesel pilot injection on the combustion and emissions of a turbocharged common rail dual-fuel engine at low load. Appl Energy 2015;143:130-137.

[72] Yang B, Wei X, Xi C, Liu Y, Zeng K, Lai MC. Experimental study of the effects of natural gas injection timing on the combustion performance and emissions of a turbocharged common rail dual-fuel engine. Energy Convers Manage 2014;87:297-304.

[73] Yang B, Wei X, Zeng K, Lai MC. The development of an electronic control unit for a high pressure common rail diesel/natural gas dual-fuel engine. SAE tech pap 2014-01-1168; 2014.

[74] Liu YF, Liu B, Liu L, Zeng K, Huang ZH. Combustion characteristics and particulate emission in a natural-gas direct-injection engine: effects of the injection timing and the spark timing. Proc Inst Mech Eng Part D: J. Automobile Eng 2010;224(8):1071-1080.

[75] Khalil EB, Karim GA. A kinetic investigation of the role of changes in the composition of natural gas in engine applications. J Eng Gas Turbines Power 2002;124(2):404-411.

[76] Huang J, Bushe WK. Experimental and kinetic study of autoignition in methane/ethane/air and methane/propane/air mixtures under engine-relevant conditions. Combust Flame 2006;144:74-88.

[77] Borman GL, Ragland KW. Combustion Engineering. New York, USA: McGraw-Hill; 1998.

[78] Crookes RJ. Comparative bio-fuel performance in internal combustion engines. Biomass Bioenergy 2006;30:461-468.

[79] McTaggart-Cowan GP, Rogak SN, Hill PG, Munshi SR, Bushe WK. The effects of fuel dilution in a natural-gas direct-injection engine. Proc IMechE Part D, J Automob Eng 2007;222(3):441-453.

[80] McTaggart-Cowan GP, Rogak SN, Munshi SR, Hill PG, Bushe WK. The influence of fuel composition on a heavy-duty, natural-gas direct-injection engine. Fuel 2010;89:752-759.

[81] McTaggart-Cowan GP, Rogak SN, Munshi SR, Hill PG, Bushe WK. Combustion in a heavy-duty direct-injection engine using hydrogen-methane blend fuels. Int J Eng Res 2009;10(1):1-13.

[82] Kubesh J, King S, Liss W. Effect of gas composition on octane number of natural gas fuels. SAE tech pap 922359; 1992.

[83] Khandal SV, Banapurmath NR, Gaitonde VN, Hiremath SS. Paradigm shift from mechanical direct injection diesel engines to advanced injection strategies of diesel homogeneous charge compression ignition (HCCI) engines- A comprehensive review. Renewable Sustainable Energy Revs 2017;70:369-384.

[84] Robert Bosch GmbH. Diesel-Engine Management. 4th ed. West Sussex, UK: Wiley; 2006.

[85] Hairuddin AA, Yusaf T, Wandel AP. A review of hydrogen and natural gas addition in diesel HCCI engines. Renewable Sustainable Energy Revs 2014;32:739-761.

[86] Karim GA. The dual fuel engine. In: Evans RL, editor. Automotive Engine Alternatives, New York, USA: Plenum Press; 1987, p. 83-104.

[87] Königsson F, Stålhammar P, Ångström H-E. Combustion modes in a diesel-CNG dual fuel engine. SAE tech pap 2011-01-1962; 2011.

[88] Kokjohn SL, Hanson RM, Splitter DA, Reitz RD. Experiments and modeling of dual-fuel HCCI and PCCI combustion using in-cylinder fuel blending. SAE tech pap 2009-01-2647; 2009.

[89] May I, Pedrozo V, Zhao H, Cairns A, Whelan S, Wong H, Bennicke P. Characterization and potential of premixed dual-fuel combustion in a heavy duty natural gas/diesel engine. SAE tech pap 2016-01-0790; 2016.

[90] White TR, Milton BE, Behnia M. Direct Injection of Natural Gas/Liquid Diesel Fuel Sprays. In: 15th Australas Fluid Mech Conf, The University of Sydney, Sydney, Australia; 2004.

[91] Mello P, Pelliza G, Catalun R, da Silva R. Evaluation of the maximum horsepower of vehicles converted for use with natural gas fuel. Fuel 2006;85:2180-2186.

[92] Korakianitis T, Namasivayam AM, Crookes RJ. Diesel and rapeseed methyl ester (RME) pilot fuels for hydrogen and natural gas dual-fuel combustion in compression-ignition engines. Fuel 2011;90:2384-2395.

[93] Carlucci AP, Laforgia D, Saracino R. Effects of in-cylinder bulk flow and methane supply strategies on charge stratification, combustion and emissions of a dual-fuel di diesel engine. SAE tech pap 2009-01-0949; 2009.

[94] Shiga S, Ozone S, Machacon HTC, Karasawa T, Nakamura H, Ueda T et al. A study of the combustion and emission characteristics of compressed-natural gas direct-injection stratified combustion using a rapid-compression-machine. Combust Flame 2002;129:1-10.

[95] Harrington J, Munshi S, Nedelcu C, Ouellette P, Thomson J, Whitfield S. Direct injection of natural gas in a heavy-duty diesel engine. SAE tech pap 2002-01-1630; 2002.

[96] McTaggart-Cowan G, Mann K, Huang J, Singh A, Patychuk B, Zheng ZX, Munshi S. Direct Injection of Natural Gas at up to 600 Bar in a Pilot-Ignited Heavy-Duty Engine. SAE tech pap 2015-01-0865; 2015.

[97] Westport Fuel Systems Inc. Westport High Pressure Direct Injection Technology. Available on: http://www.westport.com/is/core-technologies/combustion/hpdi (accessed 30 June 2016).

[98] Flaig U, Polach W, Ziegler G. Common rail system (CR-system) for passenger car DI diesel engines; Experiences with applications for series production projects. SAE tech pap 1999-01-0191; 1999.

[99] McTaggart-Cowan GP, Bushe WK, Hill PG, Munshi SR. A supercharged heavy-duty diesel single-cylinder research engine for high-pressure direct injection of natural gas. Int J Eng Res 2004;4(4):315-330.

[100] McTaggart-Cowan GP, Reynolds CCO, Bushe WK. Natural gas fuelling for heavy-duty on-road use: current trends and future direction. Int J Environ Stud 2006;63(4):421-440.

[101] Chen P-C, Wang W-C, Roberts WL, Fang T. Spray and atomization of diesel fuel and its alternatives from a single-hole injector using a common rail fuel injection system. Fuel 2013;103:850-861.

[102] Ismael MA, Heikal MR, Bahroom MB. Spray characteristics and wall impingement of diesel-CNG dual fuel jet using Schlieren imaging technique. Int J Mater Mech Manuf 2015; 3(3):145-151.

[103] Naber J, Siebers D. Effects of gas density and vaporization on penetration and dispersion of diesel sprays. SAE tech pap 960034; 1996.

[104] Mohan B, Yang W, Chou SK. Fuel injection strategies for performance improvement and emissions reduction in compression ignition engines - A review. Renewable Sustainable Energy Revs 2013;28:664-676.

[105] Rente T, Gjirja S, Denbratt I. Experimental investigation of the effect of needle opening (NOP) pressure on combustion and emissions formation in a heavy duty di diesel engine. SAE tech pap 2004-01-2921; 2004.

[106] Kobori S, Kamimoto T, Aradi A. A study of ignition delay of diesel fuel sprays. Int J Engine Res 2000;1(1):29-39.

[107] Wloka JA, Pflaum S, Wachtmeister G. Potential and challenges of a 3000 bar common-rail injection system considering engine behavior and emission level. SAE tech pap 2010-01-1131; 2010.

[108] McTaggart-Cowan GP, Jones HL, Rogak SN, Bushe WK, Hill PG, Munshi SR. The effects of high-pressure injection on a compression-ignition, direct injection of natural gas engine. J Eng Gas Turbines Power 2007;129:579-588.

[109] Mbarawa M, Milton BE, Casey RT. Experiments and modelling of natural gas combustion ignited by a pilot diesel fuel spray. Int J Therm Sci 2001;40:927-936.

[110] Erfan I, Chitsaz I, Ziabasharhagh M, Hajialimohammadi A, Fleck B. Injection characteristics of gaseous jet injected by a single-hole nozzle direct injector. Fuel 2015;160:24-34.

[111] Agarwal AK, Das LM. Biodiesel development and characterization for use as a fuel in compression ignition engines. J Eng Gas Turbines Power, 2001;123(2):440-447.

[112] American Society for Testing and Materials (ASTM). Standard D6751-15. Standard specification for biodiesel fuel blend stock (B100) for middle distillate fuels. Pennsylvania, USA: ASTM; 2015.

[113] European Committee for Standardization. Standard EN 14214:2012. Liquid petroleum products. Fatty acid methyl esters (FAME) for use in diesel engines and heating applications. Requirements and test methods. Brussels, Belgium: CEN; 2013.

[114] American Society for Testing and Materials (ASTM). Standard D975-15. Standard specification for diesel fuel oils. Pennsylvania, USA: ASTM; 2015.

[115] Demirbas A. Progress and recent trends in biodiesel fuels. Energy Convers Manage 2009;50:14-34.

[116] Knothe G. Biodiesel and renewable diesel: A comparison. Prog Energy Combust Sci 2010;36:364-373.

[117] Ryu K. Effects of pilot injection timing on the combustion and emissions characteristics in a diesel engine using biodiesel-CNG dual fuel. Appl Energy 2013;111:721-730.

[118] Ryu K. Effects of pilot injection pressure on the combustion and emissions characteristics in a diesel engine using biodiesel-CNG dual fuel. Energy Convers Manage 2013;76:506-516.

[119] Matzke M, Litzow U, Jess A, Caprotti R, Balfour G. Diesel lubricity requirements of future fuel injection equipment. SAE tech pap 2009-01-0848; 2009.

[120] Misra RD, Murthy MS. Straight vegetable oils usage in a compression ignition engine - A review. Renewable Sustainable Energy Revs 2010;14: 3005-3013.

[121] Subramaniam D, Murugesan A, Avinash A, Kumaravel A. Bio-diesel production and its engine characteristics - An expatiate view. Renewable Sustainable Energy Revs 2013;22: 361-370.

[122] Namasivayam AM, Crookes RJ, Korakianitis T, Olsen J. Assessment of combustion in natural gas fuelled compression ignition engines with DME and RME pilot ignition. Proc Instn Mech Engrs, Int J Engine Res 2009;10(3):165-174.

[123] Bob-Manuel KDH, Crookes RJ. Performance and emission evaluation in dual-fuel engine using renewable fuels for pilot injection. SAE tech pap 2007-01-3605; 2007.

[124] Balat M, Balat H. A critical review of bio-diesel as a vehicular fuel. Energy Convers Manage 2008;49:2727-2741.

[125] Shahid EM, Jamal Y. A review of biodiesel as vehicular fuel. Renewable Sustainable Energy Revs 2008;12: 2484-2494.

[126] Radwan MS, Ismail MA, Elfeky SMS, Abu-Elyazeed OSM. Jojoba methyl ester as a diesel fuel substitute: Preparation and characterization. Appl Therm Eng 2007;27:314-322.

[127] Selim MYE, Radwan MS, Saleh HE. Improving the performance of dual fuel engines running on natural gas/LPG by using pilot fuel derived from jojoba seeds. Renewable Energy 2008;33(6):1173-1185.

[128] Selim MYE. Reducing the viscosity of Jojoba Methyl Ester diesel fuel and effects on diesel engine performance and roughness. Energy Convers Manage 2009;50:1781-1788.

[129] Tarabet L, Loubar K, Lounici MS, Khiari K, Belmrabet T, Tazerout M. Experimental investigation of DI diesel engine operating with eucalyptus biodiesel/natural gas under dual fuel mode. Fuel 2014;133:129-138.

[130] Paul A, Panua RS, Debroy D, Bose PK. Effect of compressed natural gas dual fuel operation with diesel and Pongamia pinnata methyl ester (PPME) as pilot fuels on performance and emission characteristics of a CI (compression ignition) engine. Energy 2014;68:495-509.

[131] Karabektas M, Ergen G, Hosoz M. The effects of using diethylether as additive on the performance and emissions of a diesel engine fuelled with CNG. Fuel 2014;115:855-860.

[132] Geo VE, Nagarajan G, Nagalingam B. Studies on improving the performance of rubber seed oil fuel for diesel engine with DEE port injection. Fuel 2010;89:3559-3567.

[133] Fleisch TH, Basu A, Gradassi MJ, Masin JG. Dimethyl ether: A fuel for the 21st century. Stud Surf Sci Catal 1997;107:117-125.

[134] Semelsberger TA, Borup RL, Greene HL. Dimethyl ether (DME) as an alternative fuel. J Power Sources 2006;156:497-511.

[135] Arcoumanis C, Bae C, Crookes R, Kinoshita E. The potential of di-methyl ether (DME) as an alternative fuel for compression-ignition engines: A review. Fuel 2008;87:1014-1030.

[136] Teng H, McCandless J, Schneyer J. Thermodynamic properties of dimethyl ether - An alternative fuel for compression-ignition engines. SAE tech pap 2004-01-0093; 2004.

[137] Song C. Introduction to chemistry of diesel fuels. In: Song C, Hsu CS, Mochida I, editors. Chemistry of Diesel Fuels, New York, USA: Taylor & Francis; 2000, p. 1-60.

[138] Youn IM, Park SH, Roh HG, Lee CS. Investigation on the fuel spray and emission reduction characteristics for dimethyl ether (DME) fueled multi-cylinder diesel engine with common-rail injection system. Fuel Process Technol 2011;92:1280-1287.

[139] Xu S, Wang Y, Zhang X, Zhen X, Tao C. Development of a novel common-rail type Dimethyl ether (DME) injector. Appl Energy 2012;94:1-12.

[140] Bhide S, Morris D, Leroux J, Wain KS, Perez JM, Boehman AL. Characterization of the viscosity of blends of Dimethyl ether with various fuels and additives. Energy Fuels 2003;117:1126-1132.

[141] Thomas G, Feng B, Veeraragavan A, Cleary MJ, Drinnan N. Emissions from DME combustion in diesel engines and their implications on meeting future emission norms: A review. Fuel Process Technol 2014;119:286-304.

[142] Crookes RJ, Bob-Manuel KDH. RME or DME: A preferred alternative fuel option for future diesel engine operation. Energy Convers Manage 2007;48:2971-2977.

[143] Park SH, Lee CS. Applicability of dimethyl ether (DME) in a compression ignition engine as an alternative fuel. Energy Convers Manage 2014;86:848-863.

[144] Sorenson SC, Mikkelsen S-E. Performance and emissions of a 0.273 liter direct injection diesel engine fuelled with neat dimethyl ether. SAE tech pap 950064; 1995.

[145] Kapus P, Cartellieri W. ULEV Potential of a DI/TCI diesel passenger car engine operated on Dimethyl ether. SAE tech pap 952754; 1995.

[146] Ying W, Genbao L, Wei Z, Longbao Z. Study on the application of DME/diesel blends in a diesel engine. Fuel Process Technol 2008;89:1272-1280.

[147] Zhao Y, Wang Y, Li D, Lei X, Liu S. Combustion and emission characteristics of a DME (dimethyl ether)-diesel dual fuel premixed charge compression ignition engine with EGR (exhaust gas recirculation). Energy 2014;72:608-617.

[148] Namasivayam AM, Korakianitis T, Crookes RJ, Bob-Manuel KDH, Olsen J. Biodiesel, emulsified biodiesel and dimethyl ether as pilot fuels for natural gas fuelled engines. Appl Energy 2010;87:769-778.

[149] Olsen J, Crookes RJ, Bob-Manuel KDH. Experiments in dual fuelling a compression ignition engine by injecting Di-methyl ether as a pilot fuel to ignite varying quantities of natural gas. SAE tech pap 2007-01-3624; 2007.

[150] e Silva DFdC. DME as alternative diesel fuel: Overview. SAE tech pap 2006-01-2916; 2006.

[151] Lif A, Holmberg K. Water-in-diesel emulsions and related systems. Adv Colloid Interface Sci 2006;123-126:231-239.

[152] Namasivayam AM, Crookes RJ, Korakianitis T, Bob-Manuel KDH. Combustion characteristics of dual-fuel diesel engine using emulsified bio-fuel for pilot ignition. SAE tech pap 2009-01-0490; 2009.

[153] Lin C-Y, Chen L-W. Emulsification characteristics of three- and two-phase emulsions prepared by the ultrasonic emulsification method. Fuel Process Technol 2006;87:309-317.

[154] Armas O, Ballesteros R, Martos FJ, Agudelo JR. Characterization of light duty Diesel engine pollutant emissions using water-emulsified fuel. Fuel 2005;84:1011-1018.

[155] Lin C-Y, Chen L-W. Comparison of fuel properties and emission characteristics of two- and three-phase emulsions prepared by ultrasonically vibrating and mechanically homogenizing emulsification methods. Fuel 2008;87:2154-2161.

[156] Abu-Zaid M. An experimental study of the evaporation characteristics of emulsified liquid droplets. Heat Mass Transfer 2004;40:737-741.

[157] Nadeem M, Rangkuti C, Anuar K, Haq MRU, Tan IB, Shah SS. Diesel engine performance and emission evaluation using emulsified fuels stabilized by conventional and gemini surfactants. Fuel 2006;85:2111-2119.

[158] Kumar MS, Bellettre J, Tazerout M. The use of biofuel emulsions as fuel for diesel engines: a review. Proc Instn Mech Engrs, Part A: J Power Energy 2009;223(7):729-742.

[159] Sheng H-Z, Li Chen L, Wu C-K. The Droplet Group Micro-Explosions in W/O Diesel Fuel Emulsion Sprays. SAE tech pap 950855; 1995.

[160] Park S, Woo S, Kim H, Lee K. The characteristic of spray using diesel water emulsified fuel in a diesel engine. Appl Energy 2016;176:209-220.

[161] Abu-Zaid M. Performance of single cylinder, direct injection Diesel engine using water fuel emulsions. Energy Convers Manage 2004;45:697-705.

[162] Verhelst S, Wallner T. Hydrogen-fueled internal combustion engines. Prog Energy Combust Sci 2009;35:490-527.

[163] White CM, Steeper RR, Lutz AE. The hydrogen-fueled internal combustion engine: a technical review. Int J Hydrogen Energy 2006;31:1292-1305.

[164] Das LM. Hydrogen-fueled internal combustion engines. Compend Hydrogen Energy 2016;3(7)177-217.

[165] Alrazen HA, Abu Talib AR, Adnan R, Ahmad KA. A review of the effect of hydrogen addition on the performance and emissions of the compression-ignition engine. Renewable Sustainable Energy Revs 2016;54:785-796.

[166] Karim GA. Hydrogen as a spark ignition engine fuel. Int J Hydrogen Energy 2003;28:569-577.

[167] Karim GA, Wierzba I, Al-Alousi Y. Methane-hydrogen mixtures as fuels. Int J Hydrogen Energy 1996;21(7)625-631.

[168] Akansu SO, Dulger Z, Kahraman N, Veziroğlu TN. Internal combustion engines fueled by natural gas-hydrogen mixtures. Int J Hydrogen Energy 2004;29:1527-1539.

[169] Anstrom JR, Collier K. Blended hydrogen-natural gas-fueled internal combustion engines and fueling infrastructure. Compend Hydrogen Energy 2016;3(8)219-232.

[170] Ma F, Wang Y, Liu H, Li Y, Wang J, Zhao S. Experimental study on thermal efficiency and emission characteristics of a lean burn hydrogen enriched natural gas engine. Int J Hydrogen Energy 2007;32:5067-5075.

[171] Ma F, Wang Y, Liu H, Li Y, Wang J, Ding S. Effects of hydrogen addition on cycle-by-cycle variations in a lean burn natural gas spark-ignition engine. Int J Hydrogen Energy 2008;33:823-831.

[172] Zheng J, Hu E, Huang Z, Ning D, Wang J. Combustion and emission characteristics of a spray guided direct-injection spark-ignition engine fueled with natural gas-hydrogen blends. Int J Hydrogen Energy 2011;36:11155-11163.

[173] Lounici MS, Boussadi A, Loubar K, Tazerout M. Experimental investigation on NG dual fuel engine improvement by hydrogen enrichment. Int J Hydrogen Energy 2014;39:21297-21306.

[174] Park C, Kim C, Choi Y, Won S, Moriyoshi Y. The influences of hydrogen on the performance and emission characteristics of a heavy duty natural gas engine. Int J Hydrogen Energy 2011;36:3739-3745.

[175] Abdelaal MM, Hegab AH. Combustion and emission characteristics of a natural gas-fueled diesel engine with EGR. Energy Convers Manage 2012;64:301-312.

[176] Daisho Y, Yaeo T, Koseki T, Saito T, Kihara R. Combustion and exhaust emissions in a direct-injection diesel engine dual-fueled with natural gas, SAE tech pap 950465; 1995.

[177] Ladommatos N, Abdelhalim S, Zhao H. The effects of exhaust gas recirculation on diesel combustion and emissions. Int J Engine Res 2000;1(1)107-126.

[178] Abd Alla GH, Soliman HA, Badr OA, Abd Rabbo MF. Effects of diluent admissions and intake air temperature in exhaust gas recirculation on the emissions of an indirect injection dual fuel engine. Energy Convers Manage 2001;42:1033-1045.

[179] Selim MYE. A Study of Some Combustion Characteristics of Dual Fuel Engine Using EGR. SAE tech pap 2003-01-0766; 2003.

[180] Ladommatos N, Abdelhalim SM, Zhao H, Hu Z. Effects of EGR on heat release in diesel combustion. SAE paper 980184; 1998.

[181] Hill PG, McTaggart-Cowan GP. Nitrogen oxide production in a diesel engine fueled by natural gas. SAE tech pap 2005-01-1727; 2005.

[182] McTaggart-Cowan GP, Munshi SR, Rogak SN, Hill PG, Bushe WK. Hydrogen-methane blend fuelling of a heavy-duty, direct-injection engine. In: Proc IMECE2007 ASME Int Mech Eng Conf Expos. Seattle, USA: 11-15 November; 2007.

[183] McTaggart-Cowan GP, Jones HL, Rogak SN, Bushe WK, Hill PG, Munshi SR. Direct-injected hydrogen-methane mixtures in a heavy duty compression ignition engine. SAE paper 2006-01-0653; 2006.

[184] Bisio G, Bosio A, Rubatto G. Thermodynamics applied to oxygen enrichment of combustion air. Energy Convers Manage 2002;43: 2589-2600.

[185] Abdelaal MM, Rabee BA, Hegab AH. Effect of adding oxygen to the intake air on a dual-fuel engine performance, emissions, and knock tendency. Energy 2013;61:612-620.

[186] Cacua K, Amell A, Cadavid F. Effects of oxygen enriched air on the operation and performance of a diesel-biogas dual fuel engine. Biomass Bioenergy 2012;45:159-167.

[187] Nwafor OMI. Knock characteristics of dual-fuel combustion in diesel engines using natural gas as primary fuel. Sadhana 2002;27(3):375-382.

[188] Rakopoulos DC, Rakopoulos CD, Giakoumis EG, Dimaratos AM. Characteristics of performance and emissions in high-speed direct injection diesel engine fueled with diethyl ether/diesel fuel blends. Energy 2012;43:214-224.

[189] Zhang W, Chen Z, Shen Y, Shu G, Chen G, Xu B, et al. Influence of water emulsified diesel & oxygen-enriched air on diesel engine NO-smoke emissions and combustion characteristics. Energy 2013;55:369-377.

[190] Liang Y, Shu G, Wei H, Zhang W. Effect of oxygen enriched combustion and water-diesel emulsion on the performance and emissions of turbocharged diesel engine. Energy Convers Manage 2013;73:69-77.

[191] Law T. The Effects of Lubrication System Modifications on Engine Friction and Thermal Behaviour. PhD thesis, Nottingham, UK, Department of Mechanical, Materials and Manufacturing Engineering, The University of Nottingham; 2007.

[192] Neale M, Needham P, Horrell R. Couplings and Shaft Alignment. London, UK: Mechanical Engineering Publications Limited; 1991.

[193] Lancaster DR, Krieger RB, Lienesch, JH. Measurement and analysis of engine pressure data. SAE tech pap 750026; 1975.

[194] Kim, KS, Kim SS. Measurement of dynamic TDC in SI engines using microwave sensor, proximity probe and pressure transducers. SAE tech pap 891823; 1989.

[195] Martyr SJ, Plint MA. Engine Testing: The Design, Building, Modification and Use of Powertrain Test Facilities. 4th ed. Oxford, UK: Butterworth-Heinemann; 2012.

[196] Brunt, MFJ, Pond CR. Evaluation of techniques for absolute cylinder pressure correction. SAE tech pap 970036; 1997.

[197] Lee K, Yoon M, Sunwoo M. A study on pegging methods for noisy cylinder pressure signal. Control Eng Pract 2008;16:922-929.

[198] Randolph LA. Methods of processing cylinder-pressure transducer signals to maximize data accuracy. SAE tech pap 900170; 1990.

[199] Brown BR. Combustion Data Acquisition and Analysis. MEng thesis, Loughborough, UK: Department of Aeronautical and Automotive Engineering, Loughborough University; 2001.

[200] Sujatha C. Vibration and Acoustics: Measurement and Signal Analysis. New Delhi, India. Tata McGraw Hill Education Private Limited; 2010.

[201] Rai, HS, Brunt MFJ, Loader CP. Quantification and reduction of IMEP errors resulting from pressure transducer thermal shock in an S.I. engine. SAE tech pap 1999-01-1329; 1999.

[202] Payri F, Luján JM, Martín J, Abbad A. Digital signal processing of in-cylinder pressure for combustion diagnosis of internal combustion engines. Mech Syst Sig Process 2010;24:1767-1784.

[203] Rosseel E, SierensR, Baert RSG. Evaluating piezo-electric transducer response to thermal shock from in-cylinder pressure data. SAE tech pap 1999-01-0935; 1999.

[204] Amann CA. Cylinder-pressure measurement and its use in engine research. SAE tech pap 852067; 1985.

[205] Dey K. Characterization and rejection of noise from in-cylinder pressure traces in a diesel engine. MASc thesis, Windsor, Canada: Department of Electrical and Computer Engineering, University of Windsor; 2012.

[206] Asad U, Kumar R, Han X, Zheng M. Precise instrumentation of a diesel single-cylinder research engine. Meas 2011;44:1261-1278.

[207] Ren Y, Randall RB, Milton BE. Influence of the resonant frequency on the control of knock in diesel engines. Proc Instn Mech Engrs, Part D: J Automob Eng 1999;213(2):127-133.

[208] Rogers DR. Engine Combustion: Pressure Measurement and Analysis. Pennsylvania, USA: SAE International; 2010.

[209] Kistler Measuring Systems and Sensors. Optimizing diesel engines using a glow plug adapter. Available on: http://www.process-controls.com/intertechnology/Kistler/pdfs/ACC_6531Q_6535Q_Glowplug_Adapter.pdf (accessed 10 Jan. 2015).

[210] Karris ST. Signals and Systems with MATLAB Computing and Simulink Modelling. 4th ed. USA: Orchard Publications; 2008.

[211] Payri F, Broatch A, Tormos B, Marant V. New methodology for in-cylinder pressure analysis in direct injection diesel engines - application to combustion noise. Meas Sci Technol 2005;16:540-547.

[212] Goering CE. Engine heat release via spread sheet. Trans ASAE 1998;41(5): 1249-1253.

[213] Homan JP. Heat Transfer. 10th ed. New York, USA: McGraw-Hill; 2010.

[214] Parra CAF. Heat Transfer Investigations in a Modern Diesel Engine. PhD thesis, Bath, UK: Department of Mechanical Engineering, University of Bath; 2008.

[215] Lounici MS, Loubar K, Balistrou M, Tazerout M. Investigation on heat transfer evaluation for a more efficient two-zone combustion model in the case of natural gas SI engines. Appl Therm Eng 2011;31:319-328.

[216] Chang J, Güralp O, Filipi Z, Assanis D, Kuo, T-W, Najt P. et al. New heat transfer correlation for an HCCI engine derived from measurements of instantaneous surface heat flux. SAE tech pap 2004-01-2996; 2004.

[217] Borman G, Nishiwaki K. Internal combustion engine heat transfer. Prog Energy Combust Sci 1987;13:1-46.

[218] Eichelberg G. Some new investigations on old combustion engine problems. Engineering 1939;148: 446-463, 547-550.

[219] Annand WJD. Heat transfer in the cylinder of reciprocating internal combustion engines. Proc Instn Mech Engrs 1963;177(1):973-990.

[220] Woschni G. A universally applicable equation for the instantaneous heat transfer coefficient in the internal combustion engine. SAE tech pap 670931; 1967.

[221] Hohenberg GF. Advanced approaches for heat transfer calculations. SAE tech pap 790825; 1979.

[222] Sastry GVJ, Chandra H. A three-zone heat release model for DI diesel engines, SAE tech pap 940671; 1994.

[223] Kevric A. Combustion characteristics of a compression ignition engine running on biodiesel and gasoline blended fuels. PhD thesis, Nottingham, UK, Department of Mechanical, Materials and Manufacturing Engineering, The University Of Nottingham; 2013.

[224] Pugh GJ. The Analysis of Heat Release in the Investigation of Split-main Fuel Injection in a Diesel Engine. PhD thesis, Nottingham, UK, Department of Mechanical, Materials and Manufacturing Engineering, The University Of Nottingham; 2004.

[225] Pulkrabek WW. Engineering Fundamentals of the Internal Combustion Engines. 1st ed. New Jersey, USA: Prentice Hall; 1997.

[226] Çengel YA, Boles MA. Thermodynamics: An Engineering Approach. 4th ed. New York, USA: McGraw-Hill; 2002.

[227] McGhee MJ. Factors Influencing Cycle-by-Cycle Combustion Characteristics of a Diesel Engine under Cold Idling Conditions. PhD thesis, Nottingham, UK, Department of Mechanical, Materials and Manufacturing Engineering, The University of Nottingham; 2012.

[228] Rochussen J, Yeo J, Kirchen P. Effect of fueling control parameters on combustion and emissions characteristics of diesel-ignited methane dual-fuel combustion. SAE tech pap 2016-01-0792; 2016.

[229] Karim GA. Combustion in Gas Fueled Compression: Ignition Engines of the Dual Fuel Type. J Eng Gas Turbines Power, 2003;125(3):827-836.

[230] Papagiannakis RG, Krishnan SR, Rakopoulos DC, Srinivasan KK, Rakopoulos CD. A combined experimental and theoretical study of diesel fuel injection timing and gaseous fuel/diesel mass ratio effects on the performance and emissions of natural gas-diesel HDDI engine operating at various loads. Fuel 2017;202:675-687.

[231] Mustafi NN, Raine RR, Verhelst S. Combustion and emissions characteristics of a dual fuel engine operated on alternative gaseous fuels. Fuel 2013;109:669-678.

[232] Karim GA, Ito K, Abraham M, Jensen L. An examination of the role of formaldehyde in the ignition processes of a dual fuel engine. SAE tech pap 912367; 1991.

[233] Azimov U, Tomita E, Kawahara N, Harada Y. Premixed mixture ignition in the end-gas region (PREMIER) combustion in a natural gas dual-fuel engine: operating range and exhaust emissions. Int J Engine Res 2011;12(5):484-497.

[234] Serrano D, Bertrand L. Exploring the potential of dual fuel diesel-CNG combustion for passenger car engine. In: SAE China, FISITA, editors. Proc FISITA 2012 World Automot Congr, Beijing, China: Nov. 2012.

[235] Badr O, Karim GA, Liu B. An examination of the flame spread limits in a dual fuel engine. Appl Therm Eng 1999;19:1071-1080.

[236] Karim GA, Liu Z, Jones W. Exhaust emissions from dual fuel engines at light load. SAE tech pap 932822; 1993.

[237] Liu C, Karim GA, Xiao F, Sohrabi A. An experimental and numerical investigation of the combustion characteristics of a dual fuel engine with a swirl chamber. SAE tech pap 2007-01-0615; 2007.

[238] Barba C, Burkhardt C, Boulouchos K, Bargende M. A Phenomenological Combustion Model for Heat Release Rate Prediction in High-Speed DI Diesel Engines with Common Rail Injection. SAE tech pap 2000-01-2933; 2000.

[239] Khalil E. Modeling the Chemical Kinetics of Combustion of Higher Hydrocarbon Fuels in Air. PhD thesis, Calgary, Canada: Schulich School of Engineering, University of Calgary; 1998.

[240] Reitz RD, Duraisamy G. Review of high efficiency and clean reactivity controlled compression ignition (RCCI) combustion in internal combustion engines. Prog Energy Combust Sci 2015;46:12-71.

[241] Kiplimo R, Tomita E, Kawahara N, Yokobe S. Effects of spray impingement, injection parameters, and EGR on the combustion and emission characteristics of a PCCI diesel engine. Appl Therm Eng 2012;37:165-175.

[242] Xu M, Cheng W, Zhang H, An T, Zhang S. Effect of diesel pre-injection timing on combustion and emission characteristics of compression ignited natural gas engine. Energy Convers Manage 2016;117:86-94.

[243] Carvalho LdeO, de Melo TCC, Neto RMdeAC. Investigation on the fuel and engine parameters that affect the half mass fraction burned (CA50) optimum crank angle. SAE tech pap 2012-36-0498; 2012.

[244] Sun L, Liu Y, Zeng K, Yang R, Hang Z. Combustion performance and stability of a dual-fuel diesel-natural-gas engine. Proc Instn Mech Engrs, Part D: J Automob Eng 2014;229(2): 235-246.

[245] Konno M, Chen Z. Ignition mechanisms of HCCI combustion process fueled with methane/DME Composite Fuel. SAE tech pap 2005-01-0182; 2005.

[246] Tsolakis A, Megaritis A. Partially premixed charge compression ignition engine with on-board H2 production by exhaust gas fuel reforming of diesel and biodiesel. Int J Hydrogen Energy 2005;30:731-745.

[247] Hegab A, La Rocca A, Shayler P. Towards keeping diesel fuel supply and demand in balance: Dual-fuelling of diesel engines with natural gas. Renewable Sustainable Energy Revs 2017;70:666-697.

[248] Aksu C, Kawahara N, Tsuboi K, Kondo M, Tomita E. Extension of PREMIER combustion operation range using split micro pilot fuel injection in a dual fuel natural gas compression ignition engine: A performance-based and visual investigation. Fuel 2016;185:243-253.

[249] Krishnan SR, Srinivasan KK, Singh S, Bell SR, Midkiff KC, Gong W, Fiveland SB, Willi M. Strategies for reduced NOx emissions in pilot-ignited natural gas engines. J Eng Gas Turbines Power, 2004;126(3):665-671.

[250] Hegab A, Shayler P. Effect of Pilot Pre-Injection on Methane-Diesel Dual Fuel Engine Combustion. In Proc. MHMT'17 2nd Int Conf Combust Sci Processes. Barcelona, Spain: April 2017.

[251] Thanapiyawanit B, Jau-Huai L. A dual-fuel system to achieve high equivalence ratio and high engine performance in homogeneous charge compression ignition (HCCI) mode. SAE tech pap 2009-32-0035; 2009.

[252] Hegab A, Shayler P. Influence of Pilot Pre-Injection Mass on Partially Premixed Dual Fuel (PPDF) Engine Combustion. In Proc. MHMT'17 2nd Int. Conf. Combust. Sci. Processes. Barcelona, Spain: April 2017.

[253] Königsson F, Stålhammar P, Ångström H-E. Characterization and potential of dual fuel combustion in a modern diesel engine. SAE tech pap 2011-01-2223; 2011.

[254] Königsson F, Kuyper J, Stålhammar P, Ångström H-E. The influence of crevices on hydrocarbon emissions from a diesel-methane dual fuel engine. SAE tech pap 2013-01-0848; 2013.

[255] Zhou L, Liu Y-F, Wu C-B, Sun L, Wang L, Zeng K, Huang Z-H. Effect of the diesel injection timing and the pilot quantity on the combustion characteristics and the fine-particle emissions in a micro-diesel pilot ignited natural-gas engine. Proc Instn Mech Engrs, Part D: J Automob Eng 2013;227(8):1142-1152.

[256] Paykani A, Kakaee A-H, Rahnama P, Reitz RD. Progress and recent trends in reactivity-controlled compression ignition engines. Int J Engine Res 2016;17(5):481-524.

[257] Yu W, Chen G, Huang Z. Influence of cetane number improver on performance and emissions of a common-rail diesel engine fueled with biodiesel-methanol blend. Front Energy 201;5(4):412-418.

[258] Hegab A, Shayler P. The use of biodiesel and its emulsions as pilot fuels for compression ignition engines dual-fuelled with NG. In: Energy Mater. Res. Conf. Lisbon, Portugal: April 2017.

[259] Muth WA. Effect of Pressure on the Flammable Limits of Some Hydrocarbon-Air Mixtures. PhD thesis, Iowa, USA: Department of Mechanical Engineering, Iowa State University; 1963.

[260] Di Blasio G, Belgiorno G, Beatrice C. Effects on performances, emissions and particle size distributions of a dual fuel (methane-diesel) light-duty engine varying the compression ratio. Appl Energy 2017;204:726-740.

[261] Saanum I, Bysveen M, Tunestål P, Johansson B. Lean burn versus stoichiometric operation with EGR and 3- way catalyst of an engine fueled with natural gas and hydrogen-enriched natural gas. SAE tech pap 2007-01-0015; 2007.

[262] Tepimonrat T, Kamsinla K, Wirojsakunchai E, Aroonsrisopon T, Wannatong k. Use of exhaust valve timing advance for high natural gas utilization in low-load diesel dual fuel operation. SAE tech pap 2011-01-1767; 2011.

[263] Törmänen J. Variable Valve Actuation and Dual-Fuel Combustion. MSc thesis, Helsinki, Finland: Department of Energy Technology, Aalto University; 2015.

[264] Pillai S, LoRusso J, Van Benschoten M. Analytical and experimental evaluation of cylinder deactivation on a diesel engine. SAE tech pap 2015-01-2809; 2015.

[265] Mo H, Huang Y, Mao X, Zhuo B. The effect of cylinder deactivation on the performance of a diesel engine. Proc Instn Mech Engrs, Part D: J Automob Eng 2014;228(2):199-205.

[266] Wilcutts M, Switkes J, Shost M, Tripathi A. Design and benefits of dynamic skip fire strategies for cylinder deactivated engines. SAE tech pap 2013-01-0359; 2013.

[267] Serrano J, Routledge G, Lo N, Shost M, Srinivasan V, Ghosh B. Methods of evaluating and mitigating NVH when operating an engine in dynamic skip fire. SAE tech pap 2014-01-1675; 2014.

[268] Tsolakis A, Abu-Jrai A, Theinnoi K, Wyszynski ML, Xu HM, Megaritis A, Cracknell R, Golunski SE, Peucheret SM. Exhaust gas fuel reforming for IC Engines using diesel type fuels. SAE tech pap 2007-01-2044; 2007.

[269] Tsolakis A, Megaritis A, Yap D. Application of exhaust gas fuel reforming in diesel and homogeneous charge compression ignition (HCCI) engines fuelled with biofuels. Energy 2008;33:462-470.

[270] Tsolakis A, Torbati R, Megaritis A, Abu-Jrai A. Low-load dual-fuel compression ignition (CI) engine operation with an on-board reformer and a diesel oxidation catalyst: Effects on engine performance and emissions. Energy Fuels 2010;24:302-308.

[271] Tira HS, Tsolakis A, Turner D, Herreros JM, Dearn KD, Theinnoi K, Wyszynski ML. Influence of fuel properties, hydrogen, and reformate additions on diesel-biogas dual-fueled engine. J Energy Eng 2014;140(3) A4014003.

[272] Königsson F, Risberg P, Ångström H-E. Nozzle coking in CNG-diesel dual fuel engines. SAE tech pap 2014-01-2700; 2014.

[273] Birgel A, Ladommatos N, Aleiferis P, Zülch S, Milovanovic N, Lafon V, Orlovic A, Lacey P, Richards P. Deposit formation in the holes of diesel injector nozzles: A critical review. SAE tech pap 2008-01-2383; 2008.

[274] Argueyrolles B, Dehoux S, Gastaldi P, Grosjean L, Levy F, Michel A, Passerel D. Influence of injector nozzle design and cavitation on coking phenomenon. SAE tech pap 2007-01-1896; 2007.

[275] Königsson F, Stålhammar P, Ångström H-E. Controlling the injector tip temperature in a diesel dual fuel engine. SAE tech pap 2012-01-0826; 2012.

[276] Wong C, Steere D. The effects of diesel fuel properties and engine operating conditions on ignition delay. SAE tech pap 821231; 1982.

[277] Feneley AJ, Pesiridis A, Andwari AM. Variable geometry turbocharger technologies for exhaust energy recovery and boosting - A review. Renewable Sustainable Energy Revs 2017;71:959-975.

[278] Talibi M, Hellier P, Ladommatos N. The effect of varying EGR and intake air boost on hydrogen-diesel co-combustion in CI engines. Int J Hydrogen Energy 2017;42:6369-6383.

[279] Mei D, Yue S, Zhao X, Hielscher K, Baar R. Effects of center of heat release on combustion and emissions in a PCCI diesel engine fuelled by DMC-diesel blend. Appl Therm Eng 2017;114:969-976.

[280] Dahlström J. Experimental Investigations of Combustion Chamber Heat Transfer in a Light-Duty Diesel Engine. PhD thesis, Lund, Sweden, Department of Energy Science, Lund University; 2016.

[281] Korakianitis T, Boruta M, Jerovsek J, Meitner PL. Performance of a single nutating disk engine in the 2 to 500 kW power range. Fuel 2009;86:2213-2221.

APPENDICES

Appendix A: Combustion Characteristics of DP-Engine vs. CR-Engines

In this appendix, heat release data and key combustion characteristics are compared for DP-Engine and CR-Engine at different engine speeds, loads, and injection timings. The effect of each of these parameters on the combustion process is discussed in the context of comparing the two different FIEs; the mechanical injection vs. the common rail, to help visualizing how this variation could alter engine combustion.

- **Effect of engine speed**

Figure A.1 shows the net HRR profiles at three different speeds of 1500, 2000 and 2500 rpm at 3 bar BMEP and 12º BTDC with no EGR, for the DP-Engine and the CR-Engine.

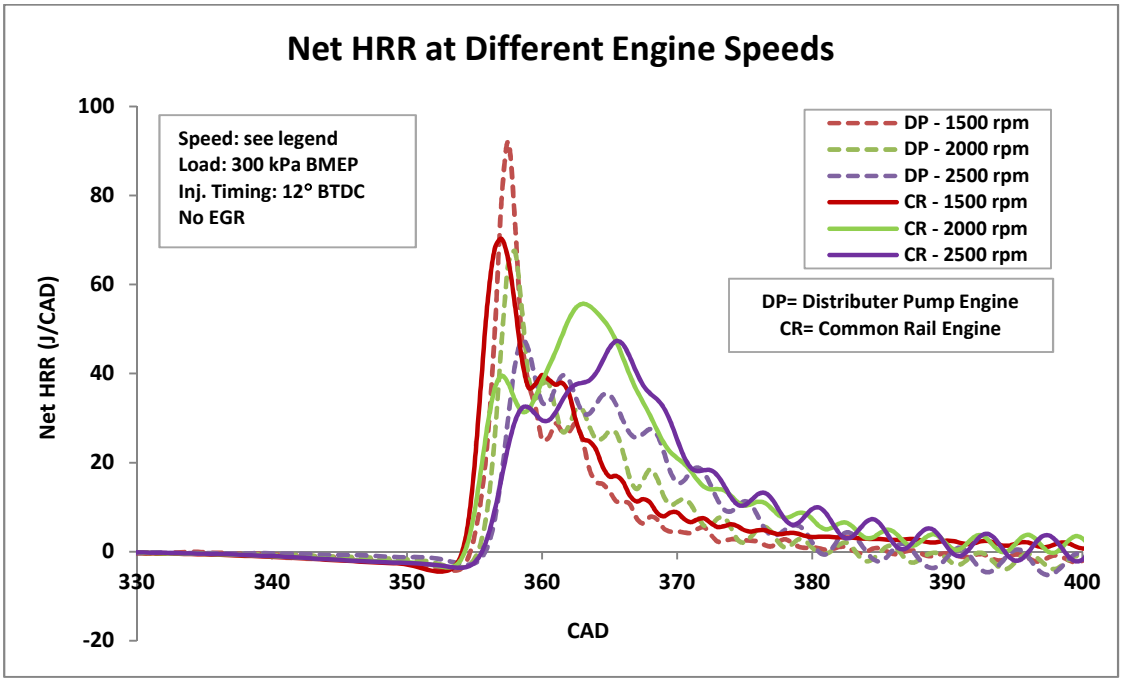


Figure A.1 **Net HRR profile at different engine speeds; 1500, 2000 and 2500 rpm, at 3 bar BMEP and injection timing of 12º BTDC; for both DP-Engine and CR-Engine.**

It can be seen that for both engines, the increase in the engine speed at constant load results in an increase in the ignition delay in crank angle degrees [276]. When measured in milliseconds, the ignition delay decreases with the increase of the engine speed, as illustrated in Fig. A.2. This is attributed to the increased degree of turbulence inside the cylinder as the speed increases, which improves the fuel/air mixing process, shortening the delay period. Also, the increased speed reduces the heat loss during the late stages of the compression stroke as noticed in Fig. A.1, raising the temperatures and pressures inside the cylinder, which improve fuel atomization and vaporization [39]. CR-Engine exhibits shorter ignition delay periods compared with the DP-Engine at all speeds; as demonstrated by Fig. A2. This is due to the high fuel injection pressure levels with the CR system as shown in Fig. A.3. While mechanical injection FIE exhibits a little change in injection pressure with engine speed, CR system involves an increased rail pressure as the fuelling quantity increases, as per the Original Equipment Manufacturer (OEM) fuel calibration map. Higher fuel injection pressure provides better fuel atomization and jet penetration; reducing the ignition delay [39].

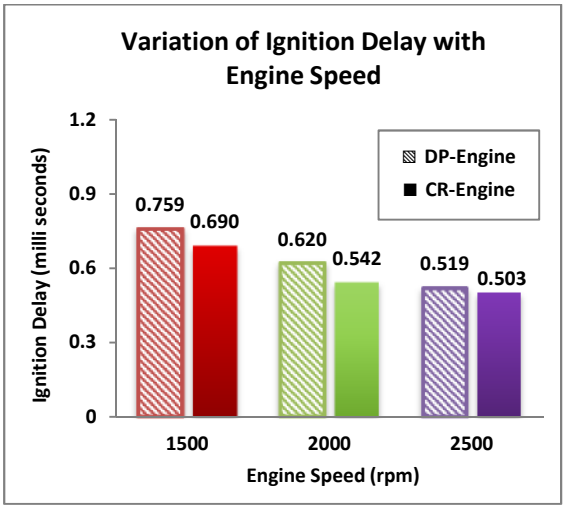


Figure A.2 Variation of ignition delay with engine speed, at constant load of 3 bar BMEP and fixed injection timing of 12º BTDC; for DP-Engine and CR-Engine.

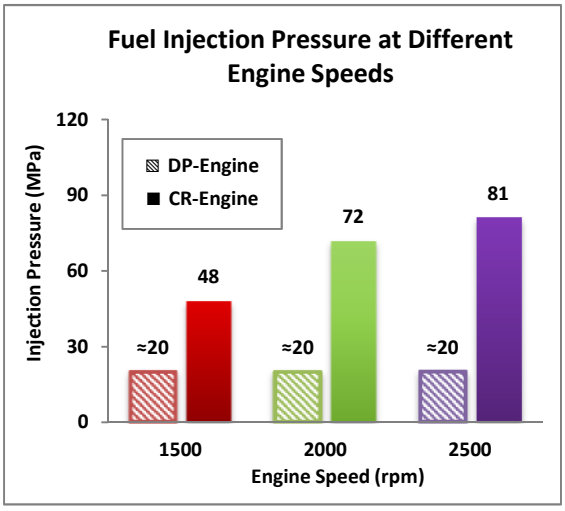


Figure A.3 Fuel injection pressure at different engine speeds. Data @ 3 bar BMEP load and 12º BTDC injection timing; for DP-Engine and CR-Engine.

In addition, the variable geometry turbine (VGT) turbocharger of the CR-Engine used in the present work generates higher boost levels, compared with the fixed geometry waste-gated turbocharger mounted on the DP-Engine [277]. This is shown by Fig. A.4

where the high boost levels and the associated turbulence created inside the cylinder enhances fuel-air mixing rates and contributes to the reduction in ignition delay [278]. The reduced ignition delay means less premixed combustion, as clearly evident in Fig. A.1. That is, MCC phase dominates over the PMC phase as the engine speed increases; where the premixed fraction of the DP-Engine decreases from ≈ 54% at 1500 rpm to ≈ 35% at 2000 rpm and further to ≈ 25% at 2500 rpm. The corresponding values with the CR-Engine are less; owing to the inherent reduction in the ignition delay at all speeds. Figure A.5 shows the premixed burn fraction, as estimated from the cumulative net HR profiles, for both engines. The less premixed fraction and lower heat release rate peak with CR-Engine are expected to generate less NOx emissions [279]. One earlier study on a HPCR engine of the same series (Ford Puma) concluded a profound correlation (direct proportionality) between the cumulative net heat release in the first 15 degrees of combustion and the level of NOx produced [224].

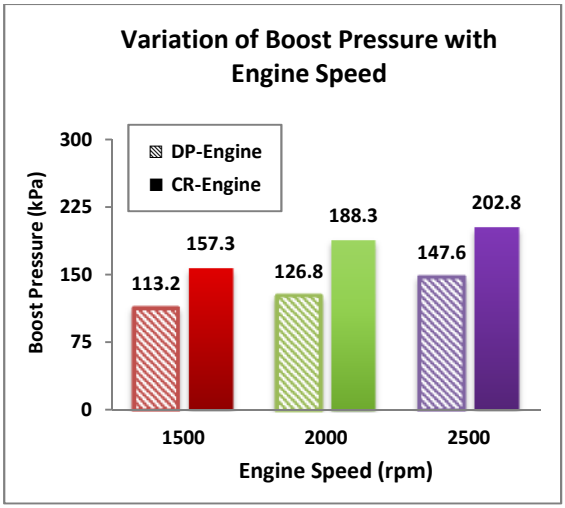


Figure A.4 Variation of boost pressure with engine speed, at constant load of 3 bar BMEP and fixed injection timing of 12° BTDC; for DP-Engine and CR-Engine.

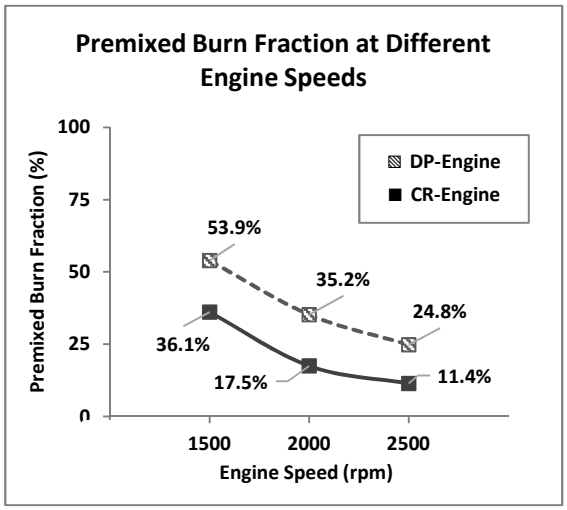


Figure A.5 Variation of premixed burn fraction with engine speed, at 3 bar BMEP and 12° BTDC inj timing; for DP-Engine and CR-Engine. Values estimated from cumulative net HR profiles.

As far as the duration of combustion (DOC) is considered, it was found that the absolute value of DOC (in milliseconds; not in CAD) reduces as the engine speed is increased. This could be attributed to the increased degree of turbulence inside the engine cylinder as the engine speed increases; where higher boost levels and improved mixing promote the combustion process. Figure A.6 shows the variation of DOC with engine speed, for

both engines. Interestingly, it can be seen that the CR-Engine experiences longer DOC than the DP-Engine at all engine speeds, despite having higher boost levels. This may suggest that the CR-Engine has a medium swirl, bowl-in-piston combustion system, compared with the DP-Engine that enjoys high swirl and deep bowl-in-piston [39]. The lower compression ratio of the CR-Engine (15.7) compared with the DP-Engine (18.4) satisfies this combustion system classification [39]. The burning rate therefore becomes slower with the more quiescent system in the CR-Engine, and hence the DOC elongates. The slower burning rate along with the reduced PMC and increased MCC mean that the center of heat release (COHR), or the CA50, with the CR-Engine is attained further away from the TDC; relative to that with DP-Engine. This is consistent throughout the entire range of speeds investigated, as demonstrated by Fig. A.7. The retardation of the COHR away from the TDC down in the expansion stroke is expected to increase both CO and HC emissions in some measure, owing to cylinder temperature decline [279].

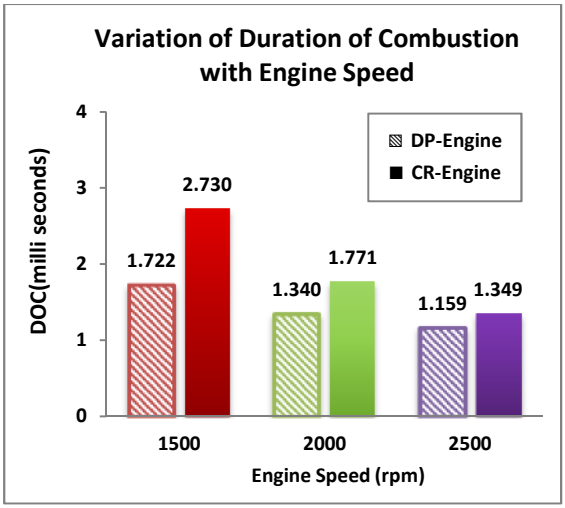


Figure A.6 Variation of DOC with engine speed, at constant load of 3 bar BMEP and fixed injection timing of 12° BTDC; for DP-Engine and CR-Engine.

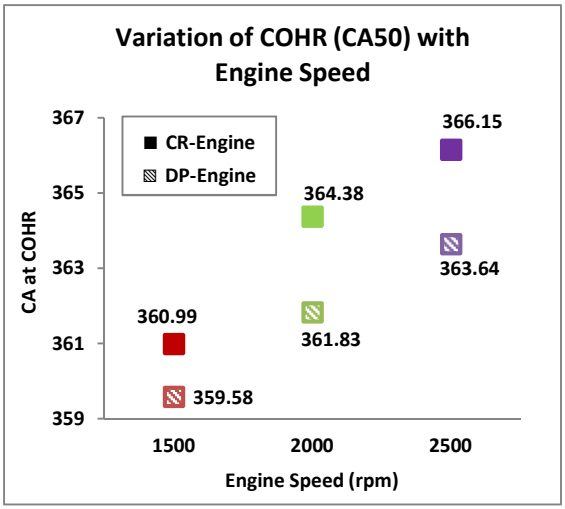


Figure A.7 Variation of COHR (CA50) with engine speed, at constant load of 3 bar BMEP and fixed injection timing of 12° BTDC; for DP-Engine and CR-Engine.

For both engines, the percentage of net HR to the total energy supplied increases as the engine speed increases, owing to the reduced heat loss to the wall [280]. The improved fuel conversion is reflected as a better gross indicated specific fuel consumption (ISFC) as the speed increases; as shown in Fig. A.8. The figure also demonstrates that the CR-Engine exhibits lower gross ISFC values compared with the DP-Engine; where this is

attributed to the higher in-cylinder pressure values over the compression and expansion strokes owing to higher boost levels. On the other hand, brake thermal efficiency (BTE) decreases for both engines as the engine speed increase as shown by Fig. A.9, where this is attributed to the increased friction as the speed increases, which reduces the brake power output. The CR-Engine suffers lower BTE values at these conditions as it works only at ≈15% of its rated power, while these conditions correspond to ≈30% of the DP-rated power; according to the characteristic maps of the two engines.

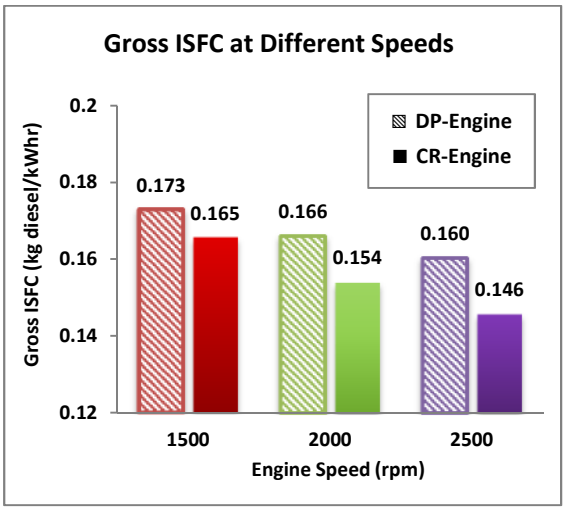


Figure A.8 Gross ISFC at different engine speeds, constant load of 3 bar BMEP and fixed injection timing of 12º BTDC; for DP-Engine and CR-Engine.

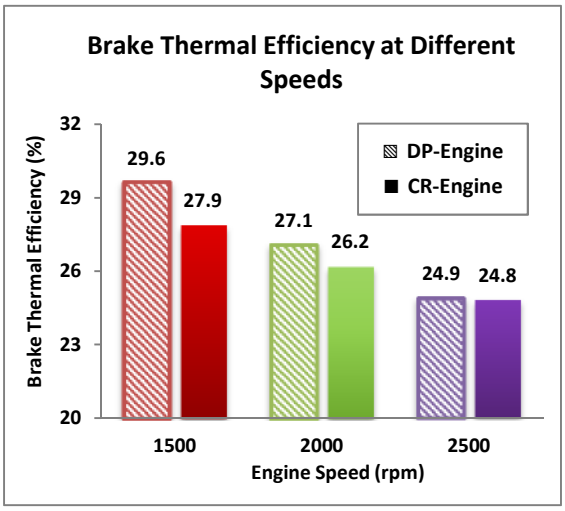


Figure A.9 Brake thermal efficiency at different engine speeds, constant load of 3 bar BMEP and fixed injection timing of 12º BTDC; for DP-Engine and CR-Engine.

- **Effect of engine load**

Figure A.10 shows the net HRR profiles at three different loads of 3, 6, and 8 bar BMEP at 1500 rpm and injection timing of 12º BTDC, for the DP-Engine and the CR-Engine. It could be seen that for both engines, ignition delay period decreases as the engine load increases. This reflects the influence of engine load change on the conditions inside the cylinder prior to injection. For one thing, as the engine load increases, the residual gas temperature, and the wall temperature increase; resulting in a higher charge temperature (and pressure, to a lesser extent), and hence ignition delay is reduced [39]. In addition, the turbocharging boost level increases as the load is increased; and consequently, inlet temperature and pressure increase; shortening the ignition delay.

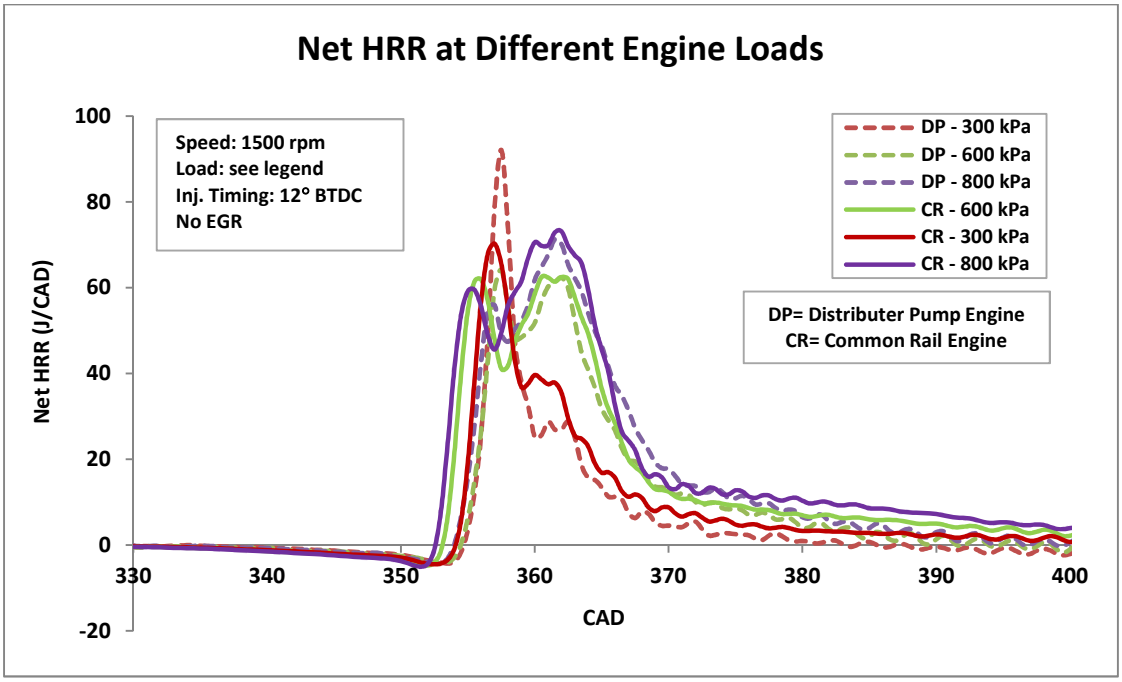


Figure A.10 **Net HRR profile at different engine loads; 3, 6 and 8 bar BMEP, at 1500 rpm and injection timing of 12º BTDC; for both DP-Engine and CR-Engine.**

Figure A.11 shows the effect of engine load on ignition delay for both engines. It could be seen that the CR-Engine always exhibits shorter ignition delay periods compared with the DP-Engine; at all load conditions. This is attributed to the higher fuel injection pressure with the CR system which improves fuel atomization, and also to the higher boost levels with the VGT turbocharger used that provide better mixing [39]. Figure A.12 presents the values of fuel injection pressure for both engines at different load conditions, while Fig. A.13 illustrates the corresponding boost pressure levels. For both engines, the shortened ignition delay and the elevated boost levels as the load increases reduce the PMC phase; from the one hand [39]. At the same time, the MCC phase itself increases since larger amount of fuel is used to attain high load conditions; where the shorter ignition delay results in the majority of the fuel to be burned in the MCC phase. As a result, the premixed fraction of the DP-Engine decreases from ≈ 54% at 3 bar BMEP to ≈ 22% at 6 bar BMEP and further to ≈ 17% at 8 bar BMEP. Once again, the corresponding values with CR-Engine are less as it experiences shorter ignition delay at all loads. Figure A.14 illustrates the premixed burn fraction, as estimated from the cumulative net HR profiles.

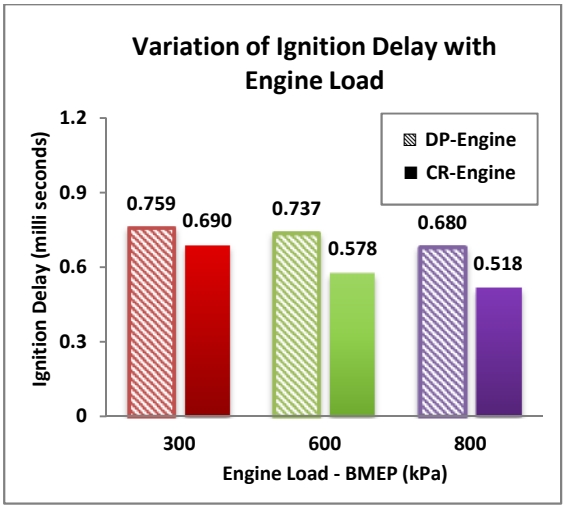


Figure A.11 Variation of ignition delay with engine load, at 1500 rpm and injection timing of 12° BTDC; for DP-Engine and CR-Engine.

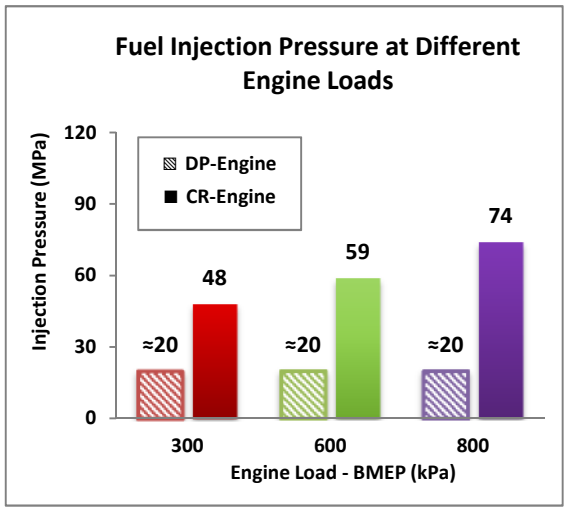


Figure A.12 Fuel injection pressure at different engine loads. Data @ 1500 rpm and 12° BTDC injection timing; for DP-Engine and CR-Engine.

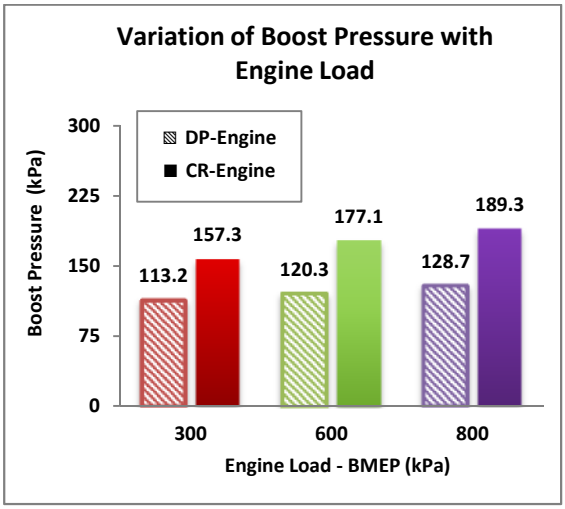


Figure A.13 Variation of boost pressure with engine load, at constant speed of 1500 rpm and fixed injection timing of 12° BTDC; for DP-Engine and CR-Engine.

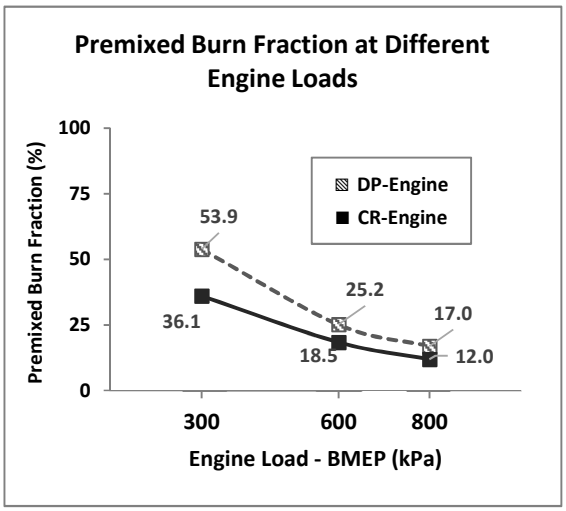


Figure A.14 Variation of the premixed burn fraction with engine load, at constant speed of 1500 rpm and fixed injection timing of 12° BTDC; for DP-Engine and CR-Engine.

Duration of combustion (DOC) for both engines elongates with the increase of engine load; understandably due to the use of larger amount of diesel fuel that requires more time to be consumed. Figure A.15 presents the variation of DOC with engine load; for both engines. It could also be seen from the figure that the CR-Engine exhibits longer DOC than the DP-Engine at all loads. As discussed earlier, this could suggest that the CR-Engine has a more quiescent system compared with the DP-Engine.

The slow burning rates are more visible in the late stages of combustion, as noticed in Fig. A.10. However, the figure also shows that the second peak that present the MCC combustion tends to drop in faster rates with the CR-Engine as the load is increased. A possible explanation for this could be a local improvement in the burning rate at this stage due to the increased pressure and temperature inside the engine cylinder as the load increases. As a result, the centre of heat release (COHR), or the CA50, with the CR-Engine is attained after that with DP-Engine only at low load (3 bar BMEP). The case is revered at 8 bar BMEP, while both engines exhibit almost the same position of the CA50 at 6 bar BMEP. Figure A.16 shows the variation of the CA50 position with engine load, for both engines.

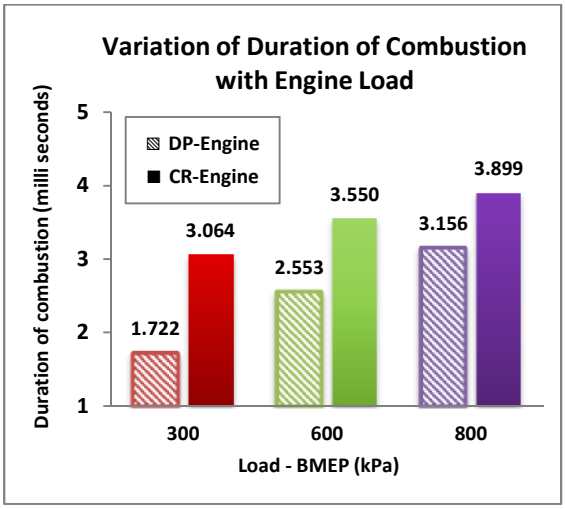


Figure A.15 Variation of DOC with engine loads, at constant speed of 1500 rpm and fixed injection timing of 12º BTDC; for DP-Engine and CR-Engine.

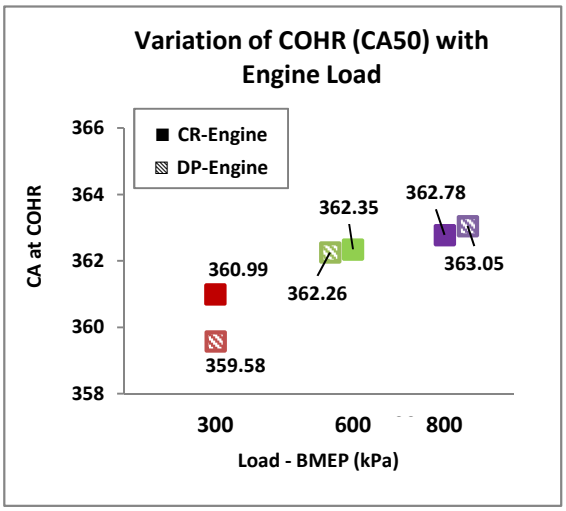


Figure A.16 Variation of COHR (CA50) with engine loads, at constant speed of 1500 rpm and fixed injection timing of 12º BTDC; for DP-Engine and CR-Engine.

As the load increases, the in-cylinder temperature increases and hence the heat transfer to the wall increases. Accordingly, the percentage of net HR to the total energy supplied to the engine decreases. The deterioration of fuel conversion into useful heat is reflected as an increased level of gross indicated specific fuel consumption (ISFC); as illustrated in Fig. A.17. The lower values of gross ISFC with the CR-Engine compared with the DP-Engine are attributed to the higher in-cylinder pressure values over the compression and expansion strokes owing to higher boost levels. Nevertheless, the reduced friction losses as the load is increased results in an improvement in the brake thermal efficiency

(BTE) [39] as illustrated by Fig. A.18. The figure also shows that the CR-Engine suffers lower values of BTE at the points investigated compared with the DP-Engine, as these points lie outside the high-performance region of its characteristic map. While the loads of 3, 6, and 8 bar BMEP at 1500 rpm stand for ≈ 30%, 60%, and 80% of the DP-Engine rated power at that speed, they only present ≈ 15%, 30%, and 40% of the CR-Engine rated power. Accordingly, higher BSFC values, or lower BTE values, are encountered.

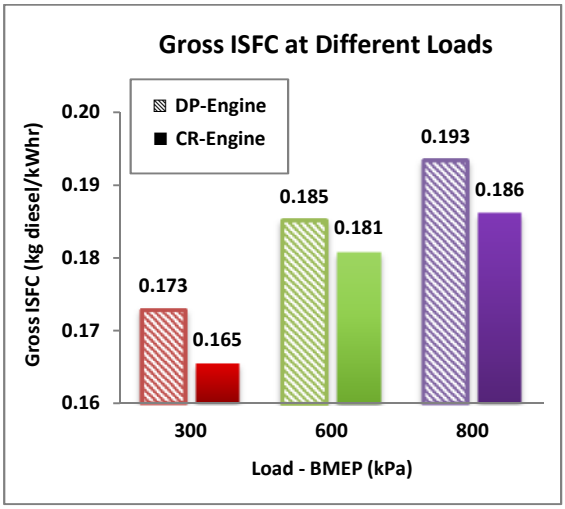


Figure A.17 Gross ISFC at different engine engine loads, at constant speed of 1500 rpm and fixed injection timing of 12° BTDC; for DP-Engine and CR-Engine.

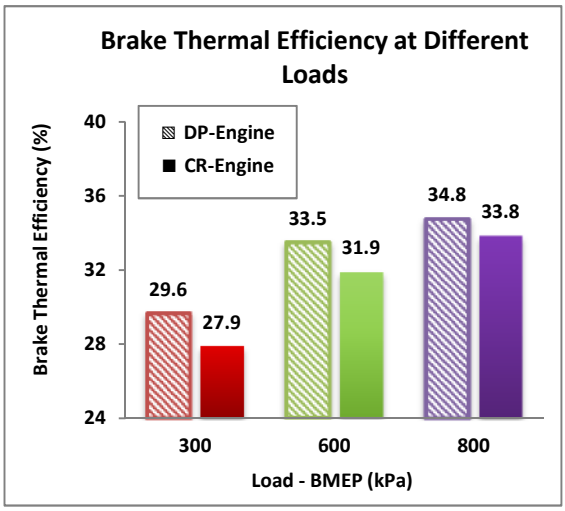


Figure A.18 Brake thermal efficiency at different engine loads, at constant speed of 1500 rpm and fixed injection timing of 12° BTDC; for DP-Engine and CR-Engine.

- **Effect of injection timing**

Figure A.19 shows the net HRR profiles at three different injection timings of 20°, 12°, and 4° BTDC, at 1500 rpm and 3 bar BMEP with no EGR, for the DP-Engine and the CR-Engine. It could be seen that for both engines, the variation of injection timing has a remarkable effect, not only on the SOC but also on the heat release profile and combustion phasing. With advanced injection timing (20°BTDC), ignition delay period increases as the temperature and pressure at the SOI are still comparatively low. As a consequence of the prolonged ignition delay, most of the fuel is injected before ignition occurs, which results in very rapid burning rates once the combustion commences. This is demonstrated by the high spike of the PMC phase, with high rates of pressure rise and high peak pressure values [39].

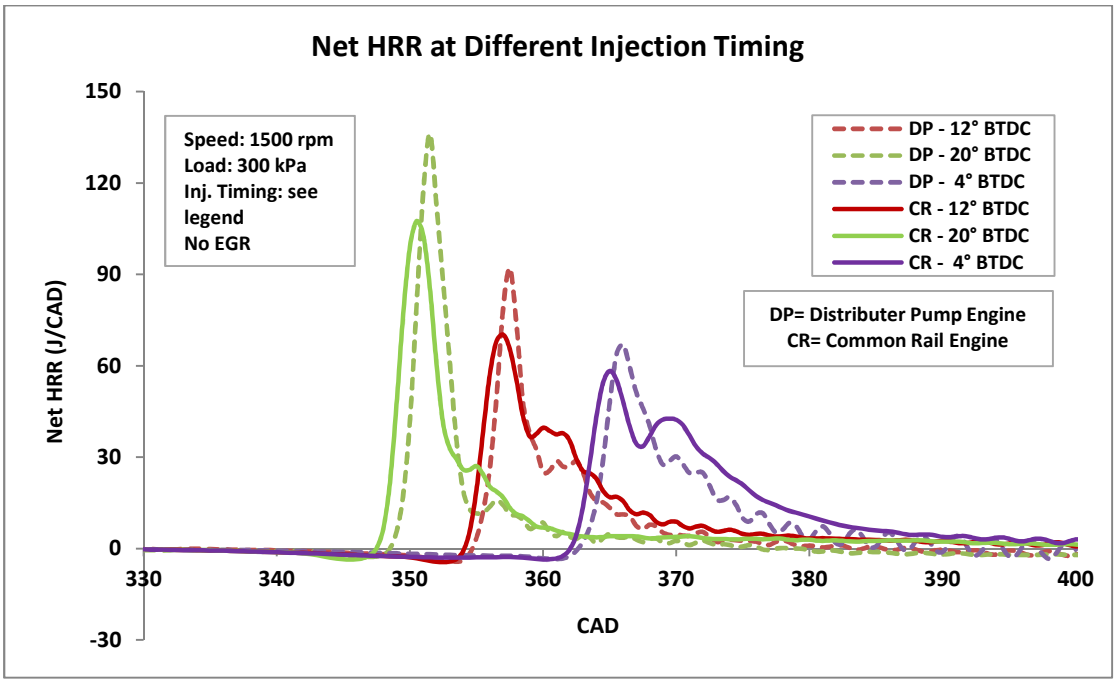


Figure A.19 **Net HRR profile at different injection timings; 20°, 12° and 4° BTDC, at 1500 rpm and load of 3 bar BMEP; for both DP-Engine and CR-Engine.**

The combustion at these conditions is therefore predominantly premixed; with a premixed fraction exceeds 70% for the DP-Engine. With the retarded injection timing (4° BTDC), in contrast, ignition delay is shortened as the fuel is injected during the high temperature and pressure near the end on the compression stroke. As a result, a smaller amount of fuel is injected before the combustion commences; and hence PMC spike becomes lower and the burning rate is slower. The premixed fraction at these conditions goes down below 50%, for the DP-Engine. As shown in Fig. A.20, the corresponding values with the CR-Engine are less, since it experiences a shorter ignition delay at all injection timings. Figure A.21 shows the variation of the ignition delay with injection timing for both engines. Once again, the shorter ignition delay with the CR-Engine is attributed to the higher fuel injection pressure and elevated boost levels, compared with the DP-Engine, as illustrated by Figs. A.22 and A.23, respectively. For the same power levels (speed-load), the change in injection timing does not influence injection pressure or boost level.

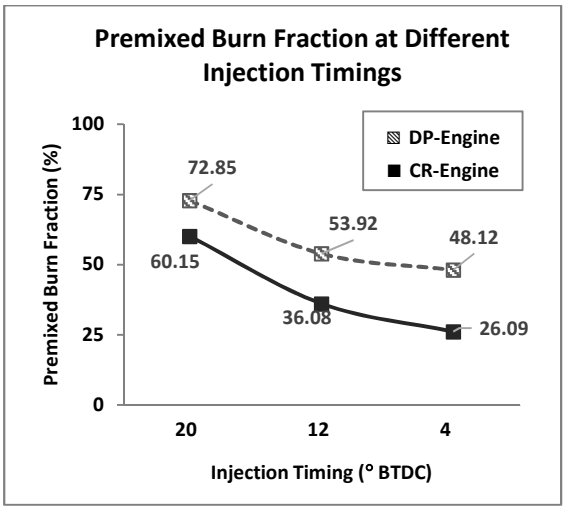


Figure A.20 Variation of the premixed burn fraction with injection timing, at 1500 rpm and 3 bar BMEP; for DP-Engine and CR-Engine.

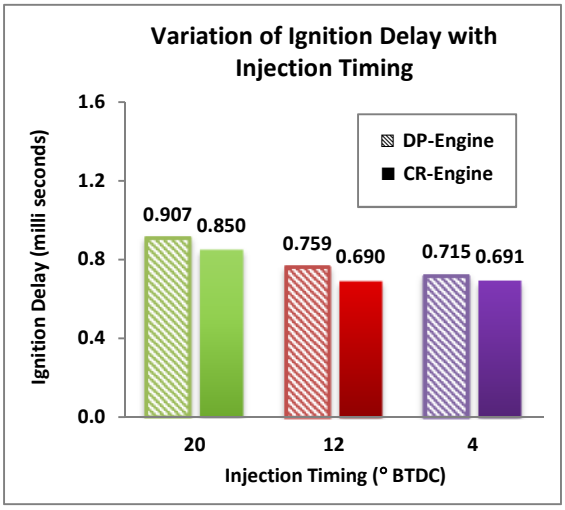


Figure A.21 Variation of ignition delay with injection timing, at 1500 rpm and 3 bar BMEP; for DP-Engine and CR-Engine.

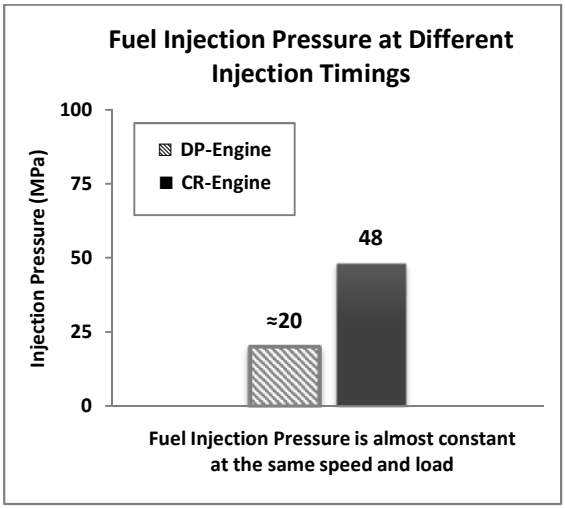


Figure A.22 Fuel injection pressure at constant speed of 1500 rpm and load of 3 bar BMEP; for DP-Engine and CR-Engine.

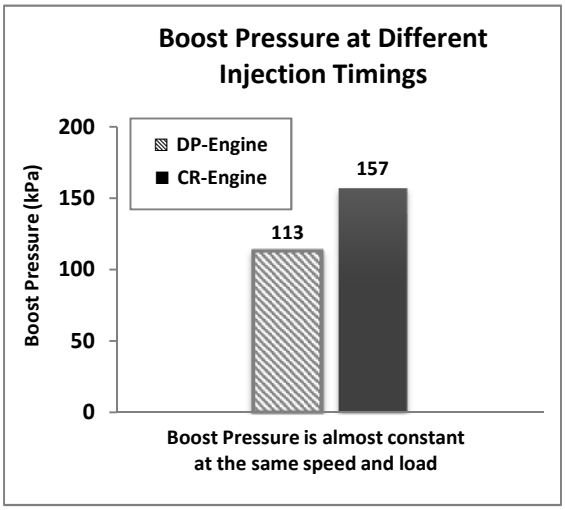


Figure A.23 Boost pressure at constant speed of 1500 rpm and load of 3 bar BMEP; for DP-Engine and CR-Engine.

The developed high pressure and temperature with the advanced injection timing bring about an increase in the heat transfer to the wall; reducing the percentage of the net HR to the total energy supplied to the engine. On the other hand, retarded injection timing results in lower pressure and temperature, and hence the heat transfer to the cylinder wall is reduced. In view of that, indicated specific fuel consumption (ISFC) for both engines increases with advanced injection timing and decreases with retarded injection

timing, as shown in Fig. A.24. The reduced ISFC values with the CR-Engine, compared with the DP-Engine are attributed to the higher gross indicated work owing to the higher cylinder pressure value.

Also, the advanced injection timing means the majority of fuel is burned and the peak in-cylinder pressure is attained before the TDC. Accordingly, a considerable portion of the power developed is wasted during the compression stroke; reducing the useful brake power output (and brake thermal efficiency; in consequence). Yet, the retarded injection timing and the associated late SOC after the TDC results in having the earlier stage of expansion stroke spent at just about motoring pressure. This diminishes the useful brake power and thermal efficiency. As shown in Fig. A.25, optimized engine performance is attained at normal injection timing; where the combustion process is completed in the appropriate crank angle interval close to the TDC [39]. It could also be seen that the CR-Engine experiences lower brake thermal efficiency (BTE) values, compared with the DP-Engine; at all injection timings. This is because the power level (speed and load) at these conditions present only ≈15% of the CR-Engine rated power; contrasting ≈30% of the DP-Engine rated power. This means higher friction losses and less useful power, and hence retarded BTE values [39].

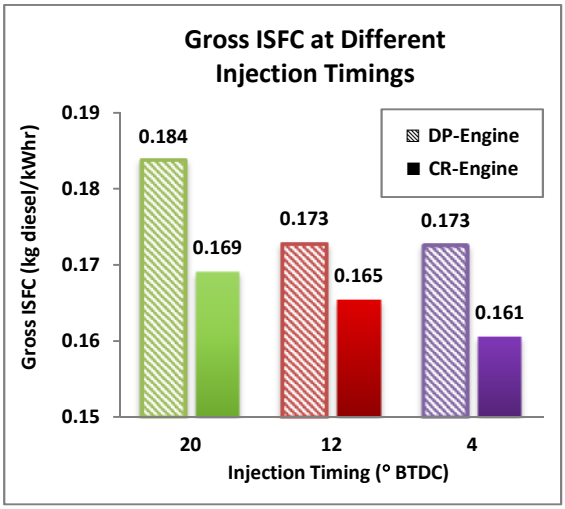


Figure A.24 Gross ISFC at different injection timings, at 1500 rpm and 3 bar BMEP; for DP-Engine and CR-Engine.

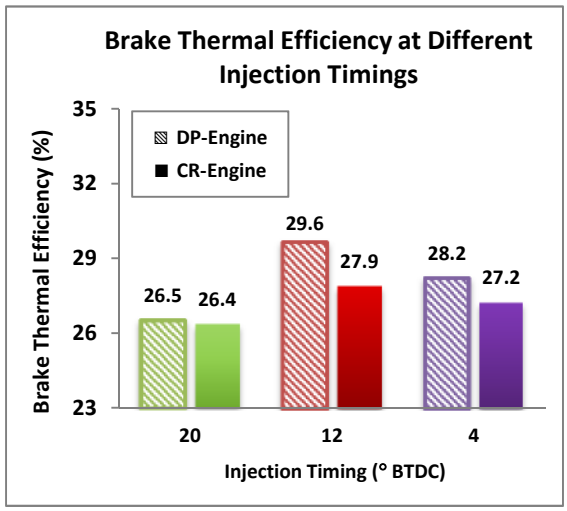


Figure A.25 Brake thermal efficiency (BTE) at different injection timings, at 1500 rpm and 3 bar BMEP; for DP-Engine and CR-Engine.

The developed high pressure and temperature with the advanced injection timing (20° BTDC) also brings about shorter duration of combustion (DOC); compared with normal (12°BTDC) and retarded (8°BDTC) injection timings. This applies to both engines; as demonstrated by Fig. A.26. It could also be seen that the CR-Engine always exhibits longer DOC; at all injection timings. Again; this could suggest it has a more quiescent system compared with the DP-Engine. The effect is more voluminous at the retarded injection timing as it is characterized with larger, slow, MCC combustion; as evident in Fig. A.19. Figure A.27 present the positions of the center of heat release (COHR), or the CA50, at different injection timings; for both engines. Although the CR-Engine has an earlier SOC, the increased MCC on the account of PMC counterparts the reduction in ignition delay. CA50 position with the CR-Engine is therefore attained after that with the DP-Engine; at all injection timings. The difference increases as the injection timing is retarded; owing to the increased MCC with the CR-Engine. This could be observed from the HRR curves in Fig. A.19, and also inferred from Fig. A.20.

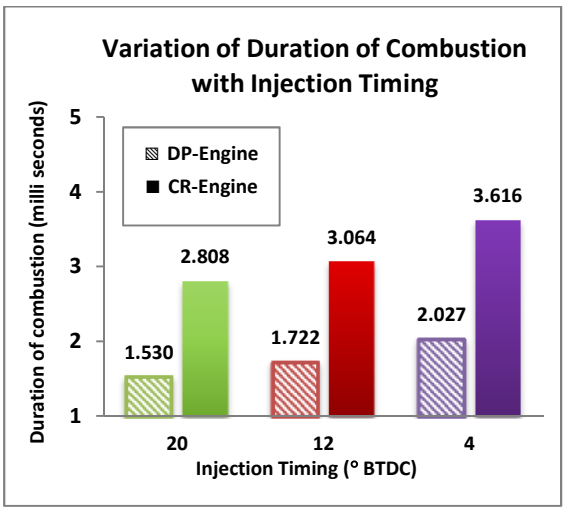


Figure A.26 Variation of DOC with injection timing, at 1500 rpm and 3 bar BMEP; for DP-Engine and CR-Engine.

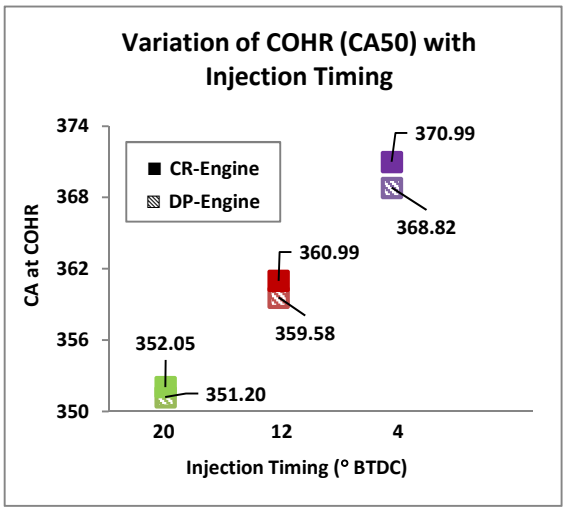


Figure A.27 Variation of COHR (CA50) with injection timing, at 1500 rpm and 3 bar BMEP; for DP-Engine and CR-Engine.

- **Conclusions**

In this appendix, the influence of fuel injection equipment (FIE) type on combustion and HR characteristics of CI engines has been investigated. The tests were performed using two engines; one has a mechanical injection distributor pump (DP) and the other has a high-pressure common rail (CR). The key conclusions of the comparison between the two engines are:

- At any given test condition, the CR-Engine always exhibits shorter ignition delay than the DP-Engine. This is attributed to the higher fuel injection pressure with the CR system which improves the fuel atomization, and also to the higher boost levels with the VGT turbocharger used that provide a better mixing.
- Reduced ignition delay with the CR-Engine results in less premixed combustion in which the MCC phase dominates over the PMC phase; at all test cases investigated. The average reduction in the premixed faction is ≈40%.
- The CR-Engine always exhibits a longer duration of combustion (DOC), compared with the DP-Engine at any given test condition, despite having higher boost levels. This suggests that the CR-Engine has a more quiescent system compared with the DP-Engine. The lower compression ratio of the CR-Engine (15.7) compared with the DP-Engine (18.4) satisfies this classification.
- The center of heat release (CA50) with the CR-Engine is attained further away from the TDC; relative to that with DP-Engine. This is attributed to the slower burning rate and increased MCC on the account of PMC. This is consistent throughout the entire range of results, except at high load conditions where the high pressure and temperature notably improve the burning rate of the MCC phase.

Appendix B: Analysis of Engine Performance Parameters

Understanding of the relationships between different performance parameters of ICEs is the key factor for guiding the research and development in that field; with regard to engine design and technology as well as the use of alternative fuels. Steady-state engine performance is governed by a set of equations; derived from the principles [39]. The engine brake thermal efficiency (η_{th}) is defined as the shaft output power ($\dot{W}$) divided by the rate of the energy supplied to the engine through the combustion of fuel:

$$\eta_{th} = \frac{\dot{W}}{\dot{m}_f . LHV_f} \tag{B.1}$$

where ($\dot{m}_f$) and (LHV_f) are the fuel's mass flow rate and lower heating value; respectively.

Incorporating the fuel-to-air ratio (FAR^{act}), which represents the actual fuel mass flow rate ($\dot{m}_f$) to the air mass flow rate ($\dot{m}_a$) used, the engine power output may be expressed as:

$$\dot{W} = \eta_{th} . \dot{m}_a . FAR^{act} . LHV_f \tag{B.2}$$

For the purpose of comparison between different fuels as well as different mixture composition conditions, it becomes more representative to express the actual FAR in terms of the equivalence ratio (ϕ) and stoichiometric FAR. Hence, from the definition of the equivalence ratio:

$$\phi = \frac{FAR^{act}}{FAR^{stoic}} \tag{B.3}$$

where (FAR^{stoic}) is the actual and stoichiometric fuel-to-air ratio; the engine power output may be expressed as:

$$\dot{W} = \eta_{th} . \dot{m}_a . \phi . FAR^{stoic} . LHV_f \tag{B.4}$$

To take into account engine design effectiveness, intake system performance, and inlet air conditions, air mass flow may be expressed in terms of volumetric efficiency, where the latter stands for the ratio of the actual air pumped into the intake system to the maximum possible mass flow rate of air that the engine geometry would allow:

$$\eta_v = \frac{\dot{m}_a}{\rho_a . V_d . k . N} \tag{B.5}$$

where (ρ_a) is air density at the engine inlet, (V_d) is the engine displacement, (k) is the number of suction strokes per engine revolution (that is; $k=1/2$ for four-stroke engine), and (N) is the engine rotational speed. Substituting Equation (B.5) in Equation (B.4); yields:

$$\dot{W} = \eta_{th} . \left(\eta_v . \rho_a . V_d . k . N\right) . \phi . FAR^{stoic} . LHV_f \tag{B.6}$$

This series of basic equations highlights the importance to engine performance of the several encountered parameters, each of which is discussed briefly herein below in the context of its relationships with some others; where this guides the vast majority of engine research work for optimized performance and exhaust emissions.

The maximum possible theoretical thermal efficiency of a particular engine is function of its compression ratio; that is, fuel conversion efficiency improves with the increase of compression ratio [39]. Nevertheless, increased compression ratio and the associated higher cylinder temperature result in increased NOx emission. The value of maximum (η_{th}) is a function of engine technology as well as geometry (principally; physical size). Decreasing the surface-to-volume ratio with large engines results in reduced relative importance of friction and heat loss per cycle; increasing the efficiency [39]. Compared with the thermal efficiency of small lawn-mower SI engine that is as low as 5%, large slow-speed marine CI engine attains efficiencies over 50%; thanks to the reduced losses [21, 39]. Increasing the engine displacement volume (V_d) not only increases the power directly but it is also advantageous in reducing losses. While engine power is directly proportional to the rotational speed (N), the latter is limited by the mean piston speed, friction, lubrication effectiveness, stress and material consideration, on top of the inertia of moving parts; basically with large engines [39]. NOx emission concentrations also increase moderately with the increasing speed. However, CO and HC emissions will be enhanced by the increase of speed if sufficient amount of oxygen is available [39].

Engine power output is also directly proportional to the air mass flow rate ($\dot{m}_a$) as well as the volumetric efficiency (η_v). The latter is largely affected by combustion chamber shape, the manifold design, and the degree of swirl [39]. Polishing the inlet and outlet manifolds, along with variable manifold geometry are used to optimize the volumetric efficiency [21]. It is preferred to introduce the fuel to the engine cylinder through direct injection rather than the induction in the intake manifold, to maximize the amount of the air mass flow and, consequently, the power. This issue is critical for most engines working on dual-fuelling strategy with gaseous fuel. The density of the inlet air to the engine (ρ_a) determines the amount of charge introduced into the engine, and it can be elevated through the use of supercharging and turbocharging. This has a significant effect upon engine torque and BMEP. For DI diesel engine of equivalent sizes, the use of turbocharger increases the maximum BMEP by 29%, and additional increase of 22% can be attained by using after-cooler along with turbocharger [39]. Still, turbocharged engines output is constrained by the stress levels in the critical mechanical components; where those levels limit the maximum cylinder pressure permissible under continuous operation. High temperatures and the resulting thermal loadings are limiting factors too. Therefore, it is a common practice to lower the compression ratio of turbocharged diesel engines (relative to naturally-aspirated engines) to keep the peak pressure and thermal loading levels within the permissible limits [39]. Smoke and NOx emission regulations are additional constraints. While increased compression ratio lowers engine resistance to knock, charge dilution may be used to damp the pressure rise rates as well as the temperature and hence the thermal NOx formation. Exhaust gas recirculation (EGR) is used frequently, although it negatively affects the air mass flow and engine volumetric efficiency.

Some researches have considered increasing the number of power strokes per crank revolution (k), to increase the engine power output. These include studies on prototype nutating disk engine with two power stroke per revolution; that is, four-times the ratio of conventional 4-stroke engines [281]. The researches on the utilization of alternative fuels in ICEs are on continuous ongoing; where fuel type is very influential on power output as per Equation (A.6), since it affects the heating value (LHV_f) the stoichiometric fuel-to-air ratio (FAR^{stoic}) and the equivalence ratio (ϕ). Fuels with higher heating values and/or higher FAR^{stoic} (relative to gasoline and diesel fuel) are desirable. Methane has

13.6% higher LHV_f yet 15.3% lower FAR^{stoic} than gasoline, and 17.6% higher LHV_f yet 15.9% lower FAR^{stoic} than diesel fuel [39]. Equivalence ratio largely influences engine operation. While lean-fuel operation ($\phi < 1$) results in lower NOx emissions and better fuel economy, it negatively affects the power output. Peak MEP is attained with slightly rich mixture; with ϕ value between 1 and 1.1. However, over rich-fuel operation ($\phi >> 1$) is not desirable because of the economic and environmental considerations (higher fuel consumption and excessive emissions) while increased power level is not realized since there will not be sufficient amount of oxygen to combust the fuel.

Appendix C: Project Safety Documents

The University of Nottingham

Faculty of Engineering

Dept. of Mechanical, Materials and Manufacturing Engineering

Ref No: 1437

Control of Substances Hazardous to Health (COSHH) Assessment Record

Room No/Place: Engine room (3) / L4 Building	**Personnel**: Abdelrahman Hegab **Status**: PhD Student			
Title of Experimental/Procedure/Process: Combustion and Exhaust Emission Characteristics of Diesel Engines Using Alternative Fuels				
Aim: The project aims at investigating the influence of fuel type, blend proportions, and injection strategy on combustion and exhaust emission characteristics of diesel engines. Three alternative fuels will be covered; typically, methane (or NG), hydrogen, and biodiesel. The results will be compared with those of conventional diesel fuel.				**Are there less hazardous alternatives?** NO
Substances involved:	**Quantity:**	**Hazards identification:**	**MSDS* attached?**	**Storage:**
Hydrogen gas (compressed) Chemical formula: H_2	50 liter gas bottle.	**Hazard statements:** -H280 Contains gas under pressure; may explode if heated. -H220 Extremely flammable gas. **Signal word:** Danger.	YES	-Bottles will be stored fairly below 50°C in a well-ventilated place, in a location free from fire risk and away from sources of heat, ignition, and combustible materials. - Bottles will be stored in the vertical position and properly secured to prevent falling over, and valve guards or caps should be in place. -Stored containers will be periodically checked for general conditions and leakage.

Page 1 of 7

		Labelling pictograms: 		
Methane gas (compressed) Chemical formula: CH_4	50 liter gas bottle.	**Hazard statements:** -H280 Contains gas under pressure; may explode if heated. -H220 Extremely flammable gas. **Signal word:** Danger. **Labelling pictograms:** 	YES	-Bottles will be stored fairly below 50°C in a well-ventilated place, in a location free from fire risk and away from sources of heat, ignition, and combustible materials. - Bottles will be stored in the vertical position and properly secured to prevent falling over, and valve guards or caps should be in place. -Stored containers will be periodically checked for general conditions and leakage.

WORK ACTIVITY

System description:

The system is located in Engine room (3) in the ground floor of L4 building. System arrangement in illustrated in Figure 1. A Full list of system components is presented in the attached Table 1. A clear description of the system is given herein below:

Basically the purpose of the arrangement is to provide the engine with the required amount of gaseous fuel supply at the required working pressure of the gaseous fuel injection system injection system. The system starts with the compressed gas bottle – 50 liters volume, supplied by BOC, and ends with the engine; 2.2L Ford Puma Common Rail Diesel engine.

All system parts in contact with the gas are made from 316L Stainless Steel. Gas pressure is first reduced from the bottle pressure of 175 bar (for Hydrogen – or 200 bar for Methane) to 15 bar via a SS single stage HP regulator; by Swagelok. The gas then flows through an arrangement of 3/8" SS seamless tube and flexible tubes by Swagelok, to a SS single stage LP regulator; where the pressure is brought down to the injectors working pressure of 7 bar. The gas then is fed into the gaseous fuel injection rail through a similar arrangement of 3/8" SS seamless tube and flexible tubes by Swagelok.

System leak-tight test:
(Refer to Figure 1 and Table 1 for parts numbers).

The complete system is going to be tested for leak prior to use. Compressed air bottle is going to be connected to the system in the place of gas bottle (#1). Shutoff valve (#11) is kept open while shutoff valve (#11*) is closed. The compressed air cylinder is then fully opened and the air is allowed to flow throughout the system. As soon as the system stabilized with no change in the pressure gauges readings, those reading are carefully recorded. The pressure gauge (#22) should read the compressed air cylinder pressure, while gauges (#23) & (#24) should read 15 bar and 7 bar, respectively; according to the pre-set values of the pressure regulators outputs. Pressure gauge (#23*) should read slightly less than 15 bar due to the pressure drop caused by friction throughout the system.

The pressure values throughout the system will be monitored for 30 minutes. If the pressure is maintained during the course of the test, the system is said to be "Leak-tight". If not, all connections are going to be checked and any possible source of leak must be addressed. Additionally, a visual leak detection test is going to be conducted at that point, where a snoop liquid lead detector is going to be sprayed over all joints and any potential leakage points such as at the point of connection of the cylinder valve with the regulator. The system should be free of any frothing. If there is any frothing, the system should be immediately depressurized and the leak corrected. The complete procedure should be repeated from the beginning.
When the system is confirmed to be leak-free; the compressed air bottle will be closed. Shutoff valve (#11) is kept open while shutoff valve (#11*) is now let opened; to allow the air vents through the vent pipe to the extractor fan.

Safety precautions:
(Refer to Figure 1 and Table 1 for parts numbers).

- The system is going to be tested for leak detection using compressed air before the introduction of any gaseous fuel; no gaseous fuel will be introduced to the system before it's assured to be "Leak-free".
- The gas bottle and delivery line is protected by a SS flashback arrestor – attached to the HP regulator at the gas bottle exit.
- The system is vented to outdoor through the extractor fan, where any excess pressure build-up in the delivery line beyond the injectors' working pressure is vented through a SS pressure relief valve by Swagelok (#18) - that opens at a predetermined value, so the gaseous fuel can be vented, through a SS flash back arrestor with an integrated check valve by WITT gas (#21) – to protect the system against dangerous reverse gas flow and eliminate any possibility of flashbacks into the system as the gaseous fuel comes into contact with air.
- Gaseous fuel injection section in the engine intake manifold is equipped with a sensitive thermal fuse that melts if the temperature goes higher than a 75°C – indicating that there is flashback of the flame inside the intake manifold. As the fuse melts, it sends out a signal to the Engine Control Unit (ECU) so it shuts of the H_2 supply to the gas injector immediately. Any pressure developed in the delivery line will be released through the pressure relief valve and the flame arrestor arrangement safely to the venting system; as outlined above.
- The system will be purged from any residuals of gaseous fuel after each experiment. The gas bottle will be fully closed, the shutoff valves (#11) is kept open while the shutoff valve (#11*) is now let fully opened; to allow the gaseous fuel inside the system to be vented out through the flashback arrestor down to the outdoor.

***MSDS Manufacturers Safety Data Sheets are attached.**

Duration of Exposure: (not duration of procedure)		
No occupational exposure limit.		
Frequency of Exposure:		
No occupational exposure limit.		
How could the materials be absorbed into the body?		
The materials can be absorbed by inhalation into the lungs.		
Is a written protocol in safe handling required: NO	**Will all persons in the vicinity be informed of the hazards and control measures:** YES	**Is air monitoring required:** NO
Are health checks required? NO	**If YES, have health checks been arranged?** N/A	**Name of person(s) requiring health checks** **N/A**

Give details of control measures to be adopted (including personal protective equipment):

- Gas bottles are stored and used at the ambient temperature; fairly below 50°C, and away from any direct source of flame or ignition.
- Only one gas bottle will be used at once.
- Gas bottle in use are protected from any reverse flow or gas flash using a flashback arrestor.
- Gas supply system are protected against any excess pressure developed; using a pressure relief valve.
- The gas pipe system is complemented with a dedicated vent system; also protected by a flashback arrestor.
- All safety measures (pressure relief valve, flashback arrestors) will be provided with a calibration certificate; either from the supplier or from an approved third party test facility.

Eye and face protection:
Wear eye protection to EN 166 when using gases.
Skin protection and other protection:
Wear lab coat, leather safety gloves and safety shoes when handling the gas cylinders.
Respiratory protection:
Not required
Thermal hazards:
Not required

Health surveillance requirements (if applicable):

N/A

Give details of disposal procedures at all stages:

Do not discharge into areas where there is a risk of forming an explosive mixture with air. Do not discharge into any place where its accumulation could be dangerous. Contact BOC if guidance is required.

Conclusion: (indicate why the risk is acceptable, bearing in mind current control measures. List additional control measures if risk is deemed unacceptable).

The system will be checked for leak before any gaseous fuel will be introduced. The gas bottle is protected by using a flashback arrestor. The whole system is vented and any build-up pressure will be relieved instantaneously. The vent pipe is equipped with a flashback arrestor with integrated check valve. The space is double-height and well-ventilated. No more than one gas cylinder will be handled at once in the working area.

EMERGENCY PROCEDURES

Spillage/uncontrolled release:

Leak not Ignited:
Extinguish all sources of ignition in the immediate area. Close the cylinder valve. If necessary tighten the gland nut. If leak continues, evacuate the area, and avoiding sources of ignition and minimizing personal risk move the leaking cylinder to a safe outside area. Notify BOC. Post warning notices and prevent access to the area. DO NOT Attempt to tighten the cylinder valve in the body of the cylinder. DO NOT tamper with the safety devices.

Leak Ignited:
Raise fire alarm. Close cylinder valve if safe to do so. Call fire brigade. Evacuate the area. If possible apply copious quantities of water from a hose to the affected cylinder(s) from a protected position until the cylinder(s) are cold. DO NOT Move cylinders until cold.

Firefighting:

Suitable extinguishing media:
Dry power; Foam

Advice for fire-fighters:
If possible, stop flow of product. Move container away or cool with water from a protected position. Do not extinguish a leaking gas flame unless absolutely necessary.
Spontaneous/explosive re-ignition may occur. Extinguish any other fire.

First Aid:

First Aid Inhalation:
Remove victim to uncontaminated area wearing self-contained breathing apparatus. Keep victim warm and rested. Call a doctor. Apply artificial respiration if breathing stopped.

First Aid Skin / Eye:
Adverse effects not expected from this product.

First Aid Ingestion:
Ingestion is not considered a potential route of exposure.

Most important symptoms and effects, both acute and delayed:
In high concentrations may cause asphyxiation. Symptoms may include loss of mobility/consciousness. Victim may not be aware of asphyxiation.

Indication of any immediate medical attention and special treatment needed:
N/A.

Name of Assessor: ABDELRAHMAN [illegible]	**Name of Supervisor:** P SHAYLER
Status: PhD Student	**Status:** PROFESSOR
Date: 21-1-2013	**Date:** 21/1/13
Signed:	**Signed:**

This assessment must be reviewed periodically, or whenever the original assessment is no longer valid, or where there has been a significant change in the work to which the assessment relates.					
Review date:					
Signed:					

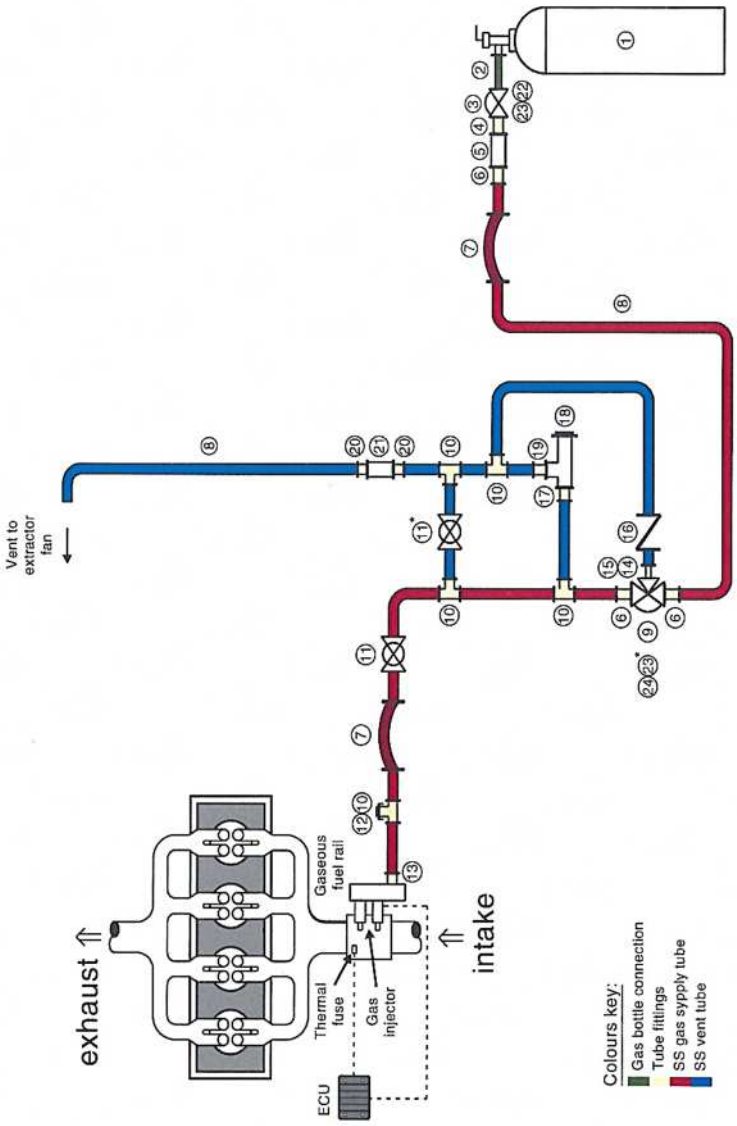


Figure (1) System components and layout. Refer to Table (1) for parts' numbers.

Table (1) System components description and parts' numbers. Refer to Figure (1) for layout.

No.	Component	Supplier	Part number	Description	Notes	End connection
1	Gas Bottle	BOC	TBC	50 Liter cylinder with side outlet and key operation	Both Hydrogen & Methane (or NG) bottles have BS4 valve outlet	BS341 No.4 (5/8")
2	SS Cylinde concection to BS341	BOC	849016	BS341 No. 4 Male LH thread x 1/4" NPT Male	Nut & stem - to connect between the gas bottle and the HP regulator	1/4" Male NPT
3	SS Single step HP regulator	Swagelok	RS-N2-02-2-NNP-NV	SS Swagelok HP regulator - 1/4" Female NPT inlet/outlet - 1/4" Female NPT pressure gauge connection	Max. pressure in 400 bar - pressure out range 0-25 bar - with gas filter - nonvented	1/4" Female NPT
4	SS pipe fitting - Nipple	Swagelok	SS-8-HRN-4	Stainless Steel Pipe Fitting, Hex Reducing Nipple, 1/2 in. Male NPT x 1/4 in. Male NPT	To connect between the 1/4" Female NPT of the HP regulatorand the 1/2" Female NPT of the HP Flashback Arrestor	1/2" Male NPT
5	SS Flashback Arrestor - HP	WITTgas	F100N-ES - 210000012	SS Flashback Arrestors, 1/2 in. Female NPT	17 bar Flashback Arrestor	1/2" Female NPT
6	SS tube fitting - Male connector	Swagelok	SS-600-1-8	SS Swagelok Tube Fitting, Male Connector, 3/8 in. Tube OD x 1/2 in. Male NPT	To connect between the 1/2" Female NPT of the HP Flashback Arrestor (and that of the LP regulator that follows) and the the 3/8" tube	3/8" Swagelok tube fitting

7	3/8" SS Flexible tube	Swagelok	SS-FM6SL6SL6-18	316L SS Convoluted (FM) Hose, 3/8 in., 316L SS Braid, 3/8 in. Tube Fittings, 18 in.	Max pressure 137 bar	3/8" Swagelok tube fitting
8	Swagelok 3/8" SS tube	Swagelok	SS-T6-S-035-20	316/316L SS Seamless Tubing, 3/8 in. OD x 0.035 in. Wall x 20 Feet	Gas tube - for both supply and vent - Max pressure 224 bar	Will always use Swagelok tube fittings for connection
9	SS Single step LP regulator	Swagelok	RS-N4-02-2-NNN-A-GN5	SS Swagelok LP regulator - 1/2" Female NPT inlet/outlet - 1/4" Female NPT pressure gauge connection - 1/8 in. ISO/BSP parallel thread vent connection - Antitamper - Gauge connection configuration GN5	Max. pressure in 70 bar - pressure out range 0-7 bar - Antitamper	1/2" Female NPT
10	SS Tube Fitting - 3/8" Union Tee	Swagelok	SS-600-3	SS Swagelok Tube Fitting, Union Tee, 3/8 in. Tube OD	To connect gas supply and vent tubes	3/8" Swagelok tube fitting
11	3/8" SS Ball Valve	Swagelok	SS-43GS6	SS 1-Piece 40 Series Ball Valve, 1.5 Cv, 3/8 in. Swagelok Tube Fitting	Max. pressure 206 bar	3/8" Swagelok tube fitting
12	SS tube fitting - Cap	Swagelok	SS-600-C	316 Stainless Steel Cap for 3/8 in. OD Tubing	Cap for attaching instrumentation	3/8" Swagelok tube fitting
13	SS tube fitting - Male connector	Swagelok	SS-600-1-10ST	SS Swagelok Tube Fitting, Male connector, 3/8 in. Tube OD x 7/8-14 Male SAE/MS Straight Thread	To connect between the 3/8" tube and the gaseous fuel rail	7/8" Male SAE/MS Straight Thread

14	SS tube fitting - Male connector	Swagelok	SS-600-1-2RS	SS Swagelok Tube Fitting, Male Connector, 3/8 in. Tube OD x 1/8 in. Male ISO Parallel Thread, Straight Shoulder	To connect between the 1/8 in. ISO/BSP parallel thread vent connection of the LP regulator and the 3/8" vent tube	3/8" Swagelok tube fitting
15	SS fitting - Buna ring	Swagelok	SS-2-RS-2B	Stainless Steel Gasket for 1/8 in. Male ISO Parallel Thread (RS) Fittings, Buna Inner Ring	Used in conjuction with the 1/8 in. Male ISO Parallel Thread (RS)	N/A
16	SS FP Poppet Check Valve	Swagelok	SS-6C-1	SS Poppet Check Valve, Fixed Pressure, 3/8 in. Swagelok Tube Fitting, 1 psig (0.07 bar)	To be connected to the thread vent port of the LP regulator - Nominal cracking pressure 0.07 bar	3/8" Swagelok tube fitting
17	SS tube fitting - Female connector	Swagelok	SS-600-7-8	SS Swagelok Tube Fitting, Female Connector, 3/8 in. Tube OD x 1/2 in. Female NPT	To connect between the 3/8" tube and the the 1/2" Male NPT of the LP relief valve	1/2" Female NPT
18	SS LP relief valve	Swagelok	SS-RL4M8F8	SS Low-Pressure Proportional Relief Valve, 1/2 in. MNPT x 1/2 in. FNPT	To relief any excess pressure in the gas suply tube downstream the LP regulator - Set pressure range 0.68-15.5 bar	1/2" Female NPT
19	SS tube fitting - Male connector	Swagelok	SS-600-1-8	SS Swagelok Tube Fitting, Male Connector, 3/8 in. Tube OD x 1/2 in. Male NPT	To connect between the 1/2" Female NPT of the LP relief valve and the 3/8" tube	3/8" Swagelok tube fitting

20	SS tube fitting - Male connector	Swagelok	SS-600-1-6	SS Swagelok Tube Fitting, Male Connector, 3/8 in. Tube OD x 3/8 in. Male NPT	To connect between the 3/8" tube and the LP Flashback Arrestor	3/8" Male NPT
21	SS Flashback Arrestor - LP	WITTgas	RF85-10N/H-ES - 143-087	SS Flashback Arrestors, 3/8 in. Female NPT	10 bar Flashback Arrestor	3/8" Female NPT
22	SS Pressure Gauge - HP	BOC	842348	SS 1/4" NPT Male connector HP gauge	For the HP regulator inlet - Max pressure 310 bar	1/4" Male NPT
23	SS Pressure Gauge - MP	BOC	842344	SS 1/4" NPT Male connector MP gauge	For the HP regulator outlet and the LP regulator inlet - Max pressure 28 bar	1/4" Male NPT
24	SS Pressure Gauge - LP	BOC	842342	SS 1/4" NPT Male connector LP gauge	For the LP regulator outlet - Max pressure 14 bar	1/4" Male NPT

Page 4 of 4

ASSESSOR (Print name): ABDELRAHMAN HEGAB	RECORD NO (leave blank): 1953	The University of Nottingham Faculty of Engineering Mechanical, Materials & Manufacturing Engineering **RISK ASSESSMENT RECORD**	
ASSESSOR'S SIGNATURE:	LOCATION OR ROOM NO: L4 BUILDING		
ASSESSMENT DATE:	LAST ASSESSMENT DATE:		
SUPERVISOR'S NAME: P SHAYLER	NEXT ASSESSMENT DATE:		
SUPERVISOR'S SIGNATURE: — 20/1/15			
PROJECT TITLE:			

SUBJECT FOR ASSESSMENT *Name the activity or project, machine, equipment, etc.*	ASSOCIATED HAZARD (something with the potential to cause harm) *List the significant hazards associated with each subject (e.g., electricity, flammable liquid, hazardous materials, fumes, noise, dust, etc.)*	PEOPLE INVOLVED *List the groups(s) of people who might be at risk (i.e., Technicians, Postgrad, Undergrad, Cleaners, Visitors etc*	ASSOCIATED RISK (the potential harm arising from the hazard) *Give a brief statement for each hazard (e.g., cut hand, eye damage, respiratory irritation, chronic illness etc.)*	EXISTING RISK-CONTROL MEASURES *List for each hazard the control procedures, equipment and devices currently used, e.g. safe method of work, LEV, safety valve, machine guarding, fume cupboard, training and specific items of PPE.*	LIKELIHOOD OF EVENT *Enter for each hazard H, M or L (3, 2 or 1)*	SEVERITY OF HARM *Enter for each hazard H, M or L (3, 2 or 1)*	RISK RATING *Enter for each hazard 1 to 9*	DEFICIENCIES & PROPOSED REMEDIAL MEASURES *Give brief statement of any observed deficiency and of any required control action(s). If not obvious, give brief reason for recommendation(s) made.*	PRIORITY *Enter for each hazard 1 to 5*
Ford Puma 2.2L Common Rail Diesel Research Engine Engine Test Rig	Noise	Research and Technical Stuff	Hearing Damage	Ear defender should be worn near engine at operating speed of 2000 rpm and higher	H	M	6		1
	Diesel Fumes	Research and Technical Stuff	Inhalation of Vaporized Hydrocarbon	COSHH Assessment No. 152. Avoid fume inhalation when re-filling the fuel tank. Extractor fan must be turned on.	M	M	5		2
	Engine Exhaust Gas	Research and Technical Stuff	Inhalation of CO and NOx	COSHH Assessment No. 120 & 189. Exhaust extraction to atmosphere. CO meter to warn of excessive concentrations of CO in the working area.	H	H	9		1
	Rotating Machinery	Research and Technical Stuff	Eye/Body Damage	Fixed-guarding around all rotating machinery to be fitted when the engine running.	H	H	9		1
	Pressurized Diesel Fuel Injection Pipes and Rails	Research and Technical Stuff	Eye Damage	COSHH Assessments No. 153. Relieve pressure in fuel lines and rails before carrying out work. Wear safety glasses during work.	M	M	5		2
	Engine Oil	Research and Technical Stuff	Skin Irritation	COSHH Assessments No. 188. Wear protective gloves and cloth.	M	M	5		2
	Engine Coolant – Water/Ethylene glycol Mixture	Research and Technical Stuff	Skin Irritation	COSHH Assessments No. 194. Wear safety glasses when caring out work involving contact with coolant.	L	H	7		2
	Compressed Gases – Nitric Oxide, Carbon Monoxide, Carbon Dioxide, Propane, Hydrogen/Helium Mixture, Nitrogen, Zero-Grade Air, Compressed Air	Research and Technical Stuff	Asphyxiation	COSHH Assessments No. 192 & 199. All connections must be checked for leak before the work is commenced.	H	M	6		1
	Compressed Gases - Hydrogen, Methane	Research and Technical Stuff	Asphyxiation, Explosion of Gas Cylinder if Heated	COSHH Assessments No. 192 & 199 & 123. All connections must be checked for leak before the work is commenced. Avoid any source of heat in the vicinity of the compressed gas cylinders.	L	H	7		2
	Diesel Spillage	Research and Technical Stuff	Slipage	Use proper granules to absorb the spillage immediately. Wear safety shoes when carrying out this work. Avoid fume inhalation.	L	M	4		3
	Lead Acid Batteries	Research and Technical Stuff	Skin Contact, Ingestion,	COSHH Assessments No. 223. Wear protective gloves when carrying out this work. Working area should be ventilated.	H	M	6		1
	Main-voltage and 3-Phase Electrical Equipments	Research and Technical Stuff	Electrocution	Work on mains voltage supply and 3-Phase equipment is carried out ONLY by qualified personnel.	M	H	8		1

Safety Office

The University of Nottingham
UNITED KINGDOM · CHINA · MALAYSIA

Standard Operating Procedure

Process Title
Combustion and Exhaust Emission Characteristics of Diesel Engines Using Alternative Fuels

Location of Work
Engine room (3) / L4 Building

Substances Involved	**Hazard**
Diesel fuel	Inhalation of vaporized hydrocarbon
Compressed gases	Asphyxiation
Engine oil	Skin irritation
Engine coolant	Skin irritation
Equipment Involved	
Rotating machinery	Eye/Body Damage
Pressurized fuel pipes	Body Damage
3-Phase electrical equipment	Electrocution
Operations Involved	
Running the engine	Inhalation of exhaust gas

Key Safety precautions/equipment that you will require

- The gas system is going to be tested for leak detection using compressed air before the introduction of any gaseous fuel.
- Only one gas bottle will be used at once.
- The gas bottle, gas delivery line, and gas vent lines are protected by flashback.
- The gas system is vented to outdoor through the extractor fan, where any excess pressure build-up in the delivery line beyond the injectors' working pressure is vented through a pressure relief valve.
- Gaseous fuel injection section in the engine intake manifold is equipped with a sensitive thermal fuse that melts if the temperature goes higher than a 75ºC – indicating that there is flashback of the flame inside the intake manifold. As the fuse melts, it sends out a signal to the Engine Control Unit (ECU) so it shuts of the H2 supply to the gas injector immediately.
- The system will be purged from any residuals of gaseous fuel after each experiment.
- The control room is equipped with a CO detector, to ensure personnel safety.
- There are 3 (three No.) emergency stop buttons that stop both the engine and the dynamometer; one attached to the dynamometer control panel, another attached to the engine control panel, and the third attached outside the room next to the engine.
- Fixed-guarding around all rotating machinery to be fitted when the engine running.
- Protective cloth will be worn when doing maintenance and inspection work.
- Battery terminals will be disconnected after the experiments end.

Page **1** of **2**

Procedure to be followed

- The whole gas system is going to be tested for leak prior to use. After insuring the system is "leak-tight", the gas bottle is insured to be closed before commencing the experiments.
- The extractor fan and the overhead vent are turned on, and also the cooling tower pump and the engine intercooler pump are turned on.
- Battery terminals are connected.
- The dynamometer is turned on to motor the engine at the desired speed, and then the engine is loaded gradually to the desired point using only the diesel fuel.
- The gaseous fuel in introduced to the engine gradually, on the account of the diesel fuel. As the experiments end, the gas supply is cut, and the engine is converted to diesel operation.
- The system will be purged from any residuals of gaseous fuel after each experiment.
- The diesel fuel supply is the cut from the engine, and then the dynamometer is stopped.
- The battery terminals are disconnected, and the pumps and fans are turned off.

Emergency/spillage procedure

- Stop the both the engine and dynamometer immediately by pressing any of the emergency buttons.
- If the leak is not ignited, extinguish all sources of ignition in the immediate area. Close the cylinder valve. If necessary tighten the gland nut. If leak continues, evacuate the area, and avoiding sources of ignition and minimizing personal risk move the leaking cylinder to a safe outside area. Notify BOC. Post warning notices and prevent access to the area. DO NOT Attempt to tighten the cylinder valve in the body of the cylinder. DO NOT tamper with the safety devices.
- If the leak is ignited, raise fire alarm. Close cylinder valve if safe to do so. Call fire brigade. Evacuate the area. If possible apply copious quantities of water from a hose to the affected cylinder(s) from a protected position until the cylinder(s) are cold. DO NOT Move cylinders until cold.

Disposal and decontamination procedures

N/A

Any specific storage requirements

- Compressed gas bottles will be stored fairly below 50°C in a well-ventilated place, in a location free from fire risk and away from sources of heat, ignition, and combustible materials.
- Bottles will be stored in the vertical position and properly secured to prevent falling over, and valve guards or caps should be in place.
- Stored containers will be periodically checked for general conditions and leakage.

Specific transport requirements [where applicable]

Gas bottles will be transported from the storage area to the work area on single-cylinder trolley one bottle at a time – only by trained personnel.

Any requirements for record keeping

ONLY authorized personnel are allowed to operate the engine.